Investigation of CD36-Induced Anti-Angiogenic Signalling Platform via Proximity Biotinylation

By

Arashdeep Saini

A thesis submitted in partial fulfillment of the requirements for the degree of

Master of Science

Department of Biochemistry

University of Alberta

Abstract

In response to hypoxic conditions, tumours secrete pro-angiogenic factors that stimulate the development of new blood vessels. Given the critical role of angiogenesis in tumour progression, therapies counteracting cancer neovascularization have been developed. However, clinical studies have shown these therapies to be only temporarily effective; thus, further research is needed to enhance our understanding of anti-angiogenic signalling. Our research has focused on elucidating the anti-angiogenic response stimulated by thrombospondin-1 (TSP-1) binding to cell surface receptor CD36. While F-actin, Fyn (an Src-family kinase), and CD36 nanoclusters are essential components of TSP1-induced anti-angiogenic response, the interactions between these molecules have yet to be discovered. Given the small size of CD36 cytosolic domains, we hypothesize that additional proteins within CD36 nanoclusters are crucial for its function. By identifying and investigating the role of these proteins, we seek to decipher the set of interactions necessary for CD36 anti-angiogenic signalling and organization. Here we developed a proximity biotinylation technique to identify proteins in the vicinity of CD36 via mass spectrometry. Proximity biotinylation has revealed a list of candidate proteins potentially important in CD36 signalling and organization. shRNA knockdown of candidate proteins revealed integrin beta-1 (ITGB1) to be essential for CD36-Fyn signalling. Furthermore, proximity ligation assay and conditional colocalization analysis provide support for a CD36, ITGB1, and CD9 molecular complex, implicated in anti-angiogenic signalling. Our approach to investigating CD36 nanodomains has not only revealed potential targets to reduce tumour angiogenesis it has also provided a roadmap to investigate the organization of other membrane proteins within their native states.

Preface

The experiments and results within this thesis were entirely and independently completed by Arashdeep Saini, the author of this work. After completing two summer studentships in the Touret lab, I opted to join the lab as an MSc. student in September of 2021. Transitioning from an undergraduate to a graduate student has been a fulfilling experience where I developed a multi-faceted skill set in my quest to unveil and investigate the CD36 interactome.

The Touret lab focuses on the mechanisms of membrane protein and receptor signal transduction. Ongoing projects within the lab are investigating how Fyn activation is modulated by its conformation and investigating the mechanism of transmembrane signal transduction of the glycosylphosphatidylinositol-anchored prion protein. My thesis investigates the anti-angiogenic signal transduction of CD36, a transmembrane protein that is expressed in microvascular endothelial cells.

Over the course of my research, I have had the opportunity to present and interact with members of the Membrane Protein Disease Research Group. Their insights have been instrumental in the development of this work. Also, I worked closely with Dr. Julien and his Ph. D student Erik Gomez in producing the mass spectrometry results presented in this thesis. This collaboration was instrumental in providing the basis for my research. My work built off the discoveries of a previous Ph.D. student in the Touret lab, John Maringa Githaka. He demonstrated that CD36 nanocluster enhancement, which was dependent on the cortical F-actin and membrane cholesterol, is needed for TSP-1-CD36 anti-angiogenic signalling. Because CD36 has short cytosolic domains with no enzymatic capacities, we believe that interacting proteins are needed for CD36 to facilitate anti-angiogenic signalling.

My research sought to discover necessary proteins for CD36 anti-angiogenic signalling and nanocluster organization. The insights provided here could be used to (re-)design anti-angiogenic therapies and improve their efficacy in clinical trials. To investigate proteins needed for CD36's

anti-angiogenic function we employed biochemical approaches and quantitative immunofluorescent microscopy. *Chapter 1* provides a holistic overview of tumour neovascularization and cancer therapies targeting anti-angiogenesis. In addition, *Chapter 1* provides general information of CD36, and the anti-angiogenic signalling cascade that it initiates in response to multi-valent ligands. Finally, the preliminary chapter of my thesis concludes by presenting our hypothesis and providing a brief history on the development of proximity labelling techniques. *Chapter 2* outlines the materials and methods utilized to produce the results presented in this thesis. In *Chapter 3*, I detail the results from CD36 biotinylation by antibody recognition (called throughout the document BAR), proximity ligation assay, conditional colocalization and experiments within our shRNA knockout cell lines which revealed role of CD36 interactors. *Chapter 4* provides a general discussion of our results and presents our predicted CD36-interaction model based on our findings.

Dedication

To my parents and my brother, Armaan, thank you for your unwavering support throughout my academic and life journey. I hope this thesis has made you proud!

Acknowledgements

Dr. Nicolas Touret, I would like to thank you for your patience and kindness during my time as an undergraduate and graduate student. The environment you have created within our lab has been key in cultivating my growth as an independent thinker. Allowing us to learn from our mistakes and providing us with the space to independently solve problems has provided me with the confidence to overcome obstacles within and outside of science. Thank you for everything you have done for me, and I will truly miss our discussions not only about science, but about basketball as well.

Thank you to my supervisory committee members, Dr. Olivier Julien, and Dr. Allan Murray for their feedback and support throughout my graduate studies. Without your insights, the research presented in this thesis would not have been possible. I would like to thank my external examiner, Dr. Ing Swie Goping for taking the time to be a part of my thesis defense.

Han, and Tolu thank you for being supportive lab members during my time within the Touret lab. Your friendship has made my graduate school experiment enjoyable. Observing your work ethic and dedication has been inspiring throughout my scientific journey. I would also like to extend a thank you to Erik Gomez who worked tirelessly with me to develop and optimize the analysis of our mass spectrometry data. I appreciate you making time for me, despite your extremely busy schedule.

I wish to extend a thank you to Canadian Institutes of Health Research, for providing me the monetary resources needed to pursue my research.

Last but certainly not least, I would like to thank my family for the support they have provided during my educational journey. You have provided me with the emotional and tangible support needed to fulfill my potential and I am forever grateful. To my brother, Armaan thank you for your patience and for providing me laughs during my lowest times. Finally, thank you to my partner,

Neha, for your support during my undergraduate and graduate studies. You have been an inspiration to me, and I am so lucky to have you in my life.

Table of contents

List of Tables

List of Figures

List of Abbreviations

AD	Alzheimer's Disease
ADP	Adenosine Di-phosphate
AF	Alexa Fluor
AKT	Ak Strain Transforming
AMP	Adenosine Monophosphate
ANOVA	Analysis of Variance
APEX	Ascorbate Peroxidase
ATP	Adenosine Triphosphate
BAR	Biotinylation by Antibody Recognition
BSA	Bovine Serum Albumin
CLESH	CD36, LIMP-2, Emp Sequence Homology
Co-IP	Co-immunoprecipitation
CSB	Cell Surface Biotinylation
DAPI	4′,6-Diamidino-2-phenylindole dihydrochloride, 2-(4-Amidinophenyl)-6-indolecarbamidine
DTT	Dithiothreitol
ECM	Extracellular Matrix
EGF	Epidermal Growth Factor
EGTA	Ethylene-bis(oxyethylenenitrilo)tetraacetic acid
EPCR	Endothelial Protein Receptor C
ER	Endoplasmic Reticulum
ERK	Extracellular signal-Regulated Kinases

FA	Fatty Acid
FAB	Fragment Antigen Binding Protein
FAK	Focal Adhesion Kinase
FDA	Food and Drug Administration
FGF	Fibroblast Growth Factor
FGFR	Fibroblast Growth Factor Receptor
FRET	Förster Resonance Energy Transfer
GFP	Green Fluorescent Protein
HIF	Hypoxia-Inducible Factor
HIV	Human Immunodeficiency Virus
HDMEC	Human Dermal Microvascular Endothelial Cells
HRP	Horseradish Peroxidase
HT	HaloTag
HUVEC	Human Umbilical Vein Endothelial Cells
IGF1	Insulin Growth Factor-1
IE	Infected Erythrocyte
JNK	c-Jun N-terminal Kinase
KD	Knockdown
KO	Knockout
LIMP	Lysosomal Integral Membrane Protein
MAM	Mitochondria-Associated ER Membranes
MAPK	Mitogen-Activated Protein Kinases
MBCD	Methyl-Beta-Cyclodextrin

MCAM	Melanoma Cell Adhesion Molecule
MMP	Matrix Metalloproteinase
MS	Mass Spectrometry
MTORC	Mammalian Target of Rapamycin Complex
MYOF	Myoferlin
NADPH	Nicotinamide Adenine Di-nucleotide Phosphate)
NB	Nanobody
NF	Necrosis Factor
NHS	N-hydroxysuccinimidobiotin
NS	Non-specific
PAGE	Polyacrylamide Gel Electrophoresis
PBS	Phosphate-buffered saline
PCR	Polymerase Chain Reaction
PDGF	Platelet-derived Growth Factor
PDGFR	Platelet-derived Growth Factor Receptor
PFA	Paraformaldehyde
PL	Proximity Labelling
PLA	Proximity Ligation Assay
PS	Phosphatidylserine
PSM	Peptide Spectral Matches
PTPε	Protein Tyrosine Phosphorylation ε
RNA	Ribonucleic Acid
ROS	Reactive Oxygen species

RPM	Revolutions per Minute
SDS	Sodium Dodecyl Sulphate
SFK	Src-Family Kinase
SR	Scavenger Receptor
STOM	Stomatin
TBST	Tris-Buffered Saline
TGF-β	Transforming Growth Factor Beta
TIE	Tyrosine-Protein Kinase Receptor
TIFF	Tag Image File Format
TIME	Human Telomerase-immortalized Microvascular Endothelial Cells
TIRFm	Total Internal Reflection Fluorescence Microscopy
TSP-1	Thrombospondin-1
TSR	Thrombospondin type 1 Repeat
TX	Triton X-100
VEGF	Vascular Endothelial Growth Factor
VEGFR	Vascular Endothelial Growth Factor Receptor

Chapter 1: Introduction

1.1 Angiogenesis

1.1.1 Angiogenesis and Tumourigenesis

Angiogenesis, the development of novel blood vessels from existing ones, is a critical physiological process that regulates embryonic development, tissue maintenance, reproduction, and wound repair (Otrock et al., 2007; Aspriţoiu et al., 2021). There are two types of angiogenesis: intussusceptive and sprouting. Intussusceptive angiogenesis, or splitting angiogenesis, occurs when a single blood vessel splits into two (Adair and Montani, 2010). Two essential vascular events, capillary development and embryo vascularization, primarily occur via intussusceptive angiogenesis (Adair and Montani, 2010). The better known angiogenic mechanism is sprouting angiogenesis, where existing endothelial cells proliferate in the direction of angiogenic stimuli (

Figure 1-1) (Adair and Montani, 2010). Angiogenesis is modulated by the balance between pro-angiogenic and anti-angiogenic factors (Figure 1-2). In adult tissue, endothelial cells are predominantly dormant and must be activated to proliferate (Ricard et al., 2021). For the ‘angiogenic switch’ to be activated, the activities of the pro-angiogenic factors must be greater than their anti-angiogenic counterparts (Bergers and Benjamin, 2003).

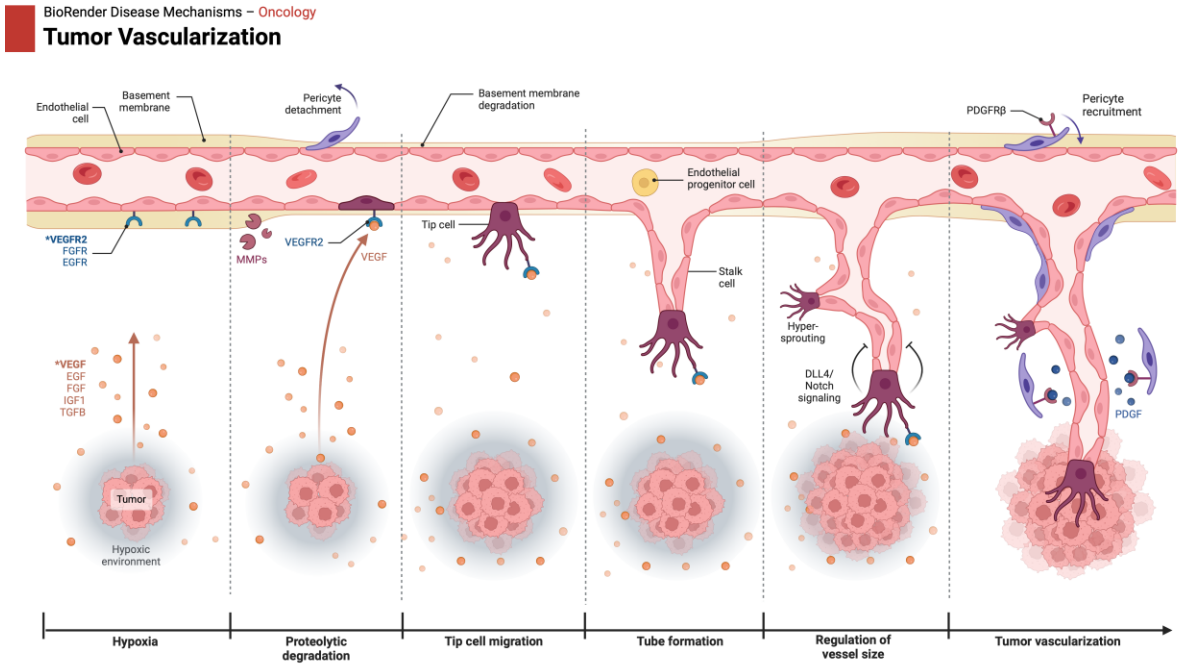

Figure 1-1: Illustration of the main events leading to tumour neo-vascularization.

In response to hypoxic conditions, tumours secrete pro-angiogenic factors vascular endothelial growth factor (VEGF), epidermal growth factor (EGF), fibroblast growth factor (FGF), insulin growth factor-1 (IGF1), and transforming growth factor beta (TGFβ), which activate the "angiogenic switch" by altering the balance between pro- and anti-angiogenic factors. Secretion of matrix metalloproteinases (MMPs) removes the physical barrier of the basement membrane and ECM, enabling endothelial cell proliferation and migration (Quintero-Fabián et al., 2019; Niland et al., 2021). Novel angiogenic sprouts are led via migrating tip cells, which migrate in a chemotactic fashion in response to the VEGF gradient produced by tumour cells (Bentley et al., 2009; Minerva et al., 2022). In the last step of tumour neo-vascularization, pericytes are recruited to novel blood vessels via endothelial and tumour cell secretion of platelet derived growth factor (PDGF) (Abramsson et al., 2003; Jiang et al., 2020). Pericytes wrap around microvascular endothelial, aiding their migration, supporting their maturation, and stabilizing novel blood vessels (Song et al., 2005). (created with Biorender).

The activation of the 'angiogenic switch' occurs during tumour development via tumour cell secretion of pro-angiogenic factors and the downregulation of anti-angiogenic factors (Bergers and Benjamin, 2003). Primary tumours develop from epigenetic and genetic factors causing uncontrolled cell proliferation. However, their growth beyond ~1mm is stunted without sufficient oxygenation and nutrients (Welch and Hurst, 2019).

Tumour neovascularization is a key milestone in tumour progression, enabling growth, survival, and metastasis (Nishida et al., 2006). In response to hypoxic conditions within the tumour

microenvironment, proteasomal degradation of transcription factor hypoxia-inducible (HIF) factor 1-α is inhibited (Ma et al., 2020). HIF-α dimerizes with HIF-1β to increase the expression of pro-angiogenic factors such as vascular endothelial cell growth factor (VEGF), platelet-derived growth factor (PDGF) and transforming growth factor-α (TGFα) (Ma et al., 2020). The binding of these factors to receptors of proximal endothelial cells induces angiogenic signalling. The signalling pathways initiated by pro-angiogenic factors contribute to angiogenesis in three ways: 1) activating proliferative signalling, 2) inducing endothelial cell migration, and 3) causing the degradation of extracellular matrix (ECM), allowing for endothelial chemotactic invasion into neighbouring tissues (Lamalice et al.,2007; Kirsch and Black 2012).

Given the critical role of angiogenesis in tumour progression and metastasis, anti-angiogenic therapies have garnered interest (Ma and Waxman, 2008). By altering the activities of anti-angiogenic or pro-angiogenic factors, these therapies are designed to tip the angiogenic scale to favour blood vessel dormancy. Enhancing our understanding of pro-angiogenic and anti-angiogenic factors has been essential in the development of novel cancer therapies limiting tumour neovascularization.

1.1.2 Pro-angiogenic and Anti-angiogenic Factors

Stimulation of angiogenesis is dependent on the activities of pro-angiogenic and anti-angiogenic factors. The balance between these factors is alerted under physiological conditions and disease. Below, we discuss the signalling pathways activated by prominent pro- and anti-angiogenic factors (summarized in Figure 1-2).

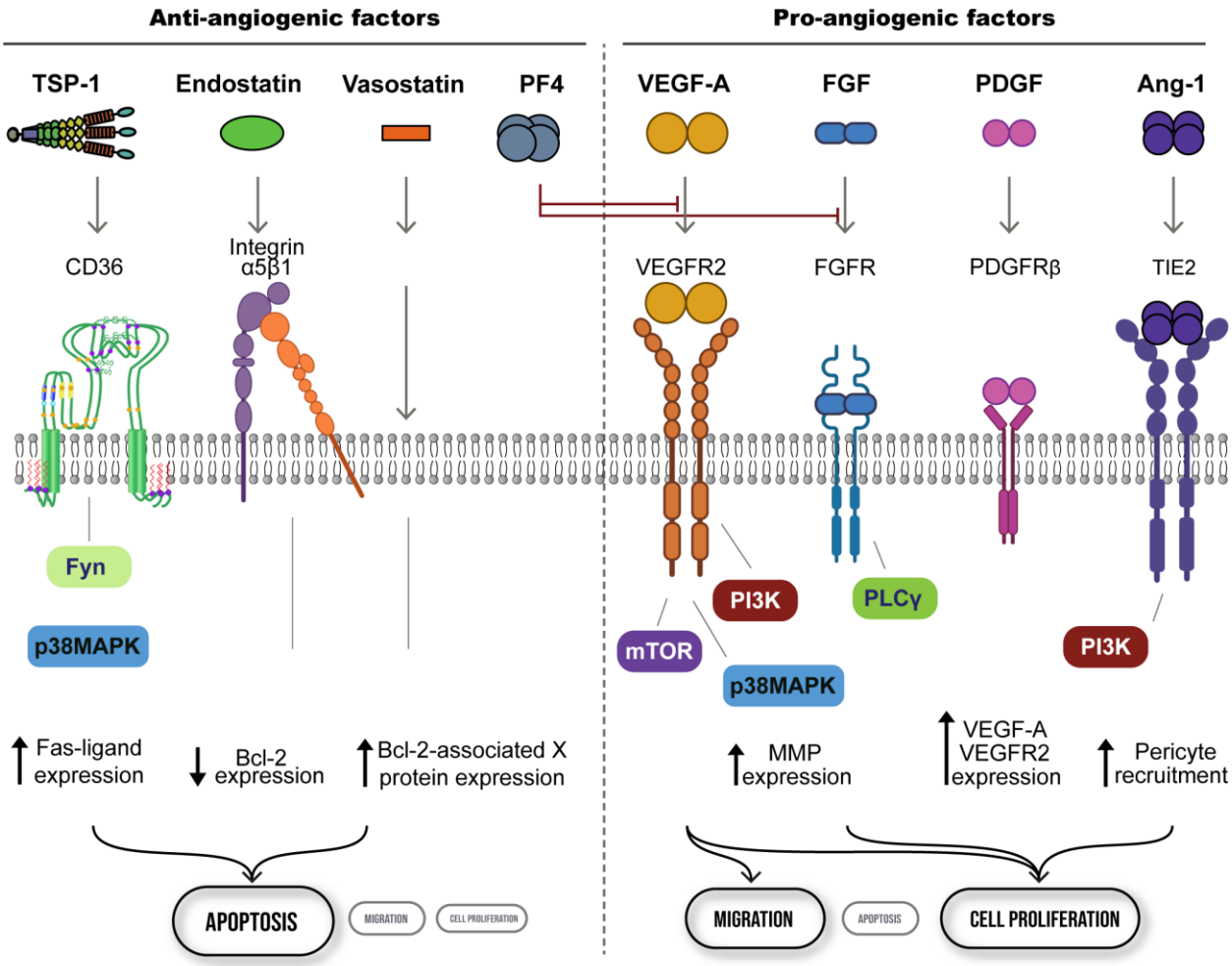

Figure 1-2: Summary of the mechanisms by which prominent pro- and anti-angiogenic modulate the angiogenic balance.

The effects of pro- (VEGF-A, FGF, PDGF, and Ang-1) and anti-angiogenic factors (TSP-1, (PF4) and endostatin and vasostatin) on endothelial signalling and proteins expression.

1.1.2.1 Pro-angiogenic Factors

1.1.2.1.1 Vascular Endothelial Growth Factor: VEGF

VEGFs are a five-membered family (VEGF-A, VEGF-B, VEGF-C, VEGF-D, and placental growth factor) of secreted dimeric glycoprotein, which regulates lymphogenesis, vasculogenesis and angiogenesis (Holmes and Zachary, 2005). VEGF activates the intrinsic kinase activity of VEGF receptors (VEGFRs) through dimerization, leading to autophosphorylation of the receptors' intracellular tyrosine resides (Ruan and Kazlauskas, 2012). Phosphorylated tyrosine residues act

as scaffolds for the recruitment of intracellular proteins promoting angiogenic signalling (Álvarez-Aznar et al., 2017). VEGF-A is the most potent VEGF member in stimulating angiogenic signalling. VEGF-A binds to VEGFR2 to initiate signalling cascades, resulting in endothelial cell proliferation and migration.

VEGF-A/VEGFR2 mediated activation of phosphoinositide 3-kinase (PI3K)/Ak strain transforming kinase (AKT) and phospholipase C gamma-1 (PLCγ) signalling pathways is needed for endothelial cell proliferation and survival. Through PI3K/AKT signalling, VEGF-A increases the expression of anti-apoptotic factors such as Bcl-2, maintaining endothelial survival (Gerber et al.,1998). PI3K/AKT downstream signalling also leads to the activation of mammalian target of rapamycin (mTOR) signalling, resulting in cell proliferation. The MTOR complexes are essential for proliferation as they increase anabolic processes, such as protein synthesis, and inhibit catabolic processes (Okumura et al., 2012). Inhibition of mTOR signalling by rapamycin has shown to inhibit early angiogenesis and decrease vascularity (Xue et al., 2009).

VEGF-A stimulation of endothelial cells also results in an increase in intracellular calcium, which is mediated through PLCγ signalling and the production of inositol 3-phosphate. Increases in intracellular Ca2+ results in the activation of the extracellular signal-regulated kinase (ERK)/mitogen-activated protein kinase (MAPK) pathway (McLaughlin and De Vries, 2001). The ERK/MAPK signalling cascade induces the activation of transcription factors, causing an increase in protein synthesis and proliferation (Takahashi et al., 1999; Mebratu and Tesfaigzi, 2009).

VEGF-A/VEGFR2 signalling stimulates endothelial cell migration by signalling through p38 MAPK. VEGF-mediated activation of p38MAPK within endothelial cells results in the reorganization of the actin cytoskeleton. These changes promote cell mobility and are characterized by an increase in actin stress fibre formation and stability of focal adhesions (Rousseau et al., 1997; Yoshizuka et al., 2012).

In addition to increased proliferation and migration, VEGF contributes to angiogenesis by increasing the expression of matrix metalloproteinase (MMP). Degradation of the ECM is needed for the liberation of proliferating endothelial cells and sequestered growth factors (Kalluri, 2003).

VEGF stimulation increases the expression and secretion of pro-MMP-9 and pro-MMP-2 (Taraboletti et al., 2002). Through inhibition studies, MMP secretion was shown to be essential in endothelial cell invasion through the reconstituted basement membrane. Although VEGF-A is the primary driver of angiogenesis, VEGF-A acts in conjunction with other growth factors to stimulate angiogenesis which are discussed below.

1.1.2.1.2 Fibroblast Growth Factor: FGF

The FGF family consists of 23 proteins (Chen et al., 2020). These proteins are needed for differentiation, proliferation, tissue repair and angiogenesis (Farooq et al., 2021). Several FGF proteins activate angiogenesis through FGF tyrosine kinase receptors (FGFRs). Activation of the intrinsic kinase domains results in proliferative and survival signalling through downstream activation of PLCγ (Chen et al., 2020). In addition, FGF contributes to angiogenesis by up-regulating proteins involved in the degradation of the ECM. FGF-2 increases the expression of MMPs, and urokinase-type plasminogen activator, a serine-protease which degrades ECM proteins. By inducing growth signalling and increasing endothelial cell migration, FGF plays an important role in promoting angiogenesis.

1.1.2.1.3 Platelet-Derived Growth Factor: PDGF

PDGFs are heterodimeric proteins that signal through tyrosine kinase receptor PDGFRβ to induce angiogenesis via two mechanisms: 1) increasing the expression of VEGF-2 and 2) initiating signalling, which stabilizes the growth of novel blood vessels (Raica and Cimpean, 2010). PDGFs are secreted from both tumours (Jiang et al., 2020) and endothelial cells (Abramsson et al., 2003) and their binding to PDGFRβ increases endothelial expression of VEGF-A and VEGFR2 (Wang et al. 1999; Magnusson et al., 2007 Trebec-Reynolds et al. 2010).

Pericytes are smooth muscles cells that wrap around endothelial cells that line capillaries (Brown et al., 2019). They are needed to guide, support maturation and stabilize developing blood vessels (Song et al., 2005). PDGF binding to PDGFRβ induces differentiation, proliferation, and recruitment of pericytes to sprouting endothelial cells (Song et al., 2005; Ribatti et al., 2011). Without the recruitment of pericytes, novel blood vessels become unstable and, hence, regress (Ribatti et al., 2011).

1.1.2.1.4 Angiopoietins

Angiopoetin-1 regulates endothelial cell survival through its binding to tyrosine kinase receptor TIE2 (Fagiani and Christofori, 2013). Angiopoetin-1 expression and secretion by pericytes and vascular smooth muscle increase in response to VEGF-A, PDGF, and hypoxia (Fagiani and Christofori, 2013). Stimulation of TIE2 by angiopoietin-1 promotes endothelial cell proliferation by inhibiting NF-κB mediated apoptosis and activating PI3K/AKT survival signalling (Kim et al., 2000; Tadros et al., 2003).

1.1.2.2 Anti-angiogenic Factors

1.1.2.2.1 Endostatin

Endostatin is a 20 kDa protein produced from the cleavage of type XVIII collagen by secreted cathepsin-L (Felbor et al., 2000; Ferreras et al., 2000; Walia et al., 2015). As a potent anti-angiogenic factor, endostatin exhibits several mechanisms reducing the proliferation and survival of endothelial cells. Endostatin binds to VEGFR-2, blocking VEGF angiogenic signalling (Walia et al., 2015). Through its interaction with α5β1, endostatin impairs integrin association with fibronectin, and therefore causing focal adhesion disassembly and impaired endothelial cell migration (Wickström et al., 2002). Through an unknown mechanism, Endostatin also disrupts Wnt/β-catenin signalling, a signalling pathway which increases the expression of Cyclin D1 (Xu et al., 2014; Hanai et al., 2002). By reducing the expression of cyclin D1, a cyclin-dependent kinase whose activity is needed for the transition of cells from G1 to S phase, endostatin induces

cell cycle arrest of endothelial cells (Hanai et al., 2002). Endostatins' ability to hamper angiogenesis through diverse mechanisms has placed it as a potential target of anti-angiogenic cancer therapies. However, issues regarding its short life time, instability, and high concentration have made its clinical application unviable (Mohajeri et al., 2017).

1.1.2.2.2 Vasostatin

Calreticulin (a protein chaperone residing in the endoplasmic reticulum) translocates to the cell membrane in response to irreversible cell damage (Panaretakis et al., 2009). Vasostatin, an anti-angiogenic fragment, is produced from the elastase-dependent cleavage of plasma membrane-localized calreticulin (Mans et al., 2012). Vasostatin inhibits endothelial cell migration and proliferation by suppressing VEGFR2 signalling (Wei et al., 2021). Like endostatin, vasostatin reduces the expression of cyclin-dependent kinases and anti-apoptotic protein Bcl-2 (Shu et al., 2014). Vasostatin further tips the angiogenic scale towards apoptosis by increasing the expression of pro-apoptotic Bcl-2-associated X protein (Shu et al., 2014). Exogenous addition of vasostatin and interleukin-12 to mice tumours has been found to decrease and inhibit tumour growth and neovascularization (Yao et al. 2000). By inhibiting different features of tumour angiogenesis, vasostatin and interleukin-12 combination represent a candidate anti-angiogenic therapy. However, vasostatin or vasostatin-derived molecules have yet to be tested in clinical trials.

1.1.2.2.3 Platelet Factor-4

Platelet factor-4 is a tetrameric chemokine released from the α-granules of activated platelets (Rauova et al., 2006). It promotes blood coagulation by inhibiting the function of antithrombin (Fiore and Kakkar, 2003). Platelet factor-4 also functions as an anti-angiogenic factor by blocking growth factor signalling and slowing endothelial cell cycle progression. The interaction of platelet factor-4 with FGF and VEGFA blocks their dimerization and activation of FGFR and VEGFR pro-angiogenic receptors (Gengrinovitch et al., 1995; Perollet et al., 1998). Platelet factor-

4 also prevents FGF-meditated cell proliferation by acting intracellularly to inhibit ERK/MAPK signalling (Sulpice et al., 2002). In addition, platelet factor-4 inhibits cell cycle progression by preventing the downregulating cyclin-dependent kinase inhibitor, p21 (Gentilini et al., 1999). While the effects of platelet factor-4 on the cell cycle are known, their mechanisms remain elusive. Therefore, further research is needed to better understand platelet factor-4 mode of action and identify its therapeutic potential.

1.1.2.2.4 Thrombospondin-1: TSP-1

TSP-1 is a homotrimeric matricellular protein released from the alpha granules of activated platelets. It is a part of the five-membered thrombospondin superfamily (TSP-1 to 5) (Sun et al., 2020). TSP-1 anti-angiogenic properties stem from its ability to antagonize growth factor signalling and induce endothelial cell apoptosis through cell surface receptor CD36 (Lawler and Lawler, 2012). TSP-1 inhibits angiogenic signalling by binding and sequestering VEGF and FGF (Inoki et al., 2002; Colombo et al., 2010). The bioavailability of VEGF is further reduced by low-density lipoprotein receptor-related protein-1 mediated internalization of the TSP-1/VEGF complexes (Greenaway et al., 2007).

TSP-1 binding to CD36 in microvascular endothelial cells initiates a signalling cascade resulting in the death of endothelial cells (Jiménez et al., 2000). The initial step of this pathway is the activation of Fyn, an Src-family kinase (SFK). Fyn downstream signalling leads to the activation of death protease caspase-3 and increased secretion of FAS ligand (Jiménez et al. 2000; Volpert et al. 2002). Proteins involved in CD36 anti-angiogenic signalling will be discussed in more detail in section 1.4.

1.1.3 Clinical Potential of Anti-Angiogenic Approaches

In 1971, Dr. Judah Folkman published a review hypothesizing that tumour viability can be reduced by inhibiting tumour neovascularization (Folkman, 1971; Ribatti, 2008). This influential

review ignited a new area of research within the field of oncology, exploring mechanisms to inhibit tumour angiogenesis. Research efforts have culminated in the development of anti-angiogenic therapies. Most of these therapies are targeted towards the inhibition of the pro-angiogenic VEGF signalling by antagonizing VEGF binding or inhibiting the VEGFR kinase domains. Activation of anti-angiogenic signalling have also been developed, such as TSP-1 mimetics targeting CD36. However, TSP-1 mimetic therapies have shown limited efficacy in clinical trials (Huang et al., 2017). The purpose of this current study was to enhance the understanding of CD36-induced anti-angiogenic signalling, and therefore aid the development of novel TSP-1 mimetics.

1.1.3.1 Inhibition of Pro-Angiogenic Pathways

Bevacizumab, the first FDA-approved anti-angiogenic therapy, is a monoclonal antibody against VEGF (Jain et al., 2006). As a monotherapy, it failed to improve the survival of colorectal and lung cancer patients. However, its use as co-therapy with toxic agents in phase III clinical trials improved the survival of colorectal, breast and lung cancer patients. Although Bevacizumab-cytotoxic therapies have shown success, some studies have demonstrated Bevacizumab to antagonize cytotoxic agents. By inhibiting tumour vascularization, it is thought Bevacizumab may reduce the delivery of cytotoxic agents to tumours. Therefore, further studies are needed to determine the cellular and vascular conditions where Bevacizumab is effective. Alfivercept is a VEGF decoy receptor that binds to VEGF (Montemagno and Pagès, 2020). It has been shown *in vitro* to greatly suppress tumour growth; however, it has been less effective than Bevacizumab in clinical trials (Montemagno and Pagès, 2020).

In contrast to Bevacizumab, receptor tyrosine kinase inhibitors have shown effectiveness as monotherapies within phase III clinical trials (Jain et al., 2006). These inhibitors prevent VEGF, FGF and PDGFR signalling by occupying the ATP-binding pocket of the intracellular kinase domains (Yamaoka et al., 2018; Pottier et al., 2020). Over 43 tyrosine kinase inhibitors have been FDA-approved for oncological treatments (Pottier et al., 2020). Despite their effectiveness,

tumours readily develop resistance to these treatments by mutating receptor tyrosine kinases (Pottier et al., 2020). Cancer-expressing efflux pumps also play a role in resistance by transporting cancer drugs out of the cell (Shukla et al., 2012). In addition, receptor kinase inhibitors exhibit high levels of toxicity due to their ability to inhibit other receptor tyrosine kinase inhibitors and intracellular kinases (Broekman et al., 2011: Pottier et al., 2020). Anti-angiogenic therapies antagonizing pro-angiogenic therapies are believed to have the greatest effectiveness when used in conjunction with other cancer therapeutics with diverse mechanisms of action (Elebiyo et al., 2022).

1.1.3.2 Activation of Anti-Angiogenic Pathways

TSP-1 mimetics have shown poor efficacy in clinical studies. ABT-510, a TSR mimetic, failed to improve the survival of renal cell carcinoma patients in phase two clinical trials as a monotherapy (Huang et al., 2017). It also causes adverse side effects such as thrombosis and pulmonary embolism (Ebbinghaus et al., 2005; Baker et al., 2016). A second-generation TSR peptide mimetic, ABT-898, has been shown to reduce angiogenesis in primates but has yet to be tested on humans (Campbell et al., 2011). The lack of effectiveness of these TSP-1 mimetics could be due to their monovalent nature. Our lab has investigated the effectiveness of multivalent ligands and shown that they are needed to enhance CD36 clustering and initiate anti-angiogenic signalling (Githika et al., 2016). CVX-045, a multivalent TSP-1 mimetic produced by attaching TSP-1 peptides to an antibody scaffold, was the first multivalent TSP-1 ligand to reach clinical trials (Jeanne et al., 2015). However, CVX-045 had limited success and produced adverse side effects in phase I clinical trials (Jeanne et al., 2015). Overall, anti-angiogenic therapies have had disappointing results. Therefore, further investigation of anti-angiogenic signalling is needed to improve the effectiveness of these therapies. The research presented here was directed to elucidate the molecular mechanisms of CD36-Fyn signal transduction to further support the enhancement of anti-angiogenic therapies.

1.1.3.3 Effect of Anti-Angiogenic Therapies on Tumour Vasculature Normalization and Cytotoxic Drug Delivery

The classical view of anti-angiogenic cancer therapies, as treatments which “starve” and reduce metastasis by downregulating tumour neo-vascularization, has led to the belief that their combination with chemotherapy would be antagonizing; given chemotherapies require adequate vascularization for their delivery to tumours (Jain, 2001; Goel et al., 2011; Liu et al. 2023). However, the addition of anti-angiogenic therapies, primarily bevacizumab, to classical chemotherapies has shown to improve survival in some malignancies (Hurwitz Herbert et al., 2004; Giantonio et al., 2007; Saltz et al., 2008; Reck et al., 2009; Welch et al., 2010; Cheng et al., 2019). To reconcile this discrepancy, Jain (2001) proposed a novel role for anti-angiogenic therapies as normalizers of tumour vasculature, enhancing the delivery of chemotherapies. It was also postulated that there is a “window” post-anti-angiogenic treatment where chemotherapies will have a maximal therapeutic effect.

In response to chronic and excessive pro-angiogenic signalling, tumour vessels acquire a tortured phenotype characterized by excessive branching, defective pericyte coverage, increased leakiness, abnormal bulges and impaired smooth muscle function (Carmeliet and Jain, 2000; De Palma et al., 2017). These vascular conditions limit the delivery and effectiveness of cytotoxic cancer therapies (Jain, 1998; Carmeliet and Jain, 2000). By normalizing tumour vasculature, anti-angiogenic therapies have been shown to improve drug delivery to tumours *in vivo*.

Treatment of tumour-bearing mice with bevacizumab prior to intravenous injection of chemotherapies reduced vessel length, leakiness and chaotic organization of tumour vasculature (Dickson et al., 2007). The normalization of tumour blood vessels enhanced intratumoral drug penetration. However, the “window” post-angiogenic treatment where cytotoxic drug delivery was maximized was altered based on the tumour-type and chemotherapy used, suggesting that the optimal “window” is modulated by these two factors. In addition, bevacizumab combination with

chemotherapies has improved the survival of patients suffering from colorectal (Hurwitz Herbert et al., 2004; Giantonio et al., 2007; Saltz et al., 2008; Welch et al., 2010), lung (Reck et al. 2009), and liver cancer (Cheng et al., 2019). The above literature has resulted in a paradigm shift in anti-angiogenic therapies as they are now perceived as co-therapies which improve the efficacy of cytotoxic cancer drugs (Ma and Waxman 2008).

1.2 CD36

1.2.1 CD36 Domain Organization

CD36 is a member of the class B scavenger receptor family. This family also includes cholesterol transport protein, scavenger receptor class B type I (SR-BI) and lysosomal integral membrane protein II (LIMP-II) (Febbraio et al., 2001). CD36 is expressed in a variety of cells: platelets (Ghosh et al., 2007; Ghosh et al., 2011), skeletal (Pelsers et al., 1999), smooth muscle (Greenwalt et al., 1995), macrophages/monocytes (Huh et al., 1996; Lonati et al., 1996; Sampson et al., 2003), adipocytes (Sfeir et al., 1997), dendritic cells (Albert et al., 1998), and microvascular endothelial cells (Swerlick et al., 1992; Farhangkhoee et al., 2005). CD36's ability to bind to a diversity of ligands allows it to play central roles in atherosclerosis and immunity (Taban et al., 2022).

CD36 is a 472 amino acid protein which features two transmembrane, a large extracellular and two short cytosolic domains (Figure 1-3) (Tandon et al., 1989; Tao et al., 1996; Aboulaich et al., 2004; Hsieh et al., 2016). The N-terminal and C-terminal cytosolic domains are 7 and 11 amino acids, respectively (Tandon et al., 1989; Hsieh et al., 2016). The four intracellular cysteines are post-translationally modified by palmitoylation (Tao et al., 1996). Palmitoylation of CD36 is critical for cell trafficking as mutation to these sites cause CD36 endoplasmic reticulum retention (Thorne et al., 2010). Palmitoylation also aids in CD36's localization to membrane domains, which is critical for its internalization and signalling functions (Thorne et al., 2010). CD36 is glycosylated at 9 of the 10 available sites glycosylation sites (Hoosdally et al., 2009). Glycosylation shifts CD36

from its predicted molecular weight of 53 kDa to 88 kDa (Hoosdally et al., 2009). The extracellular domain features 3 di-sulfide bridges in the following arrangement: C271-C332 and C12-C321, C242-C310 (Rasmussen et al., 1998). Finally, CD36 has been shown to be phosphorylated at Thr92 by PKCα. This ectodomain phosphorylation reduces CD36's extracellular ligand binding and signalling (Ho et al., 2005; Chu and Silverstein, 2012).

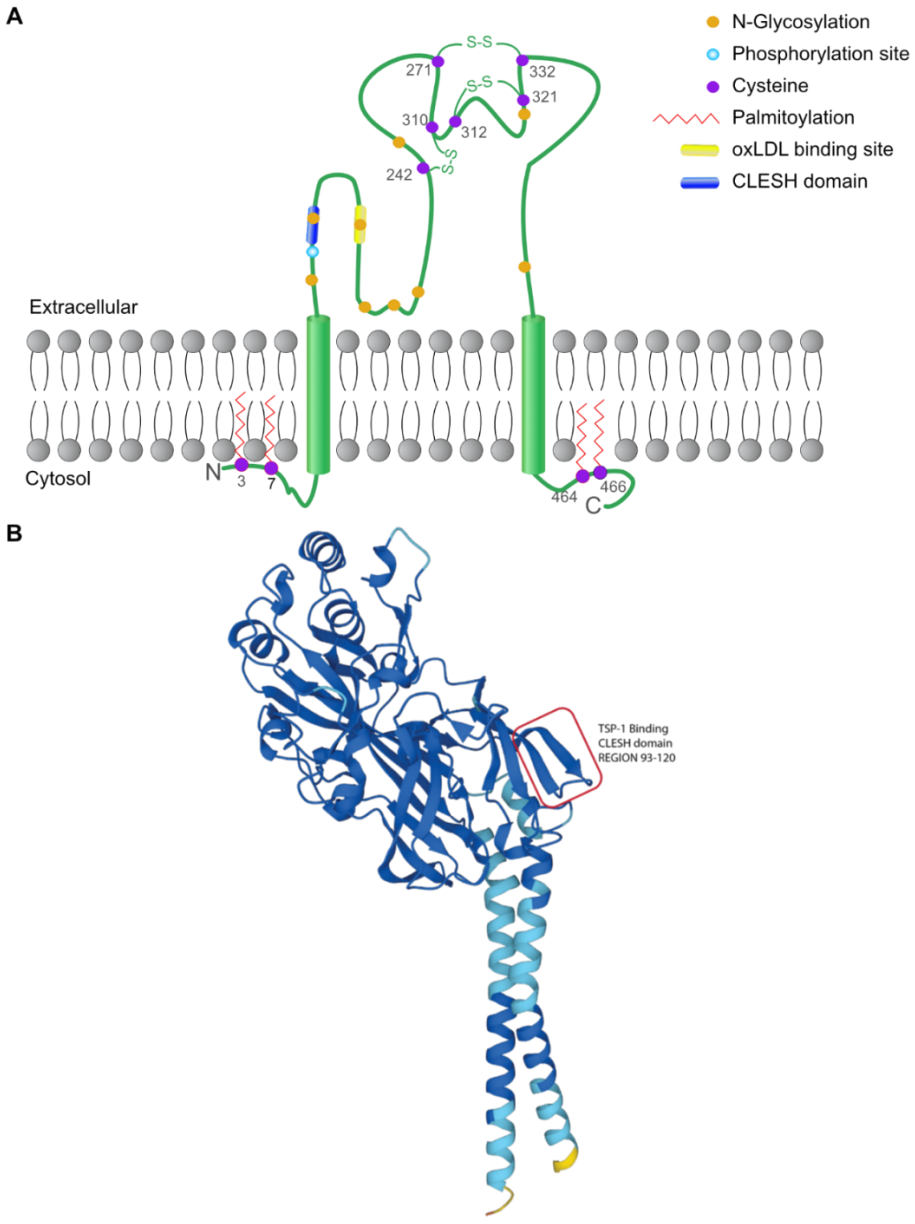

Figure 1-3: CD36 domain organization (A) and crystal structure of CD36 (B).

(A) CD36 is a transmembrane scavenger receptor that features two transmembrane domains, and a heavily glycosylated ectodomain. The extracellular domain also contains 6 cysteines which form 3 disulfide bonds in the

arrangement of C271-C332, C242-C310, and C312-C321. TSP-1 and oxLDL, two ligands of CD36, bind at the CD36, LIMP-2, Emp sequence homology (CLESH) domain, and oxLDL binding site. Palmitoylation of the short cytosolic N-terminal and C-terminal domains is needed for CD36 trafficking and membrane anchorage. (Schematic adapted from Nicolas Touret.) (B) AlphaFold prediction (AF-P16671-F1) based on the crystal structure of CD36's extracellular domain bound the Plasmodium falciparum erythrocyte membrane protein 1 (PfEMP1) (Hsieh et al., 2016). The CLESH domain, which TSP-1 binds to, is outlined in red.

The crystal structure of CD36's extracellular domain bound the *Plasmodium falciparum* erythrocyte membrane protein 1 (PfEMP1) was determined in 2016 (PDB: 5LGD and (Hsieh et al., 2016)) (Figure 1-3, B). These structures confirmed the presence of a β-barrel tunnel which transverses the length of the extracellular domain (Hsieh et al., 2016). Fatty acids were shown to occupy this cavity, and therefore it is believed that the β-barrel tunnel translocates lipids into the plasma membrane (Hsieh et al., 2016). An extracellular α-helical bundle mediates the binding of PfEMP1 to CD36 (Hsieh et al., 2016). CD36 homology modelling studies also provide support for the α-helical bundle to meditate CD36-lipid binding (Neculai et al., 2013).

1.2.2 CD36 Ligands and Cellular Responses

CD36 is implicated in diverse biological phenomena due to its ability to bind numerous ligands: oxidized LDL (oxLDL) (Nicholson et al., 1995), oxidized phospholipids (Podrez et al., 2002), pfEMP1 (Baruch et al., 1996), β-amyloid (El Khoury et al., 2002), fatty acids (FA) (Abumrad et al., 1999; Coburn et al., 2000), TSP-1 (Dawson et al., 1997), and anionic phospholipids (Rigotti et al. 1995). Here we will discuss the role of CD36 and its associated ligands in disease and cell immunity.

- oxLDL

Although CD36 binds to a diverse repertoire of ligands, its primary role is to regulate lipid metabolism by mediating oxLDL uptake and transporting FA in adipocytes (Rigotti et al., 1995), enterocytes (Stahl et al., 1999), and cardiac and skeletal muscle (Luiken et al., 1999). CD36 also mediates the uptake of oxLDL in macrophages (Navazo et al., 1996). CD36 knockout mice have

shown the importance of CD36 in maintaining lipid homeostasis (Febbraio et al., 1999). Although CD36 knockout mice were viable and phenotypically normal, they featured elevated levels of serum cholesterol, FA, and triacylglycerols. Adipocytes and macrophages of CD36 knockout mice had impaired oleate and oxLDL uptake, respectively.

CD36 transports FA and oxLDL through two different mechanisms. FA triggers adipocyte internalization of CD36 via caveolae-dependent endocytosis (Hao et al., 2020). The binding of FA causes CD36 de-palmitoylation, which is essential for internalization and the recruitment of dynamin adaptor protein VAV (Kar et al., 2008). Amino acids 157-171 constitute the binding site of oxLDL to CD36 (Kar et al., 2008). Although CD36-mediated oxLDL internalization needs further investigation, it is clear that oxLDL is endocytosed through a pathway distinct from clathrin and caveolae-mediated endocytosis (Zeng et al., 2003).

CD36-mediated internalization of oxLDL in macrophages plays a crucial role in the progression of atherosclerotic lesions. Foam cells are formed when lipid accumulation within macrophages surpasses the homeostatic capacity of the cell (Guerrini and Gennaro, 2019). Foam cells accumulate to form the core of atherosclerotic plaques (Gui et al., 2022). In states of inflammation and high reactive oxygen species (ROS) levels, CD36-mediated internalization of oxLDL contributes to the lipid dysregulation of macrophages (Liu et al., 2014). CD36 internalization of oxLDL activates transcription factor PPARγ (Collot-Teixeira et al., 2007). PPARγ activation induces transcriptional changes in the cell, including increased CD36 expression (Collot-Teixeira et al., 2007). This vicious positive feedback loop causes oxLDL uptake beyond the homeostatic capacity of macrophages leading to lipid accumulation with lipid droplets and foam cell formation (Collot-Teixeira et al., 2007).

- β-amyloid

As a ligand for β-amyloid plaques, CD36 contributes to Alzheimer's disease (AD) pathology. CD36-mediated binding of β-amyloid to microglial cells leads to the production of cytokines,

chemokines, and reactive oxygen species and produces a pro-inflammatory response which is characteristic and associated with AD (Coraci et al., 2002; El Khoury et al., 2003). In addition to chronic inflammation, AD is also characterized by cerebral amyloid angiopathy (CAA) which occurs in response to β-amyloid plaque accumulation in cortical arteries, arterioles, capillaries, and veins (Attems, 2005; Thal et al., 2008). CD36 causes β-amyloid accumulation in the cerebral vasculature and therefore promotes CAA, causing impaired blood vessel integrity, vasculature function, and cognitive function (Park et al., 2011; Park et al., 2013). Therefore, it is believed that the development of novel therapies targeting CD36 could potentially ameliorate the vascular dysfunction associated with CAA and AD (Park et al., 2011).

- PfEMP1

Malaria is one of the leading causes of mortality and morbidity in developing countries (Talapko et al., 2019). Female mosquitos of the *anopheles* species transmit causative agents of malaria such as *P. malariae*, *P. falciparum*, *P. vivax*, *P. ovale*, and *P. knowlesi* through their proboscis (Talapko et al., 2019). *P. falciparum* infections cause the most severe cases of malaria as their invasions of erythrocytes, cause erythrocyte adherence to the vasculature (Bachmann et al. 2022). Not only does this allow *P. falciparum* infected erythrocytes (IEs) to evade the immune system, but it also leads to obstruction of blood flow to vital organs (Idro et al., 2005; Hanson et al., 2012; da Silva et al., 2017; White, 2022). To sequester within blood vessels, IEs express a family of membrane proteins including PfEMP1, which binds to CD36 on endothelial cells (Baruch et al. 1997; Davis et al. 2012; Davis et al. 2013). IEs binding to CD36 leads to the activation of Src-family kinases (SFKs), which increases CD36 clustering (Davis et al., 2012) and recruits integrin $\alpha_5\beta_1$ (Davis et al., 2013) to the site of adhesion. These changes in membrane organization enhance IEs cytoadherence (Davis et al., 2012; Davis et al., 2013).

- Phosphatidylserine

Apoptotic cells are also cleared via phagocytosis by macrophages in a CD36-dependent manner. Phosphatidylserine (PS) exposure to the outer leaflet occurs during apoptosis serves as a ligand for macrophage recognition and internalization (Bratton et al.,1997, Bochkov et al., 2010). CD36 binds to oxPS, produced by PS reaction with free radicals, at the surface of apoptotic cells mediates their phagocytosis. CD36 is crucial for apoptotic cell clearance as knockout CD36 mice had three times more apoptotic cells than wild-type mice (Bratton et al.,1997, Bochkov et al., 2010). Also, transfection of CD36 enabled cells with limited phagocytic capacity to internalize apoptotic neutrophils, lymphocytes and fibroblasts (Greenberg et al., 2006).

- TSP-1

TSP-1 stimulation of CD36 in microvascular endothelial cells initiates anti-angiogenic signalling resulting in the inhibition of cell migration and apoptosis (Jiménez et al., 2000). My thesis research has focused on elucidating critical proteins for this signalling pathway. In section 1.2.3, I will describe the TSP-1-CD36 anti-angiogenic signalling pathway.

1.2.3 CD36 Anti-Angiogenic Signalling

This section will cover the domain organization, membrane organization, function and activation of proteins pertinent to CD36-induced anti-angiogenic signalling. The interplay between these pertinent proteins is brought together through comprehensive overview of TSP-1-CD36 anti-angiogenic signalling, which concludes this section.

1.2.3.1 Thrombospondin-1

TSP-1 is a 450 kDa homotrimer matricellular glycoprotein that is a part of the five-membered thrombospondin family (TSP-1 to 5) (Figure 1-4) (Gutierrez and Gutierrez, 2021). Monomers of TSP-1 are linked via inter-subunit disulphide bonds (Murphy-Ullrich, 2022). This family is divided into two subgroups, with group A containing TSP-1 and 2, and group B containing TSP-3, -4, and

-5 (Chen et al., 2000). The monomers of class A thrombospondins (TSP-1 and -2) contain an N-terminal domain, procollagen domain, three type-I repeats (also known as TSR), three type-II repeats, seven type-III repeats, and a C-terminal domain. Class B thrombospondins do not have type-I repeats. However, they feature an extra type-II repeat (Zhang et al., 2020). These domains facilitate the binding of TSP-1 to a diversity of ligands, matricellular proteins, receptors, cytokines and proteases (Resovi et al., 2014; Zhang et al., 2020)

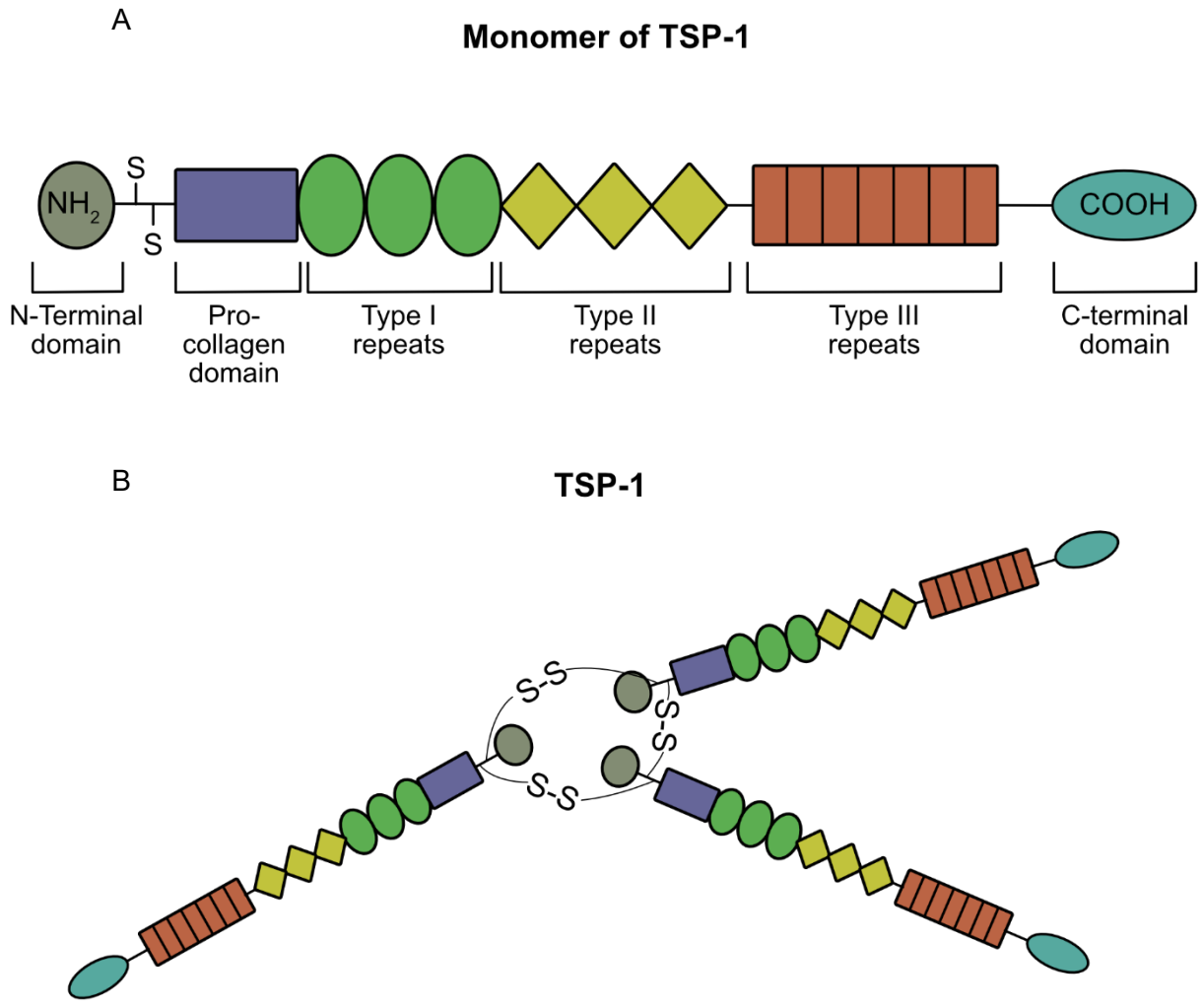

Figure 1-4: TSP-1 domain organization.

TSP-1 monomer domain organization, and TSP-1 homotrimer schematic. (A) TSP-1 monomer domains are highlighted via label and color (adapted from Murphy-Ullrich (2022)). (B) TSP-1 homotrimer linked via inter-subunit disulfide bonds.

Endothelial, macrophages, smooth muscle cells, and platelets express and secrete TSP-1 (Ahmed and Lutty, 2016). However, platelets play a predominant role in modulating plasma levels of TSP-1. Thrombospondins are the major constituents of platelet α-granules, and 25% of proteins secreted by platelets are thrombospondins (Tuszynski et al., 1988). TSP-1 contributes to hemostasis by promoting platelet aggregation and thrombus formation (Isenberg et al., 2008; Kuijpers et al., 2014; Aburima et al., 2021). TSP-1 knockout mice exhibit increased bleeding and defective thrombosis (Aburima et al., 2021).

TSP-1 induces its anti-angiogenic effect by stimulating CD36 on microvascular endothelial cells (Dawson et al. 1997; Jiménez et al. 2000). This interaction is mediated by electrostatic interaction between type-I repeats and the CLESH domain (93-120 a.a) of CD36 (Collot-Teixeira et al., 2007; Klenotic et al., 2013). The initial step of the anti-angiogenic signalling cascade is the activation of SFK Fyn. Below, we will introduce Fyn and discuss its biological roles.

1.2.3.2 Fyn

Fyn belongs to the 59kDa SFK family, which consists of the following proteins: Blk, Brk, Fgr, Frk, Hck, Lck, Lyn, c-Src, Srm, and c-Yes (Matrone et al., 2020). SFKs play a crucial role in regulating and initiating signal transduction for diverse cell surface receptors (Parsons and Parsons, 2004). Fyn regulates diverse cellular functions such as cell growth, survival, adhesion, cytoskeleton remodelling, and immune signalling (Matrone et al., 2020). Four domains, which are conserved among SFK, compose Fyn: SH4, SH3 (83-143 a.a), SH2 (149-246 a.a), and SH1 (271-524 a.a) (Figure 1-5). The SH4 domain is N-myristoylated (Gly 2) and palmitoylated at residues Cys3 and Cys6 (Figure 1-5) (Wolven et al.,1997; Udenwobele et al., 2017). These lipid modifications are necessary for Fyn localization and anchoring to the inner leaflet of plasma membrane (Wolven et al. 1997; Udenwobele et al. 2017). Palmitoylation is also critical for Fyn localization into membrane domains (Shenoy-Scaria et al., 1994; Fragoso et al., 2003; Kim et al., 2013).

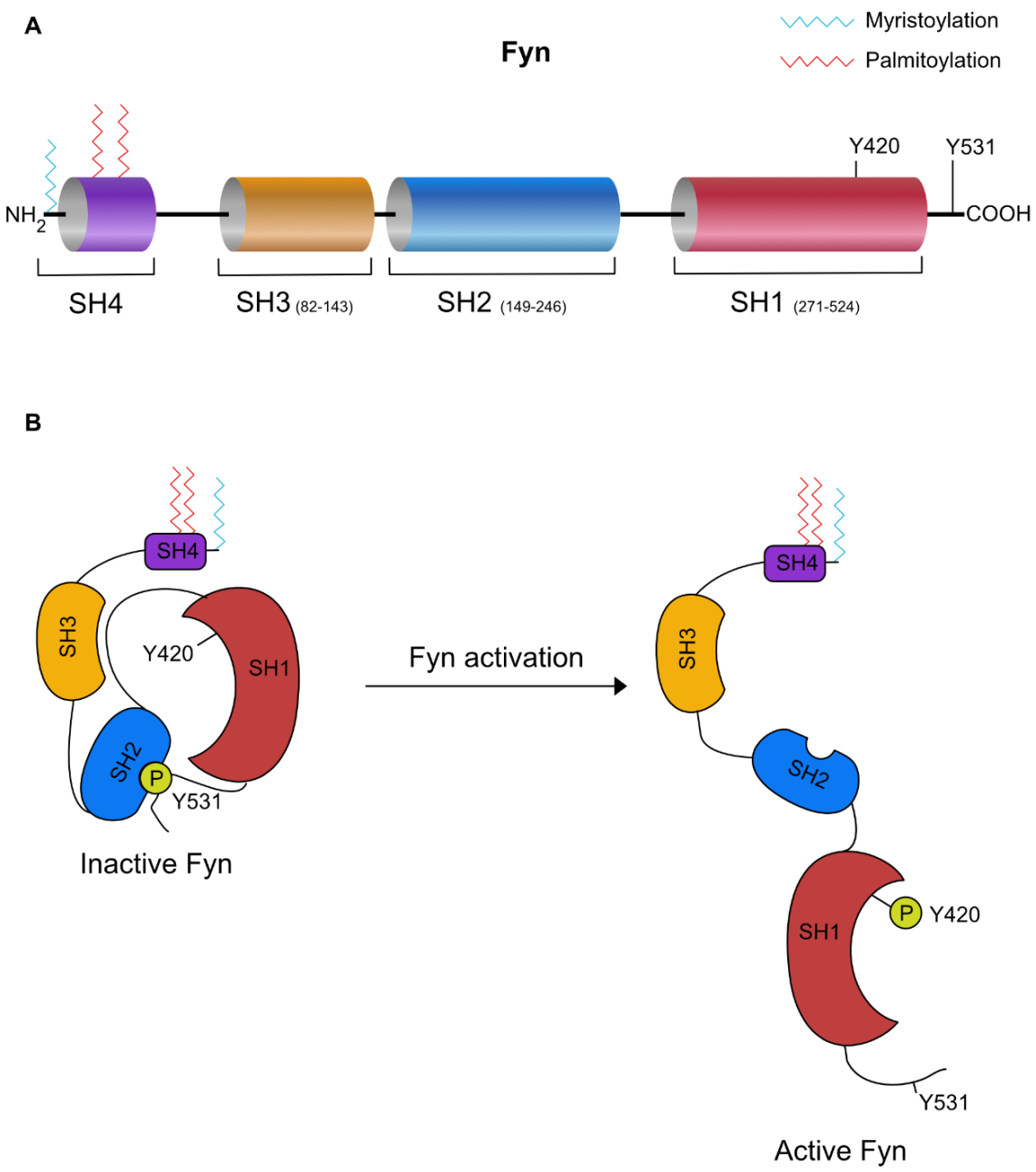

Figure 1-5: Fyn domain organization and activation schematic.

Fyn domain organization and activation schematic is adapted from Martínez-Mármol et al. (2023). (A) Fyn SH4, SH3, SH2, and SH1 domains and their corresponding amino acids are outlined. (B) Fyn depicted in its inactive, closed state with the SH2 domain binding to the inhibitory phosphate at Y531 is opened via dephosphorylation. Trans-autophosphorylation of Y420 of the SH1 domain activates Fyn, therefore allowing it phosphorylates substrates.

The SH1 catalytic domain phosphorylates tyrosine residues of target proteins (Mjartínez-Mármol et al., 2023). Fyn inactive and active conformations are modulated by two critical phosphorylation sites: Y420 and Y531 (Martínez-Mármol et al., 2023). Phosphorylation at Y531 causes Fyn to adopt a closed, inactive conformation (Martínez-Mármol et al., 2023). The closed conformation is stabilized by intramolecular binding of the SH2 domain to the inhibitory Y531 phosphate present at the C-terminus (Martínez-Mármol et al., 2023). Removal of the inhibitory phosphate by phosphatases, such as PTPα (Xu et al., 2015), CD45 (Gerbec et al., 2015), and PTPƐ (Granot-Attas and Elson, 2004), allows Fyn to adopt its open conformation. In the open conformation, trans-autophosphorylation of Y420 residue within the SH1 domain completes the activation cycle (Martínez-Mármol et al., 2023). The activation of Fyn, which is necessary for CD36 anti-angiogenic signalling, depends on changes in CD36 membrane organization (Githaka et al., 2016). The pertinence of CD36 nanocluster organization to anti-angiogenic signalling will be discussed in the next section.

1.2.3.3 CD36 Membrane Organization

Since the proposal of the fluid mosaic model by Singer and Nicolson in 1972 (Singer and Nicolson, 1972), the perspective on plasma membrane organization has shifted drastically. With the development of FRET anisotropy, super-resolution microscopy, and single-molecule tracking, we have learned that the constituent of cell membranes are not randomly, or homogenously distributed (as implied by the fluid mosaic model) but instead present in laterally segregated nanodomains (Truong Quang and Lenne, 2014). Nanodomains are areas within the plasma membrane enriched in specific proteins and lipids (Garcia-Parajo et al., 2014). They are formed due to favourable protein-protein, protein-lipid, and lipid interactions (Garcia-Parajo et al., 2014). Cytoskeleton interaction with proteins and lipids is also critical for the segregation and formation of nanodomains (Garcia-Parajo et al., 2014). By increasing the density of proteins and lipids within a confined area, nanodomains act as signalling platforms that initiate rapid responses to cellular

stimuli (Simons and Toomre, 2000). Nanodomains have been shown to support the signalling of multiple membrane receptors, including B-cell receptors (Togayachi et al., 2010), T-cell receptors (Zech et al., 2009), and integrins (Gagnoux-Palacios et al., 2003; Bodin et al., 2005; Sun et al., 2016).

CD36 signalling is also modulated by nanodomain dynamics. Githaka et al. (2016) determined that ~40% of CD36 exists in nanoclusters with a radius of ~70nm at rest in human microvascular endothelial cells. Upon TSP-1 stimulation or multivalent ligand binding (such as an IgM directed to CD36), the size and density of CD36 nanodomains increase. The enhancement of CD36 nanoclusters is needed for Fyn activation. Perturbation of membrane cholesterol and cortical F-actin were shown to abolish CD36 nanocluster enhancement and hence inhibited Fyn activation. With the fundamentals of CD36 anti-angiogenic signalling acknowledged, the pathway will be discussed in detail below.

1.2.3.4 TSP-1-CD36 Anti-Angiogenic Signalling Pathway

TSP-1 binding to CD36 initiates the anti-angiogenic signalling cascade (Figure 1-6). The endpoint of this cascade is inhibition of migration, proliferation and eventually results in the apoptosis of endothelial cells (Dawson et al., 1997; Jiménez et al., 2000). TSP-1's anti-angiogenic effect was shown to be mediated through CD36, as TSP-1 had no effect on FGF-induced endothelial migration in CD36 null mice (Jiménez et al., 2000). Dawson et al. (1997) showed that various ligands, oxLDL, collagen, and anti-CD36 IgM inhibited human microvascular cell migration. The binding of TSP-1 or multivalent ligands induces enhancement of CD36 nanocluster density and size (Githaka et al., 2016). Although CD36 nanocluster enhancement increases the density and number of CD36 molecules, the level of Fyn within the cluster is not altered. In addition, no changes are observed in cluster localization within high-actin areas after TSP-1 stimulation. Nevertheless, changes in CD36 membrane organization are needed to provide the

necessary cluster enhancement and Fyn activation leading to the anti-angiogenic signalling pathway activation (Githaka et al., 2016).

Fyn is necessary for anti-angiogenic signalling, as TSP-1 could not inhibit neovascularization in Fyn null mice (Jiménez et al., 2000). Neutralizing antibodies to Fyn also inhibited TSP-1-induced anti-angiogenic signalling in human dermal microvascular endothelial cells (HDMECs) (Jiménez et al., 2000). Signalling downstream of Fyn results in the activation of p38MAPK (Jiménez et al., 2000). Phosphorylation of p38MAPK results in its translocation to the nucleus, where it activates transcriptional factors upregulating the expression of caspase-3 and FAS ligand (Jiménez et al., 2000; Volpert et al., 2002; Wang and Li, 2019). The increased expression of these pro-apoptotic proteins results in the death of endothelial cells. Although key regulators of CD36 anti-angiogenesis signalling have been identified, pertinent questions regarding the mechanism of Fyn activation and CD36's relationship remain.

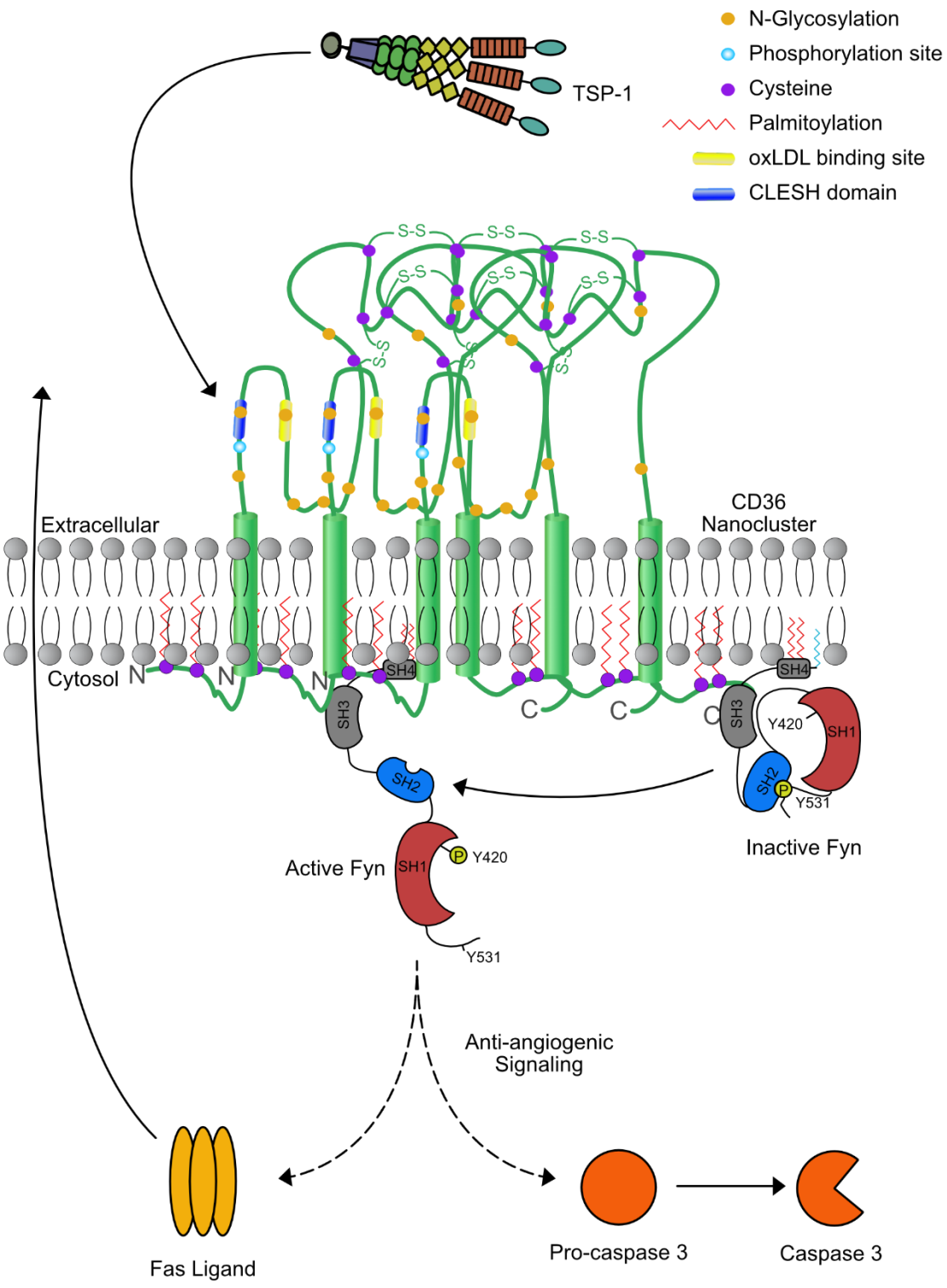

Figure 1-6: TSP-1 - CD36 signalling cascade.

TSP-1 binding to the CD36 causes CD36 nanocluster enhancement which is essential for Fyn activation. Fyn initiates a downstream signalling cascade resulting in the activation of p38MAPK. P38MAPK phosphorylates transcriptional activators resulting in the increased expression of pro-caspase 3 and FAS-ligand. Increased expression of these pro-apoptotic proteins results in microvascular endothelial cell death.

1.3 Rationale and Hypothesis

As one of the leading causes of death worldwide, cancer accounted for ~ 10 million fatalities in 2020 (Dal-Ré, 2011; Ferlay et al., 2021). Although cancer rates are slowly declining, developing novel cancer therapies is needed to reduce morbidity and mortality associated with this disease (Brenner et al., 2022). Given the importance of neovascularization for tumour growth and metastasis, anti-angiogenic therapies have been developed. However, the effectiveness of these therapies has been disappointing in clinical trials. The CD36 anti-angiogenic signalling pathway has been targeted by cancer therapies such as ABT-510 and CXV-045. However, these therapies have failed to progress past phase II clinical trials (Jeanne et al., 2015; Huang et al., 2017). Therefore, further research is needed to enhance our understanding of anti-angiogenic signalling.

Previous research in the Touret lab, conducted by Dr. Githaka, has shown that TSP-1, CD36 nanoclusters, Fyn, and the cortical F-actin are necessary components of anti-angiogenic signalling. However, how the interactions between these molecules remains unknown. Since CD36 lacks actin-binding domains, it is unlikely that CD36 independently binds to the cortical F-actin (Tandon et al., 1989; Hsieh et al., 2016). CD36 is also unlikely to solely activate Fyn as its cytosolic domains lack kinase or phosphatase activity. ***Therefore, we hypothesize that interacting proteins are needed for CD36 organization and signalling.***

My thesis research had two central aims: 1) discover proteins in the proximity of CD36 using proximity labelling (PL) and 2) determine their role in CD36 organization and anti-angiogenic signalling. In Chapter 2, I will outline the methods and material I used to investigate these aims. Results from CD36 BAR, proximity ligation and conditional colocalization are presented in Chapter 3. Chapter 4 concludes the thesis with a discussion of the results in the context of anti-angiogenic signalling and the presentation of a novel model for CD36-Fyn signalling based on these findings and future directions. Given PL provides the framework for this study, a brief history of the development of PL is discussed below.

1.4 Proximity Labelling

Proteins rarely function alone; they form molecular complexes to fulfill diverse cellular functions. Therefore, investigating protein-protein interactions is critical to understanding the molecular mechanisms of biological phenomena (Chang et al., 2017; Holthenrich et al., 2019; Sanchez et al., 2021; Yang, 2023). Viewing protein-protein interactions through a dynamic lens provides information on how changes in protein complexes facilitate cellular events (Chua et al.,2021; Vélot et al., 2021; Perez Verdaguer et al., 2022; Zhuo et al., 2023). Aberrant protein-protein interaction is observed in neurodegenerative, cancer and infectious diseases (Shangary and Wang, 2009; Brown and Horrocks, 2020; Terracciano et al., 2021). Therefore, learning about protein-protein interactions is key to our understanding of biological functions but could also provide cues in the development of effective and specific therapies.

Protein-protein interactions have conventionally (and conveniently) been investigated via co-immunoprecipitation (Co-IP). Although Co-IP enables the probing of strong interactions, the reliance on detergent solubilization and extensive washing steps are major limitations to the investigation of more transient and less stable complexes. Detergents not only abolishes transient interactions but by they can also induce artificial protein aggregation. Detergents are the casual reason for the high false-positive and false-negative rates associated with Co-IP studies (Ralston, 1985; Rees et al., 2015).

Proximity labelling (PL) utilizes promiscuous biotinylation enzymes to convert inert substrates to reactive biotin species. The short half of the reactive species allows for confined biotin labelling around a target protein. Subsequent capture of these biotinylated proteins with streptavidin and analysis via tandem mass spectrometry (LC-MS/MS) enables identification and quantification of proteins that were present in the vicinity of the target protein during the labelling period. PL circumvents the limitations of Co-IP as weak-transient interactions are still identified. Also, the high-affinity streptavidin-biotin interaction enables stringent wash conditions to remove

artificial interactions. PL's compatibility with live cell labelling, rapid labelling times, and confined labelling radius provide the spatial and temporal resolution needed to determine changes in protein-protein interactions. Revealing these dynamics is critical to elucidating and understanding cellular processes.

1.4.1 Peroxidase-based PL

PL comes in two flavours, peroxidase-based and biotin-ligase-based approaches. Peroxidase-based PL utilizes plant-based peroxidases to convert biotin-phenol in the presence of hydrogen peroxide to biotin-phenol radicals, which covalently link predominantly to nearby tyrosine residues (Zafra and Piniella, 2022). The short half-life of the biotin-phenol radical (<0.1ms) enables rapid labelling of proteins in proximity to the target (Martell et al., 2012).

Monomeric ascorbate peroxidase (APEX) is derived from plant-based ascorbates with mutations engineered to increase catalytic activity (Martell et al., 2012;). The A134P mutation of APEX, denoted as APEX2, increased its catalytic activity, thermal stability, and resistance to concentrations of higher concentrations of hydrogen peroxide (Lam et al., 2015). Proximity labelling via APEX features a labelling radius of ~20nm, which provides high spatial resolution (Martell et al., 2012; Hwang and Espenshade, 2016)

Horseradish peroxidase (HRP) is also utilized in PL. It is approximately two times larger than APEX (44 kDa vs 28 kDa); however, it features a much higher catalytic activity than APEX2 (Zafra and Piniella, 2022). HRP is therefore more suitable for PL studies requiring high temporal resolution. However, HRP features a labelling radius of ~200-300nm, which is approximately ten times greater than APEX (Kotani et al., 2008; Rees et al., 2015; Oakley et al., 2022). Of all promiscuous enzymes used for proximity labelling, HRP offers the poorest temporal resolution.

Despite the rapid labelling time, peroxidase-based PL has limited application in intracellular labelling. HRP-target protein fusion PL is restricted to the ER lumen and extracellular space as

the reducing environment of the cytosol abolishes 4 critical di-sulphide bonds needed for HRP structure and function (Hopkins et al., 2000; Zafra and Piniella, 2022). The low membrane permeability of biotin-phenol reduces the effectiveness of APEX-target fusion protein PL (Zafra and Piniella, 2022). The oxidative stress produced by hydrogen peroxide also decreases peroxidase-based PL live cell compatibility.

1.4.2 Biotin Ligase-based PL

Biotin ligase-based PL utilizes a promiscuous biotin ligase to convert, in the presence of ATP, biotin to biotin-AMP, which reacts with the primary amines of lysine residues. Biotin ligase-based PL allows for live cell and intracellular labelling, given biotin's high membrane permeability and low toxicity. The first biotin-ligase PL technique, BioID, was developed by Roux et al. (2012). By mutating biotin ligase (BirA) expressed in *Escherichia coli* (*E. coli*), they abolished substrate specificity to develop the first promiscuous biotin ligase. (Roux et al., 2012). The fusion of BirA* (35 kDa) with target proteins enables proximity labelling with a radius of ~10nm within live cells (Roux et al., 2012). However, a major drawback of BioID is the limited temporal resolution as it requires biotin incubation of ~24 hours. Therefore, BioID cannot resolve changes in protein-protein interactions due to its long labelling times (Branon et al., 2018).

Improvements have been made to reduce BirA* size and increase its catalytic activity (Cho et al. 2020). BioID2 utilizes a smaller biotin ligase from *Aquifex aeolicus*, which retains its activity at high temperatures (Kim et al., 2016). However, labelling times of 18 hours are still needed for sufficient biotinylation needed for mass spectrometry analysis (Cho et al., 2020). BASU BioID utilizes a biotin-ligase from *Bacillus subtilis* and it was used to investigate protein-RNA interactions. Biotin-ligase is fused to a Nɣ protein which binds to a BoxB stem-loop flanked with mRNA sequence of interest. Although the biotin-ligase used in BASU has a higher catalytic activity than BirA*, long labelling times are still needed (Ramanathan et al., 2018; Cho et al., 2020). AirID, an ancestral BirA for proximity-dependent biotinylation, reduces labelling times to 3

hours. However, given the rapid nature of biological processes, this technique still lacks the temporal resolution to probe rapid changes in protein-protein interactions (Kido et al., 2020).

TurboID and miniTurboID enzymes were engineered from BirA* to overcome the low catalytic activity of BioID techniques (Branon et al., 2018). Branon et al. (2018) utilized error-prone PCR to produce mutants of BirA*-R118S. These mutants were displayed on yeast surface. The addition of biotin and ATP to the yeast mutants allowed for biotinylation. Fluorescent streptavidin staining followed by fluorescence-activated cell sorting sorted the yeast with the highest amount of biotinylation. 29 rounds of selection yielded two promiscuous biotin ligases: miniTurboID (28kDa) and TurboID (35kDa). TurboID and miniTurboID feature 15 and 13 mutations in their coding sequence relative to BirA*. The increased catalytic activity requires only ~10min labelling for both enzymes. After years of progress, the development of TurboID and miniTurboID has finally provided PL with the temporal resolution needed to elucidate changes in protein-protein interactions during biological processes.

The higher activity of TurboID and miniTurboID comes at a cost as the labelling radius increases to ~35nm from the ~10nm achieved by BioID (May et al., 2020). Biotin is a prosthetic group for enzymes implicated in cellular metabolism (León-Del-Río, 2019). Sequestration of biotin by ubiquitous expression of TurboID or miniTurboID can therefore lead to metabolic dysfunction. Without biotin supplementation, Drosophila melanogaster and Caenorhabditis elegans expressing TurboID suffered from reduced viability and development delays, respectively (Branon et al., 2018). Despite these limitations, TurboID and miniTurboID represent the new gold standard for PL due to their application in live cells and high catalytic activity.

1.4.3 Split-based PL

Split-based approaches utilize protein fusions of promiscuous labelling enzyme fragments with target proteins. These approaches enhance the specificity of PL, as PL can only be performed when the two fragments are in close proximity allowing the reconstitution of the full and active promiscuous enzyme. APEX (Han et al., 2019) and TurboID (Cho et al., 2020) enzymes have been successfully designed as split systems.

Cho et al. (2020) developed a split-APEX system and fused one half to the ER membrane protein cb5 and the second half to an outer mitochondrial membrane receptor TOM20 to perform PL at mitochondrial-associated membranes (MAMs). This study unveiled novel MAM proteins, which were validated by biochemical fractionation to localize at MAM sites (Cho et al., 2020). G-coupled protein receptor and arrestin split-TurboID constructs have also been utilized to study the activation of these receptors by PL (Cho et al. 2020). Finally, split-based approaches can be utilized to validate protein-protein interactions, as biotinylation will only occur if the fusion proteins are in proximity to one another. Altering the linker size of the fusion target-PL enzyme fragment can be modulated to measure the proximity between proteins.

1.4.4 Antibody-based PL

Creating antibodies-PL enzyme fusion proteins increases the flexibility of PL. Biotinylation by Antibody Recognition called BAR, a method for proximity labelling developed by Bar et al. (2018), utilizes the specificity of a primary antibody and catalytic activity of a secondary antibody conjugated to HRP to biotinylate proteins within ~250 nm (Oakley et al., 2022). Although BAR offers great generalizability, as the PL of any target can be performed with the requisite antibodies, the large antibody complex reduces HRP's proximity to the target. Utilizing protein-A PL enzyme constructs or fragment antigen binding protein (FAB)-PL enzyme constructs can help reduce the

complex size. However, BAR will never attain the proximity of labelling achieved by target-PL enzyme constructs. BAR also suffers from the limitations of peroxidase-based PL approaches.

Construction of nanobody (NB)-PL enzyme fusions protein allows greater proximity of the PL enzyme to the target as NB is only ~3-6nm. Utilizing TurboID or miniTurboID fused to recombinant antibodies can also enable live cell labelling. NB-GFP TurboID biotinylation has been successfully applied to whole organisms expressing GFP (Xiong et al. 2021; Holzer et al. 2022).

Each biotinylation method has advantages and limitations; these qualities need to be considered for objective of PL experiments (Table 1-1). Next the methodology for capture and identification of biotinylated proteins are discussed.

Table 1-1: Summary of the properties, advantages, and limitation of different PL approaches.

Proximity labelling approach	Peroxidase	Peroxidase	Biotin Ligase	Biotin Ligase	Biotin Ligase	Split	Antibody
Enzyme	APEX	HRP	BirA*	TurboID	miniTurboID	Peroxidase/ biotin ligase	Peroxidase/ biotin ligase
Enzyme size	28 kDa	44 kDa	35 kDa	35 kDa	28 kDa	Variable	Variable
Labelling radius	~20nm	~200-300 nm	~10nm	~35nm	~35nm	Variable	Variable
Advantages	- rapid labelling - small labelling radius	- rapid labelling	- small labelling radius - low toxicity - capable of intracelluar labelling	- rapid labelling - low toxicity - capable of intracelluar labelling	- rapid labelling -smaller than TurboID - low toxicity - capable of intracelluar labelling	- increased labelling specificity	- flexible approach enabling biotinylation of diverse targets
Limitations	- highly toxic - lower catalytic activity than HRP - incompatible with intracellular labelling	- highly toxic - large labelling radius - incompatible with intracellular labelling	- low catalytic activity	- larger than miniTurboID - larger labelling radius than BioID	- larger labelling radius than BioID	- Need to clone split system	-Antibody complexes increases distance of enzyme from target

1.5 Streptavidin Pulldown of Biotinylated Proteins

Streptavidin-biotin interaction is one of the strongest non-covalent interactions found in nature (Holmberg et al., 2005). Streptavidin is a part of the avidins protein family. These biotin-binding proteins have multimeric protein structures and can bind up to 4 biotin molecules (Laitinen et al., 2021). The first known avidin was isolated from the chicken egg white in 1941 (Eakin et al., 1940). 24 years later, the first bacterial avidin, named streptavidin, was isolated from *Streptomyces avidinii* (Tausig and Wolf, 1964). The function of avidin expression in eukaryotic cells is believed to be antibiotic, as a sequestering of biotin can reduce microbe viability (Kunnas et al., 1993). This is evidenced by the induction of avidin expression in the intestine and oviduct of chickens infected with *E. coli* (Kunnas et al., 1993). Bacterial expression of avidins is also believed to play a role in bacterial defence against other microbes (Laitinen et al., 2021). These high-affinity interactions have been applied to biotechnology to improve immunoprecipitation, protein detection, and protein purification. PL has taken advantage of this interaction to purify biotinylated protein. Following purification, biotinylated proteins are prepared and analyzed by LC-MS/MS for protein identification and quantification.

1.6 References

Aboulaich N, Vainonen JP, Strålfors P, Vener AV. 2004. Vectorial proteomics reveal targeting, phosphorylation and specific fragmentation of polymerase I and transcript release factor (PTRF) at the surface of caveolae in human adipocytes. Biochem J. 383(Pt 2):237–248. doi:10.1042/BJ20040647.

Abramsson A, Lindblom P, Betsholtz C. 2003. Endothelial and nonendothelial sources of PDGF-B regulate pericyte recruitment and influence vascular pattern formation in tumours. J Clin Invest. 112(8):1142–1151. doi:10.1172/JCI200318549.

Abumrad N, Coburn C, Ibrahimi A. 1999. Membrane proteins implicated in long-chain fatty acid uptake by mammalian cells: CD36, FATP and FABPm. Biochimica et Biophysica Acta (BBA) - Molecular and Cell Biology of Lipids. 1441(1):4–13. doi:10.1016/S1388-1981(99)00137-7.

Aburima A, Berger M, Spurgeon BEJ, Webb BA, Wraith KS, Febbraio M, Poole AW, Naseem KM. 2021. Thrombospondin-1 promotes hemostasis through modulation of cAMP signalling in blood platelets. Blood. 137(5):678–689. doi:10.1182/blood.2020005382.

Adair TH, Montani J-P. 2010. Overview of Angiogenesis. Morgan & Claypool Life Sciences. [accessed 2023 Apr 25]. https://www.ncbi.nlm.nih.gov/books/NBK53238/.

Ahmed Z, Lutty GA. 2016. Anti-angiogenic properties of vitreous. In: The Curated Reference Collection in Neuroscience and Biobehavioral Psychology. Elsevier Science Ltd. p. 112–119. [accessed 2023 Apr 29]. https://jhu.pure.elsevier.com/en/publications/anti-angiogenic-properties-of-vitreous.

Albert ML, Pearce SF, Francisco LM, Sauter B, Roy P, Silverstein RL, Bhardwaj N. 1998. Immature dendritic cells phagocytose apoptotic cells via alphavbeta5 and CD36, and cross-present antigens to cytotoxic T lymphocytes. J Exp Med. 188(7):1359–1368. doi:10.1084/jem.188.7.1359.

Álvarez-Aznar A, Muhl L, Gaengel K. 2017. VEGF Receptor Tyrosine Kinases: Key Regulators of Vascular Function. Curr Top Dev Biol. 123:433–482. doi:10.1016/bs.ctdb.2016.10.001.

Aspriţoiu VM, Stoica I, Bleotu C, Diaconu CC. 2021. Epigenetic Regulation of Angiogenesis in Development and Tumours Progression: Potential Implications for Cancer Treatment. Frontiers in Cell and Developmental Biology. 9. [accessed 2023 Apr 25]. https://www.frontiersin.org/articles/10.3389/fcell.2021.689962.

Attems J. 2005. Sporadic cerebral amyloid angiopathy: pathology, clinical implications, and possible pathomechanisms. Acta Neuropathol. 110(4):345–359. doi:10.1007/s00401-005-1074-9.

Bachmann A, Metwally NG, Allweier J, Cronshagen J, Del Pilar Martinez Tauler M, Murk A, Roth LK, Torabi H, Wu Y, Gutsmann T, et al. 2022. CD36-A Host Receptor Necessary for Malaria Parasites to Establish and Maintain Infection. Microorganisms. 10(12):2356. doi:10.3390/microorganisms10122356.

Baker LH, Rowinsky EK, Mendelson D, Humerickhouse RA, Knight RA, Qian J, Carr RA, Gordon GB, Demetri GD. 2016 Sep 22. Randomized, Phase II Study of the Thrombospondin-1-Mimetic

Angiogenesis Inhibitor ABT-510 in Patients With Advanced Soft Tissue Sarcoma. Journal of Clinical Oncology. doi:10.1200/JCO.2008.17.4706. [accessed 2024 Mar 24]. https://ascopubs.org/doi/10.1200/JCO.2008.17.4706.

Bar DZ, Atkatsh K, Tavarez U, Erdos MR, Gruenbaum Y, Collins FS. 2018. Biotinylation by antibody recognition—a method for proximity labelling. Nat Methods. 15(2):127–133. doi:10.1038/nmeth.4533.

Baruch DI, Gormely JA, Ma C, Howard RJ, Pasloske BL. 1996. Plasmodium falciparum erythrocyte membrane protein 1 is a parasitized erythrocyte receptor for adherence to CD36, thrombospondin, and intercellular adhesion molecule 1. Proceedings of the National Academy of Sciences. 93(8):3497–3502. doi:10.1073/pnas.93.8.3497.

Baruch DI, Ma XC, Singh HB, Bi X, Pasloske BL, Howard RJ. 1997. Identification of a region of PfEMP1 that mediates adherence of Plasmodium falciparum infected erythrocytes to CD36: conserved function with variant sequence. Blood. 90(9):3766–3775.

Bentley K, Mariggi G, Gerhardt H, Bates PA. 2009. Tipping the Balance: Robustness of Tip Cell Selection, Migration and Fusion in Angiogenesis. PLoS Comput Biol. 5(10):e1000549. doi:10.1371/journal.pcbi.1000549.

Bergers G, Benjamin LE. 2003. Tumourigenesis and the angiogenic switch. Nat Rev Cancer. 3(6):401–410. doi:10.1038/nrc1093.

Bochkov VN, Oskolkova OV, Birukov KG, Levonen A-L, Binder CJ, Stöckl J. 2010. Generation and Biological Activities of Oxidized Phospholipids. Antioxidants & Redox Signalling. 12(8):1009–1059. doi:10.1089/ars.2009.2597.

Bodin S, Soulet C, Tronchère H, Sié P, Gachet C, Plantavid M, Payrastre B. 2005. Integrin-dependent interaction of lipid rafts with the actin cytoskeleton in activated human platelets. J Cell Sci. 118(Pt 4):759–769. doi:10.1242/jcs.01648.

Branon TC, Bosch JA, Sanchez AD, Udeshi ND, Svinkina T, Carr SA, Feldman JL, Perrimon N, Ting AY. 2018. Efficient proximity labelling in living cells and organisms with TurboID. Nat Biotechnol. 36(9):880–887. doi:10.1038/nbt.4201.

Bratton DL, Fadok VA, Richter DA, Kailey JM, Guthrie LA, Henson PM. 1997. Appearance of phosphatidylserine on apoptotic cells requires calcium-mediated nonspecific flip-flop and is enhanced by loss of the aminophospholipid translocase. J Biol Chem. 272(42):26159–26165. doi:10.1074/jbc.272.42.26159.

Brenner DR, Poirier A, Woods RR, Ellison LF, Billette J-M, Demers AA, Zhang SX, Yao C, Finley C, Fitzgerald N, et al. 2022. Projected estimates of cancer in Canada in 2022. CMAJ. 194(17):E601–E607. doi:10.1503/cmaj.212097.

Broekman F, Giovannetti E, Peters GJ. 2011. Tyrosine kinase inhibitors: Multi-targeted or single-targeted? World J Clin Oncol. 2(2):80–93. doi:10.5306/wjco.v2.i2.80.

Brown J, Horrocks MH. 2020. A sticky situation: Aberrant protein-protein interactions in Parkinson's disease. Semin Cell Dev Biol. 99:65–77. doi:10.1016/j.semcdb.2018.05.006.

Brown LS, Foster CG, Courtney J-M, King NE, Howells DW, Sutherland BA. 2019. Pericytes and Neurovascular Function in the Healthy and Diseased Brain. Frontiers in Cellular Neuroscience. 13. [accessed 2023 Apr 25]. https://www.frontiersin.org/articles/10.3389/fncel.2019.00282.

Campbell N, Greenaway J, Henkin J, Petrik J. 2011. ABT-898 induces tumour regression and prolongs survival in a mouse model of epithelial ovarian cancer. Mol Cancer Ther. 10(10):1876–1885. doi:10.1158/1535-7163.MCT-11-0402.

Carmeliet P, Jain RK. 2000. Angiogenesis in cancer and other diseases. Nature. 407(6801):249–257. doi:10.1038/35025220.

Chang L, Chen Yi-Ju, Fan C-Y, Tang C-J, Chen Y-H, Low P-Y, Ventura A, Lin C-C, Chen Yu-Ju, Angata T. 2017. Identification of Siglec Ligands Using a Proximity Labelling Method. J Proteome Res. 16(10):3929–3941. doi:10.1021/acs.jproteome.7b00625.

Chen H, Herndon ME, Lawler J. 2000. The cell biology of thrombospondin-1. Matrix Biol. 19(7):597–614. doi:10.1016/s0945-053x(00)00107-4.

Chen M, Bao L, Zhao M, Cao J, Zheng H. 2020. Progress in Research on the Role of FGF in the Formation and Treatment of Corneal Neovascularization. Front Pharmacol. 11:111. doi:10.3389/fphar.2020.00111.

Cheng A-L, Qin S, Ikeda M, Galle P, Ducreux M, Zhu A, Kim T-Y, Kudo M, Breder V, Merle P, et al. 2019. LBA3 - IMbrave150: Efficacy and safety results from a ph III study evaluating atezolizumab (atezo) + bevacizumab (bev) vs sorafenib (Sor) as first treatment (tx) for patients (pts) with unresectable hepatocellular carcinoma (HCC). Annals of Oncology. 30:ix186–ix187. doi:10.1093/annonc/mdz446.002.

Cheng S-S, Yang G-J, Wang W, Leung C-H, Ma D-L. 2020. The design and development of covalent protein-protein interaction inhibitors for cancer treatment. Journal of Hematology & Oncology. 13(1):26. doi:10.1186/s13045-020-00850-0.

Cho KF, Branon TC, Rajeev S, Svinkina T, Udeshi ND, Thoudam T, Kwak C, Rhee H-W, Lee I-K, Carr SA, et al. 2020. Split-TurboID enables contact-dependent proximity labelling in cells. Proc Natl Acad Sci U S A. 117(22):12143–12154. doi:10.1073/pnas.1919528117.

Cho KF, Branon TC, Udeshi ND, Myers SA, Carr SA, Ting AY. 2020. Proximity labelling in mammalian cells with TurboID and split-TurboID. Nat Protoc. 15(12):3971–3999. doi:10.1038/s41596-020-0399-0.

Chu L-Y, Silverstein RL. 2012. CD36 Ectodomain Phosphorylation Blocks Thrombospondin-1 Binding. Arteriosclerosis, Thrombosis, and Vascular Biology. 32(3):760–767. doi:10.1161/ATVBAHA.111.242511.

Chua XY, Aballo T, Elnemer W, Tran M, Salomon A. 2021. Quantitative Interactomics of Lck-TurboID in Living Human T Cells Unveils T Cell Receptor Stimulation-Induced Proximal Lck Interactors. J Proteome Res. 20(1):715–726. doi:10.1021/acs.jproteome.0c00616.

Coburn CT, Knapp FF, Febbraio M, Beets AL, Silverstein RL, Abumrad NA. 2000. Defective Uptake and Utilization of Long Chain Fatty Acids in Muscle and Adipose Tissues of CD36 Knockout Mice *. Journal of Biological Chemistry. 275(42):32523–32529. doi:10.1074/jbc.M003826200.

Collot-Teixeira S, Martin J, McDermott-Roe C, Poston R, McGregor JL. 2007. CD36 and macrophages in atherosclerosis. Cardiovasc Res. 75(3):468–477. doi:10.1016/j.cardiores.2007.03.010.

Colombo G, Margosio B, Ragona L, Neves M, Bonifacio S, Annis DS, Stravalaci M, Tomaselli S, Giavazzi R, Rusnati M, et al. 2010. Non-peptidic thrombospondin-1 mimics as fibroblast growth factor-2 inhibitors: an integrated strategy for the development of new antiangiogenic compounds. J Biol Chem. 285(12):8733–8742. doi:10.1074/jbc.M109.085605.

Coraci IS, Husemann J, Berman JW, Hulette C, Dufour JH, Campanella GK, Luster AD, Silverstein SC, El Khoury JB. 2002. CD36, a Class B Scavenger Receptor, Is Expressed on Microglia in Alzheimer's Disease Brains and Can Mediate Production of Reactive Oxygen Species in Response to β-Amyloid Fibrils. The American Journal of Pathology. 160(1):101–112. doi:10.1016/S0002-9440(10)64354-4.

Dal-Ré R. 2011. Worldwide Clinical Interventional Studies on Leading Causes of Death: A Descriptive Analysis. Annals of Epidemiology. 21(10):727–731. doi:10.1016/j.annepidem.2011.03.010.

Davis SP, Amrein M, Gillrie MR, Lee K, Muruve DA, Ho M. 2012. Plasmodium falciparum-induced CD36 clustering rapidly strengthens cytoadherence via p130CAS-mediated actin cytoskeletal rearrangement. FASEB J. 26(3):1119–1130. doi:10.1096/fj.11-196923.

Davis SP, Lee K, Gillrie MR, Roa L, Amrein M, Ho M. 2013. CD36 Recruits α5β1 Integrin to Promote Cytoadherence of P. falciparum-Infected Erythrocytes. PLOS Pathogens. 9(8):e1003590. doi:10.1371/journal.ppat.1003590.

Dawson DW, Pearce SFA, Zhong R, Silverstein RL, Frazier WA, Bouck NP. 1997. CD36 Mediates the In Vitro Inhibitory Effects of Thrombospondin-1 on Endothelial Cells. Journal of Cell Biology. 138(3):707–717. doi:10.1083/jcb.138.3.707.

Dayanir V, Meyer RD, Lashkari K, Rahimi N. 2001. Identification of tyrosine residues in vascular endothelial growth factor receptor-2/FLK-1 involved in activation of phosphatidylinositol 3-kinase and cell proliferation. J Biol Chem. 276(21):17686–17692. doi:10.1074/jbc.M009128200.

De Palma M, Biziato D, Petrova TV. 2017. Microenvironmental regulation of tumour angiogenesis. Nat Rev Cancer. 17(8):457–474. doi:10.1038/nrc.2017.51.

Dickson PV, Hamner JB, Sims TL, Fraga CH, Ng CYC, Rajasekeran S, Hagedorn NL, McCarville MB, Stewart CF, Davidoff AM. 2007. Bevacizumab-Induced Transient Remodeling of the Vasculature in Neuroblastoma Xenografts Results in Improved Delivery and Efficacy of Systemically Administered Chemotherapy. Clinical Cancer Research. 13(13):3942–3950. doi:10.1158/1078-0432.CCR-07-0278.

Eakin RE, McKinley WA, Williams RJ. 1940. Egg-White Injury in Chicks and Its Relationship to a Deficiency of Vitamin H (Biotin). Science. 92(2384):224–225. doi:10.1126/science.92.2384.224.

Ebbinghaus SW, Hussain M, Tannir NM, Gordon MS, Desai AA, Knight RA, Carlson DM, Figlin RA. 2005. A randomized phase 2 study of the thrombospondin-mimetic peptide ABT-510 in patients with previously untreated advanced renal cell carcinoma. JCO. 23(16_suppl):4607–4607. doi:10.1200/jco.2005.23.16_suppl.4607.

El Khoury JB, Moore K, Freeman M, Luster AD. 2002. CD36 null mice reveal a key role for CD36 in β-amyloid induced microglial activation. Journal of Neurochemistry. 81(s1):71–71. doi:10.1046/j.1471-4159.2002.00064.x.

El Khoury JB, Moore KJ, Means TK, Leung J, Terada K, Toft M, Freeman MW, Luster AD. 2003. CD36 Mediates the Innate Host Response to β-Amyloid. J Exp Med. 197(12):1657–1666. doi:10.1084/jem.20021546.

Elebiyo TC, Rotimi D, Evbuomwan IO, Maimako RF, Iyobhebhe M, Ojo OA, Oluba OM, Adeyemi OS. 2022. Reassessing vascular endothelial growth factor (VEGF) in anti-angiogenic cancer therapy. Cancer Treatment and Research Communications. 32:100620. doi:10.1016/j.ctarc.2022.100620.

Fagiani E, Christofori G. 2013. Angiopoietins in angiogenesis. Cancer Letters. 328(1):18–26. doi:10.1016/j.canlet.2012.08.018.

Farhangkhoee H, Khan ZA, Barbin Y, Chakrabarti S. 2005. Glucose-induced up-regulation of CD36 mediates oxidative stress and microvascular endothelial cell dysfunction. Diabetologia. 48(7):1401–1410. doi:10.1007/s00125-005-1801-8.

Farooq M, Khan AW, Kim MS, Choi S. 2021. The Role of Fibroblast Growth Factor (FGF) Signalling in Tissue Repair and Regeneration. Cells. 10(11):3242. doi:10.3390/cells10113242.

Febbraio M, Abumrad NA, Hajjar DP, Sharma K, Cheng W, Pearce SF, Silverstein RL. 1999. A null mutation in murine CD36 reveals an important role in fatty acid and lipoprotein metabolism. J Biol Chem. 274(27):19055–19062. doi:10.1074/jbc.274.27.19055.

Febbraio M, Hajjar DP, Silverstein RL. 2001. CD36: a class B scavenger receptor involved in angiogenesis, atherosclerosis, inflammation, and lipid metabolism. J Clin Invest. 108(6):785–791. doi:10.1172/JCI14006.

Felbor U, Dreier L, Bryant RAR, Ploegh HL, Olsen BR, Mothes W. 2000. Secreted cathepsin L generates endostatin from collagen XVIII. The EMBO Journal. 19(6):1187–1194. doi:10.1093/emboj/19.6.1187.

Ferlay J, Colombet M, Soerjomataram I, Parkin DM, Piñeros M, Znaor A, Bray F. 2021. Cancer statistics for the year 2020: An overview. International Journal of Cancer. 149(4):778–789. doi:10.1002/ijc.33588.

Ferreras M, Felbor U, Lenhard T, Olsen BR, Delaissé J-M. 2000. Generation and degradation of human endostatin proteins by various proteinases. FEBS Letters. 486(3):247–251. doi:10.1016/S0014-5793(00)02249-3.

Fiore MM, Kakkar VV. 2003. Platelet factor 4 neutralizes heparan sulfate-enhanced antithrombin inactivation of factor Xa by preventing interaction(s) of enzyme with polysaccharide. Biochemical and Biophysical Research Communications. 311(1):71–76. doi:10.1016/j.bbrc.2003.09.171.

Folkman J. 1971. Tumour angiogenesis: therapeutic implications. N Engl J Med. 285(21):1182–1186. doi:10.1056/NEJM197111182852108.

Fragoso R, Ren D, Zhang X, Su MW-C, Burakoff SJ, Jin Y-J. 2003. Lipid raft distribution of CD4 depends on its palmitoylation and association with Lck, and evidence for CD4-induced lipid raft aggregation as an additional mechanism to enhance CD3 signalling. J Immunol. 170(2):913–921. doi:10.4049/jimmunol.170.2.913.

Gagnoux-Palacios L, Dans M, van't Hof W, Mariotti A, Pepe A, Meneguzzi G, Resh MD, Giancotti FG. 2003. Compartmentalization of integrin α6β4 signalling in lipid rafts. J Cell Biol. 162(7):1189–1196. doi:10.1083/jcb.200305006.

Garcia-Parajo MF, Cambi A, Torreno-Pina JA, Thompson N, Jacobson K. 2014. Nanoclustering as a dominant feature of plasma membrane organization. Journal of Cell Science. 127(23):4995–5005. doi:10.1242/jcs.146340.

Gengrinovitch S, Greenberg SM, Cohen T, Gitay-Goren H, Rockwell P, Maione TE, Levi BZ, Neufeld G. 1995. Platelet factor-4 inhibits the mitogenic activity of VEGF121 and VEGF165 using several concurrent mechanisms. J Biol Chem. 270(25):15059–15065. doi:10.1074/jbc.270.25.15059.

Gentilini G, Kirschbaum NE, Augustine JA, Aster RH, Visentin GP. 1999. Inhibition of human umbilical vein endothelial cell proliferation by the CXC chemokine, platelet factor 4 (PF4), is associated with impaired downregulation of p21(Cip1/WAF1). Blood. 93(1):25–33.

Gerbec ZJ, Thakar MS, Malarkannan S. 2015. The Fyn–ADAP Axis: Cytotoxicity Versus Cytokine Production in Killer Cells. Frontiers in Immunology. 6. [accessed 2023 Apr 29]. https://www.frontiersin.org/articles/10.3389/fimmu.2015.00472.

Gerber HP, Dixit V, Ferrara N. 1998. Vascular endothelial growth factor induces expression of the antiapoptotic proteins Bcl-2 and A1 in vascular endothelial cells. J Biol Chem. 273(21):13313–13316. doi:10.1074/jbc.273.21.13313.

Ghosh A, Li Z, Kan C, Qing W, Maria F, John B, Roy SL. 2007. Variability of CD36 Expression on Platelets Is Determined in Part by Genetic Polymorphisms and Can Influence Platelet Function. Blood. 110(11):3643. doi:10.1182/blood.V110.11.3643.3643.

Ghosh A, Murugesan G, Chen K, Zhang L, Wang Q, Febbraio M, Anselmo RM, Marchant K, Barnard J, Silverstein RL. 2011. Platelet CD36 surface expression levels affect functional responses to oxidized LDL and are associated with inheritance of specific genetic polymorphisms. Blood. 117(23):6355–6366. doi:10.1182/blood-2011-02-338582.

Giantonio BJ, Catalano PJ, Meropol NJ, O'Dwyer PJ, Mitchell EP, Alberts SR, Schwartz MA, Benson AB. 2007. Bevacizumab in Combination With Oxaliplatin, Fluorouracil, and Leucovorin (FOLFOX4) for Previously Treated Metastatic Colorectal Cancer: Results From the Eastern

Cooperative Oncology Group Study E3200. JCO. 25(12):1539–1544. doi:10.1200/JCO.2006.09.6305.

Githaka JM, Vega AR, Baird MA, Davidson MW, Jaqaman K, Touret N. 2016 Jan 1. Ligand-induced growth and compaction of CD36 nanoclusters enriched in Fyn induces Fyn signalling. Journal of Cell Science.:jcs.188946. doi:10.1242/jcs.188946.

Goel S, Duda DG, Xu L, Munn LL, Boucher Y, Fukumura D, Jain RK. 2011. Normalization of the Vasculature for Treatment of Cancer and Other Diseases. Physiological Reviews. 91(3):1071–1121. doi:10.1152/physrev.00038.2010.

Granot-Attas S, Elson A. 2004. Protein tyrosine phosphatase epsilon activates Yes and Fyn in Neu-induced mammary tumour cells. Exp Cell Res. 294(1):236–243. doi:10.1016/j.yexcr.2003.11.003.

Greenaway J, Lawler J, Moorehead R, Bornstein P, Lamarre J, Petrik J. 2007. Thrombospondin-1 inhibits VEGF levels in the ovary directly by binding and internalization via the low density lipoprotein receptor-related protein-1 (LRP-1). J Cell Physiol. 210(3):807–818. doi:10.1002/jcp.20904.

Greenberg ME, Sun M, Zhang R, Febbraio M, Silverstein R, Hazen SL. 2006. Oxidized phosphatidylserine-CD36 interactions play an essential role in macrophage-dependent phagocytosis of apoptotic cells. J Exp Med. 203(12):2613–2625. doi:10.1084/jem.20060370.

Greenwalt DE, Scheck SH, Rhinehart-Jones T. 1995. Heart CD36 expression is increased in murine models of diabetes and in mice fed a high fat diet. J Clin Invest. 96(3):1382–1388. doi:10.1172/JCI118173.

Guerrini V, Gennaro ML. 2019. Foam cells: one size doesn't fit all. Trends Immunol. 40(12):1163–1179. doi:10.1016/j.it.2019.10.002.

Gui Y, Zheng H, Cao RY. 2022. Foam Cells in Atherosclerosis: Novel Insights Into Its Origins, Consequences, and Molecular Mechanisms. Frontiers in Cardiovascular Medicine. 9. [accessed 2023 Apr 29]. https://www.frontiersin.org/articles/10.3389/fcvm.2022.845942.

Gupta SK, Singh JP. 1994. Inhibition of endothelial cell proliferation by platelet factor-4 involves a unique action on S phase progression. J Cell Biol. 127(4):1121–1127. doi:10.1083/jcb.127.4.1121.

Gutierrez LS, Gutierrez J. 2021. Thrombospondin 1 in Metabolic Diseases. Frontiers in Endocrinology. 12. [accessed 2023 Apr 29]. https://www.frontiersin.org/articles/10.3389/fendo.2021.638536.

Han Y, Branon TC, Martell JD, Boassa D, Shechner D, Ellisman MH, Ting A. 2019. Directed Evolution of Split APEX2 Peroxidase. ACS Chem Biol. 14(4):619–635. doi:10.1021/acschembio.8b00919.

Hanai J, Dhanabal M, Karumanchi SA, Albanese C, Waterman M, Chan B, Ramchandran R, Pestell R, Sukhatme VP. 2002. Endostatin Causes G1 Arrest of Endothelial Cells through Inhibition of Cyclin D1*. Journal of Biological Chemistry. 277(19):16464–16469. doi:10.1074/jbc.M112274200.

Hanson J, Lam SWK, Mahanta KC, Pattnaik R, Alam S, Mohanty S, Hasan MU, Hossain A, Charunwatthana P, Chotivanich K, et al. 2012. Relative Contributions of Macrovascular and Microvascular Dysfunction to Disease Severity in Falciparum Malaria. The Journal of Infectious Diseases. 206(4):571–579. doi:10.1093/infdis/jis400.

Hao J-W, Wang J, Guo H, Zhao Y-Y, Sun H-H, Li Y-F, Lai X-Y, Zhao N, Wang X, Xie C, et al. 2020. CD36 facilitates fatty acid uptake by dynamic palmitoylation-regulated endocytosis. Nat Commun. 11(1):4765. doi:10.1038/s41467-020-18565-8.

Ho M, Hoang HL, Lee KM, Liu N, MacRae T, Montes L, Flatt CL, Yipp BG, Berger BJ, Looareesuwan S, et al. 2005. Ectophosphorylation of CD36 Regulates Cytoadherence of Plasmodium falciparum to Microvascular Endothelium under Flow Conditions. Infection and Immunity. 73(12):8179–8187. doi:10.1128/IAI.73.12.8179-8187.2005.

Holmberg A, Blomstergren A, Nord O, Lukacs M, Lundeberg J, Uhlén M. 2005. The biotin-streptavidin interaction can be reversibly broken using water at elevated temperatures. ELECTROPHORESIS. 26(3):501–510. doi:10.1002/elps.200410070.

Holmes DI, Zachary I. 2005. The vascular endothelial growth factor (VEGF) family: angiogenic factors in health and disease. Genome Biology. 6(2):209. doi:10.1186/gb-2005-6-2-209.

Holthenrich A, Drexler HCA, Chehab T, Naß J, Gerke V. 2019. Proximity proteomics of endothelial Weibel-Palade bodies identifies novel regulator of von Willebrand factor secretion. Blood. 134(12):979–982. doi:10.1182/blood.2019000786.

Holzer E, Rumpf-Kienzl C, Falk S, Dammermann A. 2022. A modified TurboID approach identifies tissue-specific centriolar components in C. elegans. PLoS Genet. 18(4):e1010150. doi:10.1371/journal.pgen.1010150.

Hoosdally SJ, Andress EJ, Wooding C, Martin CA, Linton KJ. 2009. The Human Scavenger Receptor CD36: GLYCOSYLATION STATUS AND ITS ROLE IN TRAFFICKING AND FUNCTION *. Journal of Biological Chemistry. 284(24):16277–16288. doi:10.1074/jbc.M109.007849.

Hopkins C, Gibson A, Stinchcombe J, Futter C. 2000. Chimeric molecules employing horseradish peroxidase as reporter enzyme for protein localization in the electron microscope. In: Thorner J, Emr SD, Abelson JN, editors. Methods in Enzymology. Vol. 327. Academic Press. (Applications of Chimeric Genes and Hybrid Proteins - Part B: Cell Biology and Physiology). p. 35–45. [accessed 2023 Apr 7]. https://www.sciencedirect.com/science/article/pii/S0076687900272650.

Hsieh F-L, Tartaglia L. 2016. The CIDRa domain from MCvar1 PfEMP1 bound to CD36. doi:https://doi.org/10.2210/pdb5LGD/pdb.

Hsieh F-L, Turner L, Bolla JR, Robinson CV, Lavstsen T, Higgins MK. 2016. The structural basis for CD36 binding by the malaria parasite. Nat Commun. 7(1):12837. doi:10.1038/ncomms12837.

Huang T, Sun L, Yuan X, Qiu H. 2017. Thrombospondin-1 is a multifaceted player in tumour progression. Oncotarget. 8(48):84546–84558. doi:10.18632/oncotarget.19165.

Huh HY, Pearce SF, Yesner LM, Schindler JL, Silverstein RL. 1996. Regulated Expression of CD36 During Monocyte-to-Macrophage Differentiation: Potential Role of CD36 in Foam Cell Formation. Blood. 87(5):2020–2028. doi:10.1182/blood.V87.5.2020.2020.

Hurwitz Herbert, Fehrenbacher Louis, Novotny William, Cartwright Thomas, Hainsworth John, Heim William, Berlin Jordan, Baron Ari, Griffing Susan, Holmgren Eric, et al. 2004. Bevacizumab plus Irinotecan, Fluorouracil, and Leucovorin for Metastatic Colorectal Cancer. New England Journal of Medicine. 350(23):2335–2342. doi:10.1056/NEJMoa032691.

Hwang J, Espenshade PJ. 2016. Proximity-dependent biotin labelling in yeast using the engineered ascorbate peroxidase APEX2. Biochem J. 473(16):2463–2469. doi:10.1042/BCJ20160106.

Idro R, Jenkins NE, Newton CR. 2005. Pathogenesis, clinical features, and neurological outcome of cerebral malaria. The Lancet Neurology. 4(12):827–840. doi:10.1016/S1474-4422(05)70247-7.

Inoki I, Shiomi T, Hashimoto G, Enomoto H, Nakamura H, Makino K, Ikeda E, Takata S, Kobayashi K, Okada Y. 2002. Connective tissue growth factor binds vascular endothelial growth factor (VEGF) and inhibits VEGF-induced angiogenesis. FASEB J. 16(2):219–221. doi:10.1096/fj.01-0332fje.

Jain RK. 1998. The next frontier of molecular medicine: Delivery of therapeutics. Nat Med. 4(6):655–657. doi:10.1038/nm0698-655.

Jain RK. 2001. Normalizing tumour vasculature with anti-angiogenic therapy: a new paradigm for combination therapy. Nat Med. 7(9):987–989. doi:10.1038/nm0901-987.

Jain RK, Duda DG, Clark JW, Loeffler JS. 2006. Lessons from phase III clinical trials on anti-VEGF therapy for cancer. Nat Rev Clin Oncol. 3(1):24–40. doi:10.1038/ncponc0403.

Jeanne A, Schneider C, Martiny L, Dedieu S. 2015. Original insights on thrombospondin-1-related antireceptor strategies in cancer. Front Pharmacol. 6:252. doi:10.3389/fphar.2015.00252.

Jiang X, Wang J, Deng X, Xiong F, Zhang S, Gong Z, Li Xiayu, Cao K, Deng H, He Y, et al. 2020. The role of microenvironment in tumour angiogenesis. Journal of Experimental & Clinical Cancer Research. 39(1):204. doi:10.1186/s13046-020-01709-5.

Jiménez B, Volpert OV, Crawford SE, Febbraio M, Silverstein RL, Bouck N. 2000. Signals leading to apoptosis-dependent inhibition of neovascularization by thrombospondin-1. Nat Med. 6(1):41–48. doi:10.1038/71517.

Jiménez B, Volpert OV, Reiher F, Chang L, Muñoz A, Karin M, Bouck N. 2001. c-Jun N-terminal kinase activation is required for the inhibition of neovascularization by thrombospondin-1. Oncogene. 20(26):3443–3448. doi:10.1038/sj.onc.1204464.

Kalluri R. 2003. Basement membranes: structure, assembly and role in tumour angiogenesis. Nat Rev Cancer. 3(6):422–433. doi:10.1038/nrc1094.

Kar NS, Ashraf MZ, Valiyaveettil M, Podrez EA. 2008a. Mapping and Characterization of the Binding Site for Specific Oxidized Phospholipids and Oxidized Low Density Lipoprotein of Scavenger Receptor CD36. J Biol Chem. 283(13):8765–8771. doi:10.1074/jbc.M709195200.

Kar NS, Ashraf MZ, Valiyaveettil M, Podrez EA. 2008b. Mapping and Characterization of the Binding Site for Specific Oxidized Phospholipids and Oxidized Low Density Lipoprotein of Scavenger Receptor CD36 *. Journal of Biological Chemistry. 283(13):8765–8771. doi:10.1074/jbc.M709195200.

Kido K, Yamanaka S, Nakano S, Motani K, Shinohara S, Nozawa A, Kosako H, Ito S, Sawasaki T. 2020. AirID, a novel proximity biotinylation enzyme, for analysis of protein–protein interactions. Cole PA, Dötsch V, Dötsch V, Cronan JE, editors. eLife. 9:e54983. doi:10.7554/eLife.54983.

Kim DI, Jensen SC, Noble KA, Kc B, Roux KH, Motamedchaboki K, Roux KJ. 2016. An improved smaller biotin ligase for BioID proximity labelling. MBoC. 27(8):1188–1196. doi:10.1091/mbc.E15-12-0844.

Kim I, Kim HG, So J-N, Kim JH, Kwak HJ, Koh GY. 2000. Angiopoietin-1 Regulates Endothelial Cell Survival Through the Phosphatidylinositol 3′-Kinase/Akt Signal Transduction Pathway. Circulation Research. 86(1):24–29. doi:10.1161/01.RES.86.1.24.

Kim K, Park I, Kim J, Kang M-G, Choi WG, Shin H, Kim J-S, Rhee H-W, Suh JM. 2021. Dynamic tracking and identification of tissue-specific secretory proteins in the circulation of live mice. Nat Commun. 12(1):5204. doi:10.1038/s41467-021-25546-y.

Kim KS, Kim JS, Park J-Y, Suh YH, Jou I, Joe E-H, Park SM. 2013. DJ-1 associates with lipid rafts by palmitoylation and regulates lipid rafts-dependent endocytosis in astrocytes. Hum Mol Genet. 22(23):4805–4817. doi:10.1093/hmg/ddt332.

Kirsch M, Black PM. 2012. Angiogenesis in Brain Tumours. Springer Science & Business Media.

Klenotic PA, Page RC, Li W, Amick J, Misra S, Silverstein RL. 2013. Molecular basis of antiangiogenic thrombospondin-1 type 1 repeat domain interactions with CD36. Arterioscler Thromb Vasc Biol. 33(7):1655–1662. doi:10.1161/ATVBAHA.113.301523.

Kotani N, Gu J, Isaji T, Udaka K, Taniguchi N, Honke K. 2008. Biochemical visualization of cell surface molecular clustering in living cells. Proceedings of the National Academy of Sciences. 105(21):7405–7409. doi:10.1073/pnas.0710346105.

Kuijpers MJE, de Witt S, Nergiz-Unal R, van Kruchten R, Korporaal SJA, Verhamme P, Febbraio M, Tjwa M, Voshol PJ, Hoylaerts MF, et al. 2014. Supporting Roles of Platelet Thrombospondin-1 and CD36 in Thrombus Formation on Collagen. Arteriosclerosis, Thrombosis, and Vascular Biology. 34(6):1187–1192. doi:10.1161/ATVBAHA.113.302917.

Kunnas TA, Wallén MJ, Kulomaa MS. 1993. Induction of chicken avidin and related mRNAs after bacterial infection. Biochimica et Biophysica Acta (BBA) - Gene Structure and Expression. 1216(3):441–445. doi:10.1016/0167-4781(93)90012-3.

Laitinen OH, Kuusela TP, Kukkurainen S, Nurminen A, Sinkkonen A, Hytönen VP. 2021. Bacterial avidins are a widely distributed protein family in Actinobacteria, Proteobacteria and Bacteroidetes. BMC Ecology and Evolution. 21(1):53. doi:10.1186/s12862-021-01784-y.

Lam SS, Martell JD, Kamer KJ, Deerinck TJ, Ellisman MH, Mootha VK, Ting AY. 2015. Directed evolution of APEX2 for electron microscopy and proximity labelling. Nat Methods. 12(1):51–54. doi:10.1038/nmeth.3179.

Lamalice L, Le Boeuf F, Huot J. 2007. Endothelial Cell Migration During Angiogenesis. Circulation Research. 100(6):782–794. doi:10.1161/01.RES.0000259593.07661.1e.

Lawler PR, Lawler J. 2012. Molecular basis for the regulation of angiogenesis by thrombospondin-1 and -2. Cold Spring Harb Perspect Med. 2(5):a006627. doi:10.1101/cshperspect.a006627.

Leitinger B, Hogg N. 2002. The involvement of lipid rafts in the regulation of integrin function. Journal of Cell Science. 115(5):963–972. doi:10.1242/jcs.115.5.963.

León-Del-Río A. 2019. Biotin in metabolism, gene expression, and human disease. Journal of Inherited Metabolic Disease. 42(4):647–654. doi:10.1002/jimd.12073.

Liu W, Yin Y, Zhou Z, He M, Dai Y. 2014. OxLDL-induced IL-1beta secretion promoting foam cells formation was mainly via CD36 mediated ROS production leading to NLRP3 inflammasome activation. Inflamm Res. 63(1):33–43. doi:10.1007/s00011-013-0667-3.

Liu Z-L, Chen H-H, Zheng L-L, Sun L-P, Shi L. 2023. Angiogenic signalling pathways and anti-angiogenic therapy for cancer. Sig Transduct Target Ther. 8(1):1–39. doi:10.1038/s41392-023-01460-1.

Lobingier BT, Hüttenhain R, Eichel K, Miller KB, Ting AY, von Zastrow M, Krogan NJ. 2017. An Approach to Spatiotemporally Resolve Protein Interaction Networks in Living Cells. Cell. 169(2):350-360.e12. doi:10.1016/j.cell.2017.03.022.

Lonati A, Mommaas MA, Pasolini G, Lavazza A, Rowden G, De Panfilis G. 1996. Macrophages, but Not Langerhans Cell-like Cells of Dendritic Lineage, Express the CD36 Molecule in Normal Human Dermis: Relevance to Downregulatory Cutaneous Immune Responses? Journal of Investigative Dermatology. 106(1):96–101. doi:10.1111/1523-1747.ep12328158.

Lopes-Coelho F, Martins F, Pereira SA, Serpa J. 2021. Anti-Angiogenic Therapy: Current Challenges and Future Perspectives. Int J Mol Sci. 22(7):3765. doi:10.3390/ijms22073765.

Luiken JJFP, Schaap FG, van Nieuwenhoven FA, van der Vusse GJ, Bonen A, Glatz JFC. 1999. Cellular fatty acid transport in heart and skeletal muscle as facilitated by proteins. Lipids. 34(S1Part2):S169–S175. doi:10.1007/BF02562278.

Ma J, Waxman DJ. 2008a. Combination of Anti-angiogenesis with Chemotherapy for More Effective Cancer Treatment. Molecular cancer therapeutics. 7(12):3670. doi:10.1158/1535-7163.MCT-08-0715.

Ma J, Waxman DJ. 2008b. Combination of antiangiogenesis with chemotherapy for more effective cancer treatment. Molecular Cancer Therapeutics. 7(12):3670–3684. doi:10.1158/1535-7163.MCT-08-0715.

Ma Q, Reiter RJ, Chen Y. 2020. Role of melatonin in controlling angiogenesis under physiological and pathological conditions. Angiogenesis. 23(2):91–104. doi:10.1007/s10456-019-09689-7.

Magnusson PU, Looman C, Åhgren A, Wu Y, Claesson-Welsh L, Heuchel RL. 2007. Platelet-Derived Growth Factor Receptor-β Constitutive Activity Promotes Angiogenesis In Vivo and In Vitro. Arteriosclerosis, Thrombosis, and Vascular Biology. 27(10):2142–2149. doi:10.1161/01.ATV.0000282198.60701.94.

Mans S, Banz Y, Mueller BU, Pabst T. 2012. The angiogenesis inhibitor vasostatin is regulated by neutrophil elastase–dependent cleavage of calreticulin in AML patients. Blood. 120(13):2690–2699. doi:10.1182/blood-2012-02-412759.

Martell JD, Deerinck TJ, Sancak Y, Poulos TL, Mootha VK, Sosinsky GE, Ellisman MH, Ting AY. 2012. Engineered ascorbate peroxidase as a genetically encoded reporter for electron microscopy. Nat Biotechnol. 30(11):1143–1148. doi:10.1038/nbt.2375.

Martínez-Mármol R, Small C, Jiang A, Palliyaguru T, Wallis TP, Gormal RS, Sibarita J-B, Götz J, Meunier FA. 2023. Fyn nanoclustering requires switching to an open conformation and is enhanced by FTLD-Tau biomolecular condensates. Mol Psychiatry. 28(2):946–962. doi:10.1038/s41380-022-01825-y.

Matrone C, Petrillo F, Nasso R, Ferretti G. 2020. Fyn Tyrosine Kinase as Harmonizing Factor in Neuronal Functions and Dysfunctions. Int J Mol Sci. 21(12):4444. doi:10.3390/ijms21124444.

May DG, Scott KL, Campos AR, Roux KJ. 2020. Comparative Application of BioID and TurboID for Protein-Proximity Biotinylation. Cells. 9(5):1070. doi:10.3390/cells9051070.

McLaughlin AP, De Vries GW. 2001. Role of PLCgamma and Ca(2+) in VEGF- and FGF-induced choroidal endothelial cell proliferation. Am J Physiol Cell Physiol. 281(5):C1448-1456. doi:10.1152/ajpcell.2001.281.5.C1448.

Mebratu Y, Tesfaigzi Y. 2009. How ERK1/2 Activation Controls Cell Proliferation and Cell Death Is Subcellular Localization the Answer? Cell Cycle. 8(8):1168–1175.

Medinger M, Mross K. 2010. Clinical trials with anti-angiogenic agents in hematological malignancies. J Angiogenes Res. 2:10. doi:10.1186/2040-2384-2-10.

Minerva D, Othman NL, Nakazawa T, Ito Y, Yoshida M, Goto A, Suzuki T. 2022. A New Chemotactic Mechanism Governs Long-Range Angiogenesis Induced by Patching an Arterial Graft into a Vein. Int J Mol Sci. 23(19):11208. doi:10.3390/ijms231911208.

Mohajeri A, Sanaei S, Kiafar F, Fattahi A, Khalili M, Zarghami N. 2017. The Challenges of Recombinant Endostatin in Clinical Application: Focus on the Different Expression Systems and Molecular Bioengineering. Adv Pharm Bull. 7(1):21–34. doi:10.15171/apb.2017.004.

Montemagno C, Pagès G. 2020. Resistance to Anti-angiogenic Therapies: A Mechanism Depending on the Time of Exposure to the Drugs. Frontiers in Cell and Developmental Biology. 8. [accessed 2023 Apr 27]. https://www.frontiersin.org/articles/10.3389/fcell.2020.00584.

Murphy-Ullrich JE. 2022. Thrombospondin-1 Signalling Through the Calreticulin/LDL Receptor Related Protein 1 Axis: Functions and Possible Roles in Glaucoma. Frontiers in Cell and Developmental Biology. 10. [accessed 2023 May 9]. https://www.frontiersin.org/articles/10.3389/fcell.2022.898772.

Navazo MDP, Daviet L, Ninio E, McGregor JL. 1996. Identification on Human CD36 of a Domain (155-183) Implicated in Binding Oxidized Low-Density Lipoproteins (Ox-LDL). Arteriosclerosis, Thrombosis, and Vascular Biology. 16(8):1033–1039. doi:10.1161/01.ATV.16.8.1033.

Neculai D, Schwake M, Ravichandran M, Zunke F, Collins RF, Peters J, Neculai M, Plumb J, Loppnau P, Pizarro JC, et al. 2013. Structure of LIMP-2 provides functional insights with implications for SR-BI and CD36. Nature. 504(7478):172–176. doi:10.1038/nature12684.

Nicholson AC, Frieda S, Pearce A, Silverstein RL. 1995. Oxidized LDL Binds to CD36 on Human Monocyte-Derived Macrophages and Transfected Cell Lines. Arteriosclerosis, Thrombosis, and Vascular Biology. 15(2):269–275. doi:10.1161/01.ATV.15.2.269.

Niland S, Riscanevo AX, Eble JA. 2021. Matrix Metalloproteinases Shape the Tumour Microenvironment in Cancer Progression. Int J Mol Sci. 23(1):146. doi:10.3390/ijms23010146.

Nishida N, Yano H, Nishida T, Kamura T, Kojiro M. 2006. Angiogenesis in Cancer. Vasc Health Risk Manag. 2(3):213–219.

Oakley JV, Buksh BF, Fernández DF, Oblinsky DG, Seath CP, Geri JB, Scholes GD, MacMillan DWC. 2022. Radius measurement via super-resolution microscopy enables the development of a variable radii proximity labelling platform. Proceedings of the National Academy of Sciences. 119(32):e2203027119. doi:10.1073/pnas.2203027119.

Okumura N, Yoshida H, Kitagishi Y, Murakami M, Nishimura Y, Matsuda S. 2012. PI3K/AKT/PTEN Signalling as a Molecular Target in Leukemia Angiogenesis. Adv Hematol. 2012:843085. doi:10.1155/2012/843085.

Otrock ZK, Mahfouz RAR, Makarem JA, Shamseddine AI. 2007. Understanding the biology of angiogenesis: Review of the most important molecular mechanisms. Blood Cells, Molecules, and Diseases. 39(2):212–220. doi:10.1016/j.bcmd.2007.04.001.

Panaretakis T, Kepp O, Brockmeier U, Tesniere A, Bjorklund A-C, Chapman DC, Durchschlag M, Joza N, Pierron G, van Endert P, et al. 2009. Mechanisms of pre-apoptotic calreticulin exposure in immunogenic cell death. The EMBO Journal. 28(5):578–590. doi:10.1038/emboj.2009.1.

Park L, Wang G, Zhou P, Zhou J, Pitstick R, Previti ML, Younkin L, Younkin SG, Van Nostrand WE, Cho S, et al. 2011. Scavenger receptor CD36 is essential for the cerebrovascular oxidative stress and neurovascular dysfunction induced by amyloid-β. Proceedings of the National Academy of Sciences. 108(12):5063–5068. doi:10.1073/pnas.1015413108.

Park L, Zhou J, Zhou P, Pistick R, El Jamal S, Younkin L, Pierce J, Arreguin A, Anrather J, Younkin SG, et al. 2013. Innate immunity receptor CD36 promotes cerebral amyloid angiopathy. Proc Natl Acad Sci U S A. 110(8):3089–3094. doi:10.1073/pnas.1300021110.

Parsons SJ, Parsons JT. 2004. Src family kinases, key regulators of signal transduction. Oncogene. 23(48):7906–7909. doi:10.1038/sj.onc.1208160.

Pelsers MM, Lutgerink JT, Nieuwenhoven FA, Tandon NN, van der Vusse GJ, Arends JW, Hoogenboom HR, Glatz JF. 1999. A sensitive immunoassay for rat fatty acid translocase (CD36) using phage antibodies selected on cell transfectants: abundant presence of fatty acid

translocase/CD36 in cardiac and red skeletal muscle and up-regulation in diabetes. Biochem J. 337(Pt 3):407–414.

Perez Verdaguer M, Zhang T, Surve S, Paulo JA, Wallace C, Watkins SC, Gygi SP, Sorkin A. 2022. Time-resolved proximity labelling of protein networks associated with ligand-activated EGFR. Cell Reports. 39(11):110950. doi:10.1016/j.celrep.2022.110950.

Perollet C, Han ZC, Savona C, Caen JP, Bikfalvi A. 1998. Platelet factor 4 modulates fibroblast growth factor 2 (FGF-2) activity and inhibits FGF-2 dimerization. Blood. 91(9):3289–3299.

Podrez EA, Poliakov E, Shen Z, Zhang R, Deng Y, Sun M, Finton PJ, Shan L, Gugiu B, Fox PL, et al. 2002. Identification of a Novel Family of Oxidized Phospholipids That Serve as Ligands for the Macrophage Scavenger Receptor CD36 *. Journal of Biological Chemistry. 277(41):38503–38516. doi:10.1074/jbc.M203318200.

Pohl J, Ring A, Korkmaz Ü, Ehehalt R, Stremmel W. 2005. FAT/CD36-mediated Long-Chain Fatty Acid Uptake in Adipocytes Requires Plasma Membrane Rafts. MBoC. 16(1):24–31. doi:10.1091/mbc.e04-07-0616.

Pottier C, Fresnais M, Gilon M, Jérusalem G, Longuespée R, Sounni NE. 2020. Tyrosine Kinase Inhibitors in Cancer: Breakthrough and Challenges of Targeted Therapy. Cancers. 12(3):731. doi:10.3390/cancers12030731.

Qin W, Cho KF, Cavanagh PE, Ting AY. 2021. Deciphering molecular interactions by proximity labelling. Nat Methods. 18(2):133–143. doi:10.1038/s41592-020-01010-5.

Quintero-Fabián S, Arreola R, Becerril-Villanueva E, Torres-Romero JC, Arana-Argáez V, Lara-Riegos J, Ramírez-Camacho MA, Alvarez-Sánchez ME. 2019. Role of Matrix Metalloproteinases in Angiogenesis and Cancer. Front Oncol. 9:1370. doi:10.3389/fonc.2019.01370.

Raica M, Cimpean AM. 2010. Platelet-Derived Growth Factor (PDGF)/PDGF Receptors (PDGFR) Axis as Target for Antitumour and Antiangiogenic Therapy. Pharmaceuticals (Basel). 3(3):572–599. doi:10.3390/ph3030572.

Ralston GB. 1985. Protein-Protein Interactions in Cell Membranes. In: Structure and Properties of Cell Membrane Structure and Properties of Cell Membranes. CRC Press. 21 p.

Ramanathan M, Majzoub K, Rao DS, Neela PH, Zarnegar BJ, Mondal S, Roth JG, Gai H, Kovalski JR, Siprashvili Z, et al. 2018. RNA–protein interaction detection in living cells. Nat Methods. 15(3):207–212. doi:10.1038/nmeth.4601.

Rasmussen JT, Berglund L, Rasmussen MS, Petersen TE. 1998. Assignment of disulfide bridges in bovine CD36. Eur J Biochem. 257(2):488–494. doi:10.1046/j.1432-1327.1998.2570488.x.

Rauova L, Zhai L, Kowalska MA, Arepally GM, Cines DB, Poncz M. 2006. Role of platelet surface PF4 antigenic complexes in heparin-induced thrombocytopenia pathogenesis: diagnostic and therapeutic implications. Blood. 107(6):2346–2353. doi:10.1182/blood-2005-08-3122.

Reck M, von Pawel J, Zatloukal P, Ramlau R, Gorbounova V, Hirsh V, Leighl N, Mezger J, Archer V, Moore N, et al. 2009. Phase III trial of cisplatin plus gemcitabine with either placebo or bevacizumab as first-line therapy for nonsquamous non-small-cell lung cancer: AVAil. J Clin Oncol. 27(8):1227–1234. doi:10.1200/JCO.2007.14.5466.

Rees Johanna S., Li X-W, Perrett S, Lilley KS, Jackson AP. 2015. Protein Neighbors and Proximity Proteomics. Mol Cell Proteomics. 14(11):2848–2856. doi:10.1074/mcp.R115.052902.

Rees Johanna Susan, Li X-W, Perrett S, Lilley KS, Jackson AP. 2015. Selective Proteomic Proximity Labelling Assay Using Tyramide (SPPLAT): A Quantitative Method for the Proteomic Analysis of Localized Membrane-Bound Protein Clusters. Curr Protoc Protein Sci. 80:19.27.1-19.27.18. doi:10.1002/0471140864.ps1927s80.

Resovi A, Pinessi D, Chiorino G, Taraboletti G. 2014. Current understanding of the thrombospondin-1 interactome. Matrix Biol. 37:83–91. doi:10.1016/j.matbio.2014.01.012.

Ribatti D. 2008. Judah Folkman, a pioneer in the study of angiogenesis. Angiogenesis. 11(1):3–10. doi:10.1007/s10456-008-9092-6.

Ribatti D, Nico B, Crivellato E. 2011. The role of pericytes in angiogenesis. The International Journal of Developmental Biology. 55(3):261–268. doi:10.1387/ijdb.103167dr.

Ricard N, Bailly S, Guignabert C, Simons M. 2021. The quiescent endothelium: signalling pathways regulating organ-specific endothelial normalcy. Nat Rev Cardiol. 18(8):565–580. doi:10.1038/s41569-021-00517-4.

Rigotti A, Acton SL, Krieger M. 1995. The Class B Scavenger Receptors SR-BI and CD36 Are Receptors for Anionic Phospholipids *. Journal of Biological Chemistry. 270(27):16221–16224. doi:10.1074/jbc.270.27.16221.

Rousseau S, Houle F, Landry J, Huot J. 1997. p38 MAP kinase activation by vascular endothelial growth factor mediates actin reorganization and cell migration in human endothelial cells. Oncogene. 15(18):2169–2177. doi:10.1038/sj.onc.1201380.

Roux KJ, Kim DI, Raida M, Burke B. 2012. A promiscuous biotin ligase fusion protein identifies proximal and interacting proteins in mammalian cells. Journal of Cell Biology. 196(6):801–810. doi:10.1083/jcb.201112098.

Ruan G-X, Kazlauskas A. 2012. VEGF-A engages at least three tyrosine kinases to activate PI3K/Akt. Cell Cycle. 11(11):2047–2048. doi:10.4161/cc.20535.

Saltz LB, Clarke S, Díaz-Rubio E, Scheithauer W, Figer A, Wong R, Koski S, Lichinitser M, Yang T-S, Rivera F, et al. 2008. Bevacizumab in combination with oxaliplatin-based chemotherapy as first-line therapy in metastatic colorectal cancer: a randomized phase III study. J Clin Oncol. 26(12):2013–2019. doi:10.1200/JCO.2007.14.9930.

Sampson MJ, Davies IR, Braschi S, Ivory K, Hughes DA. 2003. Increased expression of a scavenger receptor (CD36) in monocytes from subjects with Type 2 diabetes. Atherosclerosis. 167(1):129–134. doi:10.1016/s0021-9150(02)00421-5.

Sanchez AD, Branon TC, Cote LE, Papagiannakis A, Liang X, Pickett MA, Shen K, Jacobs-Wagner C, Ting AY, Feldman JL. 2021. Proximity labelling reveals non-centrosomal microtubule-organizing center components required for microtubule growth and localization. Curr Biol. 31(16):3586-3600.e11. doi:10.1016/j.cub.2021.06.021.

Sfeir Z, Ibrahimi A, Amri E, Grimaldi P, Abumrad N. 1997. Regulation of FAT/CD36 gene expression: further evidence in support of a role of the protein in fatty acid binding/transport. Prostaglandins Leukot Essent Fatty Acids. 57(1):17–21. doi:10.1016/s0952-3278(97)90487-7.

Shangary S, Wang S. 2009. Small-Molecule Inhibitors of the MDM2-p53 Protein-Protein Interaction to Reactivate p53 Function: A Novel Approach for Cancer Therapy. Annual Review of Pharmacology and Toxicology. 49(1):223–241. doi:10.1146/annurev.pharmtox.48.113006.094723.

Shenoy-Scaria AM, Dietzen DJ, Kwong J, Link DC, Lublin DM. 1994. Cysteine3 of Src family protein tyrosine kinase determines palmitoylation and localization in caveolae. J Cell Biol. 126(2):353–363. doi:10.1083/jcb.126.2.353.

Shu Q, Li W, Li H, Sun G. 2014. Vasostatin Inhibits VEGF-Induced Endothelial Cell Proliferation, Tube Formation and Induces Cell Apoptosis under Oxygen Deprivation. International Journal of Molecular Sciences. 15(4):6019–6030. doi:10.3390/ijms15046019.

Shukla S, Chen Z-S, Ambudkar SV. 2012. Tyrosine kinase inhibitors as modulators of ABC transporter-mediated drug resistance. Drug Resist Updat. 15(1–2):70–80. doi:10.1016/j.drup.2012.01.005.

da Silva GB, Pinto JR, Barros EJG, Farias GMN, Daher EDF. 2017. Kidney involvement in malaria: an update. Rev Inst Med Trop Sao Paulo. 59:e53. doi:10.1590/S1678-9946201759053.

Simons K, Toomre D. 2000. Lipid rafts and signal transduction. Nat Rev Mol Cell Biol. 1(1):31–39. doi:10.1038/35036052.

Singer SJ, Nicolson GL. 1972. The fluid mosaic model of the structure of cell membranes. Science. 175(4023):720–731. doi:10.1126/science.175.4023.720.

Song S, Ewald AJ, Stallcup W, Werb Z, Bergers G. 2005. PDGFRβ+ perivascular progenitor cells in tumours regulate pericyte differentiation and vascular survival. Nat Cell Biol. 7(9):870–879. doi:10.1038/ncb1288.

Stahl A, Hirsch DJ, Gimeno RE, Punreddy S, Ge P, Watson N, Patel S, Kotler M, Raimondi A, Tartaglia LA, et al. 1999. Identification of the Major Intestinal Fatty Acid Transport Protein. Molecular Cell. 4(3):299–308. doi:10.1016/S1097-2765(00)80332-9.

Sulpice E, Bryckaert M, Lacour J, Contreres J-O, Tobelem G. 2002. Platelet factor 4 inhibits FGF2-induced endothelial cell proliferation via the extracellular signal-regulated kinase pathway but not by the phosphatidylinositol 3-kinase pathway. Blood. 100(9):3087–3094. doi:10.1182/blood.V100.9.3087.

Sun S, Dong H, Yan T, Li Junchen, Liu B, Shao P, Li Jie, Liang C. 2020. Role of TSP-1 as prognostic marker in various cancers: a systematic review and meta-analysis. BMC Medical Genetics. 21(1):139. doi:10.1186/s12881-020-01073-3.

Sun X, Fu Y, Gu M, Zhang L, Li D, Li H, Chien S, Shyy JY-J, Zhu Y. 2016. Activation of integrin α5 mediated by flow requires its translocation to membrane lipid rafts in vascular endothelial cells. Proceedings of the National Academy of Sciences. 113(3):769–774. doi:10.1073/pnas.1524523113.

Swerlick RA, Lee KH, Wick TM, Lawley TJ. 1992. Human dermal microvascular endothelial but not human umbilical vein endothelial cells express CD36 in vivo and in vitro. J Immunol. 148(1):78–83.

Taban Q, Mumtaz PT, Masoodi KZ, Haq E, Ahmad SM. 2022. Scavenger receptors in host defense: from functional aspects to mode of action. Cell Communication and Signalling. 20(1):2. doi:10.1186/s12964-021-00812-0.

Tadros A, Hughes DP, Dunmore BJ, Brindle NPJ. 2003. ABIN-2 protects endothelial cells from death and has a role in the antiapoptotic effect of angiopoietin-1. Blood. 102(13):4407–4409. doi:10.1182/blood-2003-05-1602.

Takahashi T, Ueno H, Shibuya M. 1999. VEGF activates protein kinase C-dependent, but Ras-independent Raf-MEK-MAP kinase pathway for DNA synthesis in primary endothelial cells. Oncogene. 18(13):2221–2230. doi:10.1038/sj.onc.1202527.

Talapko J, Škrlec I, Alebić T, Jukić M, Včev A. 2019. Malaria: The Past and the Present. Microorganisms. 7(6):179. doi:10.3390/microorganisms7060179.

Tandon NN, Lipsky RH, Burgess WH, Jamieson GA. 1989. Isolation and characterization of platelet glycoprotein IV (CD36). J Biol Chem. 264(13):7570–7575.

Tao N, Wagner SJ, Lublin DM. 1996. CD36 is palmitoylated on both N- and C-terminal cytoplasmic tails. J Biol Chem. 271(37):22315–22320. doi:10.1074/jbc.271.37.22315.

Taraboletti G, D'Ascenzo S, Borsotti P, Giavazzi R, Pavan A, Dolo V. 2002. Shedding of the matrix metalloproteinases MMP-2, MMP-9, and MT1-MMP as membrane vesicle-associated components by endothelial cells. Am J Pathol. 160(2):673–680. doi:10.1016/S0002-9440(10)64887-0.

Tausig F, Wolf FJ. 1964. Streptavidin- a substance with avidin-like properties produced by microorganisms. Biochemical and Biophysical Research Communications. 14:205–209.

Terracciano R, Preianò M, Fregola A, Pelaia C, Montalcini T, Savino R. 2021. Mapping the SARS-CoV-2–Host Protein–Protein Interactome by Affinity Purification Mass Spectrometry and Proximity-Dependent Biotin Labelling: A Rational and Straightforward Route to Discover Host-Directed Anti-SARS-CoV-2 Therapeutics. International Journal of Molecular Sciences. 22(2):532. doi:10.3390/ijms22020532.

Thal DR, Griffin WST, Braak H. 2008. Parenchymal and vascular Aβ-deposition and its effects on the degeneration of neurons and cognition in Alzheimer's disease. Journal of Cellular and Molecular Medicine. 12(5b):1848–1862. doi:10.1111/j.1582-4934.2008.00411.x.

Thorne RF, Ralston KJ, de Bock CE, Mhaidat NM, Zhang XD, Boyd AW, Burns GF. 2010. Palmitoylation of CD36/FAT regulates the rate of its post-transcriptional processing in the endoplasmic reticulum. Biochimica et Biophysica Acta (BBA) - Molecular Cell Research. 1803(11):1298–1307. doi:10.1016/j.bbamcr.2010.07.002.

Togayachi A, Kozono Y, Ikehara Y, Ito H, Suzuki N, Tsunoda Y, Abe S, Sato T, Nakamura K, Suzuki M, et al. 2010. Lack of lacto/neolacto-glycolipids enhances the formation of glycolipid-enriched microdomains, facilitating B cell activation. Proc Natl Acad Sci U S A. 107(26):11900–11905. doi:10.1073/pnas.0914298107.

Trebec-Reynolds DP, Voronov I, Heersche JNM, Manolson MF. 2010. VEGF-A expression in osteoclasts is regulated by NF-κB induction of HIF-1α. Journal of Cellular Biochemistry. 110(2):343–351. doi:10.1002/jcb.22542.

Truong Quang B-A, Lenne P-F. 2014. Membrane microdomains: from seeing to understanding. Frontiers in Plant Science. 5. [accessed 2023 May 1]. https://www.frontiersin.org/articles/10.3389/fpls.2014.00018.

Tuszynski GP, Rothman VL, Murphy A, Siegler K, Knudsen KA. 1988. Thrombospondin promotes platelet aggregation. Blood. 72(1):109–115.

Udenwobele DI, Su R-C, Good SV, Ball TB, Varma Shrivastav S, Shrivastav A. 2017. Myristoylation: An Important Protein Modification in the Immune Response. Front Immunol. 8:751. doi:10.3389/fimmu.2017.00751.

Vélot L, Lessard F, Bérubé-Simard F-A, Tav C, Neveu B, Teyssier V, Boudaoud I, Dionne U, Lavoie N, Bilodeau S, et al. 2021. Proximity-dependent Mapping of the Androgen Receptor Identifies Kruppel-like Factor 4 as a Functional Partner. Molecular & Cellular Proteomics. 20:100064. doi:10.1016/j.mcpro.2021.100064.

Volpert OV, Zaichuk T, Zhou W, Reiher F, Ferguson TA, Stuart PM, Amin M, Bouck NP. 2002. Inducer-stimulated Fas targets activated endothelium for destruction by anti-angiogenic thrombospondin-1 and pigment epithelium-derived factor. Nat Med. 8(4):349–357. doi:10.1038/nm0402-349.

Walia A, Yang JF, Huang Y, Rosenblatt MI, Chang J-H, Azar DT. 2015. Endostatin's Emerging Roles in Angiogenesis, Lymphangiogenesis, Disease, and Clinical Applications. Biochim Biophys Acta. 1850(12):2422–2438. doi:10.1016/j.bbagen.2015.09.007.

Wang D, Huang HJ, Kazlauskas A, Cavenee WK. 1999. Induction of vascular endothelial growth factor expression in endothelial cells by platelet-derived growth factor through the activation of phosphatidylinositol 3-kinase. Cancer Res. 59(7):1464–1472.

Wang J, Li Y. 2019. CD36 tango in cancer: signalling pathways and functions. Theranostics. 9(17):4893–4908. doi:10.7150/thno.36037.

Wei R, Wu Q, Ai N, Wang L, Zhou M, Shaw C, Chen T, Ye RD, Ge W, Siu SWI, et al. 2021. A novel bioengineered fragment peptide of Vasostatin-1 exerts smooth muscle pharmacological activities and anti-angiogenic effects via blocking VEGFR signalling pathway. Comput Struct Biotechnol J. 19:2664–2675. doi:10.1016/j.csbj.2021.05.003.

Welch DR, Hurst DR. 2019. Defining the Hallmarks of Metastasis. Cancer Res. 79(12):3011–3027. doi:10.1158/0008-5472.CAN-19-0458.

Welch S, Spithoff K, Rumble RB, Maroun J. 2010. Bevacizumab combined with chemotherapy for patients with advanced colorectal cancer: a systematic review. Annals of Oncology. 21(6):1152–1162. doi:10.1093/annonc/mdp533.

White NJ. 2022. Severe malaria. Malaria Journal. 21(1):284. doi:10.1186/s12936-022-04301-8.

Wickström SA, Alitalo K, Keski-Oja J. 2002. Endostatin Associates with Integrin α5β1 and Caveolin-1, and Activates Src via a Tyrosyl Phosphatase-dependent Pathway in Human Endothelial Cells1. Cancer Research. 62(19):5580–5589.

Wolven A, Okamura H, Rosenblatt Y, Resh MD. 1997. Palmitoylation of p59fyn is reversible and sufficient for plasma membrane association. Mol Biol Cell. 8(6):1159–1173. doi:10.1091/mbc.8.6.1159.

Xiong Z, Lo HP, McMahon K-A, Martel N, Jones A, Hill MM, Parton RG, Hall TE. 2021. In vivo proteomic mapping through GFP-directed proximity-dependent biotin labelling in zebrafish. Solnica-Krezel L, White RM, Solnica-Krezel L, Major BM, editors. eLife. 10:e64631. doi:10.7554/eLife.64631.

Xu J, Kurup P, Foscue E, Lombroso PJ. 2015. Striatal-enriched protein tyrosine phosphatase regulates the PTPα/Fyn signalling pathway. J Neurochem. 134(4):629–641. doi:10.1111/jnc.13160.

Xu X, Mao W, Chen Q, Zhuang Q, Wang L, Dai J, Wang H, Huang Z. 2014. Endostar, a Modified Recombinant Human Endostatin, Suppresses Angiogenesis through Inhibition of Wnt/β-Catenin Signalling Pathway. PLOS ONE. 9(9):e107463. doi:10.1371/journal.pone.0107463.

Xue Q, Nagy JA, Manseau EJ, Phung TL, Dvorak HF, Benjamin LE. 2009. Rapamycin Inhibition of the Akt/mTOR Pathway Blocks Select Stages of VEGF-A164–Driven Angiogenesis, in Part by Blocking S6Kinase. Arteriosclerosis, Thrombosis, and Vascular Biology. 29(8):1172–1178. doi:10.1161/ATVBAHA.109.185918.

Yamaoka T, Kusumoto S, Ando K, Ohba M, Ohmori T. 2018. Receptor Tyrosine Kinase-Targeted Cancer Therapy. Int J Mol Sci. 19(11):3491. doi:10.3390/ijms19113491.

Yang L. 2023. Proximity labelling reveals a BIN2 signalling network. The Plant Cell. 35(3):958–959. doi:10.1093/plcell/koad006.

Yao L, Pike SE, Setsuda J, Parekh J, Gupta G, Raffeld M, Jaffe ES, Tosato G. 2000. Effective targeting of tumour vasculature by the angiogenesis inhibitors vasostatin and interleukin-12. Blood. 96(5):1900–1905. doi:10.1182/blood.V96.5.1900.

Yoshizuka N, Chen RM, Xu Z, Liao R, Hong L, Hu W-Y, Yu G, Han J, Chen L, Sun P. 2012. A Novel Function of p38-Regulated/Activated Kinase in Endothelial Cell Migration and Tumour Angiogenesis. Mol Cell Biol. 32(3):606–618. doi:10.1128/MCB.06301-11.

Zafra F, Piniella D. 2022. Proximity labelling methods for proteomic analysis of membrane proteins. Journal of Proteomics. 264:104620. doi:10.1016/j.jprot.2022.104620.

Zech T, Ejsing CS, Gaus K, de Wet B, Shevchenko A, Simons K, Harder T. 2009. Accumulation of raft lipids in T-cell plasma membrane domains engaged in TCR signalling. EMBO J. 28(5):466–476. doi:10.1038/emboj.2009.6.

Zeng Y, Tao N, Chung K-N, Heuser JE, Lublin DM. 2003. Endocytosis of oxidized low density lipoprotein through scavenger receptor CD36 utilizes a lipid raft pathway that does not require caveolin-1. J Biol Chem. 278(46):45931–45936. doi:10.1074/jbc.M307722200.

Zhang K, Li M, Yin L, Fu G, Liu Z. 2020. Role of thrombospondin-1 and thrombospondin-2 in cardiovascular diseases (Review). Int J Mol Med. 45(5):1275–1293. doi:10.3892/ijmm.2020.4507.

Zhuo Y, Robleto VL, Marchese A. 2023. Proximity Labelling to Identify β-Arrestin1 Binding Partners Downstream of Ligand-Activated G Protein-Coupled Receptors. International Journal of Molecular Sciences. 24(4):3285. doi:10.3390/ijms24043285.

Chapter 2: Methods and Materials

2.1 Materials

2.1.1 Cell Culture

Human telomerase (hTERT)-immortalized microvascular endothelial cells isolated from human foreskin (TIME (ATCC® CRL-4025)) expressing mEmerald-CD36 or HaloTag(HT)-CD36 were cultured in Vascular Cell Basal Medium (ATCC® PCS-100-030) supplemented with Microvascular Endothelial Cell Growth Kit-VEGF (ATCC® PCS-110-041), 0.5mg/ml Penicillin/Streptomycin, 0.5mg/ml G418, 12.5ug/ml blasticidin, and 1ug/mL puromycin and grown at 37°C in 5%CO2 atmosphere.

2.1.2 Generation of Stable TIME Cell Lines

Lentiviral transduction was used to generate stable TIME cell lines expressing HaloTag (HT)-CD36 or mEmerald-CD36 under the control of a tetracycline-inducible promoter. HT-CD36 and mEmerald-CD36 were first cloned into transfer vector pLVX. HEK293T cells were transfected in parallel with pMD2G (encoding the VSV-G envelope protein), pCMVR8.74 (encoding HIV-1 Gag, Pol, Tat and Rev proteins) and either pLVX-mEmerald/HT-CD36 (transfer vector with mEmerald-CD36 or HT-CD36) or pLVX-Tet3G (transfer plasmid containing the tetracycline-dependent transactivator, rtTA). Media containing viral particles were harvested after 48h, filtered (0.45µm pore size) and mixed with 10µg/mL polybrene. To generate the tetracycline-inducible TIME cell lines, both (pLVX-mEmerald/HT-CD36 and pLVX-Tet3G) viral supernatants were added to TIME cells at 50% confluency and incubated for 72h before applying 0.5 µg/mL of G418 (resistance gene contained in pLVX-Tet3G) and 2 µg/mL of puromycin (resistance gene for mEmerald/HT-CD36). After two weeks of selection, surviving cells were collected and plated in parallel on coverslips to evaluate the inducible expression of mEmerald-CD36. Stable cell lines were created by Dr. Nicolas Touret.

2.1.3 Generation of TIME CD9 and ITGB1 shRNA Knockdown Stable Cell Lines

Lentiviral transduction was used to generate TIME HT-CD36 and TIME mEmerald-CD36 constitutively expressing ITGB1 or CD9 shRNA. Plasmids expressing scrambled, ITGB1 or CD9 shRNA were cloned into a pLV vector under the control of a constitutively active U6 promoter (VectorBuilder Inc., IL, USA). HEK293T cells were transfected in parallel with pMD2G (encoding the VSV-G envelope protein), pCMVR8.74 (encoding HIV-1 Gag, Pol, Tat, and Rev proteins), and pLV-scrambled/CD9/ITGB1-shRNA transfer vector. Media containing viral particles were harvested after 48h, filtered (0.45µm pore size), and mixed with 10µg/mL polybrene. To generate the scrambled shRNA, CD9 shRNA, or ITGB1 shRNA knockdown (KD) cell lines, TIME HT-CD36, mApple-CD36, and TIME mEmerald-CD36 were transduced at 70% confluency for 48 hours with lentiviruses containing plasmids expressing scrambled, CD9 or ITGB1 shRNA. Following the transduction period, cells were incubated with TIME cell media supplemented with 0.2mg/mL hygromycin (resistance gene for scrambled/CD9/ITGB1-shRNA). After 1 week of selection, surviving cells were collected and their lysate was analyzed via immunoblotting to confirm candidate protein KD.

2.2 Cell Handling

2.2.1 Mouse anti-IgM Stimulation

Cells were serum starved for 3 hours in MBCD-131 media (Gibco, ThermoFisher, Waltman, MA, USA). Following serum starvation, cells were stimulated with 10µg/mL mouse anti-IgM (Santa Cruz Biotechnology, Dallas, TX, USA) for 15 minutes.

2.3 Biochemistry

2.3.1 Immunoblotting

Lysates from the CD36 BAR and shRNA KD experiments were resolved on 10% SDS-PAGE for 1hr at 150V. Proteins were transferred to nitrocellulose membranes for 1 hour at 110V

and then blocked using 3% BSA dissolved in Tris Buffered Saline Tween (TBST) at room temperature for 45 minutes. Membranes were incubated overnight with primary antibody solution at 4°C (Table 2-1). Following primary antibody incubation, membranes were washed three times with TBST and then incubated with secondary antibody solutions for 1 hour at room temperature (Table 2-1). Membranes were visualized using Li-Cor Odyssey (Li-Cor Bioscience, Lincoln, NE, USA).

Table 2-1: List of primary and secondary antibodies utilized for immunoblot experiments.

Primary Antibodies	Specificity	Species	Concentration	Provider	Catalog no.
Anti-GFP antibody	GFP	Rabbit	1:1000	Abcam	ab290
Anti-HaloTag	HaloTag	Rabbit	1:1000	Promega	
Actin Antibody (I-19)	Actin	Rabbit	1:1000	Santa Cruz Biotechnologies	sc-1616
Recombinant Anti-CD9 antibody [EPR23105-125]	CD9	Rabbit	1:1000	Abcam	ab263019
Anti-Integrin beta-1 antibody [12G10]	Integrin beta-1	Mouse	1:1000	Abcam	ab30394
Alpha-Tubulin Antibody	Tubulin	Mouse	1:1000	Rockland	200-301-880
Anti-alpha Tubulin	Tubulin	Rabbit	1:5000	Abcam	Ab18251
Secondary antibodies	Specificity	Species	Concentration	Provider	Catalog no.
Steptavidin IRDye 680RD	Biotin	N/A	1:5000	Licor Biosciences	926-68079

IRDye 680RD anti-Rabbit IgG	anti-Rabbit IgG	Donkey	1:2500	Licor Biosciences	926-68073
IRDye 680RD anti-Mouse IgG	anti-Mouse IgG	Donkey	1:2500	Licor Biosciences	926-32222
IRDye 800RD anti-Rabbit IgG	anti-Rabbit IgG	Donkey	1:2500	Licor Biosciences	926-32213
IRDye 800RD anti-Mouse IgG	anti-Mouse IgG	Donkey	1:2500	Licor Biosciences	926-32212

2.3.2 CD36 Biotinylation by Antibody Recognition (BAR)

TIME-mEmerald-CD36 cells were grown to ~80-90% confluency in 6 cm tissue culture dishes or coverslips and induced with 0.5µg of doxycycline for 18 hours prior to performing CD36 BAR. Cells were fixed with 4% PFA (Electron Microscopy Sciences, Hatfield, PA, USA) for 20 minutes on ice and then for 5 minutes at room temperature. Following fixation, 1mL of 3% BSA was added to the cells for 1 hour at room temperature. Subsequently, 1mL of`1:1000 mouse anti-CD36 was added for 1 hour at room temperature. Cells were then washed three times with PBS. 1mL of Goat anti-mouse FAB conjugated to HRP (Rockland, Baltimore, MD, USA) was diluted 1:1000 and incubated with the cells for 1 hour at room temperature. Following three washes with PBS, Biotin-XX-tyramide (Biotium, San Franscisco, CA, USA) diluted 1:1000 in the tyramide amplification buffer (Biotium, San Franscisco, CA, USA) was added to cells for 10 minutes at room temperature. Cells were protected from light, as the tyramide reaction is light sensitive. Following the reaction, cells were washed three times with PBS.

For analysis of cell lysate via immunoblot, biotin amplification buffer was aspirated and replaced with lysis buffer (150mM NaCl, 50mM Tris-HCl at pH 7.2, 0.2% SDS, 1% Triton X-100, protease inhibitor cocktail) for 30 min on ice. Cell homogenate was harvested using a cell scrapper

and centrifuged at 14,000 RPM for 20 minutes at 4°C. A fraction of the supernatant was kept as whole-cell lysate; the remaining supernatant was kept for streptavidin capture.

For analysis via microscopy, coverslips were incubated for 1 hour with AF 647 streptavidin (Jackson Immunoresearch, Philadelphia, PA, USA) and donkey-anti mouse Cy3 (Jackson Immunoresearch, Philadelphia, PA, USA) diluted 1:500 in 3% bovine serum albumin (BSA). Subsequently, cells were washed three times in PBS and post-fixed with 4% PFA (Electron Microscopy Sciences, Hatfield, PA, USA) for 10 minutes at room temperature. Cells treated with CD36 BAR were imaged via widefield microscopy.

2.3.3 Cell Surface Biotinylation

TIME-mEmerald-CD36 cells were grown to ~80-90% confluency in 6 cm tissue culture dishes or coverslips and induced with 0.5µg/mL of doxycycline for 18 hours prior to biotinylation. Cells were washed twice with a borate buffer (10mM Boric Acid, 154nM NaCl, 7.2mM KCl, 1.8mM, pH 8.3). Following washes, 1mL of Sulfo-NHS-Sulfosuccinimidobiotin (ThermoFisher, Waltman, MA, USA) dissolved in borate buffer (0.5mg/mL) was added to the cells for 15 min at 16°C. After a second incubation with 1mL of Sulfo-NHS-Sulfosuccinimidobiotin (0.5mg/mL), cells were rinsed three times with 500uL of quenching buffer (Borate Buffer complemented with 100mM Glycine and 50 mM Tris-base). Cells were processed for immunostaining or lysed in the same manner as CD36 BAR experiments.

2.3.4 Streptavidin Capture and Tandem Mass Spectrometry

CD36 BAR lysate, Pierce Streptavidin Magnetic Beads (ThermoFisher, Waltman, MA, USA) and lysis buffer were added to a deep 96 well plate (ThermoFisher, Waltman, MA, USA). The KingFisher Duo Prime System Purification System incubated the streptavidin beads with CD36 BAR lysate for 18 hours at 4°C. Following streptavidin capture, beads were transferred to a second plate containing 100 mM NH_4CO_3, 50 mM iodoacetamide and 100 mM dithiothreitol (DTT).

Streptavidin beads were incubated in 10 mM DTT to reduce biotinylated proteins. Biotinylated proteins were subsequently alkylated in 50 mM iodoacetamide and then washed with 100 mM NH_4CO_3. Finally, proteins were trypsinized with trypsin dissolved in mass spectrometry grade H_2O and digested off of streptavidin beads for 8 hours. Reduction, alkylation and trypsinization were all performed at 37°C.

Trypsinized peptides were transferred to 1.5mL tubes and concentrated using speed-vacuum evaporation. Trypsinized peptides were desalted using Thermo Scientific Pierce C18 Spin tips per the manufacturer's instructions (ThermoFisher, Waltman, MA, USA). 2µg of digested protein was analyzed with a 60-minute gradient using the Orbitrap Fusion Lumos Tribrid Mass Spectrometer. Output from LC-MS/MS includes peptide spectral matched (PSM), number of peptides, and protein intensity. PSM describes the total number of peptides identified that match a protein sequence, whereas the number of peptides describes the indicates number of unique peptides identified for a protein ("Proteome Discoverer User Guide"). Protein intensity is the sum of the signal intensity for all the peptides corresponding to an identified protein (Vogel and Marcotte, 2009).

2.3.5 F-actin Fractionation

TIME-mEmerald-CD36 cells were grown to ~90% confluency in 6 well plates and induced with 0.5ug of doxycycline for 18 hours prior to performing F-actin separation. After aspirating TIME cell media, cells were lysed using warm 250µL of cytoskeleton stabilizing buffer (50 mM PIPES at pH 6.9, 50 mM NaCl, 5 mM MgCl2, 5 mM EGTA, 5% (v/v) Glycerol, 0.1% Nonidet P40, 0.1%Triton X-100, 0.1% Tween 20, 0.1% 2-mercapto-ethanol) supplemented with 1 mM ATP solution and 1X protease inhibitor cocktail. Cell homogenate was collected using a cell scraper, and then mixed by pipetting up and down 8-10 times. Following mixing, cell lysate was incubated at 37°C for 10 min. Cells were later centrifuged at 2000 RPM at room temperature for 5 min to pellet unbroken cells. 50µL was of the cell lysate was saved before proceeding to

ultracentrifugation. The remaining 200µL was ultracentrifuged at 200,000g at room temperature for 1 hour. Following, Eppendorf tubes were immediately placed on ice. The G-actin fraction (supernatant) was saved in a separate Eppendorf tube, and the remaining F-actin pellet then was depolymerized using F-actin depolymerization buffer (140 mM NaCl, 20 mM Tris at pH 7.2, 2 mM EGTA, 10 µM Cytochalsin B) accompanied by 1X protease inhibitor and 1% Triton X-100 on ice for 1 h. F- and G-actin fraction were then analyzed via immunoblotting.

2.4 Immunofluorescence

2.4.1 Duolink Proximity Ligation Assay Immunostaining Protocol

TIME-mEmerald-CD36 cells were grown to 80% confluency on coverslips and induced with 0.5µg of doxycycline for 18 hours prior to performing Proximity ligation assay (PLA). After 18 hours, cells were fixed using 4% paraformaldehyde (Electron Microscopy Sciences, Hatfield, PA, USA) for 15 minutes on ice and then 5 minutes at room temperature.

Following fixation, cells were washed three times with PBS and stained with lectin-binding protein concanavalin A Alexa-Fluor (AF) 488 (ThermoFisher, Waltman, MA, USA). By binding to terminal α-D-mannosyl and α-D-glucosyl residues of N-glycosylated proteins, concanavalin, A AF488 provides a cell mask used for quantification of PLA images (Kiernan, 1975). 10ug of concanavalin A AF488 dissolved was 3% bovine serum albumin (Equitech-BioInc, Kerrville, TX, USA) was added to each coverslip and incubated for 30 minutes.

Cells are washed three times with PBS to remove unbound concanavalin A AF488, then permeabilized with 3% BSA + 0.1% Triton X-100 (Avantor, Radnor, PN, USA) for 30 minutes at room temperature. Cells were subsequently washed with PBS once, and two drops of Duolink blocking solution (1% BSA) (Millipore Sigma, Burlington, MA, USA) were added to each coverslip to block for 45min at 37°C. Following blocking, primary antibodies were diluted in the Duolink blocking solution and added to coverslips for 1-hour incubation at room temperature (Table 2-2).

To remove unbound primary antibodies, Coverslips were washed two times with Wash Buffer A (50mM NaCl, Tris-base 10mM, tween 0.05%, pH 7.4) for 5 minutes each at room temperature. PLA donkey-anti-rabbit PLUS and donkey-anti-mouse MINUS probes were diluted 1:5 in Duolink blocking solution, and 40uL of the antibody solution was added to each coverslip for 1 hour at 37°C (ThermoFisher, Waltman, MA, USA).

Coverslips were washed twice with Wash Buffer A for 5 minutes each at room temperature. For probe ligation, Ligation Stock Buffer (Millipore Sigma, Burlington, MA, USA) was diluted 1:5 in double distilled water, and Ligase (Millipore Sigma, Burlington, MA, USA) from the PLA kit was added at a 1:40 dilution to the diluted ligase solution. 40uL of the diluted Ligase solution was added to each coverslip and incubated at 37°C for 30 minutes.

Following the incubation, coverslips were washed twice with Wash Buffer A for 5 minutes at room temperature. For amplification, Amplification Stock Buffer (Millipore Sigma, Burlington, MA, USA) was diluted 1:5 in double distilled water, and Polymerase (Millipore Sigma, Burlington, MA, USA) from the PLA kit was added 1:80 to the diluted amplification solution. 40uL of the diluted amplification buffer was added to each coverslip and incubated at 37°C for 100 minutes.

Coverslips were washed twice with Wash Buffer B (100mM NaCl, 35mM Tris -base, Tris-HCl 215mM, pH 7.4) for 10 minutes at room temperature. For quantification of PLA, 4′,6-Diamidino-2-phenylindole dihydrochloride, 2-(4-Amidinophenyl)-6-indolecarbamidine (DAPI) (Millipore Sigma, Burlington, MA, USA), was diluted 1:500 in 3% BSA and incubated with coverslips for 30 minutes at room temperature. Coverslips were quickly rinsed twice with Wash Buffer B and then post-fixed using 4% PFA at room temperature for 10 minutes. Finally, cells were washed with 0.01x Wash Buffer B for 1 minute and mounted with Prolong Glass Antifade mounting media (ThermoFisher, Waltman, MA, USA).

Table 2-2: List of primary antibodies utilized in PLA experiments.

Primary Antibodies	Specificity	Species	Concentration	Provider	Catalog No.
Purified anti-human CD9 Antibody	CD9	Mouse	1:1000	Biolegend	312102
Anti-CD36	CD36	Mouse	1:1000	N/A	N/A
Anti-human CD59	CD59	Mouse	1:1000	Biolegend	304702
Anti-Cd146 antibody	CD146	Mouse	1:1000	Abcam	ab24577
Anti-CD151 antibody	CD151	Mouse	1:500	Abcam	ab33315
Anti-GFP antibody	GFP	Rabbit	1:1000	Abcam	ab290
Anti-GFP antibody	GFP	Mouse	1:1000	Abcam	ab1218
Human EPCR Antibody	Endothelial Protein Receptor C	Mouse	1:200	R&D Systems	MAB22451-SP
Anti-Integrin beta-1 antibody [12G10]	Integrin beta-1	Mouse	1:1000	Abcam	ab30394
Anti-Mitofilin antibody [2E4AD5]	Mitofilin	Mouse	1:1000	Abcam	ab110329
Recombinant Anti-Myoferlin antibody [EPR18887]	Myoferlin	Rabbit	1:200	Abcam	ab178386
Anti-PTP1B antibody [4F8F11]	Protein tyrosine phosphatase 1B	Mouse	1:100	Abcam	ab201974
Anti-RAB1B antibody	Ras-related protein Rab-1B	Mouse	1:100	Abcam	ab234717
Anti-Stomatin antibody	Stomatin	Rabbit	1:200	Abcam	ab169524

2.4.2 TIME HT-CD36 IgM Stimulation and Immunostaining Protocol

TIME HT-CD36 cells, and TIME HT-CD36 cells expressing CD9, ITGB1, and scrambled shRNA were grown to 50-60% confluency on coverslips and incubated with 0.5µg of doxycycline for 18 hours, and then serum starved for 3 hours in MBCD-131 media (Gibco, ThermoFisher, Waltman, MA, USA). Following serum starvation, TIME HT-CD36 were stimulated with 10µg/mL mouse anti-IgM (Santa Cruz Biotechnology, Dallas, TX, USA) for 15 minutes at 37°C. For our negative control, TIME HT-CD36 were incubated with MBCD-131 media without mouse anti-IgM (Santa Cruz Biotechnology, Dallas, TX, USA). Cells were fixed using 4% PFA (Electron Microscopy Sciences, Hatfield, PA, USA) for 15 minutes at room temperature. Following fixation, cells were washed three times with PBS and then permeabilized with ice-cold PBS + 0.1% Triton X-100 (Avantor, Radnor, PN, USA) for 10 minutes. Coverslips were subsequently blocked using 3% BSA (Equitech-BioInc, Kerrville, TX, USA) dissolved in PBS for 1 hour at room temperature. Rabbit anti-phospho-SRC (Tyr419) Polyclonal Antibody (ThermoFisher, Waltman, MA, USA) diluted 1:100 in 3% BSA (Equitech-BioInc, Kerrville, TX, USA) and added to coverslips for 1 hour at room temperature. Cells were washed three times with PBS and then incubated with AF 488 AffiniPure Anti-Rabbit IgG (H+L) (Rockland, Baltimore, MD, USA) and Invitrogen™ AF 568 Phalloidin diluted 1:500 (Waltham, Massachusetts, USA) for 1 hour. Subsequently, coverslips were washed three times in PBS and post-fixed with 4% PFA (Electron Microscopy Sciences, Hatfield, PA, USA) for 10 minutes at room temperature. Finally, coverslips were washed three times in PBS and then imaged via Total Internal Reflection Fluorescence microscopy (TIRFm).

2.4.3 Conditional Colocalization Immunofluorescence Staining and Analysis

TIME CD36-HT cells were grown to 50-60% confluency on coverslips and incubated with 0.5µg of doxycycline for 18 hours prior to immunostaining. JFX549-HaloTag ligand was diluted to 0.25nM in MBCD-131 media (Gibco, ThermoFisher, Waltman, MA, USA) and added to cells for 15 minutes incubation at 37°C. For CD36 stimulation experiments, the live cell labelling solution

was supplemented with 10µg/ml of mouse anti-CD36 IgM (Santa Cruz Biotechnology, Dallas, TX, USA). Cells were fixed using 4% PFA (Electron Microscopy Sciences, Hatfield, PA, USA) for 15 minutes at room temperature. Following fixation, cells were washed three times with PBS and then permeabilized with ice-cold PBS + 0.1% Triton X-100 (Avantor, Radnor, PN, USA) for 10 minutes. Coverslips were subsequently blocked using 3% BSA (Equitech-BioInc, Kerrville, TX, USA) dissolved in PBS for 1 hour at room temperature. Primary antibodies were diluted in 3% BSA (Equitech-BioInc, Kerrville, TX, USA) and added to coverslips for 1 hour at room temperature (Table 2-3). Cells were washed three times with PBS and then incubated with secondary antibodies diluted in 3% BSA (Table 2-3). After three washes with PBS, cells were incubated with primary antibodies conjugated to fluorescent dyes for 1 hour at room temperature (Table 2-3). Subsequently, coverslips were washed three times in PBS and post-fixed with 4% PFA (Electron Microscopy Sciences, Hatfield, PA, USA) for 10 minutes at room temperature. Finally, coverslips were washed three times in PBS and then imaged via Total Internal Reflection Fluorescence microscopy (TIRFm).

Table 2-3: List of all primary and secondary antibodies used in conditional colocalization experiments.

Primary Antibodies	Specificity	Species	Concentration	Provider	Catalog No.
Anti-Integrin beta 1 antibody [12G10] (Alexa Fluor® 488)	ITGB1	Mouse	1:20,000	Abcam	ab202641
Recombinant Alexa Fluor® 488 Anti-CD9 antibody [EPR23105-121]	CD9	Rabbit	1:10,000	Abcam	Ab267502

Recombinant Alexa Fluor® 647 Anti-CD9 antibody [EPR23105-121]	CD9	Rabbit	1:10,000	Abcam	ab267503
Phospho-SRC (Tyr419) Polyclonal Antibody, Alexa Fluor 488	Src phosphorylated at Y419	Rabbit	1:1000	Thermo Fisher Scientific	44-660A1
Secondary Antibodies	Specificity	Species	Concentration	Provider	Catalog No.
AF 488 AffiniPure Anti-Rabbit IgG (H+L)	anti-Rabbit IgG	Donkey	1:500	Jackson ImmunoResearch	711-545-152

2.5 Image Analysis Methods

2.5.1 Quantification of PLA Dot Density per Cell

PLA images taken in confocal mode of an Olympus IX81 stand using a 60x 1.49 NA objective were loaded into CellProfiler (Stirling et al., 2021). These three colour TIFF images were composed of the DAPI (blue channel), concanavalin A AF488 (green channel), and PLA signal (far red channel). The blue, green and far-red channels were split into greyscale images using the ‘colortogreymodule’. Segmentation of each cell was performed using concanavalin A-AF488 cell mask and the ‘IdentifyObjectManually’ module. The cell masks obtained from the ‘IdentifySecondaryObject’ were converted to binary images. The integrated intensities for the binary images were determined using the ‘MeasureObjectIntensity’ module. Pixels containing the cell masks were given intensities of 1 in the binary image, and therefore the integrated intensities allowed us to determine the area, in pixels, of each cell.

The module 'IdentifyPrimaryObject' was utilized to segment and count the number of PLA dots in each image. Minimum Cross-Entropy thresholding was used in segmenting PLA dots. Minimum Cross-entropy algorithm assigns a thresholding value for each pixel, which minimizes the probability of misclassifying the background or foreground. The number of PLA dots per cell was determined using the cell mask obtained from the 'IdentifySecondaryObject' module.

Segmented images were saved using the 'Save Images' module. Finally, the number of PLA dots per cell and the area of each cell were exported using the 'ExportToSpreadsheet' module. To normalize for cell size, the density of PLA dots per cell was calculated using the following equation:

$$Density\ of\ PLA\ dots\ per\ Cell = \frac{Number\ of\ PLA\ dots\ per\ Cell}{Area\ of\ cell\ in\ pixels} \quad \textbf{Equation (1)}$$

For statistical comparisons of PLA experiments, a Krushkal-Wallis test non-parametric ANOVA test was performed followed by a Dunn's post hoc test (Kruskal and Wallis 1952; Dunn, 1964). p-values were adjusted using Bonferroni correction (Etymologia, 2015). An α-value of 0.05 was chosen for significance.

2.5.2 Quantification of Density of P-Y420-Fyn Intensity per Cell

Fyn activation TIRFm images were taken using a 100x, 1.45 numeral aperture oil objective lens and loaded into a customized quantification pipeline developed in CellProfiler. Two color TIFF 16-bit images were composed of the phalloidin 568 (red channel) and rabbit anti-Phospho-SRC (Tyr419) Polyclonal Antibody (green channel). The green and far-red channels were split into greyscale images using the 'colortogreymodule'. Segmentation of each cell was performed using phalloidin 568 and the 'IdentifyObjectManually' module. The area of the cell masks obtained from 'IdentifyObjectManually' were measured using the 'MeasureImageAreaOccupied' module.

The determine the total intensity of activated Fyn, we inputted the rabbit anti-Phospho-SRC (Tyr419) Polyclonal Antibody (green channel) into the "MeasureImageAreaOccupied" module.

Finally, the total intensity of activated Fyn and the area of each cell were exported using the 'ExportToSpreadsheet' module. To normalize for cell size, the density of activated Fyn intensity per cell was calculated using the following equation:

$$Density\ of Activated\ Fyn\ Intensity\ per\ Cell = \frac{Total\ Activated\ Fyn\ Intensity}{Area\ of\ cell\ in\ pixels}$$ **Equation (2)**

For statistical comparisons of CD36 stimulation experiments, a non-parametric T-test was performed (Welch, 1947). An α-value of 0.05 was chosen for significance.

2.5.3 Conditional Colocalization Analysis

Conditional colocalized images were analyzed using the conditional colocalization package developed by Vega-Lugo et al. (2022). Three color TIFF images were saved into a movie list. Channels were assigned to three groups: 'target,' 'reference,' or 'condition' (Figure 2-1). The 'point-source detection' particle detection algorithm was implemented to determine the center coordinates of the punctate objects (Table 2-5). Objects were determined to colocalize if the distance between the centers of two punctate objects was ≦ 1 pixel. The region of interest for each image was determined manually using the freehand draw tool. Wilcoxon rank sum test (or Mann-Whitney U test) was used to determine the statistical significance (Pratt, 1959). Thresholds for three molecular colocalization significance were calculated using Dunn-Sidak correction (Dunn, 1964; Sidak, 1967). For statistical comparison of conditional colocalization values between unstimulated and stimulated treatments a non-parametric T-test was performed (Welch, 1947). An α-value of 0.05 was chosen for significance for all conditional colocalization comparisons. To learn more about the conditional colocalization method, refer to Vega-Lugo et al. (2022).

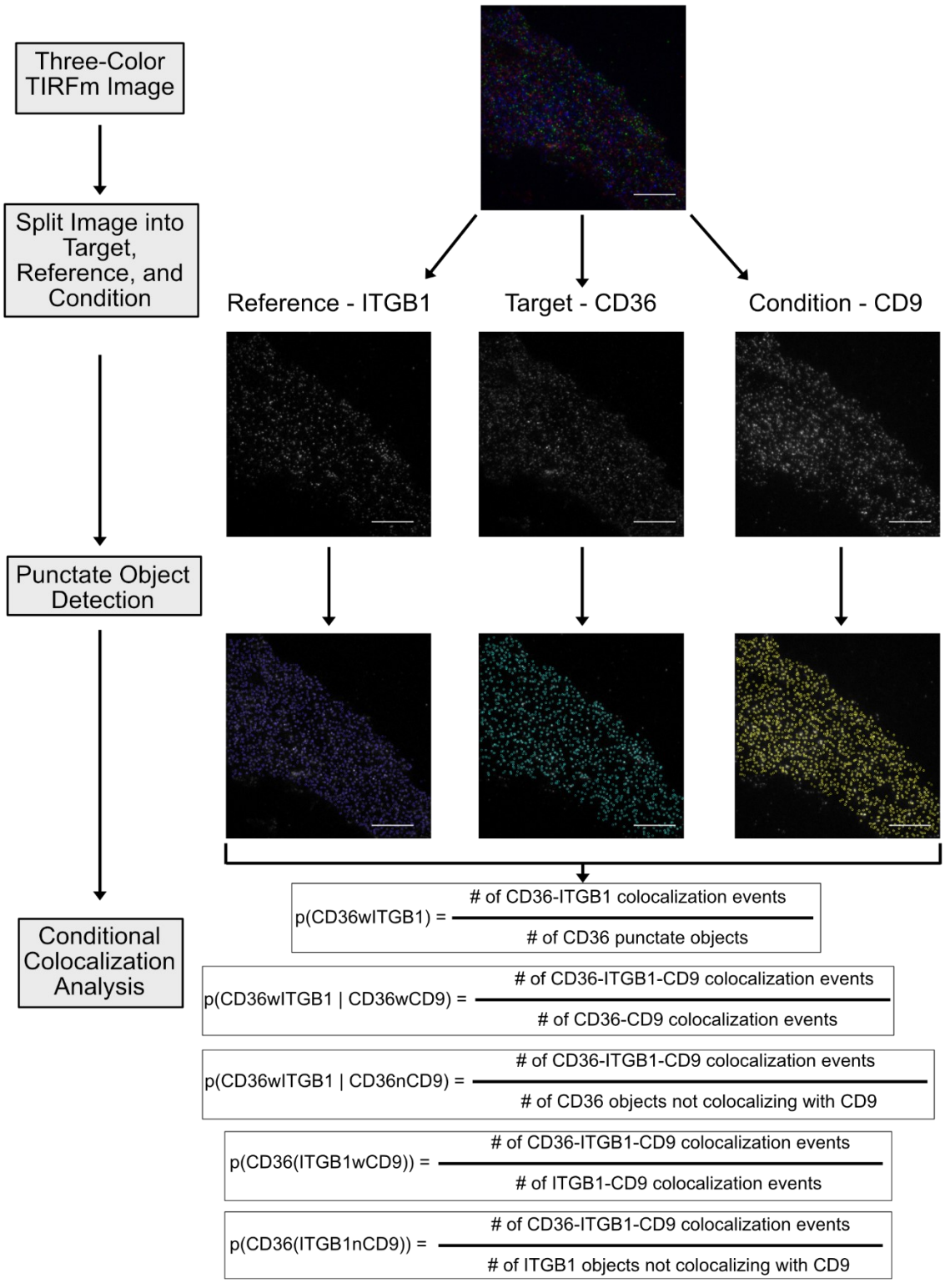

Figure 2-1: Conditional colocalization analysis workflow.

Three-color TIRFm images are split into three groups: target, reference, and condition. In this example, we denote CD36 as the target, ITGB1 as the reference, and CD9 as the condition. The puncta present in each channel is detected using a point source detection algorithm (see table 2.4 for parameters used for object detection). After object detection,

conditional colocalization analysis was performed with a colocalization radius of 2 pixels. Conditional colocalization provides three measures p(CD36wITGB1), p(CD36wITGB1 | CD36wCD9) and p(CD36(ITGB1wCD9)) to determine the effect of CD9 on CD36's colocalization with ITGB1.

Table 2-4: Description of output obtained from conditional colocalization analysis.

Conditional Colocalization Fractions	Description
p(TwR)	Fraction of target objects colocalizing with a reference object
p(TwR | TwC)	Fraction of target-condition colocalization events colocalizing with reference objects
p(TwR | TnC)	Fraction of target objects not colocalizing with the condition which colocalize with reference objects
p^{rs}(Tw(RwC)	Fraction of reference-condition colocalizing events that also colocalize with the target
p^{rs}(Tw(RnC)	Fraction of reference objects not colocalizing with the condition which colocalize with the target

Table 2-5: The α-values and point spread function-σ used for point source detection of CD36, ITGB1, CD9, P-Y420-Fyn, and TfR.

Protein	α-value	point spread function-σ
CD36	0.01	1.4
ITGB1	0.05	1.2
CD9	0.05	1.31619
P-Y420-Fyn	0.1	1.2
TfR	0.05	1.31619

2.6 Microscopy

2.6.1 Confocal Imaging

Confocal imaging was completed on the confocal mode of an Olympus IX81, equipped with Diskovery module (Quorum Technologies, Guelph, Canada). Acquisition was performed using a

60x, 1.49 numerical object oil object with a Hamamatsu EM-CDD camera (ImageEM91013, Hamamatsu) using Volocity software (Quorum Technologies, Guelph, Canada). A pinhole size of 50µm was utilized for all confocal images.

2.6.2 TIRFm Imaging

Total Internal Reflection microscopy (TIRFm) images were captured on an Olympus IX-81 motorized inverted base installed by Quorum Technologies (Guelph, ON, Canada). Acquisition was performed using a 100x, 1.45 numeral aperture oil objective lens with a Hamamatsu EM-CDD camera (ImageEM91013, Hamamatsu) using Volocity software (Quorum Technologies, Guelph, Canada).

2.6.3 Widefield Imaging

Widefield imaging was performed in widefield mode of an Olympus IX81 stand equipped with Diskovery module. Aquisition was performed using a 60x, 1.49 numerical object oil object with a Hamamatsu EM-CDD camera (ImageEM91013, Hamamatsu) using Volocity software (Quorum Technologies, Guelph, Canada).

2.7 Graphical Representation and Statistical Analysis

Data from PLA, conditional colocalization, and CD36-IgM stimulation experiments were displayed using boxplots. The median of the data set is represented by the central line (Figure 2-2). Above and below the median line are notches indicating the 95% confidence interval of the median line (Figure 2-2). The edges of the boxplot represent the 25^{th} and 75^{th} percentiles and the whiskers display the maximum and minimum data points that were not outliers' line (Figure 2-2). Data points outside the whiskers of the boxplot are considered outliers line (Figure 2-2). For PLA, CD36 stimulation, and conditional colocalization experiments statistical and graphical analysis was pre-formed using SciPy (Virtanen et al., 2020). Graphing and statistics of conditional colocalization data was preformed using MATLAB (MathWorks, Natick, MA, USA).

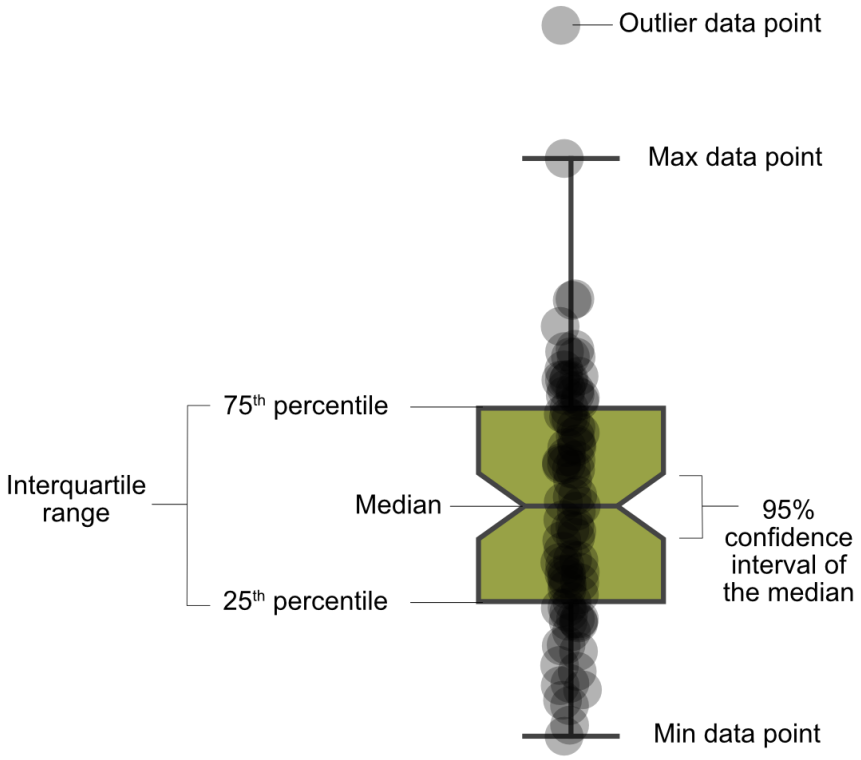

Figure 2-2: Schematic outlining key features of a boxplot.

For each boxplot, the median is indicated with a central line. The two adjacent notches represent the 95% confidence interval of the median, whereas the edges represent the 75th and 25th percentile data points. The colored box indicates the interquartile range. The minimum and maximum data points are outlined by whiskers, and points outside are denoted as outliers.

.

2.8 References

Dunn Olive Jean. 1964. Multiple Comparisons Using Rank Sums. Technometrics. 6(3):241–252. doi:10.1080/00401706.1964.10490181.

Dunn Olive Jean. 1964. Multiple Comparisons Using Rank Sums. Technometrics. 6(3):241–252. doi:10.1080/00401706.1964.10490181.

Etymologia: Bonferroni Correction. 2015. Emerg Infect Dis. 21(2):289. doi:10.3201/eid2102.ET2102.

Fredriksson S, Gullberg M, Jarvius J, Olsson C, Pietras K, Gústafsdóttir SM, Östman A, Landegren U. 2002. Protein detection using proximity-dependent DNA ligation assays. Nat Biotechnol. 20(5):473–477. doi:10.1038/nbt0502-473.

Kiernan JA. 1975. Localization of α-d-glucosyl and α-d-mannosyl groups of mucosubstances with concanavalin A and horseradish peroxidase. Histochemistry. 44(1):39–45. doi:10.1007/BF00490419.

Kruskal WH, Wallis WA. 1952. Use of Ranks in One-Criterion Variance Analysis. Journal of the American Statistical Association. 47(260):583–621. doi:10.1080/01621459.1952.10483441.

Marques PE, Nyegaard S, Collins RF, Troise F, Freeman SA, Trimble WS, Grinstein S. 2019. Multimerization and Retention of the Scavenger Receptor SR-B1 in the Plasma Membrane. Developmental Cell. 50(3):283-295.e5. doi:10.1016/j.devcel.2019.05.026.

Oakley JV, Buksh BF, Fernández DF, Oblinsky DG, Seath CP, Geri JB, Scholes GD, MacMillan DWC. 2022. Radius measurement via super-resolution microscopy enables the development of a variable radii proximity labelling platform. Proceedings of the National Academy of Sciences. 119(32):e2203027119. doi:10.1073/pnas.2203027119.

Pratt JW. 1959. Remarks on Zeros and Ties in the Wilcoxon Signed Rank Procedures. Journal of the American Statistical Association. 54(287):655–667. doi:10.1080/01621459.1959.10501526.

Proteome Discoverer User Guide.

Sidak Z. 1967. Rectangular Confidence Regions for the Means of Multivariate Normal Distributions. Journal of the American Statistical Association. 62(318):626–633. doi:10.2307/2283989.

Stirling DR, Swain-Bowden MJ, Lucas AM, Carpenter AE, Cimini BA, Goodman A. 2021. CellProfiler 4: improvements in speed, utility and usability. BMC Bioinformatics. 22(1):433. doi:10.1186/s12859-021-04344-9.

Vega-Lugo J, da Rocha-Azevedo B, Dasgupta A, Jaqaman K. 2022. Analysis of conditional colocalization relationships and hierarchies in three-color microscopy images. J Cell Biol. 221(7). doi:10.1083/jcb.202106129. [accessed 2023 Apr 3]. https://rupress.org/jcb/article/221/7/e202106129/213216/Analysis-of-conditional-colocalization.

Virtanen P, Gommers R, Oliphant TE, Haberland M, Reddy T, Cournapeau D, Burovski E, Peterson P, Weckesser W, Bright J, et al. 2020. SciPy 1.0: fundamental algorithms for scientific computing in Python. Nat Methods. 17(3):261–272. doi:10.1038/s41592-019-0686-2.

Vogel C, Marcotte EM. 2009. Absolute abundance for the masses. Nat Biotechnol. 27(9):825–826. doi:10.1038/nbt0909-825.

Welch BL. 1947. The generalisation of student's problems when several different population variances are involved. Biometrika. 34(1–2):28–35. doi:10.1093/biomet/34.1-2.28.

Chapter 3: Investigating CD36-Induced Anti-Angiogenic Signalling Platform via Proximity Labelling

3.1 Identification of Potential CD36 Interactors via Biotinylation by Antibody Recognition (BAR)

To identify protein residing within or in proximity to CD36, we employed biotinylation by antibody recognition targeting CD36 (CD36 BAR) on TIME (hTERT Immortalized Microvascular Endothelial cells, page 56) cell lines engineered to express mEmerald-CD36 under the control of a *tet*-on promoter. Following an 18-hour doxycycline induction (0.5µg), we added mouse anti-CD36 IgG antibody to target CD36 on fixed cells, and a secondary antibody conjugated to horseradish peroxidase (HRP, see section 2.3.2 page 59 for detailed protocol) (Figure 3-1, A). The addition of biotin-xx-tyramide and hydrogen peroxide results in the formation of biotin radicals by the peroxidase, which reacts to nearby tyrosine residues within a ~250nM radius (Bar et al., 2018; Oakley et al., 2022; Zafra and Piniella, 2022). To bring the labelling radius closer to the plasma membrane, we reduced the size of the antibody complex by using goat anti-mouse FAB conjugated to HRP instead of a full-size immunoglobulin which is ~3 times smaller. Although the ~250nm labelling radius is larger than CD36's nanocluster size of ~70-90nm (Githaka et al., 2016), CD36 BAR allows for labelling which encapsulates the entire CD36 nanocluster. Candidate proteins outside of the cluster range would be later on ruled out via *in-situ* PLA which detects protein-protein interactions within a ~40nm radius (Alam, 2022). For our negative control treatment, TIME mEmerald-CD36 were not induced with doxycycline, and no mouse-anti CD36 was added (Figure 3-1, A).

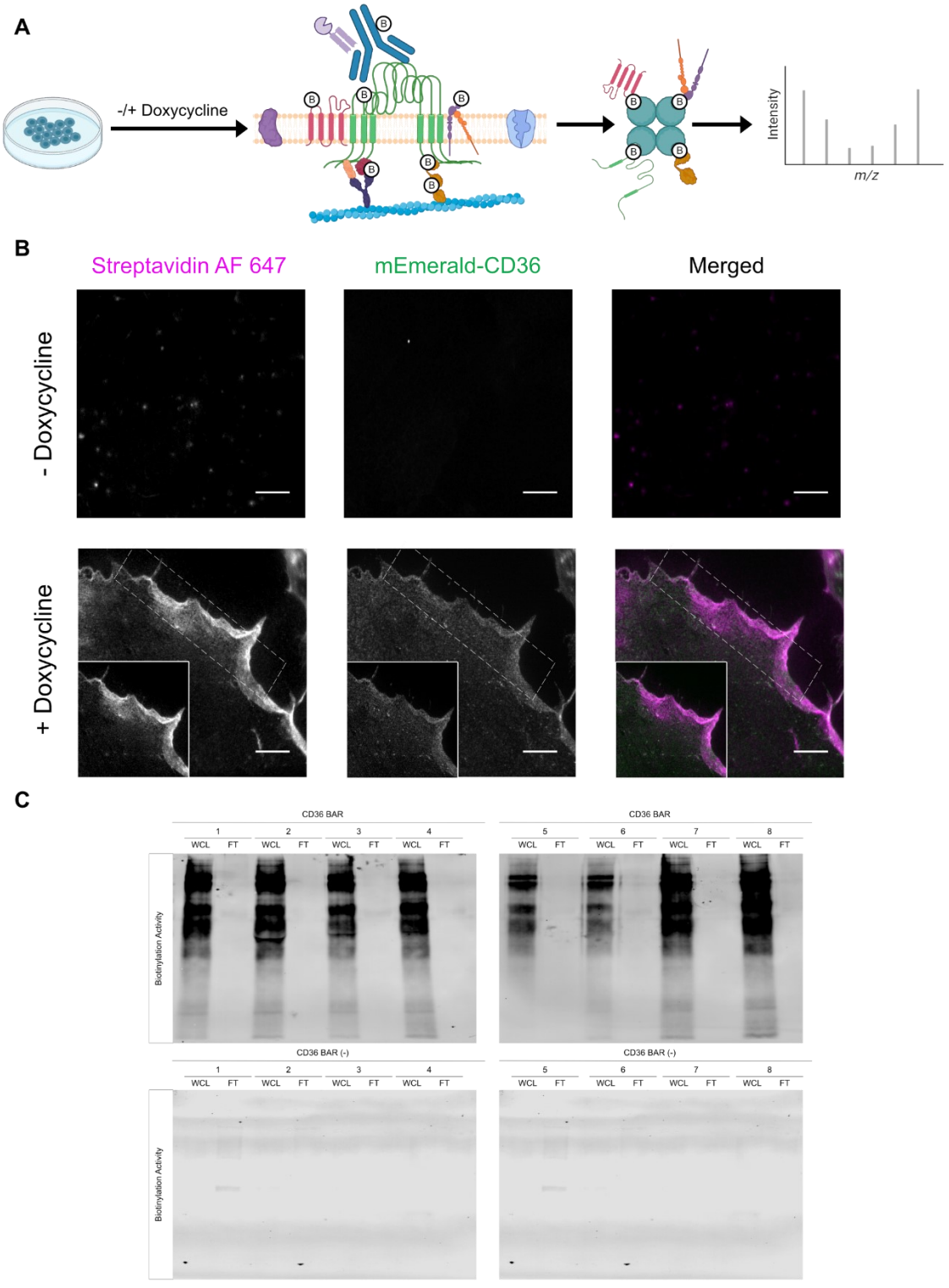

Figure 3-1: Workflow of CD36 BAR protein capture and identification.

*(**A**) Schematic of CD36 BAR workflow (created in Biorender) and **(B)** validation of CD36 BAR via widefield microscopy and immunoblotting. TIME mEmerald-CD36 cells were either uninduced (CD36 BAR control) or induced with*

doxycycline for 18 hours before fixation of cells with 4% PFA. For CD36 BAR treatment, mouse anti-CD36 was added, and for the negative control, no mouse anti-CD36 was added. Following incubation with the primary antibody, goat anti-mouse FAB conjugated to HRP was added. Following the addition of biotin-XX-tyramide and hydrogen peroxide, proteins within ~250nm of CD36 were covalently labeled with biotin. Following protein labelling, biotinylated proteins were captured via streptavidin beads and then trypsinized for identification via LC-MS/MS. Protein intensities were compared between the CD36 BAR and CD36 BAR control datasets. (B) Widefield fluorescent images of TIME mEmerald-CD36 cells treated with CD36 BAR, and CD36 BAR control. Biotinylated proteins were stained for using a 1/500 of streptavidin Alexa Fluor 647 and CD36 was stained for using Donkey anti-mouse Alexa Fluor 488. Bar scale = 10μm. (B) Immunoblot of TIME mEmerald-CD36 treated with CD36 BAR, CD36 BAR control, flow through (FT) fraction following streptavidin capture. Biotinylated proteins were detected using streptavidin IRDye 800RD.

We first validated CD36 BAR via immunofluorescence imaging and immunoblot of TIME mEmerald-CD36 cells treated with BAR. Widefield images reveal that mEmerald-CD36 expression (GFP channel, middle panel Figure 3-1, B) of TIME mEmerald-CD36 cells induced with doxycycline, whereas uninduced cells have virtually no CD36 expression (Figure 3-1, B). Following CD36 protocol, biotinylation reaction was validated by incubating cells with streptavidin-AF647 (Figure 3-1, B). For the BAR negative control treatment, with no CD36 expression, we observe low-intensity punctate streptavidin-AF647 staining, indicative of low level of non-specific biotinylation (Figure 3-1, B). In contrast, streptavidin-AF647 signal was more robust (same imaging and image contrast parameters between conditions) on induced cells and images reveal strong colocalization of streptavidin-AF647 with CD36 in high CD36-mEmerald areas, demonstrating the specificity of the labelling. Immunoblot of CD36 BAR and CD36 BAR negative control treatments also confirm the specificity of BAR as biotinylated proteins were detected in CD36 BAR lysate, whereas little to no biotinylated proteins were visualized in the CD36 BAR control lysate (Figure 3-1, C). To estimate the efficiency of the biotinylated proteins capture, the flow through recovered after binding was compared with the initial whole cell lysate using membrane blotting with streptavidin-680 (see section 6.1 page 176 for comparison of streptavidin beads capture efficiency). Streptavidin protein capture was effective as no biotinylated proteins were detected in the flow-through fraction for both CD36 BAR and CD36 BAR control samples (Figure 3-1, C).

LC-MS/MS was able to validate our CD36 BAR technique as the abundance of CD36 itself is ~140-fold greater in CD36 BAR than in CD36 BAR negative control (Figure 3-2, A). The downstream effector of TSP-1 and CD36, Fyn, was also found enriched ~15 times more in the CD36 BAR samples compared to CD36 BAR negative control (Figure 3-2, A). Proteins with ratios greater than 2, and whose average protein intensities in CD36 BAR were statistically different from CD36 control were shortlisted (Table 6-3). Of the 153 shortlisted proteins, ~25% of them were membrane-associated and ~25% corresponded to cytosolic proteins (Figure 3-2, B). The proportion of membrane proteins enriched in CD36 BAR was ~3-fold greater than the proportion of membrane proteins composing the TIME mEmerarld-CD36 proteome (Figure 6-8). Although biotin-phenol is impermeable to the cell membrane, intracellular proteins were identified in our CD36 BAR LC-MS/MS dataset. The permeabilization of the cell membrane is potentially due to paraformaldehyde fixation, allowing biotin-tyramide radicals produced by HRP to travel across the membrane and covalently react with intracellular proteins (Cheng et al., 2019).

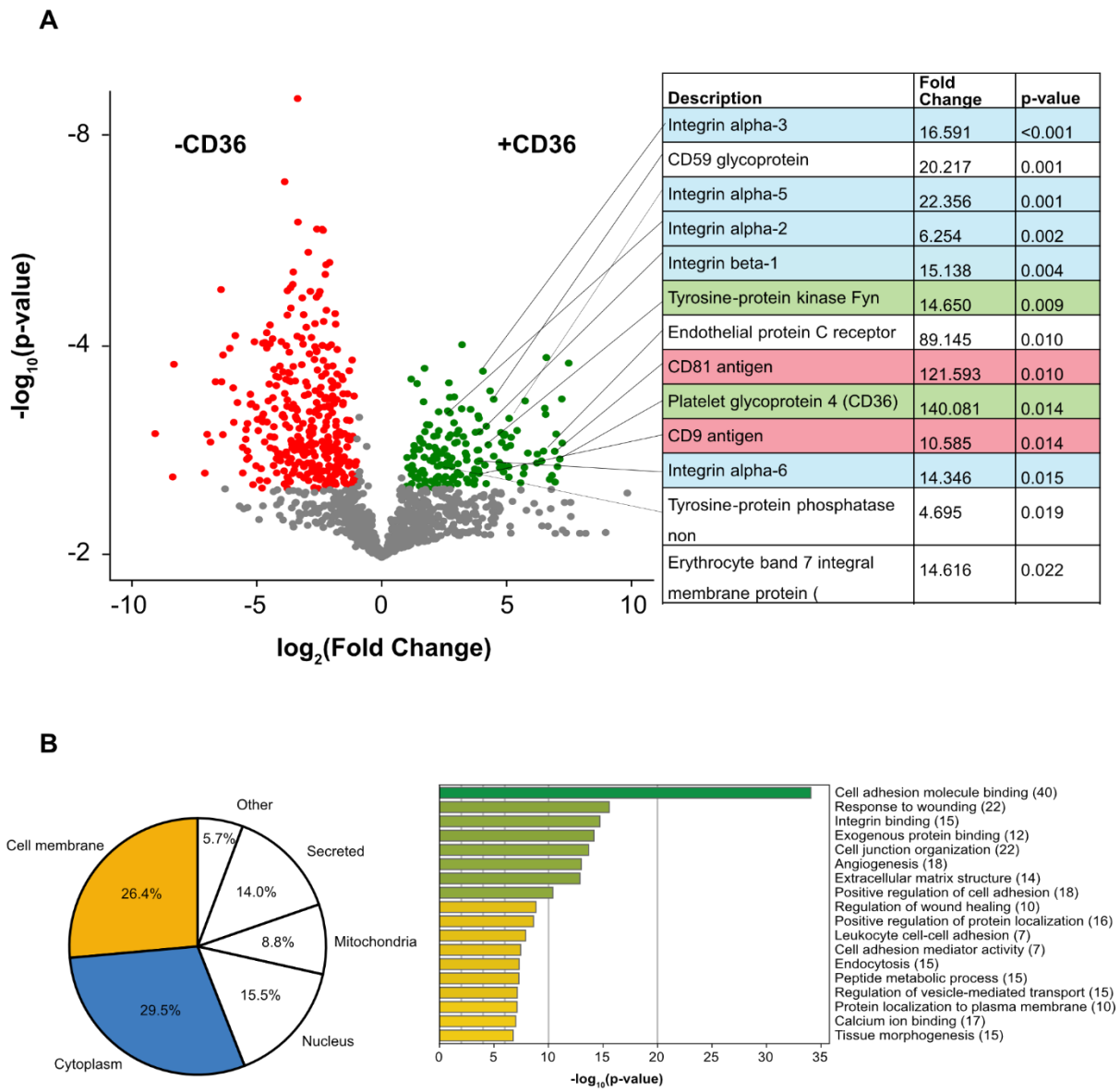

Description	Fold Change	p-value
Integrin alpha-3	16.591	<0.001
CD59 glycoprotein	20.217	0.001
Integrin alpha-5	22.356	0.001
Integrin alpha-2	6.254	0.002
Integrin beta-1	15.138	0.004
Tyrosine-protein kinase Fyn	14.650	0.009
Endothelial protein C receptor	89.145	0.010
CD81 antigen	121.593	0.010
Platelet glycoprotein 4 (CD36)	140.081	0.014
CD9 antigen	10.585	0.014
Integrin alpha-6	14.346	0.015
Tyrosine-protein phosphatase non	4.695	0.019
Erythrocyte band 7 integral membrane protein (	14.616	0.022

Figure 3-2: Quantification and analysis of enriched proteins within the CD36 BAR dataset.

*(**A**) Protein intensities were compared between the CD36 BAR and CD36 BAR control datasets. Volcano plot of CD36 BAR dataset indicating enriched proteins (green) and de-enriched protein (red). Enriched proteins are labeled in green as these proteins have average intensities ratios > 2 (log2 (2) = 1), and p-values <0.05. De-enriched proteins are labeled in red as these proteins have average intensities ratios < 0.5 (log2 (0.5) = -1), and p-values < 0.05. Candidate proteins were labeled to visualize their position on the volcano plot. Ratios were determined by dividing the average protein intensity in the CD36 BAR compared to the average protein intensity in the CD36 BAR negative control. Proteins highlighted in red are members of the tetraspanin superfamily, blue are a part of the integrins family, and in green are CD36 and Fyn two proteins expected to be enriched in our CD36 BAR dataset. (**B**) The pie chart displays the distribution of CD36 BAR enriched proteins based on their subcellular localization. Metascape gene analysis also indicates the number and the enrichment of proteins within various cellular functions.*

Metascape gene analysis of enriched proteins revealed significant pathways within our CD36 BAR dataset (Zhou et al. 2019). One of the most significantly enriched pathway was angiogenesis which was expected given CD36's anti-angiogenic capacity (Figure 3-2, B). Surprisingly, we also saw the enrichment of pathways involving integrin functions such as cell adhesion, integrin binding, and cell and junction organization. In alignment with metascape data, there are 6 proteins of the integrin family and 2 tetraspanin proteins (proteins known to interact with integrins) enriched within our CD36 BAR dataset. These data suggest that integrins are in close proximity to CD36 and may play a role in CD36 function. Our next steps were to confirm the proximity of candidate proteins listed in Figure 3-2, A to CD36 via *in-situ* proximity ligation assay.

3.2 Confirmation of Candidate Protein Proximity via in-situ Proximity Ligation Assay

To confirm the proximity of candidate proteins identified by CD36 BAR, providing a ~250nm labelling radius (Oakley et al., 2022), we employed an *in-situ* PLA methodology which detects protein interactions within a ~40nm distance from CD36 receptors. Not only does PLA provide another measure of protein proximity to CD36, but it also ensures their proximity to CD36 nanoclusters, which has a radius of ~70-90nm (Githaka et al., 2016). We chose 8 proteins to further investigate via PLA from our list of 54 membrane proteins significantly enriched in the CD36 BAR dataset. The rationale for selecting these candidates was that these proteins were: 1) shown to be interactor of CD36 within microvascular endothelial cells, or other cells lines (CD9 (Miao et al., 2001; Huang et al., 2011; Kazerounian et al., 2011; Heit et al., 2013; Huang et al., 2023), CD81 (Heit et al., 2013), ITGB1 (Thorne et al., 2000; Bamberger et al., 2003; Davis et al., 2013; Heit et al., 2013), STOM (Wu et al., 2022)); 2) known to associate with "raft domains" (CD59 (Murray and Robbins, 1998; Cross, 2004; Omidvar et al., 2006; Koyama-Honda et al., 2020), STOM (Salzer and Prohaska, 2001; Mairhofer et al., 2002; Umlauf et al., 2006)); and 3) known to have signalling capacity especially towards Src-family kinases (ITGB1 (Wary et al., 1998; Chen et al., 2000; Liang et al., 2004; Quintela-López et al., 2019), CD59 (Murray and Robbins, 1998;

Suzuki et al., 2007; Koyama-Honda et al., 2020), PTP1B (Bjorge et al., 2000; Liang et al., 2005; Arias-Romero et al., 2009).

To validate the sensitivity of the PLA assay, we performed a positive control experiment utilizing 2 different primary antibodies directed to mEmerald-CD36 (mEmerald is a variant of GFP), a mouse anti-CD36 and a rabbit anti-GFP. Since mEmerald is tagged to the N-terminus of CD36, the PLA reaction, as expected, produced numerous robust PLA signals (Figure 3-3). To ensure the specificity of PLA, we performed a negative control reaction with mouse anti-mitofilin and rabbit anti-GFP. Mitofilin is an inner mitochondrial membrane protein with no known association with CD36, and the 2 molecules also reside in separate organelles. As expected, few PLA signals were produced (Figure 3-3). To quantify PLA images, we developed an analysis pipeline in CellProfiler to determine the density of PLA dots per cell (method page 67, PLA dots per cell per pixel, Figure 3-4). The density measurement allows normalization to the effect of cell size, as larger cells will produce more PLA dots due to greater protein expression relative to smaller cells. The positive control condition (CD36/GFP) produced ~18 times greater density of PLA per cell than the mitofilin negative control (CD36/mitofilin), therefore validating the specificity of the PLA experiments and quantification (Figure 3-4).

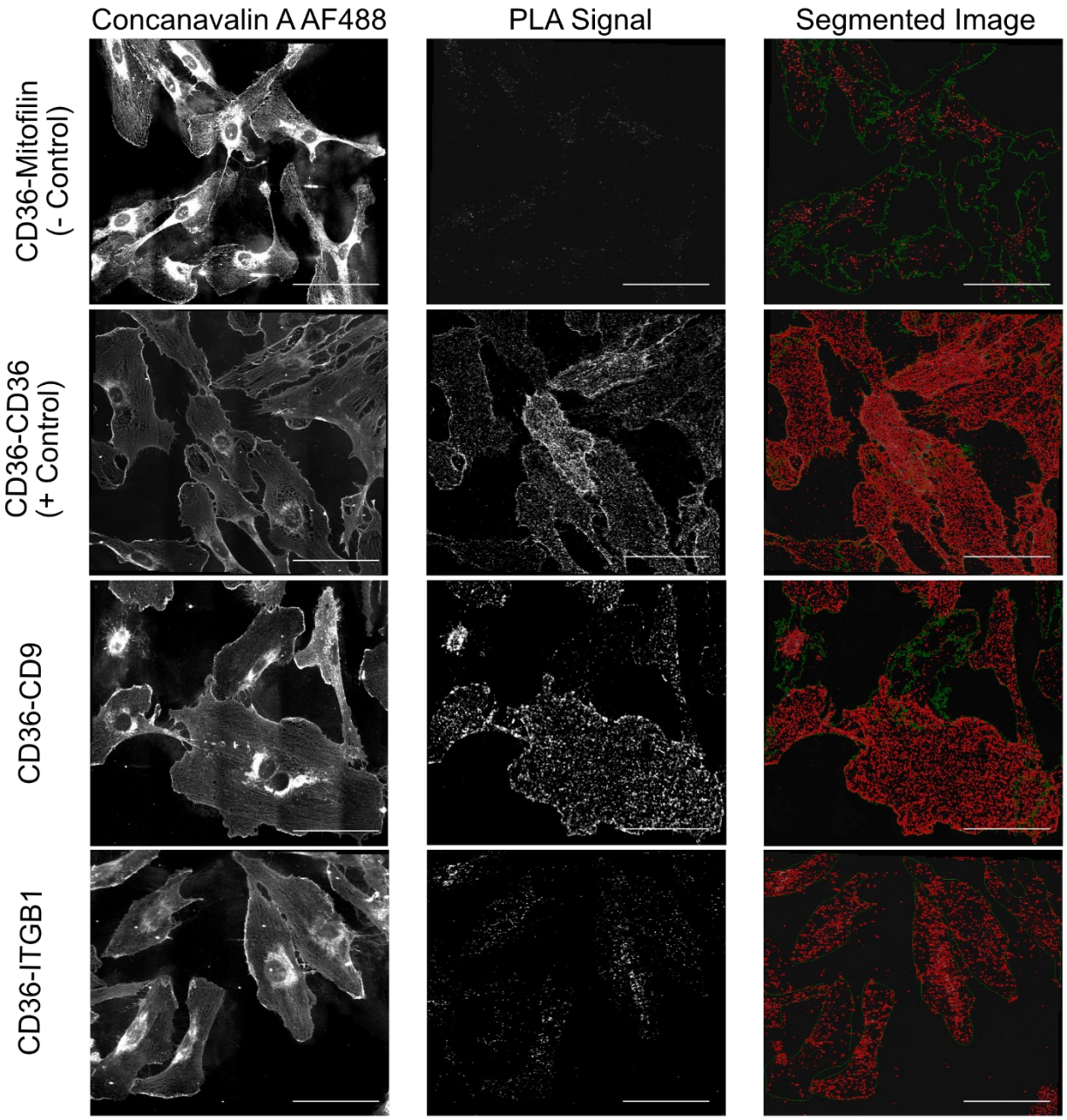

Figure 3-3: Representative images of proximity ligation assay.

CD36 interaction with the candidate proteins (CD9, CD59, CD81, ITGB1, EPCR, myoferlin) was accessed utilizing PLA. TIME mEmerald-CD36 cells were treated with Concanavalin A AF488, prior to validating candidate protein proximity to CD36 via PLA. Rabbit anti-GFP and mouse anti-CD9 antibodies or mouse anti-ITGB1 were used to determine CD9 or ITGB1 interaction with CD36. Rabbit anti-GFP or rabbit anti-mitofilin antibodies were paired with mouse anti-CD36 for positive or negative control experiments, respectively. A pipeline was developed in CellProfiler to segment cells and PLA dots to quantify the density of PLA dots per cell. Bar scale: 100μm.

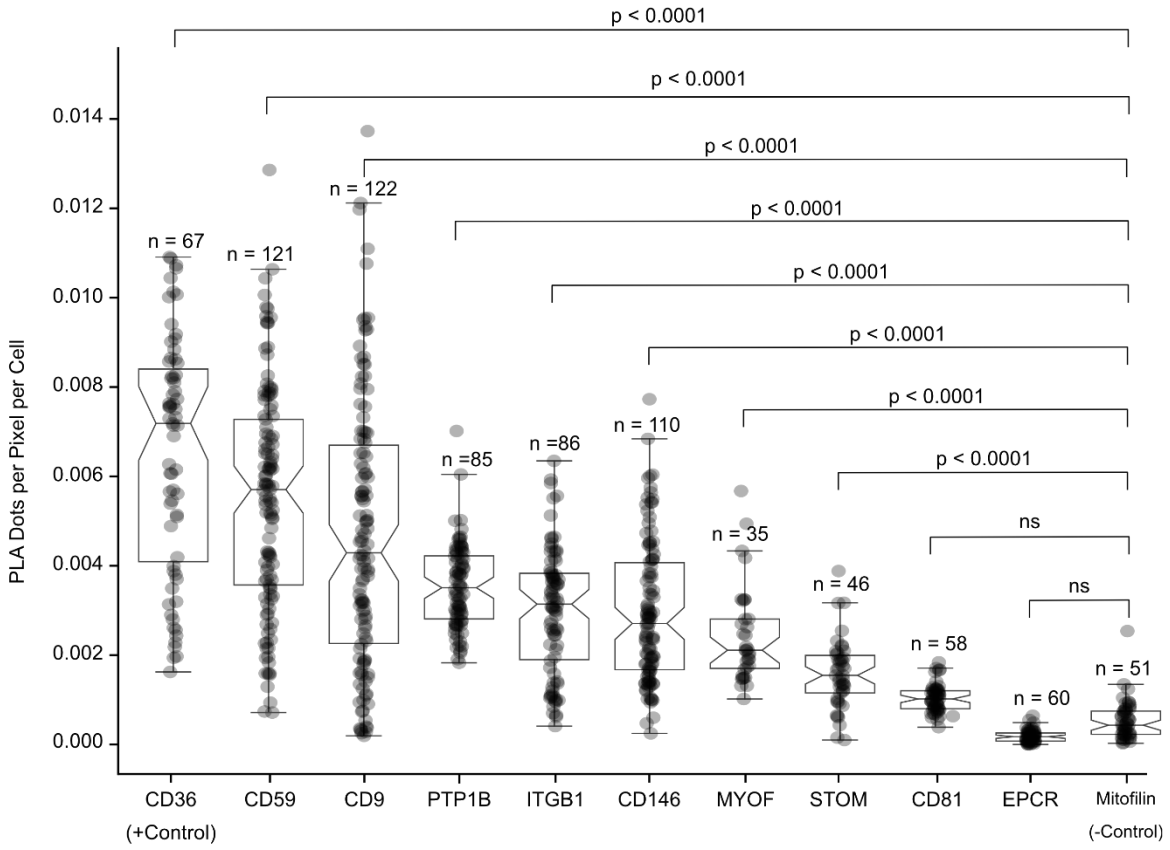

Figure 3-4: Estimation of candidate proteins' proximity to CD36 via PLA.

The boxplots indicate the PLA dots per cell per pixel produced by PLA reactions between CD36 and candidate proteins. A customized pipeline in CellProfiler was developed to segment the cell, PLA dots, and quantify the density of PLA per cell. The number of cells (n) analyzed for each candidate protein is denoted above each boxplot. Cells were imaged from a PLA single experiment was performed for each candidate protein. A non-parametric Kruskal-Wallis test was employed to determine if there were statistically significant differences between groups. Following a Kruskal-Wallis test, Dunn's post-hoc test was used to determine pairwise significance values. An α value of 0.05 was used for significance.

Candidate proteins which produced significantly greater density of PLA dots per cell in comparison to the mitofilin reaction (negative control) were classified as proteins with confirmed proximity to CD36. PLA confirmed the proximity of the following proteins: CD59, Tyrosine-protein phosphatase non-receptor type 1 (PTP1B), CD9, ITGB1, CD146, myoferlin (MYOF), and stomatin (STOM) (Figure 3-4). Although CD81, and EPCR were significantly enriched within CD36 BAR experiments, these candidate proteins failed to produce a greater level of density of PLA dots per cell than mitofilin. Therefore, PLA failed to confirm their proximity to CD36 (Figure 3-4). These

proteins were possibly identified within ~250nm radius of BAR, however, did not have intimate interactions with CD36, which were measured by PLA. Following the confirmation of candidate protein proximity to CD36, we preformed literature search to select proteins for further investigation.

3.3 Determining the Hierarchical Relationship Between CD36, ITGB1, and CD9 via Conditional Colocalization and PLA

To further elucidate the role of candidate proteins in TSP-1 - CD36 anti-angiogenic signalling, we chose to narrow our focus to CD9 and ITGB1 with the following rationale. CD9, a protein of the tetraspanin superfamily, has been shown to interact with CD36 via co-immunoprecipitation in numerous cell lines – human dermal microvascular endothelial cells (HDMEC) (Kazerounian et al., 2011), platelets (Miao et al., 2001), and macrophages (Huang et al., 2011; Heit et al., 2013; Huang et al., 2023). While the role of CD36's interaction with CD9 is unknown in HDMEC and platelets, this interaction is essential for oxLDL uptake and signalling within macrophages (Huang et al., 2011; Heit et al., 2013; Huang et al., 2023).

ITGB1 interaction with CD36 has also been shown in HDMEC (Davis et al., 2013) and macrophages (Heit et al., 2013), as well as microglia (Bamberger et al., 2003) and melanoma cells (Thorne et al., 2000). Within microglial cells, CD36 interaction with α6β1 forms a complex that binds β-amyloids fibers and induces cytokines and chemokines production (Koenigsknecht and Landreth, 2004; Bamberger et al., 2003). ITGB1 interacts with CD36 within macrophages and this interaction is dependent on CD9. These three proteins are involved in a complex needed for oxLDL uptake (Heit et al., 2013). Although the ITGB1 interaction with CD36 has been shown to strengthen *plasmodium falciparum*-infected red blood cell binding to HDMEC cells, the role of the interaction between CD36 and integrins in microvascular endothelial cells and anti-angiogenic signalling is poorly characterized (Davis et al., 2013). Therefore, the literature and our proximity data strongly suggest interactions between ITGB1, CD9 and CD36 in the membrane of

microvascular cells. Our objective is to better determine the roles, and mechanisms of action of this complex during CD36 anti-angiogenic signalling.

To determine the relationship between ITGB1, CD9 and CD36, we employed conditional colocalization analysis (Vega-Lugo et al., 2022). Conditional colocalization is a quantitative analysis program which allows exploration of the relationship between proteins within tri-colored fluorescent images. Low-level fluorescent antibody labelling, to ensure single receptor detection, enables the analysis algorithm to localize molecules and determine if the colocalization between two molecular entities is positively or negatively influenced by the colocalization of a third entity. Through this analysis, we can determine the cooperative nature of protein interactions, and define molecular complexes involved in signal transduction, nanodomain formation, and other biological phenomena. For more information on this quantitative microscopy analysis refer to Vega-Lugo et al. (2022) and section 2.5.3 of the materials and methods.

Here we employed conditional colocalization to determine whether a complex is formed between CD36, CD9 and ITGB1. Specifically, we wanted to determine whether CD36's interaction with ITGB1 was affected by CD9 and whether CD36's interaction with CD9 was affected by ITGB1. To validate this approach, we first performed a negative control conditional colocalization experiment between transferrin receptor (TfR), CD36, and ITGB1. Since TfR, has no known association with CD36 or ITGB1, we expect ITGB1 to have no effect on the colocalization between CD36 and TfR. For our positive control, we conducted conditional colocalization between CD36, Halotag (as for PLA, using the Halotag fusion portion of Halotag-CD36), and CD9, by labelling CD9 with rabbit anti-CD9 AF647 and HT-CD36 with mouse-anti CD36, donkey anti-mouse 488 and Halotag ligand-JFX-549.

Following the investigation of the CD36, CD9 and ITGB1 complex, we determined whether CD9 and ITGB1 are needed for one another's interaction with CD36 by performing PLA and

conditional colocalization within TIME mEmerald-CD36 and TIME Halotag-CD36 cell lines stably transduced with shRNA targeting ITGB1 or CD9.

3.3.1 Two-Molecular Conditional Colocalization Measures between CD36, and ITGB1, and CD9

Prior to investigating three-molecular colocalization values, we determined the extent of CD36 colocalization with itself, ITGB1, CD9, and TfR. To measure CD36's overall colocalization with these proteins we utilized the $p(TwR)$ measurement – which determines the fraction of CD36 objects (Target (T)) colocalizing with HT-CD36 (via HT-JF549X), ITGB1, CD9, or TfR (Reference (R)). As expected, CD36's colocalization with itself (positive control) exhibited the greatest colocalization extent at 25% (Figure 3-5). CD36 exhibited greater colocalization with ITGB1, 17%, than CD9, 11% (Figure 3-5). All colocalization values were significantly greater than the colocalization extent measured between CD36 and TfR measured at 7% (Figure 3-5) and likely correspond to coincidental colocalization. Here, the $p(TwR)$ colocalization measure further validates ITGB1 and CD9's proximity to CD36.

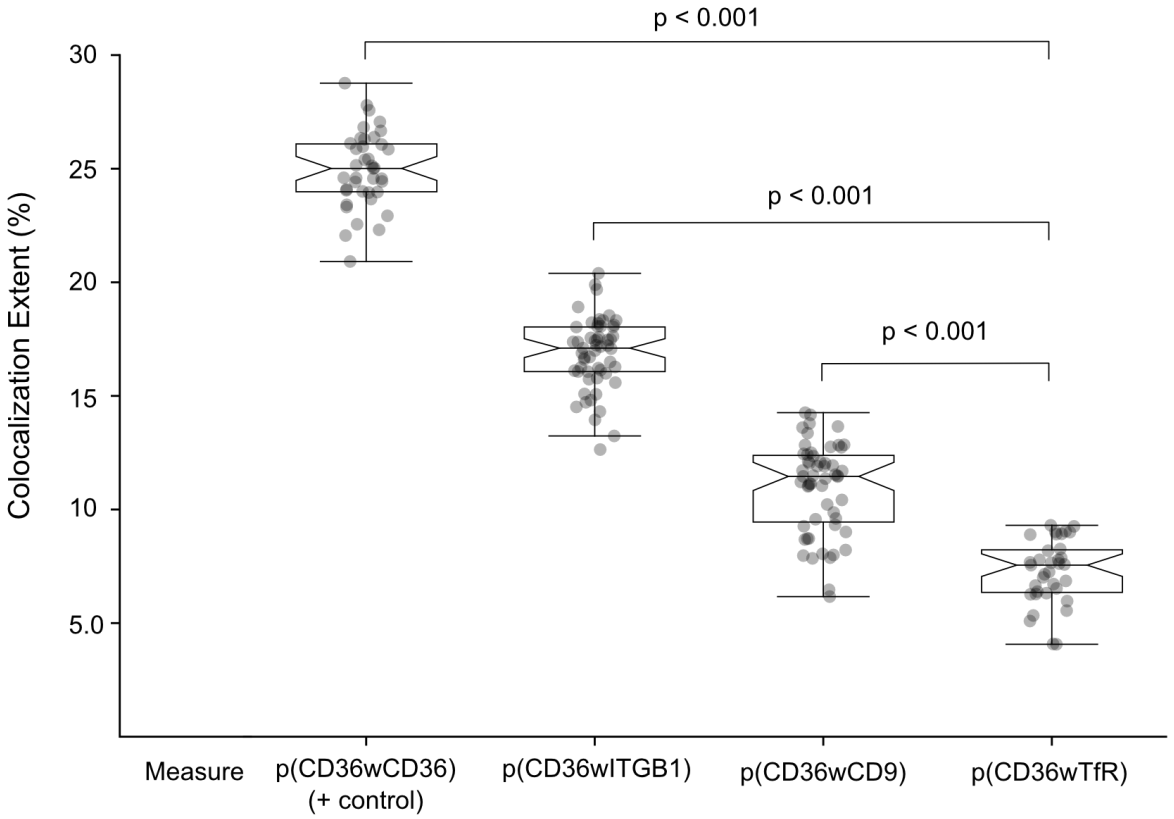

Figure 3-5: Conditional colocalization controls.

Two molecular p(TwR) colocalization measures between CD36 (Target (T)) and ITGB1, CD9 and TfR (Reference (R)). p(TwR) measures the proportion of CD36 colocalizing with CD36 (positive control), ITGB1, CD9 or TfR objects. A non-parametric Kruskal-Wallis test was employed to determine if there were statistically significant differences between groups. Following the Kruskal-Wallis test, Dunn's post-hoc test was used to determine pairwise significance values. An α value of 0.05 was used for significance. A colocalization radius of 2 pixels (~180nm) was used for conditional colocalization experiments. For positive and negative control experiments, 39 and 35 cells were imaged, respectively, over 2 experiments. 55 cells were images over 3 experiments measuring the overall colocalization of CD36 with ITGB1 or CD9.

However, in contrast to our PLA experiments, we see conditional colocalization determined ITGB1 to have greater colocalization with CD36 than CD9. This disparity is most likely due to variations in antibody concentrations needed for conditional colocalization and PLA experiments. For conditional colocalization, sparse, punctate labelling is required for object detection, whereas PLA requires strong antibody labelling for a sufficient number of connector oligomer hybridization events. Because a high proportion of proteins are labelled in PLA, proteins which are in proximity

to CD36, and with greater expression levels produce more PLA signals. Therefore CD9, which has ~ 2-fold greater expression in TIME cells than ITGB1, produces a more robust PLA signal (Cell line - CD9 - The Human Protein Atlas; Cell line - ITGB1 - The Human Protein Atlas). The low-level antibody labelling for conditional colocalization nullifies the expression effect, providing a relatively normalized approach to investigate protein interaction. Both PLA and conditional colocalization results imply, that when normalizing for protein expression, ITGB1 has a greater interaction with CD36 than CD9, although in nature, CD9 has a greater interaction with CD36 due to its high-level of expression.

3.3.2 Three Molecule Conditional Colocalization Measures between CD36, CD9, and ITGB1

To determine whether CD36, ITGB1 and CD9 form a ternary complex, we investigated three-molecular colocalization measurements. Through these measures, we are able to determine whether CD9 and ITGB1 affect one another's colocalization with CD36. To determine the effect of CD9 on the colocalization of CD36 and ITGB1, CD36 was denoted as the target (T), ITGB1 as the reference (R), and CD9 as the condition (C).

For a protein to have a significant effect on the colocalization between two proteins, the three molecular colocalization measures must be significantly greater than the two-molecular colocalization (*p(TwR)*), and the coincidental colocalization measurements, nullTR and RandC. For nullTR, the target (T) was replaced with objects randomly placed in a grid arrangement within the cell (Vega-Lugo et al., 2022). This value provides the colocalization expected by the number and spatial distribution of the reference (R) (Vega-Lugo et al., 2022). The RandC measure determines the colocalization extent when the position of the condition is randomized within the cell area (Vega-Lugo et al., 2022). For more information on the nullTR and RandC values refer to Vega-Lugo et al. (2022).

We first determined the effect of CD9 on the colocalization between CD36 and ITGB1. To investigate whether CD36's colocalization with CD9 positively influenced CD36's colocalization with ITGB1, we determined the fraction of CD36-CD9 colocalization events colocalizing with ITGB1 (p(CD36wITGB1 | CD36wCD9)). In addition, we investigated whether ITGB1's colocalization with CD9 positively influenced CD36's colocalization with ITGB1 (p(CD36w(ITGB1wCD9))). The median colocalization extent for p(CD36wITGB1 | CD36wCD9), p(CD36w(ITGB1wCD9), and p(CD36wITGB1) was ~18%, ~20%, and ~17%, respectively (Figure 3-6, A). CD36's overall colocalization with ITGB1 was significant (p(CD36wiTGB1)) (Figure 3-6, A). These results also indicate that CD36's colocalization with CD9 did not affect CD36's interaction with ITGB1 as p(CD36wITGB1 | CD36wCD9) was not significantly different from the coincidental RandC measurement nor the overall colocalization of CD36 with ITGB1 (p(CD36wITGB1)) (Figure 3-6, A). Also, the colocalization of CD36 with ITGB1 when CD36 does not colocalize with CD9 (p(CD36wITGB1 | CD36nCD9)) and colocalization of CD36 with ITGB1 when ITGB1 does not colocalize with CD9 (p(CD36w(ITGB1nCD9)) was not significantly different from the coincidental colocalization measures nor CD36's overall colocalization with CD9 (p(CD36wITGB1)) (Figure 3-6, A). However, p(CD36w(ITGB1wCD9)) was significantly greater than the coincidental colocalization measures and p(CD36wITGB1) (Figure 3-6, A). Therefore, ITGB1's colocalization with CD9 significantly enhances CD36's colocalization with ITGB1 (Figure 3-6, A).

The conditional colocalization measurements and statistical tests are summarized in Figure 3-6, B. Here, the median colocalization extent for the different measures p(CD36wITGB1), for p(CD36wITGB1 | CD36wCD9), p(CD36wITGB1 | CD36nCD9)), p(CD36w(ITGB1nCD9)), and p(CD36w(ITGB1wCD9)) are displayed in the colored circle (Figure 3-6, B). For three-molecular conditional colocalization measurements p(CD36wITGB1 | CD36wCD9), p(CD36wITGB1 | CD36nCD9)), p(CD36w(ITGB1wCD9)), and p(CD36w(ITGB1nCD9)) the least significant p-value

among three comparisons (p(CD36wITGB1), nullTR and RandC) was expressed as a $-\log_{10}$(p-value) (Figure 3-6, B). The overall colocalization of CD36 with ITGB1 (p(CD36wITGB1) was statistically compared to the nullTR measure and the significance was expressed as a $-\log_{10}$(p-value) (Figure 3-6, B). $-\log_{10}$(p-value) values greater than 1.303 (or p-values less than 0.05) were denoted as significant. For the remainder of the thesis, conditional colocalization results are displayed as the graph shown in Figure 3-6, B.

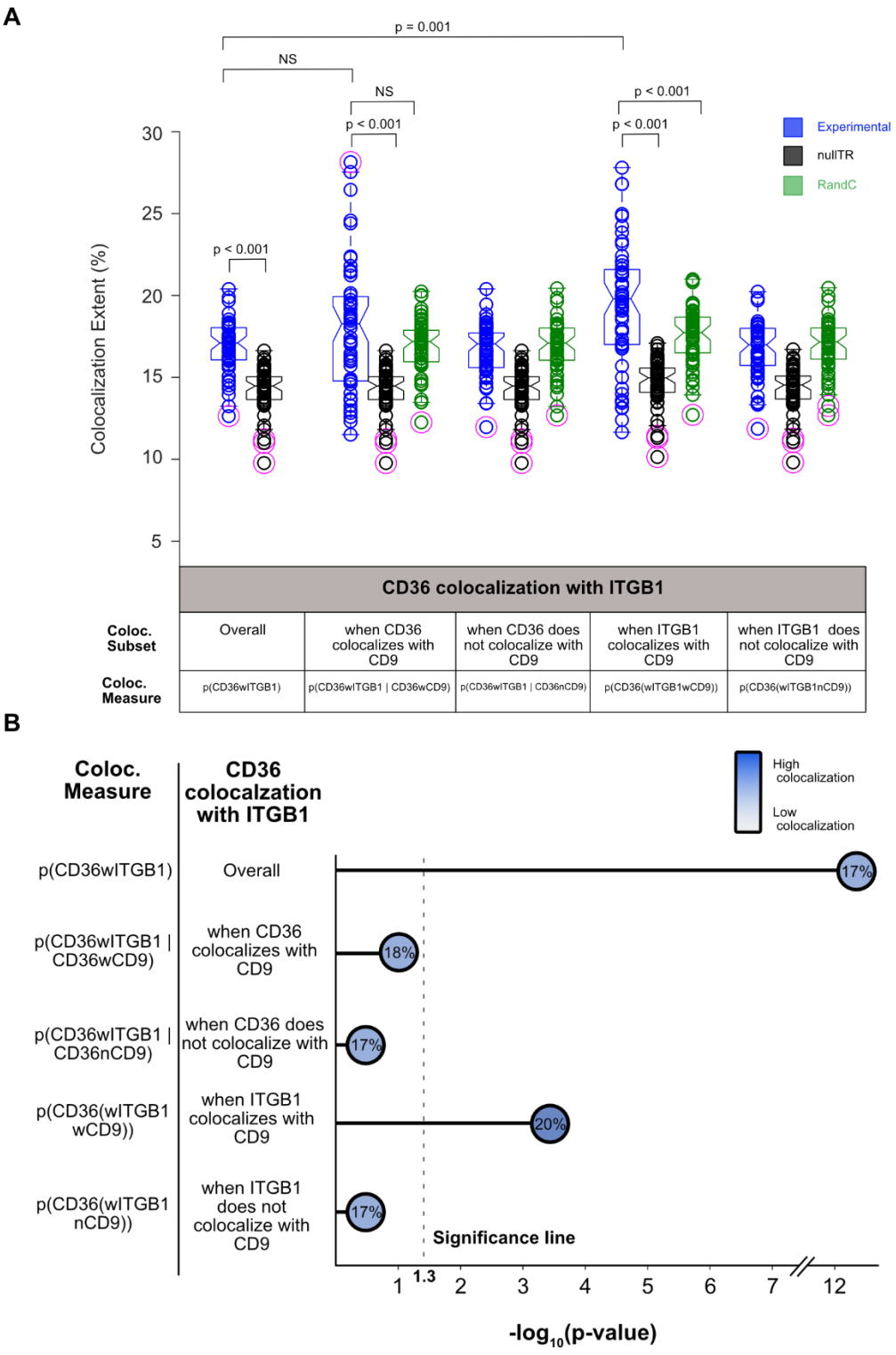

Figure 3-6: Conditional colocalization analysis measuring the effect of CD9 on the colocalization of CD36 with ITGB1.

(A) Three-molecular conditional colocalization measurements indicating the effect of CD9 on the colocalization between CD36 and ITGB1. Specifically, we determined the effect of CD36 colocalization with CD9 on CD36's

colocalization with ITGB1 (p(CD36wITGB1 | CD36wCD9)) and the effect of ITGB1 colocalization with CD9 on CD36's colocalization with CD9 (p(CD36w(ITGB1wCD9)). The colocalization of CD36 with ITGB1 when CD36 does not colocalize with CD9 (p(CD36wITGB1 | CD36nCD9)) and colocalization of CD36 with ITGB1 when ITGB1 does not colocalize with CD9 (p(CD36w(ITGB1nCD9)) was also determined. These values were compared to the coincidental colocalization measures (nullTR and RandC) and overall colocalization measure p(CD36wITGB1) to determine CD9's colocalization effect. Thresholds for three molecular colocalization significance were calculated using Dunn-Sidak correction. A colocalization radius of 2 pixels (~180nm) were used for conditional colocalization experiments. (B) Summary of conditional colocalization measurements indicating the effect of CD9 on the colocalization between CD36 and ITGB1. Median colocalization extent for each measurement is indicated within each colored circle. For three-molecular conditional colocalization measurements the least significant p-value among three comparisons (p(CD36wITGB1), nullTR and RandC) was expressed as a $-\log_{10}$(p-value). The $-\log_{10}$(p-value) for the statistical comparison between p(CD36wITGB1) and nullTR is also shown. 55 cells were imaged across 3 experiments.

In our analysis, we also investigated ITGB1 as the condition, to determine the effect of ITGB1 on the colocalization between CD36 and CD9. To measure the effect of CD36 colocalization with ITGB1 on the colocalization between CD36 and CD9, we determined the fraction of CD36-ITGB1 colocalization events which also colocalized with CD9 (p(CD36wCD9 | CD36wITGB1)). We also measured the proportion of ITGB1-CD9 colocalization events colocalizing with CD36 (p(CD36w(CD9wITGB1))) to determine whether CD9's colocalization with ITGB1 positively influences CD36 colocalization with CD9. CD36's overall colocalization with CD9 (p(CD36wCD9)) was significantly greater than the nullTR (Figure 3-7). Both, p(CD36wCD9) and p(CD36wCD9 | CD36wITGB1) were ~12%, indicating that CD36's colocalization with ITGB1 does not enhance CD36's colocalization with CD9 (Figure 3-7). Also, the colocalization of CD36 with CD9 when CD36 does not colocalize with ITGB1 (p(CD36wCD9 | CD36nITGB1)) and colocalization of CD36 with CD9 when CD9 does not colocalize with ITGB1 (p(CD36w(ITGB1nCD9))) was not significantly different from the coincidental colocalization measures nor CD36's overall colocalization with CD9 (p(CD36wCD9)) (Figure 3-7). However, p(CD36w(CD9wITGB1)) was ~13% and significantly greater than all coincidental colocalization measurements, and overall p(CD36wCD9) (Figure 3-7). Therefore, CD9's colocalization with ITGB1 enhances CD36's colocalization with CD9.

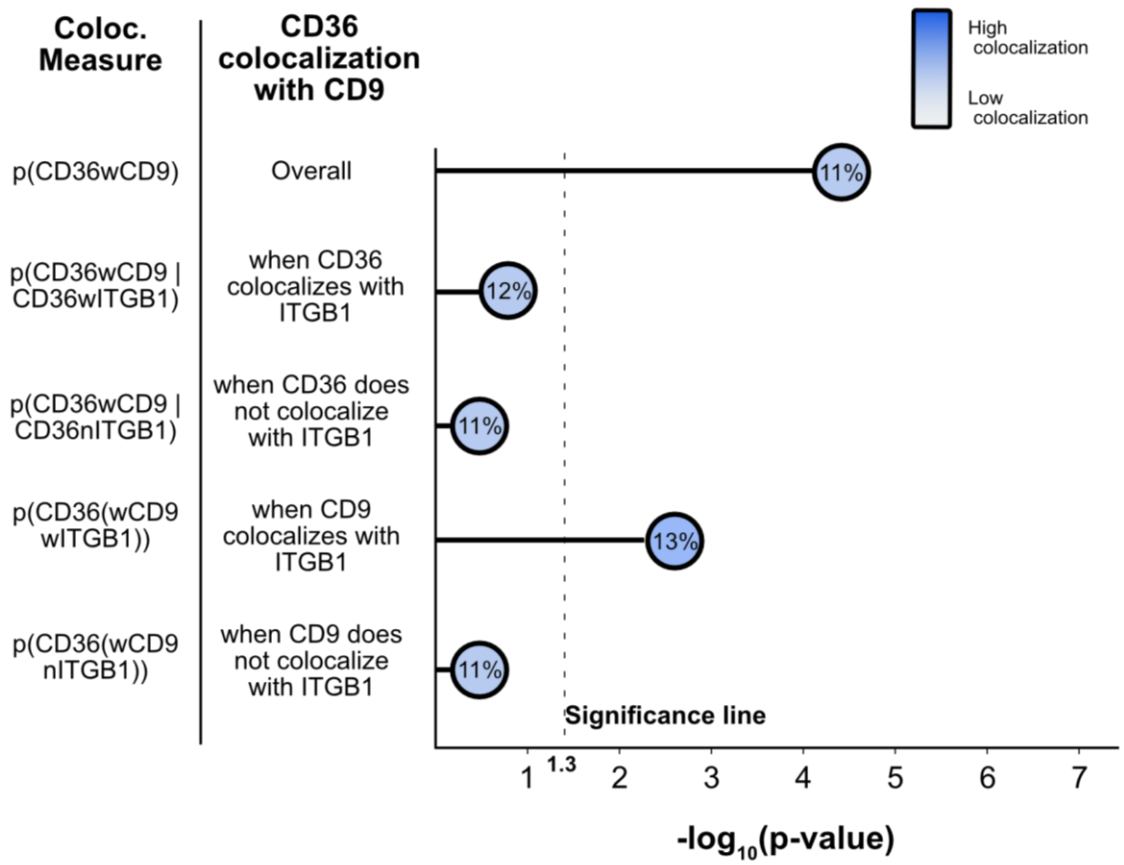

Figure 3-7: Conditional colocalization analysis measuring the effect of ITGB1 on the colocalization of CD36 with CD9.

Three-molecular conditional colocalization measures determining the effect of ITGB1 on the colocalization between CD36 and CD9. The p(CD36wCD9 | CD36wITGB1), p(CD36wCD9 | CD36nITGB1), p(CD36w(CD9wITGB1)) and p(CD36w(CD9nITGB1)) values were compared with the coincidental colocalization (nullTR and RandC) and overall colocalization measure, p(CD36wCD9,) to determine ITGB1's colocalization effect. For the three-molecular conditional colocalization measurements the least significant p-value among three comparisons (p(CD36wITGB1), nullTR and RandC) was expressed via -log$_{10}$(p-value). The -log$_{10}$(p-value) for the statistical comparison between p(CD36wCD9) and nullTR is also shown. Thresholds for three molecular colocalization significance were calculated using Dunn-Sidak correction. A colocalization radius of 2 pixels (~180nm) were used for conditional colocalization experiments. 55 cells were imaged across 3 experiments.

Conditional colocalization experiments were also performed between CD36, ITGB1 and TfR as a negative control. The p(CD36TfR | CD36wITGB1), p(CD36wTfR | CD36nITGB1), p(CD36w(TfRwITGB1)) and p(CD36w(TfRnITGB1)) measures were not significantly different from the coincidental colocalization values nor CD36's overall colocalization with TfR (p(CD36wTfR)) (Figure 3-8). As expected, ITGB1, had no influence on the colocalization between

CD36 and TfR. From these conditional colocalization experiments, we see that ITGB1's colocalization with CD9 enhances CD36 colocalization with ITGB1. In addition, we observe, to a lesser extent, that CD9's colocalization with ITGB1 enhances CD36's colocalization with CD9. The conditional effects of CD9 and ITGB1 provide evidence for ternary complex formation between CD36, CD9 and ITGB1. To further investigate the organization of the complex, we evaluated CD36 interaction with CD9, and ITGB1 via PLA at the surface of TIME-mEmerald-CD36 cell lines inactivated for CD9 and ITGB1 via stable expression of CD9 or ITGB1 shRNA.

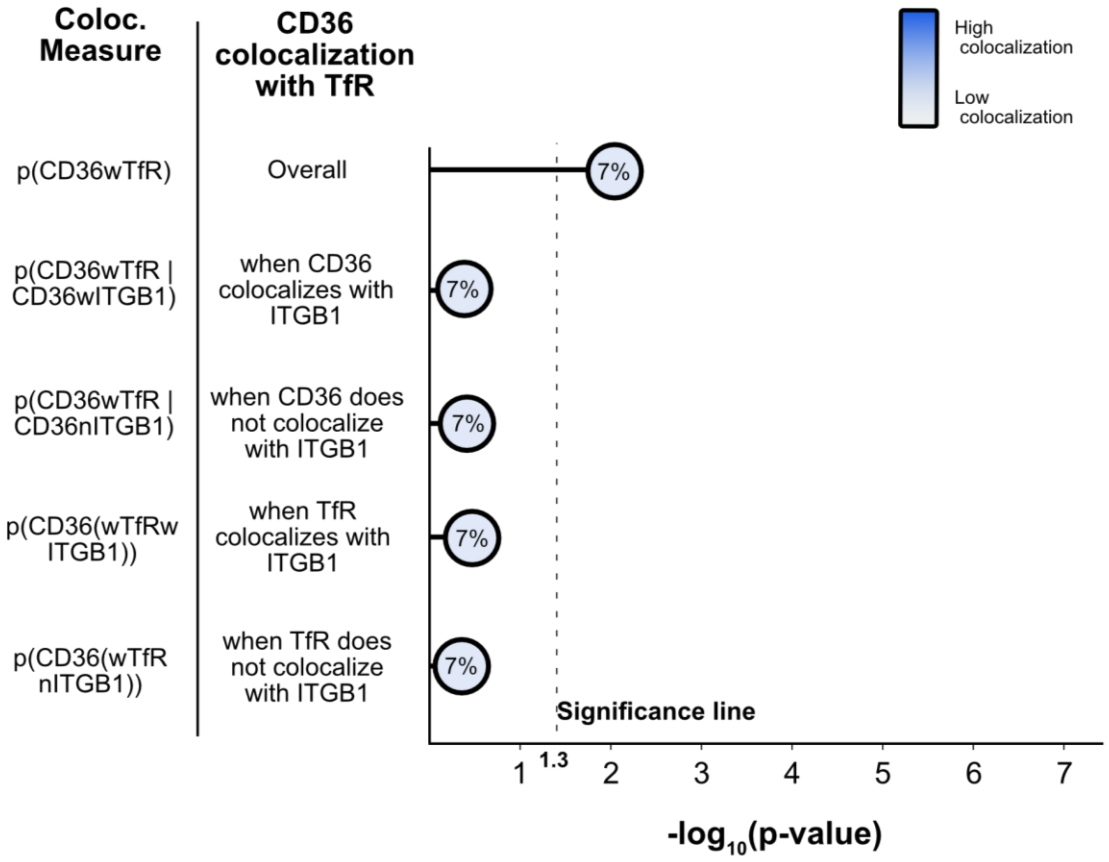

Figure 3-8: Conditional colocalization analysis measuring the effect of ITGB1 on the colocalization of CD36 with the non-interacting transferrin receptor.

Negative control conditional colocalization values measuring the effect of ITGB1 on the colocalization between CD36 and TfR. The p(CD36wTfR | CD36wITGB1), p(CD36wTfR | CD36nITGB1), p(CD36w(TfRwITGB1)) and p(CD36w(TfRnITGB1)) values were compared with the coincidental colocalization (nullTR and RandC) and overall colocalization measure p(CD36wTfR) to determine ITGB1's colocalization effect between CD36 and TfR. For the three-molecular conditional colocalization measurements the least significant p-value among three comparisons (p(CD36wTfR), nullTR and RandC) was expressed via -log$_{10}$(p-value). The -log$_{10}$(p-value) for the statistical comparison between p(CD36wTfR) and nullTR is also shown. Thresholds for three molecular colocalization significance were

calculated using Dunn-Sidak correction. A colocalization radius of 2 pixels (~180 nm) were used for conditional colocalization experiments. For the negative control experiments, 39 cells were images over 2 experiments.

3.3.3 Investigation CD36, ITGB1 and CD9 Ternary Complex via ITGB1 and CD9 shRNA inactivation

To further investigate the interactions between CD36, CD9, and ITGB1 we developed TIME mEmerald-CD36 (and HT-CD36) cell lines constitutively expressing CD9 or ITGB1 shRNA. Within TIME mEmerald-CD36 cells, ITGB1 and CD9 shRNA significantly reduced the expression of each candidate protein by ~95% and ~80%, respectively (Figure 3-9, B & C).

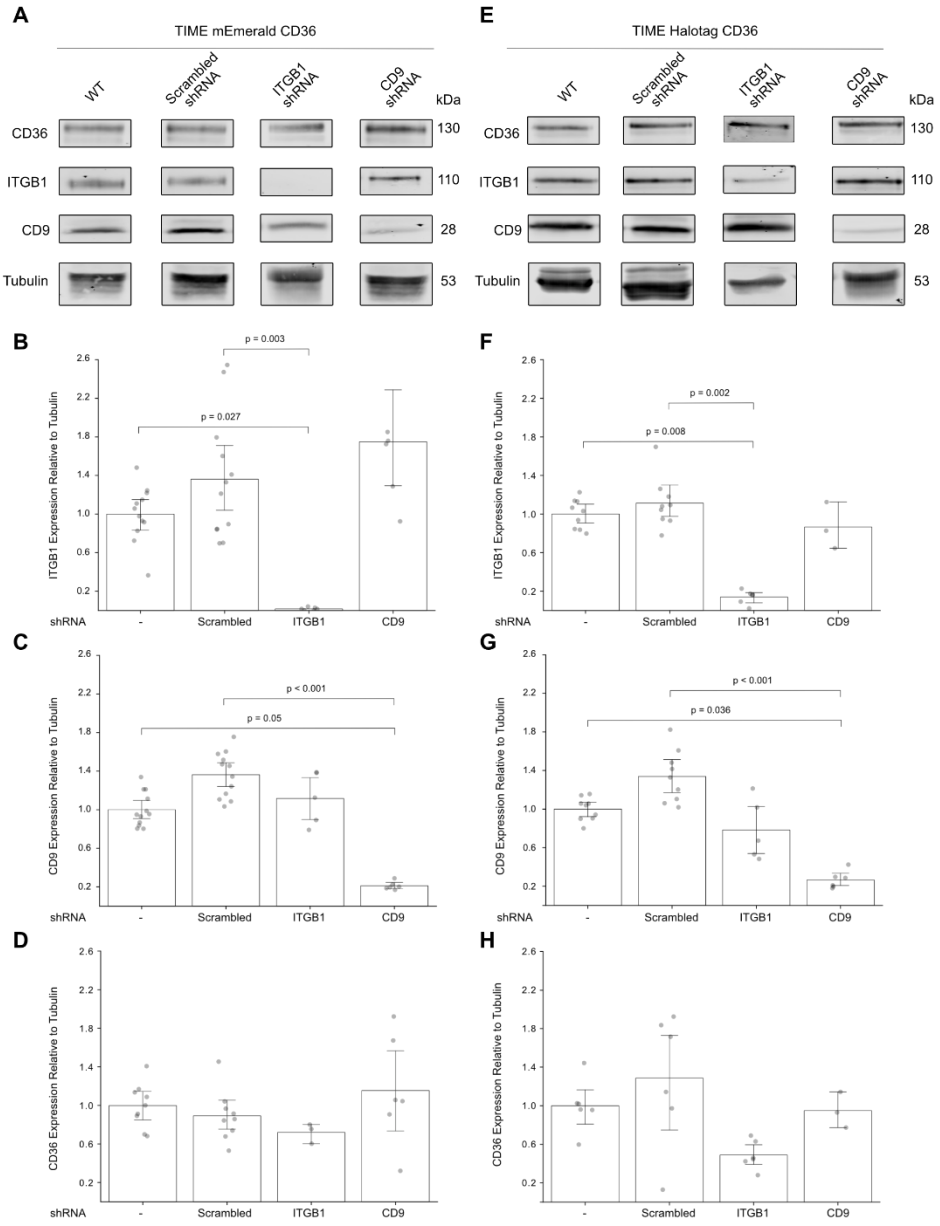

Figure 3-9: Validation of TIME mEmerald-CD36 and HaloTag-CD36 ITGB1 and CD9 shRNA KD via immunoblotting.

TIME mEmerald-CD36 and TIME HaloTag-CD36 cells were transduced with lentiviruses containing sequences for the constitutive expression of scrambled, ITGB1, or CD9 shRNA. One week following hygromycin selection, surviving cells were collected and their lysate was analyzed via immunoblotting to confirm candidate protein KD. (A) Immunoblots evaluating the expression of ITGB1, CD9, and CD36 within TIME mEmerald-CD36 cells and TIME mEmerald-CD36 cells expression scrambled, ITGB1 and CD9 shRNA. (B, C, D) Quantification of ITGB1, CD9 and CD36 expression relative to tubulin for TIME mEmerald-CD36 cells and TIME mEmerald-CD36 cells expressing scrambled, ITGB1 and CD9 shRNA. (E) Immunoblots evaluating the expression of ITGB1, CD9, and CD36 within TIME HT-CD36 cells and TIME HT-CD36 cells expression scrambled, ITGB1 and CD9 shRNA. (F,G,H) Quantification of ITGB1, CD9 and CD36 expression relative to tubulin for TIME HT-CD36 cells and TIME HT-CD36 cells expressing scrambled, ITGB1 and CD9 shRNA. A non-parametric Kruskal-Wallis test was employed to determine if there were statistically significant

differences between groups. Following a Kruskal-Wallis test, Dunn's post-hoc test was used to determine pairwise significance values. An α value of 0.05 was used for significance.

Through PLA, we were able to determine the effect of candidate protein inactivation on CD36's interaction with ITGB1 and CD9. CD36 and ITGB1 PLA experiments performed in TIME mEmerald-CD36 CD9 shRNA cells revealed a significant 25% and 38% reduction in the density of PLA dots per cell in comparison to TIME mEmerald-CD36 and TIME mEmerald-CD36 expressing scrambled shRNA (Figure 3-10 A, B). Also, ITGB1 KD significantly affected the interaction between CD36 and CD9, as the constitutive expression of ITGB1 shRNA significantly reduced the density of PLA dots produced per cell by 26% and 18% compared to TIME mEmerald-CD36 and cells constitutively expressing scrambled shRNA (Figure 3-10 A, B).

We also measured CD36 colocalization with CD9 and ITGB1 via conditional colocalization within TIME HT-CD36 cell lines following candidate proteins inactivation. Within TIME HT-CD36 cells, ITGB1 and CD9 shRNA KD significantly reduced the expression of each candidate protein by ~85% and ~75%, respectively (Figure 3-9 F, G). CD36 colocalization with ITGB1 was significantly reduced in TIME HT-CD36 expressing CD9 shRNA, compared to TIME HT-CD36 cells (Figure 6-6). However, TIME HT-CD36 cells expressing scrambled shRNA also had significantly reduced CD36 colocalization with ITGB1 compared to TIME HT-CD36 (Figure 6-6 A). CD36 colocalization with CD9 was significantly reduced in TIME HT-CD36 expressing ITGB1 shRNA, compared to TIME HT-CD36 and TIME HT-CD36 expressing scrambled shRNA (Figure 6-6 B). While conditional colocalization provides further evidence that ITGB1 shRNA KD reduces the colocalization between CD36 and CD9, we cannot determine the effect of CD9 KD on CD36's colocalization with ITGB1. The disparity in the results between conditional colocalization and PLA for our CD9 KD experiments could be due to low-level labelling needed for conditional colocalization. PLA provides a more complete overview of its effect on CD36-ITGB1 interaction due to the 10x higher concentration of antibodies compared to conditional colocalization. Because

PLA provides a more global overview of the interaction than conditional colocalization, we considered PLA results as a superior measure of two-molecule interactions.

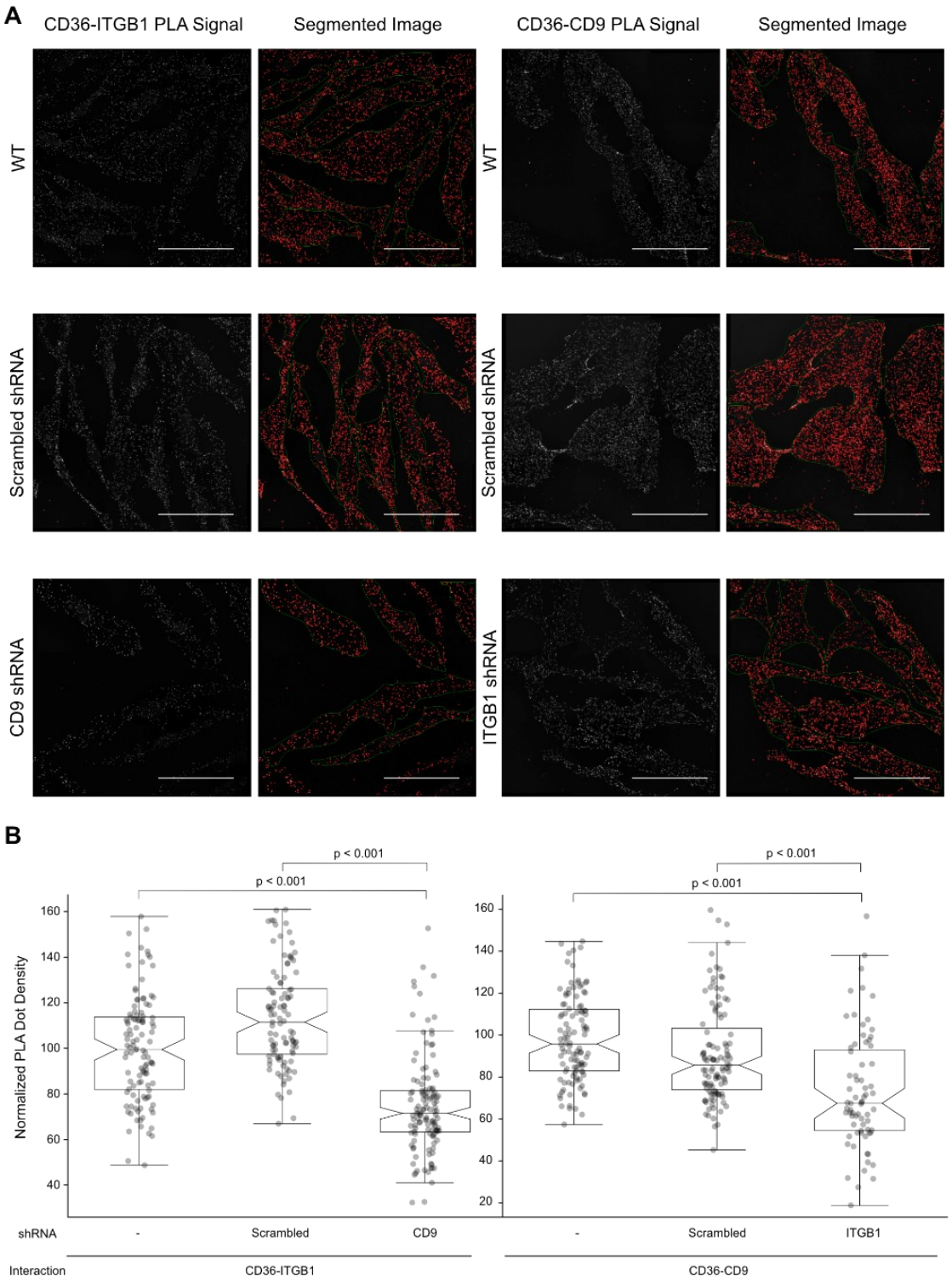

Figure 3-10: Effect of shRNA KD (CD9, ITGB1) on CD36 interaction with CD9 and ITGB1.

(A) TIME mEmerald-CD36 WT, TIME mEmerald-CD36 cells constitutively expressing scrambled shRNA, and TIME mEmerlad-CD36 cells constitutively expressing ITGB1 or CD9 shRNA were treated with Concanavalin A AF488, prior to adding primary antibodies. Mouse anti-CD36 and rabbit anti-CD9 antibodies were used to determine CD9 interaction

with CD36 following ITGB1 shRNA KD. Mouse anti-ITGB1 and rabbit anti-GFP were used to determine ITGB1 interaction with CD36 following CD9 shRNA KD. A pipeline was developed in CellProfiler to segment cells and PLA dots to quantify the density of PLA dots per cell. Bar scale: 100μm. (B) The boxplots indicate the PLA dots per cell per pixel produced by PLA reactions between CD36 and candidate proteins. A customized pipeline in CellProfiler was developed to segment the cell, PLA dots, and quantify the density of PLA per cell. A non-parametric Kruskal-Wallis test test was employed to determine if there were statistically significant differences between groups. Following a Kruskal-Wallis test, Dunn's post-hoc test was used to determine pairwise significance values. An α value of 0.05 was used for significance. For PLA between CD36-ITGB1, 124 TIME HT-CD36 WT, 101 TIME HT-CD36 cells expressing scrambled shRNA, and 112 TIME-HT CD36 CD9 KD cells were analyzed over a single experiment. For PLA between CD36-CD9, 110 TIME HT-CD36 WT, 111 TIME HT-CD36 cells expressing scrambled shRNA, and 112 TIME-HT CD36 ITGB1 KD cells were analyzed over a single experiment.

Further deciphering CD36 interaction via ITGB1 and CD9 shRNA KD cell lines revealed that CD36 interaction with ITGB1 is positively influenced by CD9 and vice versa. Compared to TIME mEmerald-CD36 cells expressing scrambled shRNA, CD9 KD cells had a larger effect on CD36's interaction with ITGB1 than ITGB1 KD on the interaction between CD36 and CD9. These findings also align with our conditional colocalization results, showing that ITGB1's colocalization with CD9 had a greater effect on CD36's interaction with ITGB1 than CD9's colocalization with ITGB1 had on CD36's interaction with CD9. Because CD9 KD had a greater effect, we believe CD9 to be an important molecule connecting CD36 to ITGB1. PLA and conditional colocalization experiments in TIME CD36 KD cell lines provide support for this ternary complex forming between CD36, ITGB1 and CD9. We next designed experiments to evaluate the role of CD9 and ITGB1 within this ternary complex in the context of anti-angiogenic signalling.

3.4 Investigating the Role of CD9, and ITGB1 in CD36-Fyn Anti-Angiogenic Signalling

To investigate the role of CD9 and ITGB1 in CD36-Fyn signalling, we stimulated CD36 using the multivalent IgM mouse anti-CD36 antibody on TIME HT-CD36 cells inactivated for ITGB1 or CD9. Following IgM stimulation of CD36, cells were stained with rabbit anti-phospho-Y420 Src to probe for activated Fyn (P-Y420-Fyn) and then imaged cells via TIRF microscopy as indicated in the material and methods (Figure 3-11, A). To normalize for cell size, the total intensity of P-Y420-Fyn was divided by the pixel area of the cell. Stimulation of TIME HT-CD36 cells resulted in a ~ 1.67-fold increase in the density of P-Y420-Fyn intensity compared to unstimulated TIME HT-

CD36 cells (Figure 3-11, B). Similarly, TIME HT-CD36 cells expressing scrambled shRNA exhibited a ~1.54-fold increase in the density of P-Y420-Fyn intensity upon stimulation (Figure 3-11, B). The significant increase in the density of P-Y420-Fyn intensity following stimulation for both cell lines verifies that multivalent stimulation of CD36 within TIME-HT CD36 cells results in Fyn activation, as reported previously in Githaka et al. (2016). However, stimulation of TIME HT-CD36 cells expressing ITGB1 shRNA resulted in virtually no change in P-Y420-Fyn intensity density (Figure 3-11, B). Stimulation of CD9 shRNA KD cell lines resulted in ~1.3-fold change in density of P-Y420-Fyn intensity, which is significant albeit attenuated in comparison to the response seen in the wildtype TIME HT-CD36 cells (Figure 3-11, B). Activation experiments within TIME shRNA KD cell lines demonstrate that CD36's capacity to activate Fyn is abolished in absence of ITGB1. Therefore, ITGB1 is required for CD36-Fyn anti-angiogenic signalling. To next thought to explore interactions modulated between CD36, CD9, ITGB1, and P-Y420-Fyn in response to anti-angiogenic signalling, we performed conditional colocalization analysis following CD36-IgM stimulation.

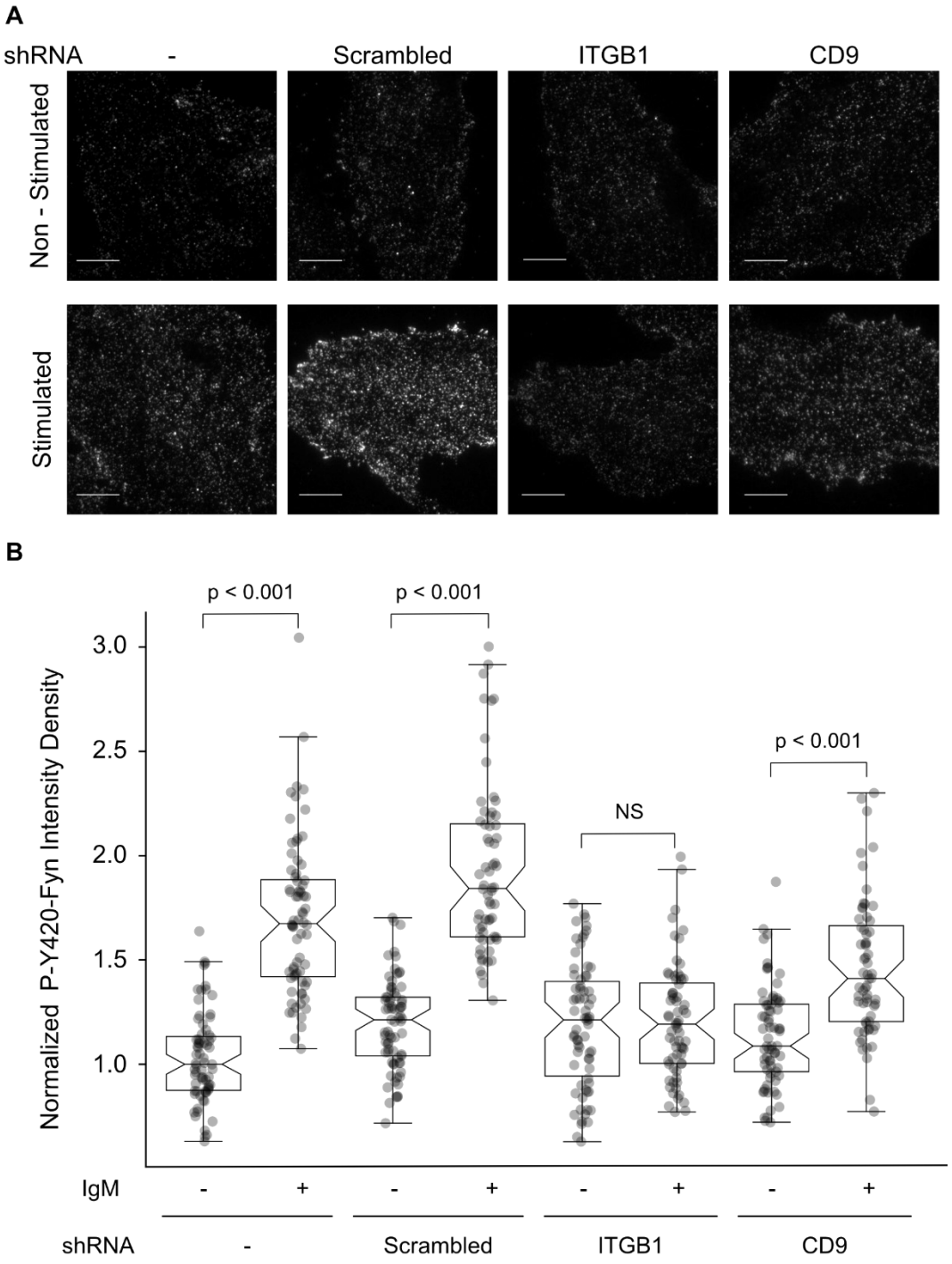

Figure 3-11: The effect of ITGB1 and CD9 shRNA KD on mouse anti-CD36 IgM induced CD36-Fyn anti-angiogenic signalling.

(A) TIRF microscopy images at 100x magnification of TIME HT-CD36 cell, and TIME HT-CD36 cell expressing scrambled, CD9 or ITGB1 shRNA unstimulated or stimulated with mouse anti-CD36 IgM. Rabbit-anti phosphorylated Src was used to probe for activated Fyn, followed by secondary staining with donkey anti-mouse AF488. The scale bar is 10 µm. (B) The boxplots indicate the density of P-Y420-Fyn intensity per pixel for cell at rest (-) and following mouse anti-CD36 IgM stimulation. A customized pipeline in CellProfiler was developed to segment the cell and quantify the

density P-Y420-Fyn intensity per cell. A non-parametric Kruskal-Wallis test was employed to determine if there were statistically significant differences between groups. Following a Kruskal-Wallis test, Dunn's post-hoc test was used to determine pairwise significance values. An α value of 0.05 was used for significance. For TIME-HT CD36 WT, 71 and 72 cells were imaged for the unstimulated and stimulated conditions, respectively. For TIME-HT CD36 cells expressing scrambled shRNA, 73 and 64 cells were imaged for the unstimulated and stimulated conditions, respectively. For TIME-HT CD36 cells expressing ITGB1 shRNA, 70 and 68 cells were imaged for the unstimulated and stimulated conditions, respectively. For TIME-HT CD36 cells expressing CD9 shRNA, 69 and 64 cells were imaged for the unstimulated and stimulated conditions, respectively. For four cell lines, cells were imaged across 3 experiments.

3.5 Investigating Changes in CD36, ITGB1 and CD9 Organization during Anti-Angiogenic Signalling via Conditional Colocalization

To investigate how CD36 interaction with CD9 and ITGB1, modulates CD36's interaction with P-Y420-Fyn we performed conditional colocalization on TIME HT-CD36 stimulated with mouse anti-CD36 IgM. At rest, ~13% of CD36 punta colocalized with P-Y420-Fyn (p(CD36w P-Y420-Fyn)) and was significantly greater than the nullTR coincidental colocalization (Figure 3-12, A). Upon IgM stimulation, there was a significant 1% increase in CD36 colocalization P-Y420-Fyn (Figure 6-6 C). This significant increase was also seen in TIME HT-CD36 expressing scrambled shRNA and ITGB1 shRNA, but not in our CD9 KD cell line (Figure 6-6, C).

However, CD36's colocalization with CD9 significantly enhanced CD36's colocalization with P-Y420-Fyn, as CD36-CD9 colocalization events had a ~2-fold increase colocalization with P-Y420-Fyn (p(CD36wP-Y420-Fyn | CD36wCD9)) in comparison to CD36 overall (p(CD36wP-Y420-Fyn)) (Figure 3-12, A). IgM stimulation of CD36 also resulted in a significant increase in p(CD36wP-Y420-Fyn | CD36wCD9) from ~27% at rest to 32% (Figure 3-12, B). The increase in the proportion of CD36-CD9 colocalization events colocalizing with P-Y420-Fyn upon CD36 IgM stimulation was also seen in TIME HT-CD36 expressing scrambled shRNA, but not in ITGB1 KD cells (Figure 3-12, B). Therefore, ITGB1 is needed for the IgM-induced increase in the proportion of the CD36-CD9 colocalization events also colocalizing with P-Y420-Fyn.

The colocalization of P-Y420-Fyn with CD9 did not enhance CD36's interaction with P-Y420-Fyn, as p(CD36w(P-Y420-FynwCD9)) was not significantly different from p(CD36wFyn)

(Figure 3-12, A). Also, the colocalization of CD36 with P-Y420-Fyn when CD36 does not colocalize with CD9 (p(CD36wP-Y420-Fyn | CD36nCD9))) and colocalization of CD36 with P-Y420-Fyn when P-Y420-Fyn does not colocalize with CD9 (p(CD36w(P-Y420-FynnCD9))) did not significantly differ from coincidental colocalization measures nor CD36's overall colocalization with P-Y420-Fyn (p(CD36wP-Y420-Fyn)) (Figure 3-12, A).

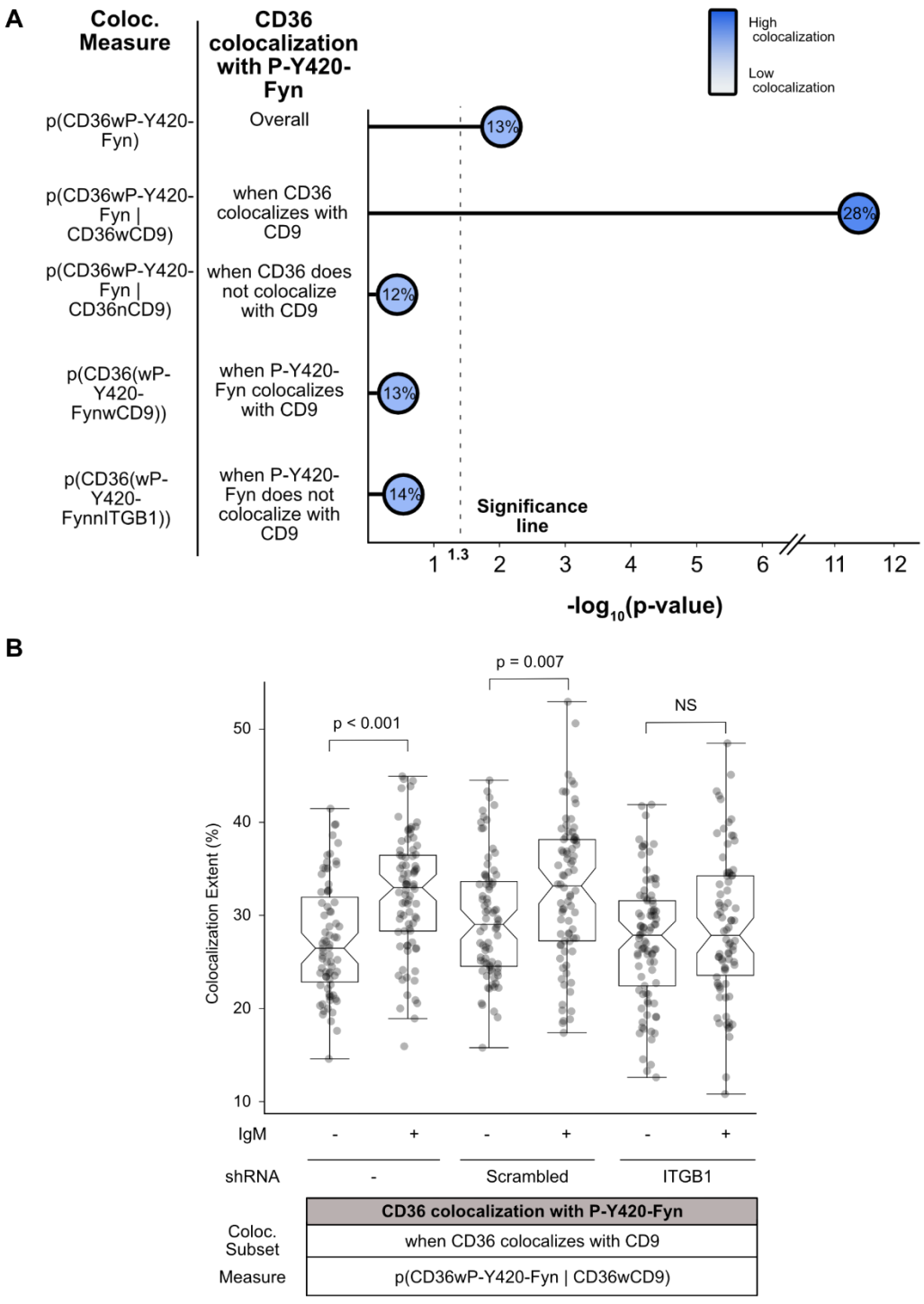

Figure 3-12: Conditional colocalization analysis of CD36, P-Y420-Fyn, and CD9 following CD36 stimulation and/or ITGB1 shRNA KD.

Overall CD36 colocalization with P-Y420-Fyn (p(CD36wP-Y420-Fyn)), CD36 colocalization with CD9 positive P-Y420-Fyn (p(CD36w(P-Y420-FynwCD9))), and CD36-CD9 subset's colocalization with P-Y420-Fyn (p(CD36wP-Y420-Fyn | CD36wCD9)) at rest. The colocalization of CD36 with P-Y420-Fyn, when CD36 does not colocalize with CD9 (p(CD36wP-Y420-Fyn | CD36nCD9)) and colocalization of CD36 with P-Y420-Fyn when P-Y420-Fyn does not

colocalize with CD9 (p(CD36w(P-Y420-FynnCD9))), was also determined. For the three-molecular conditional colocalization measurements the least significant p-value among three comparisons (p(CD36wP-Y420-Fyn), nullTR and RandC) was expressed via -log$_{10}$(p-value). The -log$_{10}$(p-value) for the statistical comparison between p(CD36wP-Y420-Fyn) and nullTR is also shown. The threshold for significance for p(CD36wP-Y420-Fyn), p(CD36wP-Y420-Fyn | CD36wCD9), p(CD36wP-Y420-Fyn | CD36nCD9), p(CD36w(P-Y420-FynwCD9)) and), p(CD36w(P-Y420-FynnCD9)) significance were calculated using Dunn-Sidak correction. 75 cells were imaged across 3 experiments (B) The effect of mouse anti-CD36 IgM stimulation (10μg/mL), scrambled shRNA, and ITGB1 shRNA was further investigated on CD9-positive CD36 colocalization with P-Y420-Fyn (p(CD36wP-Y420-Fyn | CD36wCD9)). A non-parametric T-test was used to determine the significant difference between stimulated and unstimulated conditional colocalization experiments. A conditional colocalization radius of 2 pixels was used for all analyses. For TIME-HT CD36 WT, 75 and 82 cells were imaged for the unstimulated and stimulated conditions, respectively. For TIME-HT CD36 cells expressing scrambled shRNA, 79 and 80 cells were imaged for the unstimulated and stimulated conditions, respectively. For TIME-HT CD36 cells expressing ITGB1 shRNA, 89 and 78 cells were imaged for the unstimulated and stimulated conditions, respectively. For all three cell lines, cells were imaged across 3 experiments.

Conditional colocalization also revealed changes in CD36's interaction with ITGB1 and P-Y420-Fyn in response to CD36 stimulation. At rest, we found that CD36's colocalization with ITGB1 did not affect CD36's colocalization with P-Y420-Fyn, as the proportion of CD36-ITGB1 colocalization events also colocalizing with P-Y420-Fyn (p(CD36wP-Y420-Fyn | CD36wITGB1)) did not significantly differ from CD36's overall colocalization with P-Y420-Fyn (p(CD36wP-Y420-Fyn)) (Figure 3-13, A). The colocalization of CD36 with P-Y420-Fyn when CD36 does not colocalize with ITGB1 (p(CD36wP-Y420-Fyn | CD36nITGB1)) and colocalization of CD36 with P-Y420-Fyn when P-Y420-Fyn does not colocalize with ITGB1 (p(CD36w(P-Y420-FynnITGB1))) did not significantly differ from coincidental colocalization measures nor CD36's overall colocalization with P-Y420-Fyn (p(CD36wP-Y420-Fyn)) (Figure 3-13, A).

However, P-Y420-Fyn's colocalization with ITGB1 modestly enhanced CD36's colocalization with P-Y420-Fyn as the proportion of P-Y420-Fyn-ITGB1 colocalization events also colocalizing with CD36 (p(CD36w(P-Y420-FynwITGB1)) was significantly greater than CD36's overall colocalization with (p(CD36wP-Y420-Fyn)) (Figure 3-13, A). Upon IgM stimulation the proportion of P-Y420-Fyn-ITGB1 colocalization events also colocalizing with CD36 (p(CD36w(P-Y420-FynwITGB1))) significantly increase from ~14% at rest to ~16% (Figure 3-13, B). To investigate the role of CD9 in IgM-induced increase in p(CD36w(P-Y420-FynwITGB1)) we

performed conditional colocalization experiments within TIME HT-CD36 CD9 KD cell line. Within the CD9 KD cell line, the IgM-induced increase in p(CD36w(P-Y420-FynwITGB1)) was abolished, demonstrating that the CD9 is needed for the P-Y420-Fyn-ITGB1 subset's increased colocalization with CD36 upon IgM stimulation (Figure 3-13, B).

Through conditional colocalization, we discovered CD36's colocalization with CD9 significantly enhances CD36's colocalization with P-Y420-Fyn, as the proportion of CD36-CD9 colocalization events also colocalizing with P-Y420-Fyn enhances upon IgM stimulation. Also, the importance of CD9 within anti-angiogenic signalling was further demonstrated in the CD9 KD cells, which abolished IgM-induced increase in P-Y420-Fyn-ITGB1 subsets colocalization with CD36.

ITGB1 KD abolished the IgM-induced increase in the proportion of CD36-CD9 colocalization events also colocalizing with P-Y420-Fyn. This is consistent with our finding from previous experiments showing that ITGB1 is needed for CD36-Fyn anti-angiogenic signalling (Figure 3-11). However, CD36's colocalization with ITGB1 did not enhance CD36's colocalization with P-Y420-Fyn. This indicates that other proteins must also be involved in CD36 anti-angiogenic signalling, as CD36's colocalization with ITGB1, alone, had no effect on CD36's association with P-Y420-Fyn.

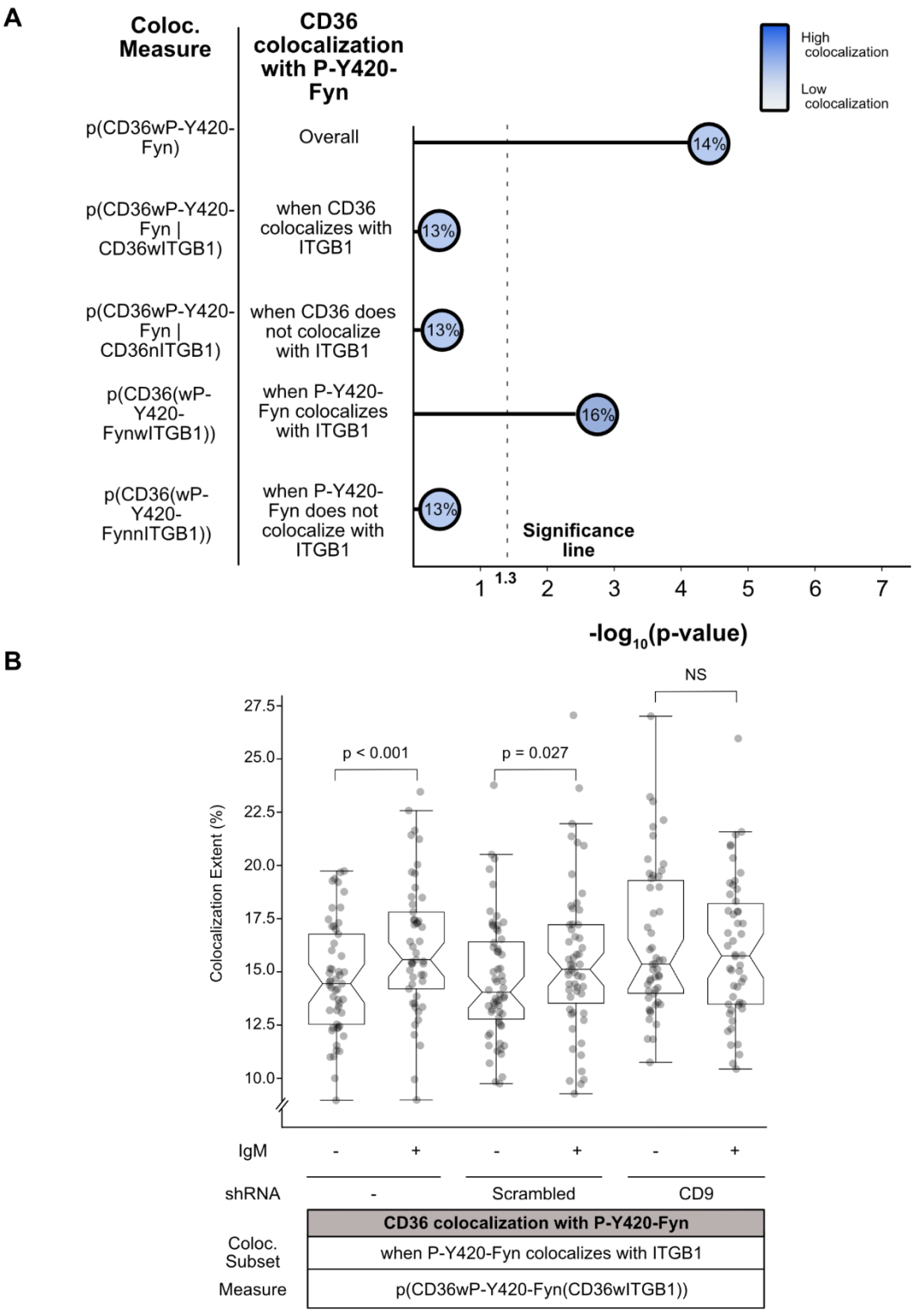

Figure 3-13: Conditional colocalization analysis of CD36, P-Y420-Fyn and ITGB1 following CD36 stimulation and/or CD9 shRNA KD.

(A) Overall CD36 colocalization with P-Y420-Fyn (p(CD36wP-Y420-Fyn)), CD36-ITGB1 subset colocalization with P-Y420-Fyn (p(CD36wP-Y420-Fyn | CD36wITGB1)), and CD36's colocalization with P-Y420-Fyn-ITGB1 subset at rest.

The colocalization of CD36 with P-Y420-Fyn, when CD36 does not colocalize with ITGB1 (p(CD36wP-Y420-Fyn | CD36nITGB1)) and colocalization of CD36 with P-Y420-Fyn when P-Y420-Fyn does not colocalize with ITGB1 (p(CD36w(P-Y420-FynnITGB1))), was also determined. For the three-molecular conditional colocalization measurements the least significant p-value among three comparisons (p(CD36wP-Y420-Fyn), nullTR and RandC) was expressed via -log$_{10}$(p-value). The -log$_{10}$(p-value) for the statistical comparison between p(CD36wP-Y420-Fyn) and nullTR is also shown. The threshold for significance for p(CD36wP-Y420-Fyn), p(CD36wP-Y420-Fyn | CD36wITGB1), p(CD36wP-Y420-Fyn | CD36nITGB1), p(CD36w(P-Y420-FynwITGB1)) and p(CD36w(P-Y420-FynnITGB1)) significance were calculated using Dunn-Sidak correction. 53 cells were imaged across 3 experiments (B) The effect of mouse anti-CD36 IgM stimulation (10µg/mL), scrambled shRNA, and CD9 shRNA was further investigated on CD36 colocalization with P-Y420-Fyn-ITGB1 subset (p(CD36w(P-Y420-Fyn(wITGB1))). A non-parametric T-test was used to determine the significant difference between stimulated and unstimulated conditional colocalization experiments. A conditional colocalization radius of 2 pixels was used for all analyses. For TIME-HT CD36 WT, 53 and 49 cells were imaged for the unstimulated and stimulated conditions, respectively. For TIME-HT CD36 cells expressing scrambled shRNA, 60 and 55 cells were imaged for the unstimulated and stimulated conditions, respectively. For TIME-HT CD36 cells expressing CD9 shRNA, 50 cells were imaged for the unstimulated and stimulated conditions, respectively. For all three cell lines, cells were imaged across 3 experiments.

Overall, the experiments here have elucidated the role of ITGB1 and CD9 in CD36 anti-angiogenic signalling. The basis for our investigation of candidate proteins began by identifying proteins in proximity to CD36 via CD36 BAR. Following BAR, candidate protein vicinity was confirmed via PLA. Further investigation of CD9 and ITGB1 via conditional colocalization and PLA experiments within our shRNA KD cells provided evidence for CD36 forming a complex with ITGB1 and CD9, where CD9 links CD36 and ITGB1. Furthermore, CD36-IgM stimulation experiments showed ITGB1 to be necessary for CD36 anti-angiogenic signalling. Through conditional colocalization, we also discovered that CD36's colocalization with CD9 enhances CD36's colocalization with P-Y420-Fyn, and CD9's effect is significantly increased upon IgM stimulation. However, the IgM-induced enhancement of CD36-CD9 colocalization events also colocalizing with P-Y420-Fyn was dependent upon ITGB1. ITGB1 also had a conditional effect on CD36-P-Y420-Fyn as P-Y420-Fyn colocalization with ITGB1 enhanced CD36's colocalization with P-Y420-Fyn. Also, the fraction of P-Y420-Fyn-ITGB1 colocalizing with CD36 was significantly increased upon IgM stimulation. However, this IgM induced enhancement was dependent upon CD9. The next chapter will discuss significance of these results and they have contributed to novel model of CD36-Fyn anti-angiogenic signalling.

3.6 References

Alam MS. 2022. Proximity Ligation Assay (PLA)Proximity ligation assay (PLA). In: Del Valle L, editor. Immunohistochemistry and Immunocytochemistry: Methods and Protocols. New York, NY: Springer US. (Methods in Molecular Biology). p. 191–201. [accessed 2024 Feb 27]. https://doi.org/10.1007/978-1-0716-1948-3_13.

Arias-Romero LE, Saha S, Villamar-Cruz O, Yip S-C, Ethier SP, Zhang Z-Y, Chernoff J. 2009. Activation of Src by Protein Tyrosine Phosphatase-1B is required for ErbB2 transformation of human breast epithelial cells. Cancer Res. 69(11):4582–4588. doi:10.1158/0008-5472.CAN-08-4001.

Bamberger ME, Harris ME, McDonald DR, Husemann J, Landreth GE. 2003. A Cell Surface Receptor Complex for Fibrillar β-Amyloid Mediates Microglial Activation. J Neurosci. 23(7):2665–2674. doi:10.1523/JNEUROSCI.23-07-02665.2003.

Bar DZ, Atkatsh K, Tavarez U, Erdos MR, Gruenbaum Y, Collins FS. 2018. Biotinylation by antibody recognition—a method for proximity labelling. Nat Methods. 15(2):127–133. doi:10.1038/nmeth.4533.

Bjorge JD, Pang A, Fujita DJ. 2000. Identification of Protein-tyrosine Phosphatase 1B as the Major Tyrosine Phosphatase Activity Capable of Dephosphorylating and Activating c-Src in Several Human Breast Cancer Cell Lines *. Journal of Biological Chemistry. 275(52):41439–41446. doi:10.1074/jbc.M004852200.

Cell line - CD9 - The Human Protein Atlas. [accessed 2024 Jan 23]. https://www.proteinatlas.org/ENSG00000010278-CD9/cell+line.

Cell line - ITGB1 - The Human Protein Atlas. [accessed 2023 Apr 18]. https://www.proteinatlas.org/ENSG00000150093-ITGB1/cell+line.

Chen L-M, Bailey D, Fernandez-Valle C. 2000. Association of β1 Integrin with Focal Adhesion Kinase and Paxillin in Differentiating Schwann Cells. J Neurosci. 20(10):3776–3784. doi:10.1523/JNEUROSCI.20-10-03776.2000.

Cross NL. 2004. Reorganization of Lipid Rafts During Capacitation of Human Sperm1. Biology of Reproduction. 71(4):1367–1373. doi:10.1095/biolreprod.104.030502.

Davis SP, Lee K, Gillrie MR, Roa L, Amrein M, Ho M. 2013. CD36 Recruits α5β1 Integrin to Promote Cytoadherence of P. falciparum-Infected Erythrocytes. PLoS Pathog. 9(8):e1003590. doi:10.1371/journal.ppat.1003590.

Githaka JM, Vega AR, Baird MA, Davidson MW, Jaqaman K, Touret N. 2016. Ligand-induced growth and compaction of CD36 nanoclusters enriched in Fyn induces Fyn signalling. Journal of Cell Science. 129(22):4175–4189. doi:10.1242/jcs.188946.

Heit B, Kim H, Cosío G, Castaño D, Collins R, Lowell CA, Kain KC, Trimble WS, Grinstein S. 2013. Multimolecular Signalling Complexes Enable Syk-Mediated Signalling of CD36 Internalization. Developmental Cell. 24(4):372–383. doi:10.1016/j.devcel.2013.01.007.

Huang W, Febbraio M, Silverstein RL. 2011. CD9 tetraspanin interacts with CD36 on the surface of macrophages: a possible regulatory influence on uptake of oxidized low density lipoprotein. PLoS One. 6(12):e29092. doi:10.1371/journal.pone.0029092.

Huang W, Li R, Zhang J, Cheng Y, Ramakrishnan DP, Silverstein RL. 2023. A CD36 transmembrane domain peptide interrupts CD36 interactions with membrane partners on macrophages and inhibits atherogenic functions. Transl Res. 254:68–76. doi:10.1016/j.trsl.2022.10.005.

Kazerounian S, Duquette M, Reyes MA, Lawler JT, Song K, Perruzzi C, Primo L, Khosravi-Far R, Bussolino F, Rabinovitz I, et al. 2011. Priming of the vascular endothelial growth factor signalling pathway by thrombospondin-1, CD36, and spleen tyrosine kinase. Blood. 117(17):4658–4666. doi:10.1182/blood-2010-09-305284.

Koyama-Honda I, Fujiwara TK, Kasai RS, Suzuki KGN, Kajikawa E, Tsuboi H, Tsunoyama TA, Kusumi A. 2020. High-speed single-molecule imaging reveals signal transduction by induced transbilayer raft phases. Journal of Cell Biology. 219(12):e202006125. doi:10.1083/jcb.202006125.

Liang F, Lee S-Y, Liang J, Lawrence DS, Zhang Z-Y. 2005. The Role of Protein-tyrosine Phosphatase 1B in Integrin Signalling *. Journal of Biological Chemistry. 280(26):24857–24863. doi:10.1074/jbc.M502780200.

Mairhofer M, Steiner M, Mosgoeller W, Prohaska R, Salzer U. 2002. Stomatin is a major lipid-raft component of platelet α granules. Blood. 100(3):897–904. doi:10.1182/blood.V100.3.897.

Miao WM, Vasile E, Lane WS, Lawler J. 2001. CD36 associates with CD9 and integrins on human blood platelets. Blood. 97(6):1689–1696. doi:10.1182/blood.v97.6.1689.

Murray EW, Robbins SM. 1998. Antibody Cross-linking of the Glycosylphosphatidylinositol-linked Protein CD59 on Hematopoietic Cells Induces Signalling Pathways Resembling Activation by Complement. Journal of Biological Chemistry. 273(39):25279–25284. doi:10.1074/jbc.273.39.25279.

Oakley JV, Buksh BF, Fernández DF, Oblinsky DG, Seath CP, Geri JB, Scholes GD, MacMillan DWC. 2022. Radius measurement via super-resolution microscopy enables the development of a variable radii proximity labelling platform. Proceedings of the National Academy of Sciences. 119(32):e2203027119. doi:10.1073/pnas.2203027119.

Omidvar N, Wang ECY, Brennan P, Longhi MP, Smith RAG, Morgan BP. 2006. Expression of Glycosylphosphatidylinositol-Anchored CD59 on Target Cells Enhances Human NK Cell-Mediated Cytotoxicity. J Immunol. 176(5):2915–2923.

Salzer U, Prohaska R. 2001. Stomatin, flotillin-1, and flotillin-2 are major integral proteins of erythrocyte lipid rafts. Blood. 97(4):1141–1143. doi:10.1182/blood.V97.4.1141.

Thorne RF, Marshall JF, Shafren DR, Gibson PG, Hart IR, Burns GF. 2000. The Integrins α3β1 and α6β1 Physically and Functionally Associate with CD36 in Human Melanoma Cells: REQUIREMENT FOR THE EXTRACELLULAR DOMAIN OF CD36*. Journal of Biological Chemistry. 275(45):35264–35275. doi:10.1074/jbc.M003969200.

Umlauf E, Mairhofer M, Prohaska R. 2006. Characterization of the Stomatin Domain Involved in Homo-oligomerization and Lipid Raft Association *. Journal of Biological Chemistry. 281(33):23349–23356. doi:10.1074/jbc.M513720200.

Vega-Lugo J, da Rocha-Azevedo B, Dasgupta A, Jaqaman K. 2022. Analysis of conditional colocalization relationships and hierarchies in three-color microscopy images. Journal of Cell Biology. 221(7):e202106129. doi:10.1083/jcb.202106129.

Wary KK, Mariotti A, Zurzolo C, Giancotti FG. 1998. A Requirement for Caveolin-1 and Associated Kinase Fyn in Integrin Signalling and Anchorage-Dependent Cell Growth. Cell. 94(5):625–634. doi:10.1016/S0092-8674(00)81604-9.

Wong HS, Jaumouillé V, Freeman SA, Doodnauth SA, Schlam D, Canton J, Mukovozov IM, Saric A, Grinstein S, Robinson LA. 2016. Chemokine Signalling Enhances CD36 Responsiveness toward Oxidized Low-Density Lipoproteins and Accelerates Foam Cell Formation. Cell Reports. 14(12):2859–2871. doi:10.1016/j.celrep.2016.02.071.

Wu S-C, Lo Y-M, Lee J-H, Chen C-Y, Chen T-W, Liu H-W, Lian W-N, Hua K, Liao C-C, Lin W-J, et al. 2022. Stomatin modulates adipogenesis through the ERK pathway and regulates fatty acid uptake and lipid droplet growth. Nat Commun. 13(1):4174. doi:10.1038/s41467-022-31825-z.

Zafra F, Piniella D. 2022. Proximity labelling methods for proteomic analysis of membrane proteins. Journal of Proteomics. 264:104620. doi:10.1016/j.jprot.2022.104620.

Chapter 4: Discussion and Conclusions

4.1 Results and Discussion

By altering the angiogenic balance to promote blood vessel dormancy, anti-angiogenic therapies represent a viable approach to reducing cancer metastasis and growth (Lopes-Coelho et al., 2021). TSP-1's capacity to induce anti-angiogenic signalling within microvascular endothelial cells by stimulating CD36 has been attempted using TSP-1 mimetics. However, monovalent and bi-valent TSP-1 mimetics have had limited efficacy in clinical trials (Huang et al., 2017; Jeanne et al., 2015). The knowledge unveiled through our study of the CD36-induced anti-angiogenic signalling via proximity labelling, fluorescent microscopy, and CD9 and ITGB1 KD could be implemented to improve and re-design existing TSP-1 mimetic therapies. Our discoveries have also led to the development of a novel model highlighting the roles of ITGB1 and CD9 in facilitating CD36-induced anti-angiogenic signalling.

To discover proteins residing within CD36 nanoclusters, we employed CD36 BAR followed by protein identification using LC-MS/MS. CD36 BAR provided us with a list of candidate proteins potentially important in CD36 signalling and organization (Table 6-3). CD36 and Fyn, as well as previously known CD36 interactors CD9 (Kazerounian et al., 2011; Heit et al., 2013), CD81 (Heit et al., 2013), ITGB1 (Heit et al., 2013), ITGA3 (Thorne et al., 2000), ITGA5 (Davis et al., 2013), ITGA6 (Thorne et al., 2000), and STOM (Wu et al., 2020) were enriched in our CD36 BAR dataset. To confirm the proximity of candidate proteins to CD36 in microvascular endothelial cells, we employed PLA, allowing us to determine if these proteins resided within a ~40m radius of CD36.

Performing PLA within TIME mEmerald-CD36 cells confirmed the proximity of CD59, CD9, PTP1B, ITGB1, CD146, MYOF, CD146, and STOM to CD36 (Figure 3-4). Despite their significance in our CD36 BAR dataset, PLA failed to confirm the proximity of CD81 and EPCR to CD36. The discrepancy between our PLA and CD36 BAR data could be attributed to several reasons. For one, the ~250nm labelling radius of BAR is approximately 5 times larger than the resolution of protein-proteins interaction achieved via PLA. Therefore, proteins enriched within

CD36 BAR, but that do not produce PLA signals, could be proteins that do not form intimate interactions with CD36, yet exist within or on the outskirts of the CD36 clusters, which feature a cluster radius of ~70-90nm. The discrepancy could also be attributed to PLA's need for strong antibody labelling. Connector oligomer hybridization is reliant on robust primary antibody staining. Therefore, candidate proteins with low expression and weaker antibodies will provide less PLA signals, even if they are in proximity to CD36. In contrast, BAR requires only strong labelling for a single primary antibody, mouse anti-CD36, and the creation of biotin-radical allows for the labelling of proteins close to CD36, irrespective of their expression. Therefore, low PLA signals do not necessarily mean that candidate proteins do not interact with CD36; however, candidate proteins that produce significant PLA signals, despite the limitations of this technique, can be considered stronger CD36 interactors.

From our narrowed candidate list, we performed a literature search to select protein for further investigation. Given that CD9 (Huang et al., 2023; Heit et al., 2013; Kazerounian et al., 2011; Huang et al., 2011; Miao et al., 2001) and ITGB1 (Davis et al., 2013; Heit et al., 2013; Koenigsknecht and Landreth, 2004; Bamberger et al., 2003; Thorne et al., 2000) interact with CD36 in diverse cell lines and have even been shown to form signalling complexes with CD36 facilitating oxLDL uptake (Heit et al., 2013), we proceeded to investigate the roles of these two proteins in CD36-induced anti-angiogenic signalling and organization.

CD9 is one of 33 members of the tetraspanin superfamily (Berditchevski and Odintsova, 2007). Tetraspanins are characterized as organizers of the cell membrane which mediate protein-protein interactions and play essential roles in biological phenomena such as immune signalling, adhesion, migration, viral pathogenesis, cancer, and trafficking (Mattila et al. 2013, Tejera et al. 2013, Kim et al. 2017; Ono 2010; Mazzocca et al. 2014; Pols and Klumperman, 2009). Along with four transmembrane domains, tetraspanin proteins contain a conserved CCG domain within its large extracellular domain named EC2 domain (see Figure 4-3 (Yang et al., 2020)). Within the

EC2 domain, there is a variable domain that allows tetraspanins to interact with specific protein partners (Shoham et al., 2006; van Deventer et al., 2017; Yang et al., 2020). Via the EC2 domain, tetraspanins interact with, and regulate the function and organization of integrins (Serru et al., 1999; Cook et al., 2002; Zhang et al., 2002; Yu et al., 2017; Rocha-Perugini et al. 2014), leukocyte receptors (Tarrant et al., 2003), transmembrane immunoglobulin superfamily proteins (Stipp et al., 2003; Sala-Valdés et al., 2006; Wang et al., 2011), and intracellular signalling enzymes (Termini et al., 2016; Zuidscherwoude et al., 2017). 'Secondary' or indirect interactions with tetraspanins are dependent upon protein palmitoylation. The association of acyl chains of palmitoylated tetraspanins, and protein partners is believed to lead to the formation and stabilization of tetraspanin-enriched microdomains (TEMs) (Hemler, 2005). Inhibition of protein palmitoylation impairs the recruitment of tetraspanins to TEM, the TEM morphology, and TEM-mediated cell functions (Berditchevski et al., 2002; Zevian et al., 2011; Termini et al., 2014). Although tetraspanins have no known signalling capacity, nor natural ligands, they modulate signalling pathways by facilitating protein-protein interactions. CD9's interaction with β1-integrin is seen within diverse cell lines and has been shown to affect integrin adhesion (Cook et al., 2002; Stipp et al., 2003), activation (Gutiérrez-López et al. 2003), clustering (Rocha-Perugini et al., 2014), and signalling (Rocha-Perugini et al., 2014).

Integrins are a family of heterodimeric proteins composed of an α and β subunit which are bonded non-covalently (Hynes, 2002). The 24 proteins which compose the integrin family are assembled from unique combinates of the 18 α and 8 β subunits (Takada et al., 2007). Integrins are sub-grouped based on their ligand-binding properties (Hynes, 2002; Takada et al., 2007). β1 subunits form integrin complexes that bind collagen (α10β1, α11β1), fibronectin (α4β1, α5β1, α8β1), laminin (α1β1, α2β1, α3β1, α4β1, α7β1), and leukocyte-specific receptors (α4β1, α9β1) (Takada et al. 2007; Barczyk et al., 2010). The α-subunit primarily regulates ligand binding specificity, however, if the α-subunit does not contain the α I domain, the β integrin subunits form

the ligand-binding domain (Zhang and Chen, 2012; Mezu-Ndubuisi and Maheshwari, 2021). Through mediating the connection between the ECM components and actin cytoskeleton, β1 integrins play essential roles in cell adhesion (Bharadwaj et al., 2017; Dao et al., 2021), migration (Jin et al., 2006; Shafaq-Zadah et al., 2016), and proliferation (Pasqualini and Hemler, 1994; Shibue and Weinberg 2009).

For integrins to bind their ligands, they must be in their high affinity or “active “state. Integrin activation is driven by two mechanisms: 1) binding to divalent cations or 2) inside-out signalling. Within the β I domain of β integrin subunits, there are three divalent cation binding sites: metal-ion dependent adhesion site (MIDAS), ADMIDAS (adjacent to MIDAS), and the synergistic metal ion-binding site (SyMBS) which regulates integrin conformation and ligand affinity (Plow et al., 2000; Zhang and Chen, 2012). Binding of Mg^{2+} or Mn^{2+} to MIDAS (Valdramidou et al., 2008; Zhang and Chen, 2012), Mn^{2+} to ADMIDAS (Humphries et al. 2003) or Ca^{2+} binding to syMBS (Zhu et al., 2008) induces conformation changes activating integrins (Figure 4-1). Ca^{2+} also has an inhibitory effect as Ca^{2+} competes with Mg^{2+} and Mn^{2+} for MIDAS (Leitinger et al., 2000), and Ca^{2+} binding to ADMIDAS stabilizes the closed conformation (Zhu et al., 2008). The second mode of (independent or necessary) activation is via inside-out signalling and it occurs in response to intracellular signalling which leads to the binding of talin and kindlin to the cytoplasmic tails of integrins. Talin binding destabilizes a salt bridge between the two subunits leading to changes in the extracellular domain conformation and enhancing ligand binding (Figure 4-1) (Vinogradova et al. 2002; Tadokoro et al. 2003; Anthis et al. 2009; Park et al. 2015; Ludwig et al. 2021). While kindlin alone cannot disrupt the salt bridge, it acts as a co-activator of talin, and therefore promotes integrin activation (Bledzka et al., 2012; Haydari et al., 2020; Lu et al., 2022). Once activated, integrins bind to the ECM-ligands resulting in the recruitment of proteins connecting integrins with the underlying cortical F-actin (talin (Chen et al., 1995; Müller et al. 2014; (Orłowski et al. 2015), paxillin (Rondas et al. 2011; Hu et al., 2014; Lu et al., 2022), vinculin

(Humphries et al., 2007; Calderwood et al., 2013), α-actinin (Smith et al., 2010; Ciobanasu et al., 2012)), and signalling proteins FAK (Klemke et al., 1998; Hu et al., 2014; Yu et al., 2018), Src (Choma et al., 2007; Machiyama et al., 2017), and PI3K (Velling et al., 2004; Matsuoka et al., 2012; Erami et al., 2019). The formation of these complexes at the integrin cytoplasmic tails leads to cell migration, proliferation, actin remodelling, adhesion strengthening and focal adhesion assembly. A summary of integrin activation and signalling is shown in Figure 4-1.

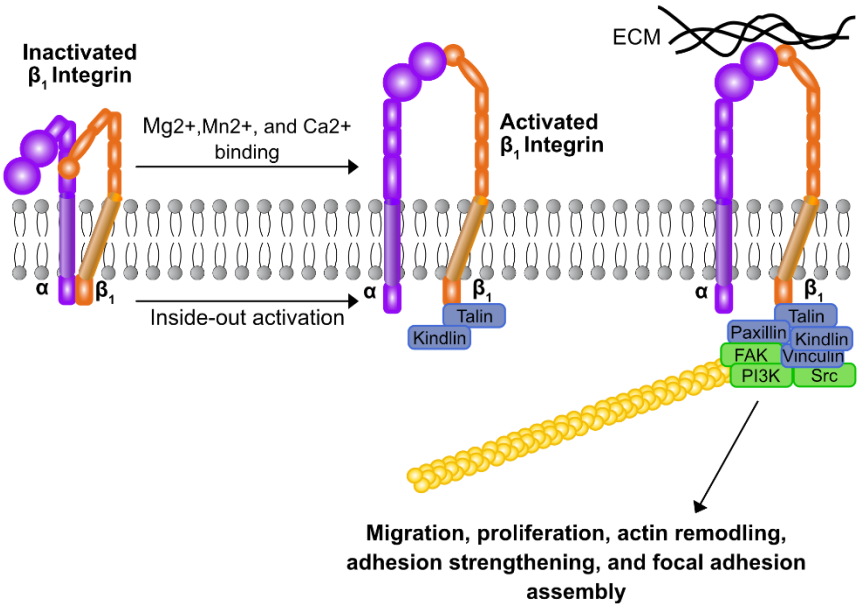

Figure 4-1: Summary of integrin activation and signalling.

Integrin activation can occur via two mechanisms – 1) divalent cation binding and 2) inside-out signalling. Binding of Mg2+, Mn^{2+}, and Ca2+ to specific divalent cation binding sites on β subunit resulting in a conformational change to the high affinity (ligand binding) state. Inside-out activation, in response to cell signalling, leads to talin and kindlin binding to the cytoplasmic tails and change in integrin conformation. Activated integrins can bind to its ligands, such as components of the ECM, leading to the recruitment of scaffolding and intracellular signalling.

Since β1 integrins can exist in different conformations, we investigated whether CD36 associates more with the active or inactive ITGB1. Using antibodies that recognize different conformations of ITGB1, conditional colocalization revealed that CD36 interacts significantly more with active ITGB1 (17%) than total (either active or inactive using antibody clone K20) ITGB1 (10%) (Figure 5-6, D). This suggests that the activated conformation of ITGB1 plays a greater role in CD36 anti-angiogenic signalling. From the CD36 BAR experiments, we also identified integrin-alpha 2, 3, 5, and 6 to be enriched, all of which form heterodimers with ITGB1 (Takada et al., 2007). The diverse signalling properties of each integrin (as discussed in Section 4.1) suggests that a specific heterodimer is needed for CD36-induced anti-angiogenic signalling. Now that a general overview of integrin and CD9 function has been given, I will now put into perspective our discoveries towards better understanding the role of these proteins in CD36-induced anti-angiogenic signalling.

To investigate the role of CD9 and ITGB1, we performed lentiviral transduction of TIME mEmerald-CD36 and TIME HT-CD36 cells with plasmids expressing CD9 or ITGB1 shRNA. These cell lines were utilized within conditional colocalization, PLA, and CD36-IgM stimulation experiments to investigate the role of CD9 and ITGB1 in TSP-1 / CD36 / Fyn signalling, and whether they played a role in the CD36 complex formation and maintenance.

Conditional colocalization experiments investigating the interaction between CD36, CD9, and ITGB1 provided support for these proteins to form a ternary complex. While colocalization of CD9 and ITGB1 with one another was shown to enhance each other's colocalization with CD36, CD9 had a greater conditional effect than ITGB1. PLA experiments in TIME mEmerald-CD36 cells also provided evidence that a ternary complex is formed as the KD of both CD9 and ITGB1, affected one another interaction with CD36. In alignment with our findings from our conditional colocalization experiments, we saw that CD9 KD resulted in a greater reduction in interaction between CD36 and ITGB1, in comparison to the effect of ITGB1 KD on CD36's interaction with

CD9. In addition to providing support for a ternary complex, these experiments have unveiled the role of CD9 as a linker connecting CD36 and ITGB1. Anti CD36-IgM stimulation experiments within shRNA KD TIME CD36 cells further revealed which components of this ternary complex were needed for anti-angiogenic signalling.

Candidate protein shRNA KD and stimulation of CD36 via mouse anti-CD36 IgM revealed ITGB1 to be essential to CD36-Fyn signalling. Interestingly CD9 shRNA KD did not abolish Fyn activation, however, it insignificantly attenuated the activation following IgM stimulation of CD36. If CD9 mediated the critical link between CD36 and ITGB1, then why does CD9 KD not abrogate CD36 anti-angiogenic signalling? One possible explanation is that other tetraspanins, given their high homology to one another, help facilitate the interaction between CD36 and ITGB1 in the absence of CD9. Studies in macrophages have shown that CD36's interaction with CD9 to be mediated by the GXXXG motif within the N-terminal transmembrane domain of CD36 (Huang et al., 2023) (Figure 4-3). Since CD9 also contains a GXXG motif in its 3rd transmembrane domain, it is hypothesized that GXXXG motifs mediate the transmembrane domain interaction between these two proteins (Teese and Langosch, 2015; Huang et al., 2023). Tetraspanin CD81, which was enriched in CD36 BAR, may facilitate CD36's interaction with ITGB1 in the absence of CD9, as it contains a transmembrane GXXXG motif and has shown to associate with CD36 (Heit et al., 2013) and ITGB1 (Serru et al. 1999; Oguri et al. 2020) in Co-IP studies. Although CD151 does not have a transmembrane GXXXG motif, Co-IP and cross-linking studies have revealed CD151 to associate with α3β1 (Yauch et al., 1998; Yauch et al., 2000; Berditchevski et al., 2002; Zhang et al., 2002) and CD36 (Kazerounian et al., 2011). Therefore, it is believed that CD36 forms a complex where CD151 connects CD36 to α3β1 (Thorne et al., 2000; Berditchevski et al., 2002). However, it is important to note that CD151 was not enriched in our proximity biotinylation data set. Performing PLA between CD36-CD81, and CD36-CD151 and conditional colocalization experiments between CD36-ITGB1-CD81/CD151 on TIME CD36 and TIME CD36 with CD9 KD

cell lines would allow us to determine whether CD81, and/or CD151 compensates the absence of CD9. Comparing CD36 anti-angiogenic signalling within TIME cells with all three tetraspanins inactivated or with only CD81 and CD151 knocked down would allow us to truly determine the role of CD9 in CD36-Fyn signalling. However, when present, we propose that CD9 plays a critical role in facilitating interactions needed for CD36 organization and signalling.

Through conditional colocalization, we also observed that the interactions between ITGB1, CD9, CD36, and activated Fyn changed during CD36 stimulation. As expected, activated Fyn's colocalization with ITGB1 enhanced CD36's colocalization with activated Fyn (Figure 3-13). The fraction of CD36 colocalizing with the ITGB1-activated Fyn subset also increases upon IgM stimulation (Figure 3-13). However, the fraction of the CD36-ITGB1 subset colocalizing with activated Fyn was similar to overall colocalization of CD36 with P-Y420-Fyn (Figure 3-13). Therefore, CD36's colocalization with ITGB1 did not enhance CD36's colocalization with activated Fyn (Figure 3-13). This suggests that additional proteins, beyond ITGB1, must be needed to initiate CD36 signalling. CD9 shRNA KD abolished this IgM-induced increase in CD36 colocalization with ITGB1-positive activated Fyn subset, providing evidence that CD9 facilitates critical interactions during anti-angiogenic signalling (Figure 3-13). CD9-positive CD36 had ~2 times greater colocalization with activated Fyn than CD36 overall (Figure 3-12). Moreover, IgM stimulation enhanced CD36-CD9 subset colocalization with activated Fyn, however, ITGB1 inactivation abolished this enhancement (Figure 3-12). These results not only elucidate the role of CD9 as a key mediator in the interactions between CD36, ITGB1 and Fyn, but they also provide further evidence that ITGB1 is an essential component of CD36-induced anti-angiogenic signalling.

In alignment with our finding, ITGB1 has been shown to be essential for Fyn activation and signalling in other biological processes such as oligodendrocyte stimulation with Aβ oligomers (Quintela-López et al., 2019), Schwann cell adhesion and differentiation (Chen et al., 2000),

integrin-signalling (Wary et al., 1998), and oligodendrocyte differentiation (Liang et al., 2004). Moreover, CD36's interaction with ITGB1 has shown to have functional significance in macrophages, as the KD of ITGB1 inhibited Src and spleen tyrosine kinase (SYK) activation upon CD36-mediated oxLDL uptake (Heit et al., 2013). CD36 has also been shown to form a complex with integrin α6β1 which is needed for ß-amyloid interaction and signalling within microglial cells (Koenigsknecht and Landreth, 2004; Bamberger et al., 2003). Antibody blocking of CD36 or ITGB1 inhibited ß-amyloid-mediated activation of Fyn and intracellular tyrosine kinase signalling (Bamberger et al., 2003). The experiments performed in this study demonstrating ITGB1 as a necessary component of CD36-induced anti-angiogenic signalling also provide support for the role of ITGB1 as an activator of Fyn. In addition, our investigation of CD9 and CD36 aligns with previous findings from co-immunoprecipitation experiments showing that CD9 is involved in supporting CD36's interaction with ITGB1 (Heit et al., 2013). Furthermore, the current study is the first one to show this complex to be implicated in anti-angiogenic signalling.

Although our findings implicate ITGB1 and CD9 as facilitators of CD36-induced angiogenic signalling, these proteins have been shown to both inhibit or promote angiogenesis. VEGF-A binding to integrin α9β1 causes the activation of ERK and paxillin leading to endothelial cell migration angiogenesis (Oommen et al., 2011). α2β1 also promotes angiogenesis as neutralizing antibodies against it reduced endothelial proliferation and tube formation in 3D collagen (Ghatak et al., 2016). The pro-angiogenic role of α2β1 has been further supported by *in vivo* studies as α2β1 KO mice also feature impaired angiogenesis (Ghatak et al., 2016). In response to collagen binding and EGF stimulation, α2β1 activates the p38MAPK pathway which promotes endothelial migration (Klekotka et al., 2001). Although p38MAPK activates pro-apoptotic transcription factors, it can also activate transcription factors leading to proliferation (Pua et al. 2022). α5β1 binding to fibronectin was also shown to promote cell migration, and proliferation through FAK and PI3K/AKT signalling (Lee and Ruoslahti, 2005; Bhaskar et al., 2007). Finally, cysteine-rich angiogenic

inducer 61 binding to integrin α6β1 induces endothelial tube formation and angiogenesis through an unknown signalling cascade (Leu et al., 2002; Leu et al., 2003). ITGB1 also inhibits angiogenesis through α3β1. TSP-1 peptide binding to α3β1 has been shown to inhibit endothelial migration and angiogenesis in response to FGF2 and VEGF. C-terminal mutation of CD36 has been shown to decrease its association with ITGB1 and abrogate TSP-1-mediated inhibition of VEGF-A signalling (Primo et al., 2005). These studies imply that a CD36/ITGB1 complex may be needed for TSP-1 to inhibit endothelial cell migration and angiogenesis (Primo et al., 2005; Zhang et al., 2009). While designing novel TSP-1 mimetics, it would be essential to consider the diverse effects of β1 integrins on angiogenesis. Based on our research and literature, enhancing the interaction between CD36 and α3β1 on the endothelial cell membrane could stimulate anti-angiogenic signalling while simultaneously inhibiting VEGF-A.

CD9, through KD and KO studies, has been characterized as a critical protein for angiogenesis. CD9 KD in HUVEC reduces microvascular sprouting (Iwasaki et al., 2013) and migration in response to VEGF and hepatocyte growth factor (HGF) (Kamisasanuki et al., 2011). Moreover, tumour implants within CD9-KO mice had decreased angiogenesis as tumour volume, metastasis, and microvascular density were reduced (Iwasaki et al., 2013). Since CD9 has been shown to promote angiogenesis, monoclonal antibodies against CD9 have been investigated as an anti-angiogenic therapy. Addition CD9 antibodies, have been shown to reduce angiogenesis in response to VEGF and HGF, and tumorigenicity of gastric cancer xenografts in mice (Nakamoto et al., 2009) Intravenous injection of monoclonal CD9 antibody, ALB6, reduced tumour microvascular density and increased gastric cancer apoptosis (Nakamoto et al., 2009). Reduction of tumour viability was not only due to the reduction of tumour neo-vascularization but also to the capacity of ALB6 to activate pro-apoptotic pathways within gastric cancer cells (Murayama et al., 2004; Nakamoto et al., 2009). ALB6 binding inhibited endothelial cell proliferation and activated pro-apoptotic signalling through the activation of p38 MAPK and caspase-3, proteins which are

also downstream effectors in CD36-Fyn anti-angiogenic signalling (Murayama et al. 2004). Whether ALB6 activates or inhibits the function of CD9 as a facilitator of protein-protein interactions is not known as literature has supported both effects (Higginbottom et al., 2000; Murayama et al., 2004; Kamisasanuki et al., 2011; Hwang et al., 2012).

Although CD9 is primarily characterized as a promoter of angiogenesis, it may facilitate both pro- or anti-angiogenesis depending on the connection it facilitates between membrane proteins and integrins. The discoveries presented here have led to the development of a novel model for CD36-induced anti-angiogenic signalling which will be further discussed in the next section.

4.2 CD36-induced Anti-Angiogenic Signalling Model

Githaka et al. (2016) discovered that cortical F-actin, cholesterol, and multivalent ligand were needed to enhance CD36 nanoclusters and hence initiate a downstream signalling cascade. However, the development of multivalent TSP-1 mimetics has had limited efficacy in clinical trials (Molckovsky and Siu, 2008). Therefore, further understanding of CD36-induced anti-angiogenic signalling is needed. Our studies build upon the discoveries of Githaka et al. (2016) by unveiling protein-protein interactions needed for CD36 signalling and organization. Through proximity labelling and quantitative fluorescent microscopy, we have determined CD36, CD9, and ITGB1 to form a ternary complex implicated in anti-angiogenic signalling. The organization of this complex was further deciphered via PLA and conditional colocalization experiments, which revealed CD9 to act as a scaffold connecting ITGB1 to CD36 (Figure 4-2). We hypothesize that CD9 associates with ITGB1 through the EC2 domain (Cook et al. 2002), and the GxxxG transmembrane motifs mediate the interaction between CD36 and CD9 (Figure 4-3) (Teese and Langosch, 2015; Huang et al., 2023).

Furthermore, ITGB1 is essential for the initiation of anti-angiogenic response induced by multivalent IgM binding to CD36. While CD9 is not needed for CD36 signalling, its interaction with CD36 facilitates interactions activation of Fyn. Overall, we have determined that CD36 interaction

of ITGB1, and CD9, two proteins residing within CD36 nanoclusters is essential for its organization and anti-angiogenic signalling capacity.

Although our research has elucidated the protein composition of CD36 clusters, our research has yet to elucidate the role of the cortical F-actin and membrane cholesterol in CD36-Fyn signalling. CD36 clustering is affected by the cytoskeleton, which imposes restrictions on membrane domain formation and size (Ritchie et al., 2003; Jaqaman et al., 2011; Garcia-Parajo et al., 2014; Matuszewska et al., 2022). CD36 connection to the cortical F-actin, possibly through ITGB1, may allow reorganization of the F-actin to enhance CD36 cluster size and density, initiating CD36-Fyn signalling. CD36 has also been shown to reside within lipid nanodomains often referred to as lipid rafts, membrane structures stabilized by cholesterol (Zeng et al., 2003; Pohl et al., 2005; Silverstein and Febbraio, 2009; Chen et al., 2022). Palmitoylated proteins such as CD36, CD9 (Zilber et al., 2005; Ishii et al., 2006; Israels and McMillan-Ward, 2006) and ITGB1 (Salani et al., 2009; Wang et al., 2010) have high affinity for lipid rafts, therefore membrane cholesterol may help recruit ITGB1, CD9 and other raftophilic proteins needed for Fyn activation to CD36 nanoclusters (Levental et al., 2010; Shelby et al., 2023). Although this current study reveals ITGB1 to be necessary for anti-angiogenic signalling, the mechanism by which ITGB1 promotes Fyn activation was not revealed. One of the ways integrins have been shown to activate SFKs in Fcγ-mediated phagocytosis is through creating an actin barrier, following Fcγ engagement, excluding bulky phosphatases from sites of phagocytosis and therefore allowing SFKs activation (Freeman et al., 2016). ITGB1 could be facilitating CD36-Fyn anti-angiogenic signalling similarly by creating an actin network surrounding CD36 clusters following stimulation, excluding phosphatases, and enabling Fyn phosphorylation and signalling.

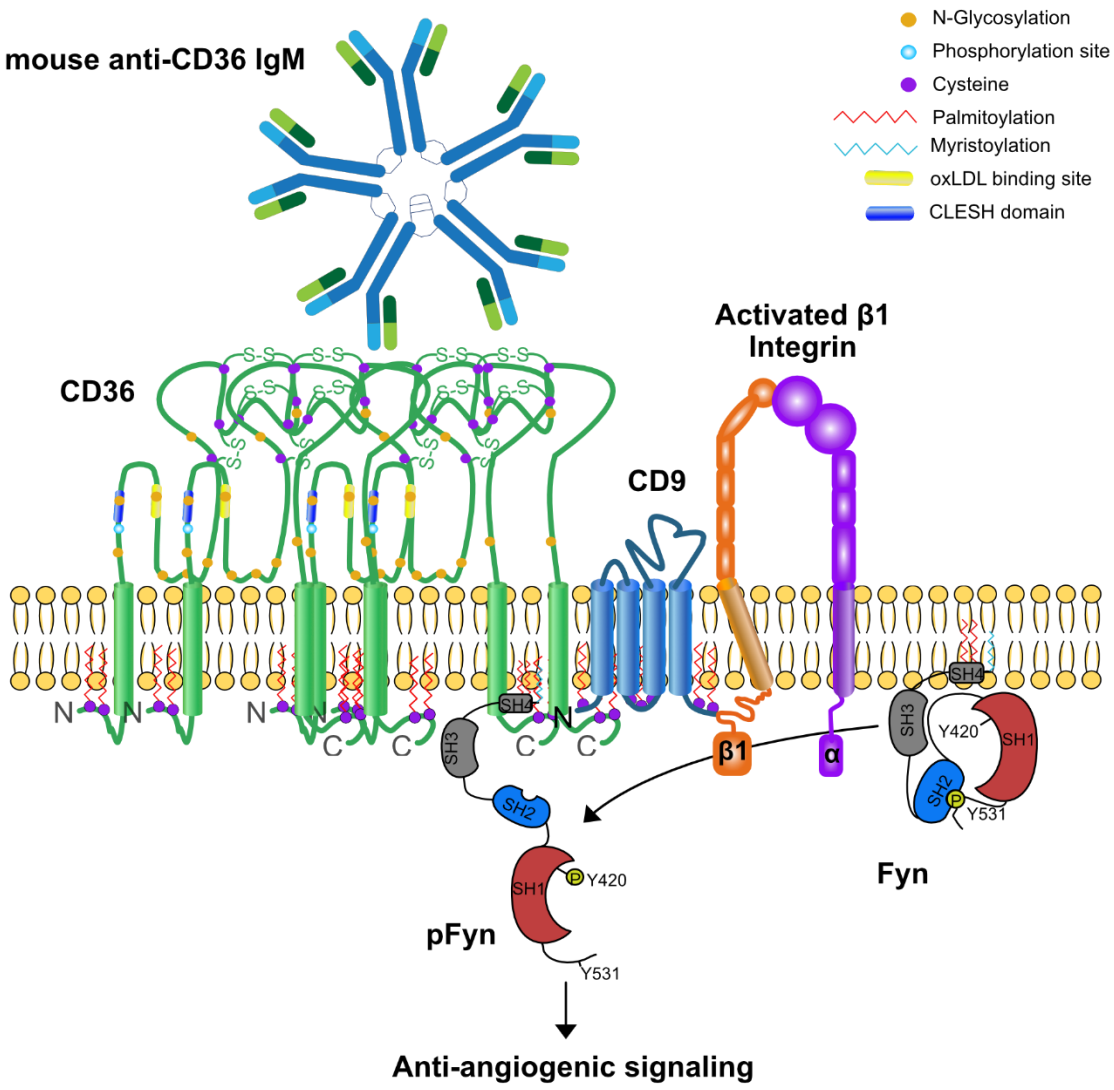

Figure 4-2: Proposed model for CD36-induced anti-angiogenic signalling.

CD36, ITGB1, and CD9 form a ternary complex that facilitates anti-angiogenic signalling. Within this complex CD9 acts as a scaffold linking CD36 to ITGB1. Furthermore, ITGB1 is essential for the activation of Fyn and the initiation of anti-angiogenic signalling induced by IgM stimulation of CD36.

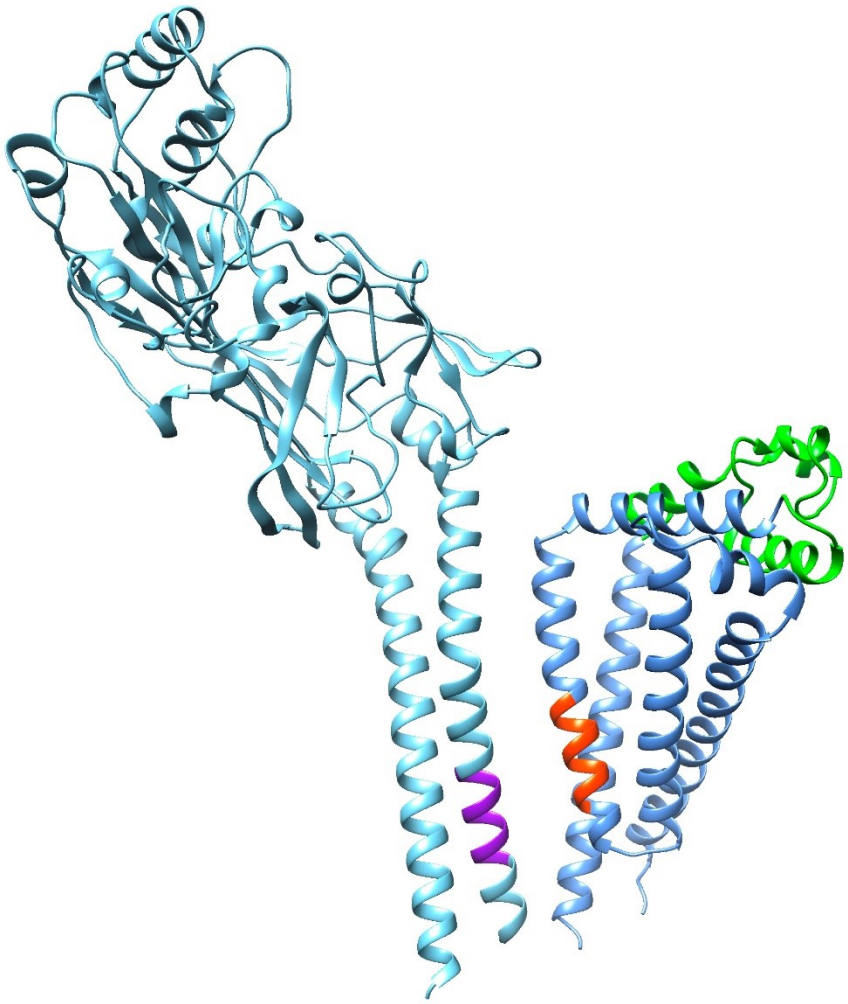

Figure 4-3: CD36 (cyan) and CD9 (blue) crystal structure with interaction domains highlighted.

In purple and red are the GxxxG transmembrane domains for the CD36 and CD9, respectively. The GxxxGxxxG motif of CD36 is N-terminal transmembrane domain (amino acids 2-8), and GxxG motif of CD9 found in the third transmembrane domain (amino acids 90 -94). Highlighted in green is the EC2 domain of CD9 which is needed for CD9's interaction with ITGB1. Designed in Chimera (https://www.cgl.ucsf.edu/chimera/) using Alphafold predictive models for CD36 (AF-P16671-F1) and CD9 (AF-P21926-F1).

4.3 Conclusions and Future Directions

Our research has revealed ITGB1 and CD9 to be pertinent regulators of CD36 organization and signalling. Establishing the signalling model of these proteins with CD36 has provided a

framework which we can build upon to provide a holistic role of ITGB1 and CD9 in CD36 function. The next steps of this project are to investigate the role of CD9 and ITGB1 in two pertinent aspects of CD36 signalling: 1) CD36's connecting to underlying dynamic cortical F-actin and 2) CD36 nanocluster enhancement upon multivalent ligand stimulation.

The cortical F-actin network plays an essential role in regulating the diverse functions of CD36. Drug-mediated perturbation of the F-actin network has been shown to affect CD36 diffusion patterns and internalization via macropinocytosis (Jaqaman et al., 2011; Collins et al., 2009). In addition, triton extraction experiments performed in macrophages provided evidence that CD36 interacts with underlying F-actin, although most likely in an indirect fashion (Jaqaman et al., 2011). F-actin is essential for CD36-induced anti-angiogenic signalling as its perturbation abolished CD36 nanocluster enhancement and hence Fyn activation upon multivalent ligand stimulation (Githaka et al., 2016). Areas with higher F-actin intensities were enriched with CD36 nanocluster and upon stimulation presented higher levels of activated Fyn (Githaka et al., 2016). Despite the importance of F-actin to CD36 function, proteins mediating this connection have yet to be discovered. Our lab has developed an F-actin fractionation protocol, based on F-actin sedimentation, that will be used to separate F-actin associated proteins from the rest of the cell components. In these experiments, we can visualize by immunoblotting the co-sedimentation of CD36 with the F-actin fraction. Preliminary experiments have shown ITGB1 inactivation to decrease the association of CD36 with the F-actin fraction, however, these experiments need to be repeated (Figure 6-7).

Given that ITGB1 links to the cortical cytoskeleton via its association with focal adhesion proteins such as talin (Orłowski et al., 2015), vinculin (Humphries et al., 2007), paxillin (Lawson and Schlaepfer, 2012), and Arp2/3 complex (Brakebusch and Fässler, 2003), we propose that ITGB1 could connect CD36 to the cortical F-actin. In addition, ITGB1-mediated regulation of the

cortical F-actin has been shown to affect CD36 clustering and binding to oxLDL (Wong et al., 2016).

CD36 plasma membrane organization into nanoclusters is essential for its capacity to activate Fyn and initiate anti-angiogenic signalling (Githaka et al., 2016). Therefore, to truly understand the role of ITGB1 and CD9 in the context of anti-angiogenic signalling, we need to determine their effect on CD36 nanocluster organization. Stochastic optical reconstruction microscopy super-resolution imaging of CD36 within TIME CD36 cells with ITGB1 and CD9 shRNA will reveal the properties of CD36 clusters at steady-state and following stimulation. This would unveil whether these proteins are needed for nanocluster formation and/or their enhancement during activation. Given that ITGB1 is needed for CD36-Fyn activation, we believe that ITGB1 KD will abolish nanocluster enhancement. For our investigation of F-actin connection and nanocluster organization within CD9 shRNA cell lines, it is important to realize that tetraspanins, such as CD81 and CD151, could facilitate essential interactions in the absence of CD9. Therefore, CD9, CD81, and CD151 triple shRNA KD may be needed to clearly define the role of CD9.

While our research has determined proteins that reside within CD36 nanoclusters, the reason, or mechanisms by which these proteins are recruited and reside within these nanodomains remain unknown. Given that CD36 is highly palmitoylated, and that membrane cholesterol is needed for CD36 nanocluster enhancement, CD9 and ITGB1 could be recruited due to their preference to interact with liquid-ordered lipids (palmitoylated proteins are known to favour this type of membrane domains (Levental et al., 2010; Shelby et al., 2023)) or domains. To investigate the role of membrane cholesterol in the interaction, we would perform plasma membrane cholesterol extraction, via addition of methyl beta-cyclodextrin, followed by PLA between CD36 and ITGB1. In addition, conditional colocalization experiments following membrane cholesterol removal would also help determine if the interactions facilitated by CD9

and ITGB1 during anti-angiogenic signal are dependent upon the formation of lipid nanodomains. In addition, transfection of TIME HT-CD36 cells with fluorescent plasma membrane markers which partition into liquid ordered-phase of the membrane, followed by conditional colocalization will allow us to determine if the interactions of CD36 and ITGB1, or CD9 preferentially occur with lipid nanodomains (Shelby et al., 2023). Conditional colocalization and PLA experiments upon F-actin perturbation with latrunculin B would also unveil if the interactions between CD36 and candidate proteins are dependent upon the actin cytoskeleton.

Integrins are heterodimeric proteins, and while we have determined ITGB1 resides in proximity to CD36, we have still to define which integrin alpha/beta heterodimer is needed for CD36-induced anti-angiogenic signalling. From the CD36 BAR experiments, we have identified integrin-alpha 2, 3, 5, and 6 to be enriched in proximity to CD36. Conditional colocalization between CD36, ITGB1, and integrin-alpha 2, 3, 5, or 6 will elucidate which integrin-alpha/ITGB1 heterodimer is needed for CD36 function and signalling. Because different integrin-alpha/ITGB1 heterodimers have unique effects on angiogenesis (as discussed in Section 4.1), determining the integrin-alpha / ITGB1 heterodimer implicated in CD36 signalling will be essential in designing novel anti-angiogenic therapeutics.

Our research has unveiled ITGB1, and CD9 as proteins that can be targeted to enhance the effectiveness of existing anti-angiogenic drugs. The addition of fibronectin mimetic, the ligand for a majority of ITGB1 heterodimers, to TSP-1 multimeric scaffolds could improve the interaction between CD36 and ITGB1 and hence enhance the stimulation of anti-angiogenic signalling in vivo (Shroff et al. 2010; Widhe et al. 2016). In addition to revealing novel targets of anti-angiogenesis, our study contributes to the debate on the existence of lipid rafts. Through CD36 BAR and PLA, we have shown that CD36, a canonical “raft protein”, has specific proteins enriched in its proximity (Pohl et al., 2005; Ehehalt et al., 2008; Glatz et al., 2022). We have also shown that two of these proteins, ITGB1 and CD9, play a crucial role in facilitating CD36 organization and function. Finally,

this investigation of CD36 has provided a roadmap that can be applied to study the organization of membrane proteins within their native states.

4.4 References

Anthis NJ, Wegener KL, Ye F, Kim C, Goult BT, Lowe ED, Vakonakis I, Bate N, Critchley DR, Ginsberg MH, et al. 2009. The structure of an integrin/talin complex reveals the basis of inside-out signal transduction. EMBO J. 28(22):3623–3632. doi:10.1038/emboj.2009.287.

Bamberger ME, Harris ME, McDonald DR, Husemann J, Landreth GE. 2003. A Cell Surface Receptor Complex for Fibrillar β-Amyloid Mediates Microglial Activation. J Neurosci. 23(7):2665–2674. doi:10.1523/JNEUROSCI.23-07-02665.2003.

Barczyk M, Carracedo S, Gullberg D. 2010. Integrins. Cell Tissue Res. 339(1):269–280. doi:10.1007/s00441-009-0834-6.

Berditchevski F, Odintsova E. 2007. Tetraspanins as Regulators of Protein Trafficking. Traffic. 8(2):89–96. doi:10.1111/j.1600-0854.2006.00515.x.

Berditchevski F, Odintsova E, Sawada S, Gilbert E. 2002. Expression of the palmitoylation-deficient CD151 weakens the association of alpha 3 beta 1 integrin with the tetraspanin-enriched microdomains and affects integrin-dependent signalling. J Biol Chem. 277(40):36991–37000. doi:10.1074/jbc.M205265200.

Bharadwaj M, Strohmeyer N, Colo GP, Helenius J, Beerenwinkel N, Schiller HB, Fässler R, Müller DJ. 2017. αV-class integrins exert dual roles on α5β1 integrins to strengthen adhesion to fibronectin. Nat Commun. 8(1):14348. doi:10.1038/ncomms14348.

Bhaskar V, Zhang D, Fox M, Seto P, Wong MH, Wales PE, Powers D, Chao DT, DuBridge RB, Ramakrishnan V. 2007. A function blocking anti-mouse integrin α5β1 antibody inhibits angiogenesis and impedes tumour growth in vivo. J Transl Med. 5(1):61. doi:10.1186/1479-5876-5-61.

Bledzka K, Liu J, Xu Z, Perera HD, Yadav SP, Bialkowska K, Qin J, Ma Y-Q, Plow EF. 2012. Spatial Coordination of Kindlin-2 with Talin Head Domain in Interaction with Integrin β Cytoplasmic Tails. J Biol Chem. 287(29):24585–24594. doi:10.1074/jbc.M111.336743.

Calderwood DA, Campbell ID, Critchley DR. 2013. Talins and kindlins: partners in integrin-mediated adhesion. Nat Rev Mol Cell Biol. 14(8):503–517. doi:10.1038/nrm3624.

Chen HC, Appeddu PA, Parsons JT, Hildebrand JD, Schaller MD, Guan JL. 1995. Interaction of focal adhesion kinase with cytoskeletal protein talin. J Biol Chem. 270(28):16995–16999. doi:10.1074/jbc.270.28.16995.

Chen L-M, Bailey D, Fernandez-Valle C. 2000. Association of β1 Integrin with Focal Adhesion Kinase and Paxillin in Differentiating Schwann Cells. J Neurosci. 20(10):3776–3784. doi:10.1523/JNEUROSCI.20-10-03776.2000.

Chen Y, Zhang J, Cui W, Silverstein RL. 2022. CD36, a signalling receptor and fatty acid transporter that regulates immune cell metabolism and fate. Journal of Experimental Medicine. 219(6):e20211314. doi:10.1084/jem.20211314.

Choma DP, Milano V, Pumiglia KM, Michael DiPersio C. 2007. Integrin α3β1-Dependent Activation of FAK/Src Regulates Rac1-Mediated Keratinocyte Polarization on Laminin-5. Journal of Investigative Dermatology. 127(1):31–40. doi:10.1038/sj.jid.5700505.

Ciobanasu C, Faivre B, Le Clainche C. 2012. Actin Dynamics Associated with Focal Adhesions. Int J Cell Biol. 2012:941292. doi:10.1155/2012/941292.

Cook GA, Longhurst CM, Grgurevich S, Cholera S, Crossno JT, Jennings LK. 2002. Identification of CD9 extracellular domains important in regulation of CHO cell adhesion to fibronectin and fibronectin pericellular matrix assembly. Blood. 100(13):4502–4511. doi:10.1182/blood.V100.13.4502.

Dao L, Blaue C, Franz CM. 2021. Integrin α2β1 as a negative regulator of the laminin receptors α6β1 and α6β4. Micron. 148:103106. doi:10.1016/j.micron.2021.103106.

Davis SP, Lee K, Gillrie MR, Roa L, Amrein M, Ho M. 2013. CD36 Recruits α5β1 Integrin to Promote Cytoadherence of P. falciparum-Infected Erythrocytes. PLOS Pathogens. 9(8):e1003590. doi:10.1371/journal.ppat.1003590.

van Deventer SJ, Dunlock V-ME, van Spriel AB. 2017. Molecular interactions shaping the tetraspanin web. Biochemical Society Transactions. 45(3):741–750. doi:10.1042/BST20160284.

Erami Z, Heitz S, Bresnick AR, Backer JM. 2019. PI3Kβ links integrin activation and PI(3,4)P2 production during invadopodial maturation. Mol Biol Cell. 30(18):2367–2376. doi:10.1091/mbc.E19-03-0182.

Freeman SA, Goyette J, Furuya W, Woods EC, Bertozzi CR, Bergmeier W, Hinz B, van der Merwe PA, Das R, Grinstein S. 2016. Integrins Form an Expanding Diffusional Barrier that Coordinates Phagocytosis. Cell. 164(1–2):128–140. doi:10.1016/j.cell.2015.11.048.

Garcia-Parajo MF, Cambi A, Torreno-Pina JA, Thompson N, Jacobson K. 2014. Nanoclustering as a dominant feature of plasma membrane organization. J Cell Sci. 127(Pt 23):4995–5005. doi:10.1242/jcs.146340.

Ghatak S, Niland S, Schulz J-N, Wang F, Eble JA, Leitges M, Mauch C, Krieg T, Zigrino P, Eckes B. 2016. Role of Integrins α1β1 and α2β1 in Wound and Tumour Angiogenesis in Mice. The American Journal of Pathology. 186(11):3011–3027. doi:10.1016/j.ajpath.2016.06.021.

Gutiérrez-López MD, Ovalle S, Yáñez-Mó M, Sánchez-Sánchez N, Rubinstein E, Olmo N, Lizarbe MA, Sánchez-Madrid F, Cabañas C. 2003. A Functionally Relevant Conformational Epitope on the CD9 Tetraspanin Depends on the Association with Activated β1Integrin *. Journal of Biological Chemistry. 278(1):208–218. doi:10.1074/jbc.M207805200.

Haydari Z, Shams H, Jahed Z, Mofrad MRK. 2020. Kindlin Assists Talin to Promote Integrin Activation. Biophys J. 118(8):1977–1991. doi:10.1016/j.bpj.2020.02.023.

Hemler ME. 2005. Tetraspanin functions and associated microdomains. Nat Rev Mol Cell Biol. 6(10):801–811. doi:10.1038/nrm1736.

Higginbottom A, Wilkinson I, McCullough B, Lanza F, Azorsa DO, Partridge LJ, Monk PN. 2000. Antibody cross-linking of human CD9 and the high-affinity immunoglobulin E receptor stimulates secretion from transfected rat basophilic leukaemia cells. Immunology. 99(4):546–552. doi:10.1046/j.1365-2567.2000.00992.x.

Hu Y-L, Lu S, Szeto KW, Sun J, Wang Y, Lasheras JC, Chien S. 2014. FAK and paxillin dynamics at focal adhesions in the protrusions of migrating cells. Sci Rep. 4(1):6024. doi:10.1038/srep06024.

Huang T, Sun L, Yuan X, Qiu H. 2017. Thrombospondin-1 is a multifaceted player in tumour progression. Oncotarget. 8(48):84546–84558. doi:10.18632/oncotarget.19165.

Huang W, Li R, Zhang J, Cheng Y, Ramakrishnan DP, Silverstein RL. 2023. A CD36 transmembrane domain peptide interrupts CD36 interactions with membrane partners on macrophages and inhibits atherogenic functions. Translational Research. 254:68–76. doi:10.1016/j.trsl.2022.10.005.

Humphries JD, Wang P, Streuli C, Geiger B, Humphries MJ, Ballestrem C. 2007. Vinculin controls focal adhesion formation by direct interactions with talin and actin. Journal of Cell Biology. 179(5):1043–1057. doi:10.1083/jcb.200703036.

Humphries MJ, Symonds EJ, Mould AP. 2003. Mapping functional residues onto integrin crystal structures. Current Opinion in Structural Biology. 13(2):236–243. doi:10.1016/S0959-440X(03)00035-6.

Hwang JR, Jo K, Lee Y, Sung B-J, Park YW, Lee J-H. 2012. Upregulation of CD9 in ovarian cancer is related to the induction of TNF-α gene expression and constitutive NF-κB activation. Carcinogenesis. 33(1):77–83. doi:10.1093/carcin/bgr257.

Hynes RO. 2002. Integrins: bidirectional, allosteric signalling machines. Cell. 110(6):673–687. doi:10.1016/s0092-8674(02)00971-6.

Ishii M, Iwai K, Koike M, Ohshima S, Kudo-Tanaka E, Ishii T, Mima T, Katada Y, Miyatake K, Uchiyama Y, et al. 2006. RANKL-Induced Expression of Tetraspanin CD9 in Lipid Raft Membrane Microdomain Is Essential for Cell Fusion During Osteoclastogenesis. Journal of Bone and Mineral Research. 21(6):965–976. doi:10.1359/jbmr.060308.

Israels SJ, McMillan-Ward EM. 2006. Platelet Tetraspanin Complexes and Their Relation to Lipid Rafts. Blood. 108(11):1530. doi:10.1182/blood.V108.11.1530.1530.

Iwasaki T, Takeda Y, Maruyama K, Yokosaki Y, Tsujino K, Tetsumoto S, Kuhara H, Nakanishi K, Otani Y, Jin Y, et al. 2013. Deletion of Tetraspanin CD9 Diminishes Lymphangiogenesis in Vivo and in Vitro. J Biol Chem. 288(4):2118–2131. doi:10.1074/jbc.M112.424291.

Jaqaman K, Kuwata H, Touret N, Collins R, Trimble WS, Danuser G, Grinstein S. 2011. Cytoskeletal control of CD36 diffusion promotes its receptor and signalling function. Cell. 146(4):593–606. doi:10.1016/j.cell.2011.06.049.

Jeanne A, Schneider C, Martiny L, Dedieu S. 2015. Original insights on thrombospondin-1-related antireceptor strategies in cancer. Front Pharmacol. 6:252. doi:10.3389/fphar.2015.00252.

Jin H, Su J, Garmy-Susini B, Kleeman J, Varner J. 2006. Integrin α4β1 Promotes Monocyte Trafficking and Angiogenesis in Tumours. Cancer Research. 66(4):2146–2152. doi:10.1158/0008-5472.CAN-05-2704.

Kamisasanuki T, Tokushige S, Terasaki H, Khai NC, Wang Y, Sakamoto T, Kosai K. 2011. Targeting CD9 produces stimulus-independent antiangiogenic effects predominantly in activated endothelial cells during angiogenesis: A novel antiangiogenic therapy. Biochemical and Biophysical Research Communications. 413(1):128–135. doi:10.1016/j.bbrc.2011.08.068.

Kazerounian S, Duquette M, Reyes MA, Lawler JT, Song K, Perruzzi C, Primo L, Khosravi-Far R, Bussolino F, Rabinovitz I, et al. 2011. Priming of the vascular endothelial growth factor signalling pathway by thrombospondin-1, CD36, and spleen tyrosine kinase. Blood. 117(17):4658–4666. doi:10.1182/blood-2010-09-305284.

Klekotka PA, Santoro SA, Zutter MM. 2001. α2 Integrin Subunit Cytoplasmic Domain-dependent Cellular Migration Requires p38 MAPK. Journal of Biological Chemistry. 276(12):9503–9511. doi:10.1074/jbc.M006286200.

Klemke RL, Leng J, Molander R, Brooks PC, Vuori K, Cheresh DA. 1998. CAS/Crk coupling serves as a “molecular switch” for induction of cell migration. J Cell Biol. 140(4):961–972. doi:10.1083/jcb.140.4.961.

Koenigsknecht J, Landreth G. 2004. Microglial Phagocytosis of Fibrillar β-Amyloid through a β_1 Integrin-Dependent Mechanism. J Neurosci. 24(44):9838–9846. doi:10.1523/JNEUROSCI.2557-04.2004.

Lee B-H, Ruoslahti E. 2005. α5β1 integrin stimulates Bcl-2 expression and cell survival through Akt, focal adhesion kinase, and Ca2+/calmodulin-dependent protein kinase IV. Journal of Cellular Biochemistry. 95(6):1214–1223. doi:10.1002/jcb.20488.

Leitinger B, McDowall A, Stanley P, Hogg N. 2000. The regulation of integrin function by Ca2+. Biochimica et Biophysica Acta (BBA) - Molecular Cell Research. 1498(2):91–98. doi:10.1016/S0167-4889(00)00086-0.

Leu S-J, Lam SC-T, Lau LF. 2002. Pro-angiogenic Activities of CYR61 (CCN1) Mediated through Integrins αvβ3 and α6β1 in Human Umbilical Vein Endothelial Cells *. Journal of Biological Chemistry. 277(48):46248–46255. doi:10.1074/jbc.M209288200.

Leu S-J, Liu Y, Chen N, Chen C-C, Lam SC-T, Lau LF. 2003. Identification of a Novel Integrin α6β1 Binding Site in the Angiogenic Inducer CCN1 (CYR61) *. Journal of Biological Chemistry. 278(36):33801–33808. doi:10.1074/jbc.M305862200.

Levental I, Lingwood D, Grzybek M, Coskun U, Simons K. 2010. Palmitoylation regulates raft affinity for the majority of integral raft proteins. Proc Natl Acad Sci U S A. 107(51):22050–22054. doi:10.1073/pnas.1016184107.

Liang X, Draghi NA, Resh MD. 2004. Signalling from Integrins to Fyn to Rho Family GTPases Regulates Morphologic Differentiation of Oligodendrocytes. J Neurosci. 24(32):7140–7149. doi:10.1523/JNEUROSCI.5319-03.2004.

Lu F, Zhu L, Bromberger T, Yang J, Yang Q, Liu J, Plow EF, Moser M, Qin J. 2022. Mechanism of integrin activation by talin and its cooperation with kindlin. Nat Commun. 13(1):2362. doi:10.1038/s41467-022-30117-w.

Ludwig BS, Kessler H, Kossatz S, Reuning U. 2021. RGD-Binding Integrins Revisited: How Recently Discovered Functions and Novel Synthetic Ligands (Re-)Shape an Ever-Evolving Field. Cancers (Basel). 13(7):1711. doi:10.3390/cancers13071711.

Machiyama H, Yamaguchi T, Watanabe TM, Fujita H. 2017. A novel c-Src recruitment pathway from the cytosol to focal adhesions. FEBS Lett. 591(13):1940–1946. doi:10.1002/1873-3468.12696.

Matsuoka T, Yashiro M, Nishioka N, Hirakawa K, Olden K, Roberts JD. 2012. PI3K/Akt signalling is required for the attachment and spreading, and growth in vivo of metastatic scirrhous gastric carcinoma. Br J Cancer. 106(9):1535–1542. doi:10.1038/bjc.2012.107.

Matuszewska K, Kortenaar S ten, Pereira M, Santry LA, Petrik D, Lo K-M, Bridle BW, Wootton SK, Lawler J, Petrik J. 2022. Addition of an Fc-IgG induces receptor clustering and increases the in vitro efficacy and in vivo anti-tumour properties of the thrombospondin-1 type I repeats (3TSR) in a mouse model of advanced stage ovarian cancer. Gynecologic Oncology. 164(1):154–169. doi:10.1016/j.ygyno.2021.11.006.

Mezu-Ndubuisi OJ, Maheshwari A. 2021. The role of integrins in inflammation and angiogenesis. Pediatr Res. 89(7):1619–1626. doi:10.1038/s41390-020-01177-9.

Miao WM, Vasile E, Lane WS, Lawler J. 2001. CD36 associates with CD9 and integrins on human blood platelets. Blood. 97(6):1689–1696. doi:10.1182/blood.v97.6.1689.

Müller MA, Brunie L, Bächer A-S, Kessler H, Gottschalk K-E, Reuning U. 2014. Cytoplasmic salt bridge formation in integrin αvß3 stabilizes its inactive state affecting integrin-mediated cell biological effects. Cell Signal. 26(11):2493–2503. doi:10.1016/j.cellsig.2014.07.013.

Murayama Y, Miyagawa J, Oritani K, Yoshida H, Yamamoto K, Kishida O, Miyazaki T, Tsutsui S, Kiyohara T, Miyazaki Y, et al. 2004. CD9-mediated activation of the p46 Shc isoform leads to apoptosis in cancer cells. Journal of Cell Science. 117(15):3379–3388. doi:10.1242/jcs.01201.

Nakamoto T, Murayama Y, Oritani K, Boucheix C, Rubinstein E, Nishida M, Katsube F, Watabe K, Kiso S, Tsutsui S, et al. 2009. A novel therapeutic strategy with anti-CD9 antibody in gastric cancers. J Gastroenterol. 44(9):889–896. doi:10.1007/s00535-009-0081-3.

Oguri Y, Shinoda K, Kim H, Alba DL, Bolus WR, Wang Q, Brown Z, Pradhan RN, Tajima K, Yoneshiro T, et al. 2020. CD81 Controls Beige Fat Progenitor Cell Growth and Energy Balance via FAK Signalling. Cell. 182(3):563-577.e20. doi:10.1016/j.cell.2020.06.021.

Oommen S, Gupta SK, Vlahakis NE. 2011. Vascular Endothelial Growth Factor A (VEGF-A) Induces Endothelial and Cancer Cell Migration through Direct Binding to Integrin α9β1. J Biol Chem. 286(2):1083–1092. doi:10.1074/jbc.M110.175158.

Orłowski A, Kukkurainen S, Pöyry A, Rissanen S, Vattulainen I, Hytönen VP, Róg T. 2015. PIP2 and Talin Join Forces to Activate Integrin. J Phys Chem B. 119(38):12381–12389. doi:10.1021/acs.jpcb.5b06457.

Park EJ, Yuki Y, Kiyono H, Shimaoka M. 2015. Structural basis of blocking integrin activation and deactivation for anti-inflammation. Journal of Biomedical Science. 22(1):51. doi:10.1186/s12929-015-0159-6.

Pasqualini R, Hemler ME. 1994. Contrasting roles for integrin beta 1 and beta 5 cytoplasmic domains in subcellular localization, cell proliferation, and cell migration. The Journal of cell biology. 125(2):447–460. doi:10.1083/jcb.125.2.447.

Plow EF, Haas TA, Zhang L, Loftus J, Smith JW. 2000. Ligand Binding to Integrins *. Journal of Biological Chemistry. 275(29):21785–21788. doi:10.1074/jbc.R000003200.

Pohl J, Ring A, Korkmaz Ü, Ehehalt R, Stremmel W. 2005. FAT/CD36-mediated Long-Chain Fatty Acid Uptake in Adipocytes Requires Plasma Membrane Rafts. MBoC. 16(1):24–31. doi:10.1091/mbc.e04-07-0616.

Primo L, Ferrandi C, Roca C, Marchiò S, di Blasio L, Alessio M, Bussolino F. 2005. Identification of CD36 molecular features required for its in vitro angiostatic activity. FASEB J. 19(12):1713–1715. doi:10.1096/fj.05-3697fje.

Pua LJW, Mai C-W, Chung FF-L, Khoo AS-B, Leong C-O, Lim W-M, Hii L-W. 2022. Functional Roles of JNK and p38 MAPK Signalling in Nasopharyngeal Carcinoma. Int J Mol Sci. 23(3):1108. doi:10.3390/ijms23031108.

Ritchie K, Iino R, Fujiwara T, Murase K, Kusumi A. 2003. The fence and picket structure of the plasma membrane of live cells as revealed by single molecule techniques (Review). Molecular Membrane Biology. 20(1):13–18. doi:10.1080/0968768021000055698.

Rocha-Perugini V, González-Granado JM, Tejera E, López-Martín S, Yañez-Mó M, Sánchez-Madrid F. 2014. Tetraspanins CD9 and CD151 at the immune synapse support T-cell integrin signalling. Eur J Immunol. 44(7):1967–1975. doi:10.1002/eji.201344235.

Salani B, Briatore L, Contini P, Passalacqua M, Melloni E, Paggi A, Cordera R, Maggi D. 2009. IGF-I induced rapid recruitment of integrin beta1 to lipid rafts is Caveolin-1 dependent. Biochem Biophys Res Commun. 380(3):489–492. doi:10.1016/j.bbrc.2009.01.102.

Sala-Valdés M, Ursa A, Charrin S, Rubinstein E, Hemler ME, Sánchez-Madrid F, Yáñez-Mó M. 2006. EWI-2 and EWI-F link the tetraspanin web to the actin cytoskeleton through their direct association with ezrin-radixin-moesin proteins. J Biol Chem. 281(28):19665–19675. doi:10.1074/jbc.M602116200.

Serru V, Le Naour F, Billard M, Azorsa DO, Lanza F, Boucheix C, Rubinstein E. 1999. Selective tetraspan-integrin complexes (CD81/alpha4beta1, CD151/alpha3beta1, CD151/alpha6beta1) under conditions disrupting tetraspan interactions. Biochem J. 340(Pt 1):103–111.

Shafaq-Zadah M, Gomes-Santos CS, Bardin S, Maiuri P, Maurin M, Iranzo J, Gautreau A, Lamaze C, Caswell P, Goud B, et al. 2016. Persistent cell migration and adhesion rely on retrograde transport of β1 integrin. Nat Cell Biol. 18(1):54–64. doi:10.1038/ncb3287.

Shelby SA, Castello-Serrano I, Wisser KC, Levental I, Veatch SL. 2023. Membrane phase separation drives responsive assembly of receptor signalling domains. Nat Chem Biol. 19(6):750–758. doi:10.1038/s41589-023-01268-8.

Shoham T, Rajapaksa R, Kuo C-C, Haimovich J, Levy S. 2006. Building of the Tetraspanin Web: Distinct Structural Domains of CD81 Function in Different Cellular Compartments. Mol Cell Biol. 26(4):1373–1385. doi:10.1128/MCB.26.4.1373-1385.2006.

Silverstein RL, Febbraio M. 2009. CD36, a Scavenger Receptor Involved in Immunity, Metabolism, Angiogenesis, and Behavior. Sci Signal. 2(72):re3. doi:10.1126/scisignal.272re3.

Smith MA, Blankman E, Gardel ML, Luettjohann L, Waterman CM, Beckerle MC. 2010. A Zyxin-Mediated Mechanism for Actin Stress Fiber Maintenance and Repair. Developmental Cell. 19(3):365–376. doi:10.1016/j.devcel.2010.08.008.

Stipp CS, Kolesnikova TV, Hemler ME. 2003. EWI-2 regulates α3β1 integrin–dependent cell functions on laminin-5. J Cell Biol. 163(5):1167–1177. doi:10.1083/jcb.200309113.

Tadokoro S, Shattil SJ, Eto K, Tai V, Liddington RC, de Pereda JM, Ginsberg MH, Calderwood DA. 2003. Talin Binding to Integrin ß Tails: A Final Common Step in Integrin Activation. Science. 302(5642):103–106. doi:10.1126/science.1086652.

Takada Y, Ye X, Simon S. 2007. The integrins. Genome Biol. 8(5):215. doi:10.1186/gb-2007-8-5-215.

Tarrant JM, Robb L, Spriel AB van, Wright MD. 2003. Tetraspanins: molecular organisers of the leukocyte surface. Trends in Immunology. 24(11):610–617. doi:10.1016/j.it.2003.09.011.

Teese MG, Langosch D. 2015. Role of GxxxG Motifs in Transmembrane Domain Interactions. Biochemistry. 54(33):5125–5135. doi:10.1021/acs.biochem.5b00495.

Termini CM, Lidke KA, Gillette JM. 2016. Tetraspanin CD82 Regulates the Spatiotemporal Dynamics of PKCα in Acute Myeloid Leukemia. Sci Rep. 6(1):29859. doi:10.1038/srep29859.

Thorne RF, Marshall JF, Shafren DR, Gibson PG, Hart IR, Burns GF. 2000. The Integrins α3β1 and α6β1 Physically and Functionally Associate with CD36 in Human Melanoma Cells: REQUIREMENT FOR THE EXTRACELLULAR DOMAIN OF CD36*. Journal of Biological Chemistry. 275(45):35264–35275. doi:10.1074/jbc.M003969200.

Valdramidou D, Humphries MJ, Mould AP. 2008. DISTINCT ROLES OF β1 MIDAS, ADMIDAS AND LIMBS CATION-BINDING SITES IN LIGAND RECOGNITION BY INTEGRIN α2β1. J Biol Chem. 283(47):32704–32714. doi:10.1074/jbc.M802066200.

Velling T, Nilsson S, Stefansson A, Johansson S. 2004. β1-Integrins induce phosphorylation of Akt on serine 473 independently of focal adhesion kinase and Src family kinases. EMBO Rep. 5(9):901–905. doi:10.1038/sj.embor.7400234.

Vinogradova O, Velyvis A, Velyviene A, Hu B, Haas T, Plow E, Qin J. 2002. A structural mechanism of integrin alpha(IIb)beta(3) “inside-out” activation as regulated by its cytoplasmic face. Cell. 110(5):587–597. doi:10.1016/s0092-8674(02)00906-6.

Wang C, Yoo Y, Fan H, Kim E, Guan K-L, Guan J-L. 2010. Regulation of Integrin β1 Recycling to Lipid Rafts by Rab1a to Promote Cell Migration*. Journal of Biological Chemistry. 285(38):29398–29405. doi:10.1074/jbc.M110.141440.

Wang H-X, Kolesnikova TV, Denison C, Gygi SP, Hemler ME. 2011. The C-terminal tail of tetraspanin protein CD9 contributes to its function and molecular organization. J Cell Sci. 124(Pt 16):2702–2710. doi:10.1242/jcs.085449.

Wang J. 2012. Pull and push: Talin activation for integrin signalling. Cell Res. 22(11):1512–1514. doi:10.1038/cr.2012.103.

Wary KK, Mariotti A, Zurzolo C, Giancotti FG. 1998. A Requirement for Caveolin-1 and Associated Kinase Fyn in Integrin Signalling and Anchorage-Dependent Cell Growth. Cell. 94(5):625–634. doi:10.1016/S0092-8674(00)81604-9.

Wu S-C, Lo Y-M, Lee J-H, Chen C-Y, Chen T-W, Liu H-W, Lian W-N, Hua K, Liao C-C, Lin W-J, et al. 2022. Stomatin modulates adipogenesis through the ERK pathway and regulates fatty acid uptake and lipid droplet growth. Nat Commun. 13(1):4174. doi:10.1038/s41467-022-31825-z.

Yang Y, Liu XR, Greenberg ZJ, Zhou F, He P, Fan L, Liu S, Shen G, Egawa T, Gross ML, et al. 2020. Open conformation of tetraspanins shapes interaction partner networks on cell membranes. EMBO J. 39(18):e105246. doi:10.15252/embj.2020105246.

Yauch RL, Berditchevski F, Harler MB, Reichner J, Hemler ME. 1998. Highly Stoichiometric, Stable, and Specific Association of Integrin α3β1 with CD151 Provides a Major Link to Phosphatidylinositol 4-Kinase, and May Regulate Cell Migration. MBoC. 9(10):2751–2765. doi:10.1091/mbc.9.10.2751.

Yauch RL, Kazarov AR, Desai B, Lee RT, Hemler ME. 2000. Direct Extracellular Contact between Integrin α3β1 and TM4SF Protein CD151 *. Journal of Biological Chemistry. 275(13):9230–9238. doi:10.1074/jbc.275.13.9230.

Yu H, Gao M, Ma Y, Wang L, Shen Y, Liu X. 2018. Inhibition of cell migration by focal adhesion kinase: Time-dependent difference in integrin-induced signalling between endothelial and hepatoblastoma cells. Int J Mol Med. 41(5):2573–2588. doi:10.3892/ijmm.2018.3512.

Yu J, Lee C-Y, Changou CA, Cedano-Prieto DM, Takada YK, Takada Y. 2017. The CD9, CD81, and CD151 EC2 domains bind to the classical RGD-binding site of integrin αvβ3. Biochemical Journal. 474(4):589–596. doi:10.1042/BCJ20160998.

Zeng Y, Tao N, Chung K-N, Heuser JE, Lublin DM. 2003. Endocytosis of Oxidized Low Density Lipoprotein through Scavenger Receptor CD36 Utilizes a Lipid Raft Pathway That Does Not Require Caveolin-1 *. Journal of Biological Chemistry. 278(46):45931–45936. doi:10.1074/jbc.M307722200.

Zhang K, Chen J. 2012. The regulation of integrin function by divalent cations. Cell Adh Migr. 6(1):20–29. doi:10.4161/cam.18702.

Zhang X, Kazerounian S, Duquette M, Perruzzi C, Nagy JA, Dvorak HF, Parangi S, Lawler J. 2009. Thrombospondin-1 modulates vascular endothelial growth factor activity at the receptor level. FASEB J. 23(10):3368–3376. doi:10.1096/fj.09-131649.

Zhang XA, Kazarov AR, Yang X, Bontrager AL, Stipp CS, Hemler ME. 2002. Function of the Tetraspanin CD151–α6β1 Integrin Complex during Cellular Morphogenesis. Mol Biol Cell. 13(1):1–11. doi:10.1091/mbc.01-10-0481.

Zhu J, Luo B-H, Xiao T, Zhang C, Nishida N, Springer TA. 2008. Structure of a complete integrin ectodomain in a physiologic resting state and activation and deactivation by applied forces. Mol Cell. 32(6):849–861. doi:10.1016/j.molcel.2008.11.018.

Zilber M-T, Setterblad N, Vasselon T, Doliger C, Charron D, Mooney N, Gelin C. 2005. MHC class II/CD38/CD9: a lipid-raft–dependent signalling complex in human monocytes. Blood. 106(9):3074–3081. doi:10.1182/blood-2004-10-4094.

Zuidscherwoude M, Dunlock V-ME, van den Bogaart G, van Deventer SJ, van der Schaaf A, van Oostrum J, Goedhart J, In ’t Hout J, Hämmerling GJ, Tanaka S, et al. 2017. Tetraspanin microdomains control localized protein kinase C signalling in B cells. Sci Signal. 10(478):eaag2755. doi:10.1126/scisignal.aag2755.

Chapter 5: Bibliography

Aboulaich N, Vainonen JP, Strålfors P, Vener AV. 2004. Vectorial proteomics reveal targeting, phosphorylation and specific fragmentation of polymerase I and transcript release factor (PTRF) at the surface of caveolae in human adipocytes. Biochem J. 383(Pt 2):237–248. doi:10.1042/BJ20040647.

Abramsson A, Lindblom P, Betsholtz C. 2003. Endothelial and nonendothelial sources of PDGF-B regulate pericyte recruitment and influence vascular pattern formation in tumors. J Clin Invest. 112(8):1142–1151. doi:10.1172/JCI200318549.

Abumrad N, Coburn C, Ibrahimi A. 1999. Membrane proteins implicated in long-chain fatty acid uptake by mammalian cells: CD36, FATP and FABPm. Biochimica et Biophysica Acta (BBA) - Molecular and Cell Biology of Lipids. 1441(1):4–13. doi:10.1016/S1388-1981(99)00137-7.

Aburima A, Berger M, Spurgeon BEJ, Webb BA, Wraith KS, Febbraio M, Poole AW, Naseem KM. 2021. Thrombospondin-1 promotes hemostasis through modulation of cAMP signaling in blood platelets. Blood. 137(5):678–689. doi:10.1182/blood.2020005382.

Adair TH, Montani J-P. 2010. Overview of Angiogenesis. Morgan & Claypool Life Sciences. [accessed 2023 Apr 25]. https://www.ncbi.nlm.nih.gov/books/NBK53238/.

Ahmed Z, Lutty GA. 2016. Anti-angiogenic properties of vitreous. In: The Curated Reference Collection in Neuroscience and Biobehavioral Psychology. Elsevier Science Ltd. p. 112–119. [accessed 2023 Apr 29]. https://jhu.pure.elsevier.com/en/publications/anti-angiogenic-properties-of-vitreous.

Alam MS. 2022. Proximity Ligation Assay (PLA)Proximity ligation assay (PLA). In: Del Valle L, editor. Immunohistochemistry and Immunocytochemistry: Methods and Protocols. New York, NY: Springer US. (Methods in Molecular Biology). p. 191–201. [accessed 2024 Feb 27]. https://doi.org/10.1007/978-1-0716-1948-3_13.

Albert ML, Pearce SF, Francisco LM, Sauter B, Roy P, Silverstein RL, Bhardwaj N. 1998. Immature dendritic cells phagocytose apoptotic cells via alphavbeta5 and CD36, and cross-present antigens to cytotoxic T lymphocytes. J Exp Med. 188(7):1359–1368. doi:10.1084/jem.188.7.1359.

Álvarez-Aznar A, Muhl L, Gaengel K. 2017. VEGF Receptor Tyrosine Kinases: Key Regulators of Vascular Function. Curr Top Dev Biol. 123:433–482. doi:10.1016/bs.ctdb.2016.10.001.

Anthis NJ, Wegener KL, Ye F, Kim C, Goult BT, Lowe ED, Vakonakis I, Bate N, Critchley DR, Ginsberg MH, et al. 2009. The structure of an integrin/talin complex reveals the basis of inside-out signal transduction. EMBO J. 28(22):3623–3632. doi:10.1038/emboj.2009.287.

Arias-Romero LE, Saha S, Villamar-Cruz O, Yip S-C, Ethier SP, Zhang Z-Y, Chernoff J. 2009. Activation of Src by Protein Tyrosine Phosphatase-1B is required for ErbB2 transformation of human breast epithelial cells. Cancer Res. 69(11):4582–4588. doi:10.1158/0008-5472.CAN-08-4001.

Aspriţoiu VM, Stoica I, Bleotu C, Diaconu CC. 2021. Epigenetic Regulation of Angiogenesis in Development and Tumors Progression: Potential Implications for Cancer Treatment. Frontiers

in Cell and Developmental Biology. 9. [accessed 2023 Apr 25]. https://www.frontiersin.org/articles/10.3389/fcell.2021.689962.

Attems J. 2005. Sporadic cerebral amyloid angiopathy: pathology, clinical implications, and possible pathomechanisms. Acta Neuropathol. 110(4):345–359. doi:10.1007/s00401-005-1074-9.

Bachmann A, Metwally NG, Allweier J, Cronshagen J, Del Pilar Martinez Tauler M, Murk A, Roth LK, Torabi H, Wu Y, Gutsmann T, et al. 2022. CD36-A Host Receptor Necessary for Malaria Parasites to Establish and Maintain Infection. Microorganisms. 10(12):2356. doi:10.3390/microorganisms10122356.

Baker LH, Rowinsky EK, Mendelson D, Humerickhouse RA, Knight RA, Qian J, Carr RA, Gordon GB, Demetri GD. 2016 Sep 22. Randomized, Phase II Study of the Thrombospondin-1-Mimetic Angiogenesis Inhibitor ABT-510 in Patients With Advanced Soft Tissue Sarcoma. Journal of Clinical Oncology. doi:10.1200/JCO.2008.17.4706. [accessed 2024 Mar 24]. https://ascopubs.org/doi/10.1200/JCO.2008.17.4706.

Bamberger ME, Harris ME, McDonald DR, Husemann J, Landreth GE. 2003. A Cell Surface Receptor Complex for Fibrillar β-Amyloid Mediates Microglial Activation. J Neurosci. 23(7):2665–2674. doi:10.1523/JNEUROSCI.23-07-02665.2003.

Bar DZ, Atkatsh K, Tavarez U, Erdos MR, Gruenbaum Y, Collins FS. 2018a. Biotinylation by antibody recognition—a method for proximity labeling. Nat Methods. 15(2):127–133. doi:10.1038/nmeth.4533.

Bar DZ, Atkatsh K, Tavarez U, Erdos MR, Gruenbaum Y, Collins FS. 2018b. Biotinylation by antibody recognition—a method for proximity labeling. Nat Methods. 15(2):127–133. doi:10.1038/nmeth.4533.

Barczyk M, Carracedo S, Gullberg D. 2010. Integrins. Cell Tissue Res. 339(1):269–280. doi:10.1007/s00441-009-0834-6.

Baruch DI, Gormely JA, Ma C, Howard RJ, Pasloske BL. 1996. Plasmodium falciparum erythrocyte membrane protein 1 is a parasitized erythrocyte receptor for adherence to CD36, thrombospondin, and intercellular adhesion molecule 1. Proceedings of the National Academy of Sciences. 93(8):3497–3502. doi:10.1073/pnas.93.8.3497.

Baruch DI, Ma XC, Singh HB, Bi X, Pasloske BL, Howard RJ. 1997. Identification of a region of PfEMP1 that mediates adherence of Plasmodium falciparum infected erythrocytes to CD36: conserved function with variant sequence. Blood. 90(9):3766–3775.

Bentley K, Mariggi G, Gerhardt H, Bates PA. 2009. Tipping the Balance: Robustness of Tip Cell Selection, Migration and Fusion in Angiogenesis. PLoS Comput Biol. 5(10):e1000549. doi:10.1371/journal.pcbi.1000549.

Berditchevski F, Odintsova E. 2007. Tetraspanins as Regulators of Protein Trafficking. Traffic. 8(2):89–96. doi:10.1111/j.1600-0854.2006.00515.x.

Berditchevski F, Odintsova E, Sawada S, Gilbert E. 2002. Expression of the palmitoylation-deficient CD151 weakens the association of alpha 3 beta 1 integrin with the tetraspanin-enriched

microdomains and affects integrin-dependent signaling. J Biol Chem. 277(40):36991–37000. doi:10.1074/jbc.M205265200.

Bergers G, Benjamin LE. 2003. Tumorigenesis and the angiogenic switch. Nat Rev Cancer. 3(6):401–410. doi:10.1038/nrc1093.

Bharadwaj M, Strohmeyer N, Colo GP, Helenius J, Beerenwinkel N, Schiller HB, Fässler R, Müller DJ. 2017. αV-class integrins exert dual roles on α5β1 integrins to strengthen adhesion to fibronectin. Nat Commun. 8(1):14348. doi:10.1038/ncomms14348.

Bhaskar V, Zhang D, Fox M, Seto P, Wong MH, Wales PE, Powers D, Chao DT, DuBridge RB, Ramakrishnan V. 2007. A function blocking anti-mouse integrin α5β1 antibody inhibits angiogenesis and impedes tumor growth in vivo. J Transl Med. 5(1):61. doi:10.1186/1479-5876-5-61.

Bjorge JD, Pang A, Fujita DJ. 2000. Identification of Protein-tyrosine Phosphatase 1B as the Major Tyrosine Phosphatase Activity Capable of Dephosphorylating and Activating c-Src in Several Human Breast Cancer Cell Lines *. Journal of Biological Chemistry. 275(52):41439–41446. doi:10.1074/jbc.M004852200.

Bledzka K, Liu J, Xu Z, Perera HD, Yadav SP, Bialkowska K, Qin J, Ma Y-Q, Plow EF. 2012. Spatial Coordination of Kindlin-2 with Talin Head Domain in Interaction with Integrin β Cytoplasmic Tails. J Biol Chem. 287(29):24585–24594. doi:10.1074/jbc.M111.336743.

Bochkov VN, Oskolkova OV, Birukov KG, Levonen A-L, Binder CJ, Stöckl J. 2010. Generation and Biological Activities of Oxidized Phospholipids. Antioxidants & Redox Signaling. 12(8):1009–1059. doi:10.1089/ars.2009.2597.

Bodin S, Soulet C, Tronchère H, Sié P, Gachet C, Plantavid M, Payrastre B. 2005. Integrin-dependent interaction of lipid rafts with the actin cytoskeleton in activated human platelets. J Cell Sci. 118(Pt 4):759–769. doi:10.1242/jcs.01648.

Branon TC, Bosch JA, Sanchez AD, Udeshi ND, Svinkina T, Carr SA, Feldman JL, Perrimon N, Ting AY. 2018. Efficient proximity labeling in living cells and organisms with TurboID. Nat Biotechnol. 36(9):880–887. doi:10.1038/nbt.4201.

Bratton DL, Fadok VA, Richter DA, Kailey JM, Guthrie LA, Henson PM. 1997. Appearance of phosphatidylserine on apoptotic cells requires calcium-mediated nonspecific flip-flop and is enhanced by loss of the aminophospholipid translocase. J Biol Chem. 272(42):26159–26165. doi:10.1074/jbc.272.42.26159.

Brenner DR, Poirier A, Woods RR, Ellison LF, Billette J-M, Demers AA, Zhang SX, Yao C, Finley C, Fitzgerald N, et al. 2022. Projected estimates of cancer in Canada in 2022. CMAJ. 194(17):E601–E607. doi:10.1503/cmaj.212097.

Broekman F, Giovannetti E, Peters GJ. 2011. Tyrosine kinase inhibitors: Multi-targeted or single-targeted? World J Clin Oncol. 2(2):80–93. doi:10.5306/wjco.v2.i2.80.

Brown J, Horrocks MH. 2020. A sticky situation: Aberrant protein-protein interactions in Parkinson's disease. Semin Cell Dev Biol. 99:65–77. doi:10.1016/j.semcdb.2018.05.006.

Brown LS, Foster CG, Courtney J-M, King NE, Howells DW, Sutherland BA. 2019. Pericytes and Neurovascular Function in the Healthy and Diseased Brain. Frontiers in Cellular Neuroscience. 13. [accessed 2023 Apr 25]. https://www.frontiersin.org/articles/10.3389/fncel.2019.00282.

Calderwood DA, Campbell ID, Critchley DR. 2013. Talins and kindlins: partners in integrin-mediated adhesion. Nat Rev Mol Cell Biol. 14(8):503–517. doi:10.1038/nrm3624.

Campbell N, Greenaway J, Henkin J, Petrik J. 2011. ABT-898 induces tumor regression and prolongs survival in a mouse model of epithelial ovarian cancer. Mol Cancer Ther. 10(10):1876–1885. doi:10.1158/1535-7163.MCT-11-0402.

Carmeliet P, Jain RK. 2000. Angiogenesis in cancer and other diseases. Nature. 407(6801):249–257. doi:10.1038/35025220.

Cell line - CD9 - The Human Protein Atlas. [accessed 2024 Jan 23]. https://www.proteinatlas.org/ENSG00000010278-CD9/cell+line.

Cell line - ITGB1 - The Human Protein Atlas. [accessed 2023 Apr 18]. https://www.proteinatlas.org/ENSG00000150093-ITGB1/cell+line.

Chang L, Chen Yi-Ju, Fan C-Y, Tang C-J, Chen Y-H, Low P-Y, Ventura A, Lin C-C, Chen Yu-Ju, Angata T. 2017. Identification of Siglec Ligands Using a Proximity Labeling Method. J Proteome Res. 16(10):3929–3941. doi:10.1021/acs.jproteome.7b00625.

Chen H, Herndon ME, Lawler J. 2000. The cell biology of thrombospondin-1. Matrix Biol. 19(7):597–614. doi:10.1016/s0945-053x(00)00107-4.

Chen HC, Appeddu PA, Parsons JT, Hildebrand JD, Schaller MD, Guan JL. 1995. Interaction of focal adhesion kinase with cytoskeletal protein talin. J Biol Chem. 270(28):16995–16999. doi:10.1074/jbc.270.28.16995.

Chen L-M, Bailey D, Fernandez-Valle C. 2000. Association of β1 Integrin with Focal Adhesion Kinase and Paxillin in Differentiating Schwann Cells. J Neurosci. 20(10):3776–3784. doi:10.1523/JNEUROSCI.20-10-03776.2000.

Chen M, Bao L, Zhao M, Cao J, Zheng H. 2020. Progress in Research on the Role of FGF in the Formation and Treatment of Corneal Neovascularization. Front Pharmacol. 11:111. doi:10.3389/fphar.2020.00111.

Chen Y, Zhang J, Cui W, Silverstein RL. 2022. CD36, a signaling receptor and fatty acid transporter that regulates immune cell metabolism and fate. Journal of Experimental Medicine. 219(6):e20211314. doi:10.1084/jem.20211314.

Cheng A-L, Qin S, Ikeda M, Galle P, Ducreux M, Zhu A, Kim T-Y, Kudo M, Breder V, Merle P, et al. 2019. LBA3 - IMbrave150: Efficacy and safety results from a ph III study evaluating atezolizumab (atezo) + bevacizumab (bev) vs sorafenib (Sor) as first treatment (tx) for patients (pts) with unresectable hepatocellular carcinoma (HCC). Annals of Oncology. 30:ix186–ix187. doi:10.1093/annonc/mdz446.002.

Cheng S-S, Yang G-J, Wang W, Leung C-H, Ma D-L. 2020. The design and development of covalent protein-protein interaction inhibitors for cancer treatment. Journal of Hematology & Oncology. 13(1):26. doi:10.1186/s13045-020-00850-0.

Cho KF, Branon TC, Rajeev S, Svinkina T, Udeshi ND, Thoudam T, Kwak C, Rhee H-W, Lee I-K, Carr SA, et al. 2020. Split-TurboID enables contact-dependent proximity labeling in cells. Proc Natl Acad Sci U S A. 117(22):12143–12154. doi:10.1073/pnas.1919528117.

Cho KF, Branon TC, Udeshi ND, Myers SA, Carr SA, Ting AY. 2020. Proximity labeling in mammalian cells with TurboID and split-TurboID. Nat Protoc. 15(12):3971–3999. doi:10.1038/s41596-020-0399-0.

Choma DP, Milano V, Pumiglia KM, Michael DiPersio C. 2007. Integrin α3β1-Dependent Activation of FAK/Src Regulates Rac1-Mediated Keratinocyte Polarization on Laminin-5. Journal of Investigative Dermatology. 127(1):31–40. doi:10.1038/sj.jid.5700505.

Chu L-Y, Silverstein RL. 2012. CD36 Ectodomain Phosphorylation Blocks Thrombospondin-1 Binding. Arteriosclerosis, Thrombosis, and Vascular Biology. 32(3):760–767. doi:10.1161/ATVBAHA.111.242511.

Chua XY, Aballo T, Elnemer W, Tran M, Salomon A. 2021. Quantitative Interactomics of Lck-TurboID in Living Human T Cells Unveils T Cell Receptor Stimulation-Induced Proximal Lck Interactors. J Proteome Res. 20(1):715–726. doi:10.1021/acs.jproteome.0c00616.

Ciobanasu C, Faivre B, Le Clainche C. 2012. Actin Dynamics Associated with Focal Adhesions. Int J Cell Biol. 2012:941292. doi:10.1155/2012/941292.

Coburn CT, Knapp FF, Febbraio M, Beets AL, Silverstein RL, Abumrad NA. 2000. Defective Uptake and Utilization of Long Chain Fatty Acids in Muscle and Adipose Tissues of CD36 Knockout Mice *. Journal of Biological Chemistry. 275(42):32523–32529. doi:10.1074/jbc.M003826200.

Collot-Teixeira S, Martin J, McDermott-Roe C, Poston R, McGregor JL. 2007. CD36 and macrophages in atherosclerosis. Cardiovasc Res. 75(3):468–477. doi:10.1016/j.cardiores.2007.03.010.

Colombo G, Margosio B, Ragona L, Neves M, Bonifacio S, Annis DS, Stravalaci M, Tomaselli S, Giavazzi R, Rusnati M, et al. 2010. Non-peptidic thrombospondin-1 mimics as fibroblast growth factor-2 inhibitors: an integrated strategy for the development of new antiangiogenic compounds. J Biol Chem. 285(12):8733–8742. doi:10.1074/jbc.M109.085605.

Cook GA, Longhurst CM, Grgurevich S, Cholera S, Crossno JT, Jennings LK. 2002. Identification of CD9 extracellular domains important in regulation of CHO cell adhesion to fibronectin and fibronectin pericellular matrix assembly. Blood. 100(13):4502–4511. doi:10.1182/blood.V100.13.4502.

Coraci IS, Husemann J, Berman JW, Hulette C, Dufour JH, Campanella GK, Luster AD, Silverstein SC, El Khoury JB. 2002. CD36, a Class B Scavenger Receptor, Is Expressed on Microglia in Alzheimer's Disease Brains and Can Mediate Production of Reactive Oxygen Species in Response to β-Amyloid Fibrils. The American Journal of Pathology. 160(1):101–112. doi:10.1016/S0002-9440(10)64354-4.

Cross NL. 2004. Reorganization of Lipid Rafts During Capacitation of Human Sperm1. Biology of Reproduction. 71(4):1367–1373. doi:10.1095/biolreprod.104.030502.

Dal-Ré R. 2011. Worldwide Clinical Interventional Studies on Leading Causes of Death: A Descriptive Analysis. Annals of Epidemiology. 21(10):727–731. doi:10.1016/j.annepidem.2011.03.010.

Dao L, Blaue C, Franz CM. 2021. Integrin α2β1 as a negative regulator of the laminin receptors α6β1 and α6β4. Micron. 148:103106. doi:10.1016/j.micron.2021.103106.

Davis SP, Amrein M, Gillrie MR, Lee K, Muruve DA, Ho M. 2012. Plasmodium falciparum-induced CD36 clustering rapidly strengthens cytoadherence via p130CAS-mediated actin cytoskeletal rearrangement. FASEB J. 26(3):1119–1130. doi:10.1096/fj.11-196923.

Davis SP, Lee K, Gillrie MR, Roa L, Amrein M, Ho M. 2013a. CD36 Recruits α5β1 Integrin to Promote Cytoadherence of P. falciparum-Infected Erythrocytes. PLOS Pathogens. 9(8):e1003590. doi:10.1371/journal.ppat.1003590.

Davis SP, Lee K, Gillrie MR, Roa L, Amrein M, Ho M. 2013b. CD36 Recruits α5β1 Integrin to Promote Cytoadherence of P. falciparum-Infected Erythrocytes. PLoS Pathog. 9(8):e1003590. doi:10.1371/journal.ppat.1003590.

Davis SP, Lee K, Gillrie MR, Roa L, Amrein M, Ho M. 2013c. CD36 Recruits α5β1 Integrin to Promote Cytoadherence of P. falciparum-Infected Erythrocytes. PLOS Pathogens. 9(8):e1003590. doi:10.1371/journal.ppat.1003590.

Dawson DW, Pearce SFA, Zhong R, Silverstein RL, Frazier WA, Bouck NP. 1997. CD36 Mediates the In Vitro Inhibitory Effects of Thrombospondin-1 on Endothelial Cells. Journal of Cell Biology. 138(3):707–717. doi:10.1083/jcb.138.3.707.

Dayanir V, Meyer RD, Lashkari K, Rahimi N. 2001. Identification of tyrosine residues in vascular endothelial growth factor receptor-2/FLK-1 involved in activation of phosphatidylinositol 3-kinase and cell proliferation. J Biol Chem. 276(21):17686–17692. doi:10.1074/jbc.M009128200.

De Palma M, Biziato D, Petrova TV. 2017. Microenvironmental regulation of tumour angiogenesis. Nat Rev Cancer. 17(8):457–474. doi:10.1038/nrc.2017.51.

van Deventer SJ, Dunlock V-ME, van Spriel AB. 2017. Molecular interactions shaping the tetraspanin web. Biochemical Society Transactions. 45(3):741–750. doi:10.1042/BST20160284.

Dickson PV, Hamner JB, Sims TL, Fraga CH, Ng CYC, Rajasekeran S, Hagedorn NL, McCarville MB, Stewart CF, Davidoff AM. 2007. Bevacizumab-Induced Transient Remodeling of the Vasculature in Neuroblastoma Xenografts Results in Improved Delivery and Efficacy of Systemically Administered Chemotherapy. Clinical Cancer Research. 13(13):3942–3950. doi:10.1158/1078-0432.CCR-07-0278.

Dunn OJ. 1964. Multiple Comparisons Using Rank Sums. Technometrics. 6(3):241–252. doi:10.1080/00401706.1964.10490181.

Eakin RE, McKinley WA, Williams RJ. 1940. Egg-White Injury in Chicks and Its Relationship to a Deficiency of Vitamin H (Biotin). Science. 92(2384):224–225. doi:10.1126/science.92.2384.224.

Ebbinghaus SW, Hussain M, Tannir NM, Gordon MS, Desai AA, Knight RA, Carlson DM, Figlin RA. 2005. A randomized phase 2 study of the thrombospondin-mimetic peptide ABT-510 in patients with previously untreated advanced renal cell carcinoma. JCO. 23(16_suppl):4607–4607. doi:10.1200/jco.2005.23.16_suppl.4607.

El Khoury JB, Moore K, Freeman M, Luster AD. 2002. CD36 null mice reveal a key role for CD36 in β-amyloid induced microglial activation. Journal of Neurochemistry. 81(s1):71–71. doi:10.1046/j.1471-4159.2002.00064.x.

El Khoury JB, Moore KJ, Means TK, Leung J, Terada K, Toft M, Freeman MW, Luster AD. 2003. CD36 Mediates the Innate Host Response to β-Amyloid. J Exp Med. 197(12):1657–1666. doi:10.1084/jem.20021546.

Elebiyo TC, Rotimi D, Evbuomwan IO, Maimako RF, Iyobhebhe M, Ojo OA, Oluba OM, Adeyemi OS. 2022. Reassessing vascular endothelial growth factor (VEGF) in anti-angiogenic cancer therapy. Cancer Treatment and Research Communications. 32:100620. doi:10.1016/j.ctarc.2022.100620.

Erami Z, Heitz S, Bresnick AR, Backer JM. 2019. PI3Kβ links integrin activation and PI(3,4)P2 production during invadopodial maturation. Mol Biol Cell. 30(18):2367–2376. doi:10.1091/mbc.E19-03-0182.

Etymologia: Bonferroni Correction. 2015. Emerg Infect Dis. 21(2):289. doi:10.3201/eid2102.ET2102.

Fagiani E, Christofori G. 2013. Angiopoietins in angiogenesis. Cancer Letters. 328(1):18–26. doi:10.1016/j.canlet.2012.08.018.

Farhangkhoee H, Khan ZA, Barbin Y, Chakrabarti S. 2005. Glucose-induced up-regulation of CD36 mediates oxidative stress and microvascular endothelial cell dysfunction. Diabetologia. 48(7):1401–1410. doi:10.1007/s00125-005-1801-8.

Farooq M, Khan AW, Kim MS, Choi S. 2021. The Role of Fibroblast Growth Factor (FGF) Signaling in Tissue Repair and Regeneration. Cells. 10(11):3242. doi:10.3390/cells10113242.

Febbraio M, Abumrad NA, Hajjar DP, Sharma K, Cheng W, Pearce SF, Silverstein RL. 1999. A null mutation in murine CD36 reveals an important role in fatty acid and lipoprotein metabolism. J Biol Chem. 274(27):19055–19062. doi:10.1074/jbc.274.27.19055.

Febbraio M, Hajjar DP, Silverstein RL. 2001. CD36: a class B scavenger receptor involved in angiogenesis, atherosclerosis, inflammation, and lipid metabolism. J Clin Invest. 108(6):785–791. doi:10.1172/JCI14006.

Felbor U, Dreier L, Bryant RAR, Ploegh HL, Olsen BR, Mothes W. 2000. Secreted cathepsin L generates endostatin from collagen XVIII. The EMBO Journal. 19(6):1187–1194. doi:10.1093/emboj/19.6.1187.

Ferlay J, Colombet M, Soerjomataram I, Parkin DM, Piñeros M, Znaor A, Bray F. 2021. Cancer statistics for the year 2020: An overview. International Journal of Cancer. 149(4):778–789. doi:10.1002/ijc.33588.

Ferreras M, Felbor U, Lenhard T, Olsen BR, Delaissé J-M. 2000. Generation and degradation of human endostatin proteins by various proteinases. FEBS Letters. 486(3):247–251. doi:10.1016/S0014-5793(00)02249-3.

Fiore MM, Kakkar VV. 2003. Platelet factor 4 neutralizes heparan sulfate-enhanced antithrombin inactivation of factor Xa by preventing interaction(s) of enzyme with polysaccharide. Biochemical and Biophysical Research Communications. 311(1):71–76. doi:10.1016/j.bbrc.2003.09.171.

Folkman J. 1971. Tumor angiogenesis: therapeutic implications. N Engl J Med. 285(21):1182–1186. doi:10.1056/NEJM197111182852108.

Fragoso R, Ren D, Zhang X, Su MW-C, Burakoff SJ, Jin Y-J. 2003. Lipid raft distribution of CD4 depends on its palmitoylation and association with Lck, and evidence for CD4-induced lipid raft aggregation as an additional mechanism to enhance CD3 signaling. J Immunol. 170(2):913–921. doi:10.4049/jimmunol.170.2.913.

Fredriksson S, Gullberg M, Jarvius J, Olsson C, Pietras K, Gústafsdóttir SM, Östman A, Landegren U. 2002. Protein detection using proximity-dependent DNA ligation assays. Nat Biotechnol. 20(5):473–477. doi:10.1038/nbt0502-473.

Freeman SA, Goyette J, Furuya W, Woods EC, Bertozzi CR, Bergmeier W, Hinz B, van der Merwe PA, Das R, Grinstein S. 2016. Integrins Form an Expanding Diffusional Barrier that Coordinates Phagocytosis. Cell. 164(1–2):128–140. doi:10.1016/j.cell.2015.11.048.

Gagnoux-Palacios L, Dans M, van't Hof W, Mariotti A, Pepe A, Meneguzzi G, Resh MD, Giancotti FG. 2003. Compartmentalization of integrin α6β4 signaling in lipid rafts. J Cell Biol. 162(7):1189–1196. doi:10.1083/jcb.200305006.

Garcia-Parajo MF, Cambi A, Torreno-Pina JA, Thompson N, Jacobson K. 2014a. Nanoclustering as a dominant feature of plasma membrane organization. Journal of Cell Science. 127(23):4995–5005. doi:10.1242/jcs.146340.

Garcia-Parajo MF, Cambi A, Torreno-Pina JA, Thompson N, Jacobson K. 2014b. Nanoclustering as a dominant feature of plasma membrane organization. J Cell Sci. 127(Pt 23):4995–5005. doi:10.1242/jcs.146340.

Gengrinovitch S, Greenberg SM, Cohen T, Gitay-Goren H, Rockwell P, Maione TE, Levi BZ, Neufeld G. 1995. Platelet factor-4 inhibits the mitogenic activity of VEGF121 and VEGF165 using several concurrent mechanisms. J Biol Chem. 270(25):15059–15065. doi:10.1074/jbc.270.25.15059.

Gentilini G, Kirschbaum NE, Augustine JA, Aster RH, Visentin GP. 1999. Inhibition of human umbilical vein endothelial cell proliferation by the CXC chemokine, platelet factor 4 (PF4), is associated with impaired downregulation of p21(Cip1/WAF1). Blood. 93(1):25–33.

Gerbec ZJ, Thakar MS, Malarkannan S. 2015. The Fyn–ADAP Axis: Cytotoxicity Versus Cytokine Production in Killer Cells. Frontiers in Immunology. 6. [accessed 2023 Apr 29]. https://www.frontiersin.org/articles/10.3389/fimmu.2015.00472.

Gerber HP, Dixit V, Ferrara N. 1998. Vascular endothelial growth factor induces expression of the antiapoptotic proteins Bcl-2 and A1 in vascular endothelial cells. J Biol Chem. 273(21):13313–13316. doi:10.1074/jbc.273.21.13313.

Ghatak S, Niland S, Schulz J-N, Wang F, Eble JA, Leitges M, Mauch C, Krieg T, Zigrino P, Eckes B. 2016. Role of Integrins α1β1 and α2β1 in Wound and Tumor Angiogenesis in Mice. The American Journal of Pathology. 186(11):3011–3027. doi:10.1016/j.ajpath.2016.06.021.

Ghosh A, Li Z, Kan C, Qing W, Maria F, John B, Roy SL. 2007. Variability of CD36 Expression on Platelets Is Determined in Part by Genetic Polymorphisms and Can Influence Platelet Function. Blood. 110(11):3643. doi:10.1182/blood.V110.11.3643.3643.

Ghosh A, Murugesan G, Chen K, Zhang L, Wang Q, Febbraio M, Anselmo RM, Marchant K, Barnard J, Silverstein RL. 2011. Platelet CD36 surface expression levels affect functional responses to oxidized LDL and are associated with inheritance of specific genetic polymorphisms. Blood. 117(23):6355–6366. doi:10.1182/blood-2011-02-338582.

Giantonio BJ, Catalano PJ, Meropol NJ, O'Dwyer PJ, Mitchell EP, Alberts SR, Schwartz MA, Benson AB. 2007. Bevacizumab in Combination With Oxaliplatin, Fluorouracil, and Leucovorin (FOLFOX4) for Previously Treated Metastatic Colorectal Cancer: Results From the Eastern Cooperative Oncology Group Study E3200. JCO. 25(12):1539–1544. doi:10.1200/JCO.2006.09.6305.

Githaka JM, Vega AR, Baird MA, Davidson MW, Jaqaman K, Touret N. 2016 Jan 1. Ligand-induced growth and compaction of CD36 nanoclusters enriched in Fyn induces Fyn signaling. Journal of Cell Science.:jcs.188946. doi:10.1242/jcs.188946.

Githaka JM, Vega AR, Baird MA, Davidson MW, Jaqaman K, Touret N. 2016. Ligand-induced growth and compaction of CD36 nanoclusters enriched in Fyn induces Fyn signaling. Journal of Cell Science. 129(22):4175–4189. doi:10.1242/jcs.188946.

Goel S, Duda DG, Xu L, Munn LL, Boucher Y, Fukumura D, Jain RK. 2011. Normalization of the Vasculature for Treatment of Cancer and Other Diseases. Physiological Reviews. 91(3):1071–1121. doi:10.1152/physrev.00038.2010.

Granot-Attas S, Elson A. 2004. Protein tyrosine phosphatase epsilon activates Yes and Fyn in Neu-induced mammary tumor cells. Exp Cell Res. 294(1):236–243. doi:10.1016/j.yexcr.2003.11.003.

Greenaway J, Lawler J, Moorehead R, Bornstein P, Lamarre J, Petrik J. 2007. Thrombospondin-1 inhibits VEGF levels in the ovary directly by binding and internalization via the low density lipoprotein receptor-related protein-1 (LRP-1). J Cell Physiol. 210(3):807–818. doi:10.1002/jcp.20904.

Greenberg ME, Sun M, Zhang R, Febbraio M, Silverstein R, Hazen SL. 2006. Oxidized phosphatidylserine-CD36 interactions play an essential role in macrophage-dependent phagocytosis of apoptotic cells. J Exp Med. 203(12):2613–2625. doi:10.1084/jem.20060370.

Greenwalt DE, Scheck SH, Rhinehart-Jones T. 1995. Heart CD36 expression is increased in murine models of diabetes and in mice fed a high fat diet. J Clin Invest. 96(3):1382–1388. doi:10.1172/JCI118173.

Guerrini V, Gennaro ML. 2019. Foam cells: one size doesn't fit all. Trends Immunol. 40(12):1163–1179. doi:10.1016/j.it.2019.10.002.

Gui Y, Zheng H, Cao RY. 2022. Foam Cells in Atherosclerosis: Novel Insights Into Its Origins, Consequences, and Molecular Mechanisms. Frontiers in Cardiovascular Medicine. 9. [accessed 2023 Apr 29]. https://www.frontiersin.org/articles/10.3389/fcvm.2022.845942.

Gupta SK, Singh JP. 1994. Inhibition of endothelial cell proliferation by platelet factor-4 involves a unique action on S phase progression. J Cell Biol. 127(4):1121–1127. doi:10.1083/jcb.127.4.1121.

Gutierrez LS, Gutierrez J. 2021. Thrombospondin 1 in Metabolic Diseases. Frontiers in Endocrinology. 12. [accessed 2023 Apr 29]. https://www.frontiersin.org/articles/10.3389/fendo.2021.638536.

Gutiérrez-López MD, Ovalle S, Yáñez-Mó M, Sánchez-Sánchez N, Rubinstein E, Olmo N, Lizarbe MA, Sánchez-Madrid F, Cabañas C. 2003. A Functionally Relevant Conformational Epitope on the CD9 Tetraspanin Depends on the Association with Activated β1Integrin *. Journal of Biological Chemistry. 278(1):208–218. doi:10.1074/jbc.M207805200.

Han Y, Branon TC, Martell JD, Boassa D, Shechner D, Ellisman MH, Ting A. 2019. Directed Evolution of Split APEX2 Peroxidase. ACS Chem Biol. 14(4):619–635. doi:10.1021/acschembio.8b00919.

Hanai J, Dhanabal M, Karumanchi SA, Albanese C, Waterman M, Chan B, Ramchandran R, Pestell R, Sukhatme VP. 2002. Endostatin Causes G1 Arrest of Endothelial Cells through Inhibition of Cyclin D1*. Journal of Biological Chemistry. 277(19):16464–16469. doi:10.1074/jbc.M112274200.

Hanson J, Lam SWK, Mahanta KC, Pattnaik R, Alam S, Mohanty S, Hasan MU, Hossain A, Charunwatthana P, Chotivanich K, et al. 2012. Relative Contributions of Macrovascular and Microvascular Dysfunction to Disease Severity in Falciparum Malaria. The Journal of Infectious Diseases. 206(4):571–579. doi:10.1093/infdis/jis400.

Hao J-W, Wang J, Guo H, Zhao Y-Y, Sun H-H, Li Y-F, Lai X-Y, Zhao N, Wang X, Xie C, et al. 2020. CD36 facilitates fatty acid uptake by dynamic palmitoylation-regulated endocytosis. Nat Commun. 11(1):4765. doi:10.1038/s41467-020-18565-8.

Haydari Z, Shams H, Jahed Z, Mofrad MRK. 2020. Kindlin Assists Talin to Promote Integrin Activation. Biophys J. 118(8):1977–1991. doi:10.1016/j.bpj.2020.02.023.

Heit B, Kim H, Cosío G, Castaño D, Collins R, Lowell CA, Kain KC, Trimble WS, Grinstein S. 2013. Multimolecular Signaling Complexes Enable Syk-Mediated Signaling of CD36 Internalization. Developmental Cell. 24(4):372–383. doi:10.1016/j.devcel.2013.01.007.

Hemler ME. 2005. Tetraspanin functions and associated microdomains. Nat Rev Mol Cell Biol. 6(10):801–811. doi:10.1038/nrm1736.

Higginbottom A, Wilkinson I, McCullough B, Lanza F, Azorsa DO, Partridge LJ, Monk PN. 2000. Antibody cross-linking of human CD9 and the high-affinity immunoglobulin E receptor stimulates secretion from transfected rat basophilic leukaemia cells. Immunology. 99(4):546–552. doi:10.1046/j.1365-2567.2000.00992.x.

Ho M, Hoang HL, Lee KM, Liu N, MacRae T, Montes L, Flatt CL, Yipp BG, Berger BJ, Looareesuwan S, et al. 2005. Ectophosphorylation of CD36 Regulates Cytoadherence of Plasmodium falciparum to Microvascular Endothelium under Flow Conditions. Infection and Immunity. 73(12):8179–8187. doi:10.1128/IAI.73.12.8179-8187.2005.

Holmberg A, Blomstergren A, Nord O, Lukacs M, Lundeberg J, Uhlén M. 2005. The biotin-streptavidin interaction can be reversibly broken using water at elevated temperatures. ELECTROPHORESIS. 26(3):501–510. doi:10.1002/elps.200410070.

Holmes DI, Zachary I. 2005. The vascular endothelial growth factor (VEGF) family: angiogenic factors in health and disease. Genome Biology. 6(2):209. doi:10.1186/gb-2005-6-2-209.

Holthenrich A, Drexler HCA, Chehab T, Naß J, Gerke V. 2019. Proximity proteomics of endothelial Weibel-Palade bodies identifies novel regulator of von Willebrand factor secretion. Blood. 134(12):979–982. doi:10.1182/blood.2019000786.

Holzer E, Rumpf-Kienzl C, Falk S, Dammermann A. 2022. A modified TurboID approach identifies tissue-specific centriolar components in C. elegans. PLoS Genet. 18(4):e1010150. doi:10.1371/journal.pgen.1010150.

Hoosdally SJ, Andress EJ, Wooding C, Martin CA, Linton KJ. 2009. The Human Scavenger Receptor CD36: GLYCOSYLATION STATUS AND ITS ROLE IN TRAFFICKING AND FUNCTION *. Journal of Biological Chemistry. 284(24):16277–16288. doi:10.1074/jbc.M109.007849.

Hopkins C, Gibson A, Stinchcombe J, Futter C. 2000. Chimeric molecules employing horseradish peroxidase as reporter enzyme for protein localization in the electron microscope. In: Thorner J, Emr SD, Abelson JN, editors. Methods in Enzymology. Vol. 327. Academic Press. (Applications of Chimeric Genes and Hybrid Proteins - Part B: Cell Biology and Physiology). p. 35–45. [accessed 2023 Apr 7]. https://www.sciencedirect.com/science/article/pii/S0076687900272650.

Hsieh F-L, Tartaglia L. 2016. The CIDRa domain from MCvar1 PfEMP1 bound to CD36. doi:https://doi.org/10.2210/pdb5LGD/pdb.

Hsieh F-L, Turner L, Bolla JR, Robinson CV, Lavstsen T, Higgins MK. 2016. The structural basis for CD36 binding by the malaria parasite. Nat Commun. 7(1):12837. doi:10.1038/ncomms12837.

Hu Y-L, Lu S, Szeto KW, Sun J, Wang Y, Lasheras JC, Chien S. 2014. FAK and paxillin dynamics at focal adhesions in the protrusions of migrating cells. Sci Rep. 4(1):6024. doi:10.1038/srep06024.

Huang T, Sun L, Yuan X, Qiu H. 2017. Thrombospondin-1 is a multifaceted player in tumor progression. Oncotarget. 8(48):84546–84558. doi:10.18632/oncotarget.19165.

Huang W, Febbraio M, Silverstein RL. 2011. CD9 tetraspanin interacts with CD36 on the surface of macrophages: a possible regulatory influence on uptake of oxidized low density lipoprotein. PLoS One. 6(12):e29092. doi:10.1371/journal.pone.0029092.

Huang W, Li R, Zhang J, Cheng Y, Ramakrishnan DP, Silverstein RL. 2023a. A CD36 transmembrane domain peptide interrupts CD36 interactions with membrane partners on macrophages and inhibits atherogenic functions. Transl Res. 254:68–76. doi:10.1016/j.trsl.2022.10.005.

Huang W, Li R, Zhang J, Cheng Y, Ramakrishnan DP, Silverstein RL. 2023b. A CD36 transmembrane domain peptide interrupts CD36 interactions with membrane partners on macrophages and inhibits atherogenic functions. Translational Research. 254:68–76. doi:10.1016/j.trsl.2022.10.005.

Huh HY, Pearce SF, Yesner LM, Schindler JL, Silverstein RL. 1996. Regulated Expression of CD36 During Monocyte-to-Macrophage Differentiation: Potential Role of CD36 in Foam Cell Formation. Blood. 87(5):2020–2028. doi:10.1182/blood.V87.5.2020.2020.

Humphries JD, Wang P, Streuli C, Geiger B, Humphries MJ, Ballestrem C. 2007. Vinculin controls focal adhesion formation by direct interactions with talin and actin. Journal of Cell Biology. 179(5):1043–1057. doi:10.1083/jcb.200703036.

Humphries MJ, Symonds EJ, Mould AP. 2003. Mapping functional residues onto integrin crystal structures. Current Opinion in Structural Biology. 13(2):236–243. doi:10.1016/S0959-440X(03)00035-6.

Hurwitz Herbert, Fehrenbacher Louis, Novotny William, Cartwright Thomas, Hainsworth John, Heim William, Berlin Jordan, Baron Ari, Griffing Susan, Holmgren Eric, et al. 2004. Bevacizumab plus Irinotecan, Fluorouracil, and Leucovorin for Metastatic Colorectal Cancer. New England Journal of Medicine. 350(23):2335–2342. doi:10.1056/NEJMoa032691.

Hwang J, Espenshade PJ. 2016. Proximity-dependent biotin labeling in yeast using the engineered ascorbate peroxidase APEX2. Biochem J. 473(16):2463–2469. doi:10.1042/BCJ20160106.

Hwang JR, Jo K, Lee Y, Sung B-J, Park YW, Lee J-H. 2012. Upregulation of CD9 in ovarian cancer is related to the induction of TNF-α gene expression and constitutive NF-κB activation. Carcinogenesis. 33(1):77–83. doi:10.1093/carcin/bgr257.

Hynes RO. 2002. Integrins: bidirectional, allosteric signaling machines. Cell. 110(6):673–687. doi:10.1016/s0092-8674(02)00971-6.

Idro R, Jenkins NE, Newton CR. 2005. Pathogenesis, clinical features, and neurological outcome of cerebral malaria. The Lancet Neurology. 4(12):827–840. doi:10.1016/S1474-4422(05)70247-7.

Inoki I, Shiomi T, Hashimoto G, Enomoto H, Nakamura H, Makino K, Ikeda E, Takata S, Kobayashi K, Okada Y. 2002. Connective tissue growth factor binds vascular endothelial growth factor (VEGF) and inhibits VEGF-induced angiogenesis. FASEB J. 16(2):219–221. doi:10.1096/fj.01-0332fje.

Ishii M, Iwai K, Koike M, Ohshima S, Kudo-Tanaka E, Ishii T, Mima T, Katada Y, Miyatake K, Uchiyama Y, et al. 2006. RANKL-Induced Expression of Tetraspanin CD9 in Lipid Raft Membrane

Microdomain Is Essential for Cell Fusion During Osteoclastogenesis. Journal of Bone and Mineral Research. 21(6):965–976. doi:10.1359/jbmr.060308.

Israels SJ, McMillan-Ward EM. 2006. Platelet Tetraspanin Complexes and Their Relation to Lipid Rafts. Blood. 108(11):1530. doi:10.1182/blood.V108.11.1530.1530.

Iwasaki T, Takeda Y, Maruyama K, Yokosaki Y, Tsujino K, Tetsumoto S, Kuhara H, Nakanishi K, Otani Y, Jin Y, et al. 2013. Deletion of Tetraspanin CD9 Diminishes Lymphangiogenesis in Vivo and in Vitro. J Biol Chem. 288(4):2118–2131. doi:10.1074/jbc.M112.424291.

Jain RK. 1998. The next frontier of molecular medicine: Delivery of therapeutics. Nat Med. 4(6):655–657. doi:10.1038/nm0698-655.

Jain RK. 2001. Normalizing tumor vasculature with anti-angiogenic therapy: a new paradigm for combination therapy. Nat Med. 7(9):987–989. doi:10.1038/nm0901-987.

Jain RK, Duda DG, Clark JW, Loeffler JS. 2006. Lessons from phase III clinical trials on anti-VEGF therapy for cancer. Nat Rev Clin Oncol. 3(1):24–40. doi:10.1038/ncponc0403.

Jaqaman K, Kuwata H, Touret N, Collins R, Trimble WS, Danuser G, Grinstein S. 2011. Cytoskeletal control of CD36 diffusion promotes its receptor and signaling function. Cell. 146(4):593–606. doi:10.1016/j.cell.2011.06.049.

Jeanne A, Schneider C, Martiny L, Dedieu S. 2015. Original insights on thrombospondin-1-related antireceptor strategies in cancer. Front Pharmacol. 6:252. doi:10.3389/fphar.2015.00252.

Jiang X, Wang J, Deng X, Xiong F, Zhang S, Gong Z, Li Xiayu, Cao K, Deng H, He Y, et al. 2020. The role of microenvironment in tumor angiogenesis. Journal of Experimental & Clinical Cancer Research. 39(1):204. doi:10.1186/s13046-020-01709-5.

Jiménez B, Volpert OV, Crawford SE, Febbraio M, Silverstein RL, Bouck N. 2000. Signals leading to apoptosis-dependent inhibition of neovascularization by thrombospondin-1. Nat Med. 6(1):41–48. doi:10.1038/71517.

Jiménez B, Volpert OV, Reiher F, Chang L, Muñoz A, Karin M, Bouck N. 2001. c-Jun N-terminal kinase activation is required for the inhibition of neovascularization by thrombospondin-1. Oncogene. 20(26):3443–3448. doi:10.1038/sj.onc.1204464.

Jin H, Su J, Garmy-Susini B, Kleeman J, Varner J. 2006. Integrin α4β1 Promotes Monocyte Trafficking and Angiogenesis in Tumors. Cancer Research. 66(4):2146–2152. doi:10.1158/0008-5472.CAN-05-2704.

Kalluri R. 2003. Basement membranes: structure, assembly and role in tumour angiogenesis. Nat Rev Cancer. 3(6):422–433. doi:10.1038/nrc1094.

Kamisasanuki T, Tokushige S, Terasaki H, Khai NC, Wang Y, Sakamoto T, Kosai K. 2011. Targeting CD9 produces stimulus-independent antiangiogenic effects predominantly in activated endothelial cells during angiogenesis: A novel antiangiogenic therapy. Biochemical and Biophysical Research Communications. 413(1):128–135. doi:10.1016/j.bbrc.2011.08.068.

Kar NS, Ashraf MZ, Valiyaveettil M, Podrez EA. 2008a. Mapping and Characterization of the Binding Site for Specific Oxidized Phospholipids and Oxidized Low Density Lipoprotein of Scavenger Receptor CD36. J Biol Chem. 283(13):8765–8771. doi:10.1074/jbc.M709195200.

Kar NS, Ashraf MZ, Valiyaveettil M, Podrez EA. 2008b. Mapping and Characterization of the Binding Site for Specific Oxidized Phospholipids and Oxidized Low Density Lipoprotein of Scavenger Receptor CD36 *. Journal of Biological Chemistry. 283(13):8765–8771. doi:10.1074/jbc.M709195200.

Kazerounian S, Duquette M, Reyes MA, Lawler JT, Song K, Perruzzi C, Primo L, Khosravi-Far R, Bussolino F, Rabinovitz I, et al. 2011. Priming of the vascular endothelial growth factor signaling pathway by thrombospondin-1, CD36, and spleen tyrosine kinase. Blood. 117(17):4658–4666. doi:10.1182/blood-2010-09-305284.

Kido K, Yamanaka S, Nakano S, Motani K, Shinohara S, Nozawa A, Kosako H, Ito S, Sawasaki T. 2020. AirID, a novel proximity biotinylation enzyme, for analysis of protein–protein interactions. Cole PA, Dötsch V, Dötsch V, Cronan JE, editors. eLife. 9:e54983. doi:10.7554/eLife.54983.

Kiernan JA. 1975. Localization of α-d-glucosyl and α-d-mannosyl groups of mucosubstances with concanavalin A and horseradish peroxidase. Histochemistry. 44(1):39–45. doi:10.1007/BF00490419.

Kim DI, Jensen SC, Noble KA, Kc B, Roux KH, Motamedchaboki K, Roux KJ. 2016. An improved smaller biotin ligase for BioID proximity labeling. MBoC. 27(8):1188–1196. doi:10.1091/mbc.E15-12-0844.

Kim I, Kim HG, So J-N, Kim JH, Kwak HJ, Koh GY. 2000. Angiopoietin-1 Regulates Endothelial Cell Survival Through the Phosphatidylinositol 3′-Kinase/Akt Signal Transduction Pathway. Circulation Research. 86(1):24–29. doi:10.1161/01.RES.86.1.24.

Kim K, Park I, Kim J, Kang M-G, Choi WG, Shin H, Kim J-S, Rhee H-W, Suh JM. 2021. Dynamic tracking and identification of tissue-specific secretory proteins in the circulation of live mice. Nat Commun. 12(1):5204. doi:10.1038/s41467-021-25546-y.

Kim KS, Kim JS, Park J-Y, Suh YH, Jou I, Joe E-H, Park SM. 2013. DJ-1 associates with lipid rafts by palmitoylation and regulates lipid rafts-dependent endocytosis in astrocytes. Hum Mol Genet. 22(23):4805–4817. doi:10.1093/hmg/ddt332.

Kirsch M, Black PM. 2012. Angiogenesis in Brain Tumors. Springer Science & Business Media.

Klekotka PA, Santoro SA, Zutter MM. 2001. α2 Integrin Subunit Cytoplasmic Domain-dependent Cellular Migration Requires p38 MAPK. Journal of Biological Chemistry. 276(12):9503–9511. doi:10.1074/jbc.M006286200.

Klemke RL, Leng J, Molander R, Brooks PC, Vuori K, Cheresh DA. 1998. CAS/Crk coupling serves as a “molecular switch” for induction of cell migration. J Cell Biol. 140(4):961–972. doi:10.1083/jcb.140.4.961.

Klenotic PA, Page RC, Li W, Amick J, Misra S, Silverstein RL. 2013. Molecular basis of antiangiogenic thrombospondin-1 type 1 repeat domain interactions with CD36. Arterioscler Thromb Vasc Biol. 33(7):1655–1662. doi:10.1161/ATVBAHA.113.301523.

Koenigsknecht J, Landreth G. 2004. Microglial Phagocytosis of Fibrillar β-Amyloid through a β_1 Integrin-Dependent Mechanism. J Neurosci. 24(44):9838–9846. doi:10.1523/JNEUROSCI.2557-04.2004.

Kotani N, Gu J, Isaji T, Udaka K, Taniguchi N, Honke K. 2008. Biochemical visualization of cell surface molecular clustering in living cells. Proceedings of the National Academy of Sciences. 105(21):7405–7409. doi:10.1073/pnas.0710346105.

Koyama-Honda I, Fujiwara TK, Kasai RS, Suzuki KGN, Kajikawa E, Tsuboi H, Tsunoyama TA, Kusumi A. 2020. High-speed single-molecule imaging reveals signal transduction by induced transbilayer raft phases. Journal of Cell Biology. 219(12):e202006125. doi:10.1083/jcb.202006125.

Kruskal WH, Wallis WA. 1952. Use of Ranks in One-Criterion Variance Analysis. Journal of the American Statistical Association. 47(260):583–621. doi:10.1080/01621459.1952.10483441.

Kuijpers MJE, de Witt S, Nergiz-Unal R, van Kruchten R, Korporaal SJA, Verhamme P, Febbraio M, Tjwa M, Voshol PJ, Hoylaerts MF, et al. 2014. Supporting Roles of Platelet Thrombospondin-1 and CD36 in Thrombus Formation on Collagen. Arteriosclerosis, Thrombosis, and Vascular Biology. 34(6):1187–1192. doi:10.1161/ATVBAHA.113.302917.

Kunnas TA, Wallén MJ, Kulomaa MS. 1993. Induction of chicken avidin and related mRNAs after bacterial infection. Biochimica et Biophysica Acta (BBA) - Gene Structure and Expression. 1216(3):441–445. doi:10.1016/0167-4781(93)90012-3.

Laitinen OH, Kuusela TP, Kukkurainen S, Nurminen A, Sinkkonen A, Hytönen VP. 2021. Bacterial avidins are a widely distributed protein family in Actinobacteria, Proteobacteria and Bacteroidetes. BMC Ecology and Evolution. 21(1):53. doi:10.1186/s12862-021-01784-y.

Lam SS, Martell JD, Kamer KJ, Deerinck TJ, Ellisman MH, Mootha VK, Ting AY. 2015. Directed evolution of APEX2 for electron microscopy and proximity labeling. Nat Methods. 12(1):51–54. doi:10.1038/nmeth.3179.

Lamalice L, Le Boeuf F, Huot J. 2007. Endothelial Cell Migration During Angiogenesis. Circulation Research. 100(6):782–794. doi:10.1161/01.RES.0000259593.07661.1e.

Lawler PR, Lawler J. 2012. Molecular basis for the regulation of angiogenesis by thrombospondin-1 and -2. Cold Spring Harb Perspect Med. 2(5):a006627. doi:10.1101/cshperspect.a006627.

Lee B-H, Ruoslahti E. 2005. α5β1 integrin stimulates Bcl-2 expression and cell survival through Akt, focal adhesion kinase, and Ca2+/calmodulin-dependent protein kinase IV. Journal of Cellular Biochemistry. 95(6):1214–1223. doi:10.1002/jcb.20488.

Leitinger B, Hogg N. 2002. The involvement of lipid rafts in the regulation of integrin function. Journal of Cell Science. 115(5):963–972. doi:10.1242/jcs.115.5.963.

Leitinger B, McDowall A, Stanley P, Hogg N. 2000. The regulation of integrin function by Ca2+. Biochimica et Biophysica Acta (BBA) - Molecular Cell Research. 1498(2):91–98. doi:10.1016/S0167-4889(00)00086-0.

León-Del-Río A. 2019. Biotin in metabolism, gene expression, and human disease. Journal of Inherited Metabolic Disease. 42(4):647–654. doi:10.1002/jimd.12073.

Leu S-J, Lam SC-T, Lau LF. 2002. Pro-angiogenic Activities of CYR61 (CCN1) Mediated through Integrins αvβ3 and α6β1 in Human Umbilical Vein Endothelial Cells *. Journal of Biological Chemistry. 277(48):46248–46255. doi:10.1074/jbc.M209288200.

Leu S-J, Liu Y, Chen N, Chen C-C, Lam SC-T, Lau LF. 2003. Identification of a Novel Integrin α6β1 Binding Site in the Angiogenic Inducer CCN1 (CYR61) *. Journal of Biological Chemistry. 278(36):33801–33808. doi:10.1074/jbc.M305862200.

Levental I, Lingwood D, Grzybek M, Coskun U, Simons K. 2010. Palmitoylation regulates raft affinity for the majority of integral raft proteins. Proc Natl Acad Sci U S A. 107(51):22050–22054. doi:10.1073/pnas.1016184107.

Liang F, Lee S-Y, Liang J, Lawrence DS, Zhang Z-Y. 2005. The Role of Protein-tyrosine Phosphatase 1B in Integrin Signaling *. Journal of Biological Chemistry. 280(26):24857–24863. doi:10.1074/jbc.M502780200.

Liang X, Draghi NA, Resh MD. 2004. Signaling from Integrins to Fyn to Rho Family GTPases Regulates Morphologic Differentiation of Oligodendrocytes. J Neurosci. 24(32):7140–7149. doi:10.1523/JNEUROSCI.5319-03.2004.

Liu W, Yin Y, Zhou Z, He M, Dai Y. 2014. OxLDL-induced IL-1beta secretion promoting foam cells formation was mainly via CD36 mediated ROS production leading to NLRP3 inflammasome activation. Inflamm Res. 63(1):33–43. doi:10.1007/s00011-013-0667-3.

Liu Z-L, Chen H-H, Zheng L-L, Sun L-P, Shi L. 2023. Angiogenic signaling pathways and anti-angiogenic therapy for cancer. Sig Transduct Target Ther. 8(1):1–39. doi:10.1038/s41392-023-01460-1.

Lobingier BT, Hüttenhain R, Eichel K, Miller KB, Ting AY, von Zastrow M, Krogan NJ. 2017. An Approach to Spatiotemporally Resolve Protein Interaction Networks in Living Cells. Cell. 169(2):350-360.e12. doi:10.1016/j.cell.2017.03.022.

Lonati A, Mommaas MA, Pasolini G, Lavazza A, Rowden G, De Panfilis G. 1996. Macrophages, but Not Langerhans Cell-like Cells of Dendritic Lineage, Express the CD36 Molecule in Normal Human Dermis: Relevance to Downregulatory Cutaneous Immune Responses? Journal of Investigative Dermatology. 106(1):96–101. doi:10.1111/1523-1747.ep12328158.

Lopes-Coelho F, Martins F, Pereira SA, Serpa J. 2021. Anti-Angiogenic Therapy: Current Challenges and Future Perspectives. Int J Mol Sci. 22(7):3765. doi:10.3390/ijms22073765.

Lu F, Zhu L, Bromberger T, Yang J, Yang Q, Liu J, Plow EF, Moser M, Qin J. 2022. Mechanism of integrin activation by talin and its cooperation with kindlin. Nat Commun. 13(1):2362. doi:10.1038/s41467-022-30117-w.

Ludwig BS, Kessler H, Kossatz S, Reuning U. 2021. RGD-Binding Integrins Revisited: How Recently Discovered Functions and Novel Synthetic Ligands (Re-)Shape an Ever-Evolving Field. Cancers (Basel). 13(7):1711. doi:10.3390/cancers13071711.

Luiken JJFP, Schaap FG, van Nieuwenhoven FA, van der Vusse GJ, Bonen A, Glatz JFC. 1999. Cellular fatty acid transport in heart and skeletal muscle as facilitated by proteins. Lipids. 34(S1Part2):S169–S175. doi:10.1007/BF02562278.

Ma J, Waxman DJ. 2008a. Combination of Anti-angiogenesis with Chemotherapy for More Effective Cancer Treatment. Molecular cancer therapeutics. 7(12):3670. doi:10.1158/1535-7163.MCT-08-0715.

Ma J, Waxman DJ. 2008b. Combination of antiangiogenesis with chemotherapy for more effective cancer treatment. Molecular Cancer Therapeutics. 7(12):3670–3684. doi:10.1158/1535-7163.MCT-08-0715.

Ma Q, Reiter RJ, Chen Y. 2020. Role of melatonin in controlling angiogenesis under physiological and pathological conditions. Angiogenesis. 23(2):91–104. doi:10.1007/s10456-019-09689-7.

Machiyama H, Yamaguchi T, Watanabe TM, Fujita H. 2017. A novel c-Src recruitment pathway from the cytosol to focal adhesions. FEBS Lett. 591(13):1940–1946. doi:10.1002/1873-3468.12696.

Magnusson PU, Looman C, Åhgren A, Wu Y, Claesson-Welsh L, Heuchel RL. 2007. Platelet-Derived Growth Factor Receptor-β Constitutive Activity Promotes Angiogenesis In Vivo and In Vitro. Arteriosclerosis, Thrombosis, and Vascular Biology. 27(10):2142–2149. doi:10.1161/01.ATV.0000282198.60701.94.

Mairhofer M, Steiner M, Mosgoeller W, Prohaska R, Salzer U. 2002. Stomatin is a major lipid-raft component of platelet α granules. Blood. 100(3):897–904. doi:10.1182/blood.V100.3.897.

Mans S, Banz Y, Mueller BU, Pabst T. 2012. The angiogenesis inhibitor vasostatin is regulated by neutrophil elastase–dependent cleavage of calreticulin in AML patients. Blood. 120(13):2690–2699. doi:10.1182/blood-2012-02-412759.

Marques PE, Nyegaard S, Collins RF, Troise F, Freeman SA, Trimble WS, Grinstein S. 2019. Multimerization and Retention of the Scavenger Receptor SR-B1 in the Plasma Membrane. Developmental Cell. 50(3):283-295.e5. doi:10.1016/j.devcel.2019.05.026.

Martell JD, Deerinck TJ, Sancak Y, Poulos TL, Mootha VK, Sosinsky GE, Ellisman MH, Ting AY. 2012. Engineered ascorbate peroxidase as a genetically encoded reporter for electron microscopy. Nat Biotechnol. 30(11):1143–1148. doi:10.1038/nbt.2375.

Martínez-Mármol R, Small C, Jiang A, Palliyaguru T, Wallis TP, Gormal RS, Sibarita J-B, Götz J, Meunier FA. 2023. Fyn nanoclustering requires switching to an open conformation and is enhanced by FTLD-Tau biomolecular condensates. Mol Psychiatry. 28(2):946–962. doi:10.1038/s41380-022-01825-y.

Matrone C, Petrillo F, Nasso R, Ferretti G. 2020. Fyn Tyrosine Kinase as Harmonizing Factor in Neuronal Functions and Dysfunctions. Int J Mol Sci. 21(12):4444. doi:10.3390/ijms21124444.

Matsuoka T, Yashiro M, Nishioka N, Hirakawa K, Olden K, Roberts JD. 2012. PI3K/Akt signalling is required for the attachment and spreading, and growth in vivo of metastatic scirrhous gastric carcinoma. Br J Cancer. 106(9):1535–1542. doi:10.1038/bjc.2012.107.

Matuszewska K, Kortenaar S ten, Pereira M, Santry LA, Petrik D, Lo K-M, Bridle BW, Wootton SK, Lawler J, Petrik J. 2022. Addition of an Fc-IgG induces receptor clustering and increases the in vitro efficacy and in vivo anti-tumor properties of the thrombospondin-1 type I repeats (3TSR) in a mouse model of advanced stage ovarian cancer. Gynecologic Oncology. 164(1):154–169. doi:10.1016/j.ygyno.2021.11.006.

May DG, Scott KL, Campos AR, Roux KJ. 2020. Comparative Application of BioID and TurboID for Protein-Proximity Biotinylation. Cells. 9(5):1070. doi:10.3390/cells9051070.

McLaughlin AP, De Vries GW. 2001. Role of PLCgamma and Ca(2+) in VEGF- and FGF-induced choroidal endothelial cell proliferation. Am J Physiol Cell Physiol. 281(5):C1448-1456. doi:10.1152/ajpcell.2001.281.5.C1448.

Mebratu Y, Tesfaigzi Y. 2009. How ERK1/2 Activation Controls Cell Proliferation and Cell Death Is Subcellular Localization the Answer? Cell Cycle. 8(8):1168–1175.

Medinger M, Mross K. 2010. Clinical trials with anti-angiogenic agents in hematological malignancies. J Angiogenes Res. 2:10. doi:10.1186/2040-2384-2-10.

Mezu-Ndubuisi OJ, Maheshwari A. 2021. The role of integrins in inflammation and angiogenesis. Pediatr Res. 89(7):1619–1626. doi:10.1038/s41390-020-01177-9.

Miao WM, Vasile E, Lane WS, Lawler J. 2001. CD36 associates with CD9 and integrins on human blood platelets. Blood. 97(6):1689–1696. doi:10.1182/blood.v97.6.1689.

Minerva D, Othman NL, Nakazawa T, Ito Y, Yoshida M, Goto A, Suzuki T. 2022. A New Chemotactic Mechanism Governs Long-Range Angiogenesis Induced by Patching an Arterial Graft into a Vein. Int J Mol Sci. 23(19):11208. doi:10.3390/ijms231911208.

Mohajeri A, Sanaei S, Kiafar F, Fattahi A, Khalili M, Zarghami N. 2017. The Challenges of Recombinant Endostatin in Clinical Application: Focus on the Different Expression Systems and Molecular Bioengineering. Adv Pharm Bull. 7(1):21–34. doi:10.15171/apb.2017.004.

Montemagno C, Pagès G. 2020. Resistance to Anti-angiogenic Therapies: A Mechanism Depending on the Time of Exposure to the Drugs. Frontiers in Cell and Developmental Biology. 8. [accessed 2023 Apr 27]. https://www.frontiersin.org/articles/10.3389/fcell.2020.00584.

Müller MA, Brunie L, Bächer A-S, Kessler H, Gottschalk K-E, Reuning U. 2014. Cytoplasmic salt bridge formation in integrin αvß3 stabilizes its inactive state affecting integrin-mediated cell biological effects. Cell Signal. 26(11):2493–2503. doi:10.1016/j.cellsig.2014.07.013.

Murayama Y, Miyagawa J, Oritani K, Yoshida H, Yamamoto K, Kishida O, Miyazaki T, Tsutsui S, Kiyohara T, Miyazaki Y, et al. 2004. CD9-mediated activation of the p46 Shc isoform leads to apoptosis in cancer cells. Journal of Cell Science. 117(15):3379–3388. doi:10.1242/jcs.01201.

Murphy-Ullrich JE. 2022. Thrombospondin-1 Signaling Through the Calreticulin/LDL Receptor Related Protein 1 Axis: Functions and Possible Roles in Glaucoma. Frontiers in Cell and Developmental Biology. 10. [accessed 2023 May 9]. https://www.frontiersin.org/articles/10.3389/fcell.2022.898772.

Murray EW, Robbins SM. 1998. Antibody Cross-linking of the Glycosylphosphatidylinositol-linked Protein CD59 on Hematopoietic Cells Induces Signaling Pathways Resembling Activation by Complement. Journal of Biological Chemistry. 273(39):25279–25284. doi:10.1074/jbc.273.39.25279.

Nakamoto T, Murayama Y, Oritani K, Boucheix C, Rubinstein E, Nishida M, Katsube F, Watabe K, Kiso S, Tsutsui S, et al. 2009. A novel therapeutic strategy with anti-CD9 antibody in gastric cancers. J Gastroenterol. 44(9):889–896. doi:10.1007/s00535-009-0081-3.

Navazo MDP, Daviet L, Ninio E, McGregor JL. 1996. Identification on Human CD36 of a Domain (155-183) Implicated in Binding Oxidized Low-Density Lipoproteins (Ox-LDL). Arteriosclerosis, Thrombosis, and Vascular Biology. 16(8):1033–1039. doi:10.1161/01.ATV.16.8.1033.

Neculai D, Schwake M, Ravichandran M, Zunke F, Collins RF, Peters J, Neculai M, Plumb J, Loppnau P, Pizarro JC, et al. 2013. Structure of LIMP-2 provides functional insights with implications for SR-BI and CD36. Nature. 504(7478):172–176. doi:10.1038/nature12684.

Nicholson AC, Frieda S, Pearce A, Silverstein RL. 1995. Oxidized LDL Binds to CD36 on Human Monocyte-Derived Macrophages and Transfected Cell Lines. Arteriosclerosis, Thrombosis, and Vascular Biology. 15(2):269–275. doi:10.1161/01.ATV.15.2.269.

Niland S, Riscanevo AX, Eble JA. 2021. Matrix Metalloproteinases Shape the Tumor Microenvironment in Cancer Progression. Int J Mol Sci. 23(1):146. doi:10.3390/ijms23010146.

Nishida N, Yano H, Nishida T, Kamura T, Kojiro M. 2006. Angiogenesis in Cancer. Vasc Health Risk Manag. 2(3):213–219.

Oakley JV, Buksh BF, Fernández DF, Oblinsky DG, Seath CP, Geri JB, Scholes GD, MacMillan DWC. 2022a. Radius measurement via super-resolution microscopy enables the development of a variable radii proximity labeling platform. Proceedings of the National Academy of Sciences. 119(32):e2203027119. doi:10.1073/pnas.2203027119.

Oakley JV, Buksh BF, Fernández DF, Oblinsky DG, Seath CP, Geri JB, Scholes GD, MacMillan DWC. 2022b. Radius measurement via super-resolution microscopy enables the development of a variable radii proximity labeling platform. Proceedings of the National Academy of Sciences. 119(32):e2203027119. doi:10.1073/pnas.2203027119.

Oakley JV, Buksh BF, Fernández DF, Oblinsky DG, Seath CP, Geri JB, Scholes GD, MacMillan DWC. 2022c. Radius measurement via super-resolution microscopy enables the development of a variable radii proximity labeling platform. Proceedings of the National Academy of Sciences. 119(32):e2203027119. doi:10.1073/pnas.2203027119.

Oguri Y, Shinoda K, Kim H, Alba DL, Bolus WR, Wang Q, Brown Z, Pradhan RN, Tajima K, Yoneshiro T, et al. 2020. CD81 Controls Beige Fat Progenitor Cell Growth and Energy Balance via FAK Signaling. Cell. 182(3):563-577.e20. doi:10.1016/j.cell.2020.06.021.

Okumura N, Yoshida H, Kitagishi Y, Murakami M, Nishimura Y, Matsuda S. 2012. PI3K/AKT/PTEN Signaling as a Molecular Target in Leukemia Angiogenesis. Adv Hematol. 2012:843085. doi:10.1155/2012/843085.

Omidvar N, Wang ECY, Brennan P, Longhi MP, Smith RAG, Morgan BP. 2006. Expression of Glycosylphosphatidylinositol-Anchored CD59 on Target Cells Enhances Human NK Cell-Mediated Cytotoxicity. J Immunol. 176(5):2915–2923.

Oommen S, Gupta SK, Vlahakis NE. 2011. Vascular Endothelial Growth Factor A (VEGF-A) Induces Endothelial and Cancer Cell Migration through Direct Binding to Integrin α9β1. J Biol Chem. 286(2):1083–1092. doi:10.1074/jbc.M110.175158.

Orłowski A, Kukkurainen S, Pöyry A, Rissanen S, Vattulainen I, Hytönen VP, Róg T. 2015. PIP2 and Talin Join Forces to Activate Integrin. J Phys Chem B. 119(38):12381–12389. doi:10.1021/acs.jpcb.5b06457.

Otrock ZK, Mahfouz RAR, Makarem JA, Shamseddine AI. 2007. Understanding the biology of angiogenesis: Review of the most important molecular mechanisms. Blood Cells, Molecules, and Diseases. 39(2):212–220. doi:10.1016/j.bcmd.2007.04.001.

Panaretakis T, Kepp O, Brockmeier U, Tesniere A, Bjorklund A-C, Chapman DC, Durchschlag M, Joza N, Pierron G, van Endert P, et al. 2009. Mechanisms of pre-apoptotic calreticulin exposure in immunogenic cell death. The EMBO Journal. 28(5):578–590. doi:10.1038/emboj.2009.1.

Park EJ, Yuki Y, Kiyono H, Shimaoka M. 2015. Structural basis of blocking integrin activation and deactivation for anti-inflammation. Journal of Biomedical Science. 22(1):51. doi:10.1186/s12929-015-0159-6.

Park L, Wang G, Zhou P, Zhou J, Pitstick R, Previti ML, Younkin L, Younkin SG, Van Nostrand WE, Cho S, et al. 2011. Scavenger receptor CD36 is essential for the cerebrovascular oxidative stress and neurovascular dysfunction induced by amyloid-β. Proceedings of the National Academy of Sciences. 108(12):5063–5068. doi:10.1073/pnas.1015413108.

Park L, Zhou J, Zhou P, Pistick R, El Jamal S, Younkin L, Pierce J, Arreguin A, Anrather J, Younkin SG, et al. 2013. Innate immunity receptor CD36 promotes cerebral amyloid angiopathy. Proc Natl Acad Sci U S A. 110(8):3089–3094. doi:10.1073/pnas.1300021110.

Parsons SJ, Parsons JT. 2004. Src family kinases, key regulators of signal transduction. Oncogene. 23(48):7906–7909. doi:10.1038/sj.onc.1208160.

Pasqualini R, Hemler ME. 1994. Contrasting roles for integrin beta 1 and beta 5 cytoplasmic domains in subcellular localization, cell proliferation, and cell migration. The Journal of cell biology. 125(2):447–460. doi:10.1083/jcb.125.2.447.

Pelsers MM, Lutgerink JT, Nieuwenhoven FA, Tandon NN, van der Vusse GJ, Arends JW, Hoogenboom HR, Glatz JF. 1999. A sensitive immunoassay for rat fatty acid translocase (CD36)

using phage antibodies selected on cell transfectants: abundant presence of fatty acid translocase/CD36 in cardiac and red skeletal muscle and up-regulation in diabetes. Biochem J. 337(Pt 3):407–414.

Perez Verdaguer M, Zhang T, Surve S, Paulo JA, Wallace C, Watkins SC, Gygi SP, Sorkin A. 2022. Time-resolved proximity labeling of protein networks associated with ligand-activated EGFR. Cell Reports. 39(11):110950. doi:10.1016/j.celrep.2022.110950.

Perollet C, Han ZC, Savona C, Caen JP, Bikfalvi A. 1998. Platelet factor 4 modulates fibroblast growth factor 2 (FGF-2) activity and inhibits FGF-2 dimerization. Blood. 91(9):3289–3299.

Plow EF, Haas TA, Zhang L, Loftus J, Smith JW. 2000. Ligand Binding to Integrins *. Journal of Biological Chemistry. 275(29):21785–21788. doi:10.1074/jbc.R000003200.

Podrez EA, Poliakov E, Shen Z, Zhang R, Deng Y, Sun M, Finton PJ, Shan L, Gugiu B, Fox PL, et al. 2002. Identification of a Novel Family of Oxidized Phospholipids That Serve as Ligands for the Macrophage Scavenger Receptor CD36 *. Journal of Biological Chemistry. 277(41):38503–38516. doi:10.1074/jbc.M203318200.

Pohl J, Ring A, Korkmaz Ü, Ehehalt R, Stremmel W. 2005a. FAT/CD36-mediated Long-Chain Fatty Acid Uptake in Adipocytes Requires Plasma Membrane Rafts. MBoC. 16(1):24–31. doi:10.1091/mbc.e04-07-0616.

Pohl J, Ring A, Korkmaz Ü, Ehehalt R, Stremmel W. 2005b. FAT/CD36-mediated Long-Chain Fatty Acid Uptake in Adipocytes Requires Plasma Membrane Rafts. MBoC. 16(1):24–31. doi:10.1091/mbc.e04-07-0616.

Pottier C, Fresnais M, Gilon M, Jérusalem G, Longuespée R, Sounni NE. 2020. Tyrosine Kinase Inhibitors in Cancer: Breakthrough and Challenges of Targeted Therapy. Cancers. 12(3):731. doi:10.3390/cancers12030731.

Pratt JW. 1959. Remarks on Zeros and Ties in the Wilcoxon Signed Rank Procedures. Journal of the American Statistical Association. 54(287):655–667. doi:10.1080/01621459.1959.10501526.

Primo L, Ferrandi C, Roca C, Marchiò S, di Blasio L, Alessio M, Bussolino F. 2005. Identification of CD36 molecular features required for its in vitro angiostatic activity. FASEB J. 19(12):1713–1715. doi:10.1096/fj.05-3697fje.

Proteome Discoverer User Guide.

Pua LJW, Mai C-W, Chung FF-L, Khoo AS-B, Leong C-O, Lim W-M, Hii L-W. 2022. Functional Roles of JNK and p38 MAPK Signaling in Nasopharyngeal Carcinoma. Int J Mol Sci. 23(3):1108. doi:10.3390/ijms23031108.

Qin W, Cho KF, Cavanagh PE, Ting AY. 2021. Deciphering molecular interactions by proximity labeling. Nat Methods. 18(2):133–143. doi:10.1038/s41592-020-01010-5.

Quintero-Fabián S, Arreola R, Becerril-Villanueva E, Torres-Romero JC, Arana-Argáez V, Lara-Riegos J, Ramírez-Camacho MA, Alvarez-Sánchez ME. 2019. Role of Matrix

Metalloproteinases in Angiogenesis and Cancer. Front Oncol. 9:1370. doi:10.3389/fonc.2019.01370.

Raica M, Cimpean AM. 2010. Platelet-Derived Growth Factor (PDGF)/PDGF Receptors (PDGFR) Axis as Target for Antitumor and Antiangiogenic Therapy. Pharmaceuticals (Basel). 3(3):572–599. doi:10.3390/ph3030572.

Ralston GB. 1985. Protein-Protein Interactions in Cell Membranes. In: Structure and Properties of Cell Membrane Structure and Properties of Cell Membranes. CRC Press. 21 p.

Ramanathan M, Majzoub K, Rao DS, Neela PH, Zarnegar BJ, Mondal S, Roth JG, Gai H, Kovalski JR, Siprashvili Z, et al. 2018. RNA–protein interaction detection in living cells. Nat Methods. 15(3):207–212. doi:10.1038/nmeth.4601.

Rasmussen JT, Berglund L, Rasmussen MS, Petersen TE. 1998. Assignment of disulfide bridges in bovine CD36. Eur J Biochem. 257(2):488–494. doi:10.1046/j.1432-1327.1998.2570488.x.

Rauova L, Zhai L, Kowalska MA, Arepally GM, Cines DB, Poncz M. 2006. Role of platelet surface PF4 antigenic complexes in heparin-induced thrombocytopenia pathogenesis: diagnostic and therapeutic implications. Blood. 107(6):2346–2353. doi:10.1182/blood-2005-08-3122.

Reck M, von Pawel J, Zatloukal P, Ramlau R, Gorbounova V, Hirsh V, Leighl N, Mezger J, Archer V, Moore N, et al. 2009. Phase III trial of cisplatin plus gemcitabine with either placebo or bevacizumab as first-line therapy for nonsquamous non-small-cell lung cancer: AVAil. J Clin Oncol. 27(8):1227–1234. doi:10.1200/JCO.2007.14.5466.

Rees Johanna S., Li X-W, Perrett S, Lilley KS, Jackson AP. 2015. Protein Neighbors and Proximity Proteomics. Mol Cell Proteomics. 14(11):2848–2856. doi:10.1074/mcp.R115.052902.

Rees Johanna Susan, Li X-W, Perrett S, Lilley KS, Jackson AP. 2015. Selective Proteomic Proximity Labeling Assay Using Tyramide (SPPLAT): A Quantitative Method for the Proteomic Analysis of Localized Membrane-Bound Protein Clusters. Curr Protoc Protein Sci. 80:19.27.1-19.27.18. doi:10.1002/0471140864.ps1927s80.

Resovi A, Pinessi D, Chiorino G, Taraboletti G. 2014. Current understanding of the thrombospondin-1 interactome. Matrix Biol. 37:83–91. doi:10.1016/j.matbio.2014.01.012.

Ribatti D. 2008. Judah Folkman, a pioneer in the study of angiogenesis. Angiogenesis. 11(1):3–10. doi:10.1007/s10456-008-9092-6.

Ribatti D, Nico B, Crivellato E. 2011. The role of pericytes in angiogenesis. The International Journal of Developmental Biology. 55(3):261–268. doi:10.1387/ijdb.103167dr.

Ricard N, Bailly S, Guignabert C, Simons M. 2021. The quiescent endothelium: signalling pathways regulating organ-specific endothelial normalcy. Nat Rev Cardiol. 18(8):565–580. doi:10.1038/s41569-021-00517-4.

Rigotti A, Acton SL, Krieger M. 1995. The Class B Scavenger Receptors SR-BI and CD36 Are Receptors for Anionic Phospholipids *. Journal of Biological Chemistry. 270(27):16221–16224. doi:10.1074/jbc.270.27.16221.

Ritchie K, Iino R, Fujiwara T, Murase K, Kusumi A. 2003. The fence and picket structure of the plasma membrane of live cells as revealed by single molecule techniques (Review). Molecular Membrane Biology. 20(1):13–18. doi:10.1080/0968768021000055698.

Rocha-Perugini V, González-Granado JM, Tejera E, López-Martín S, Yañez-Mó M, Sánchez-Madrid F. 2014. Tetraspanins CD9 and CD151 at the immune synapse support T-cell integrin signaling. Eur J Immunol. 44(7):1967–1975. doi:10.1002/eji.201344235.

Rousseau S, Houle F, Landry J, Huot J. 1997. p38 MAP kinase activation by vascular endothelial growth factor mediates actin reorganization and cell migration in human endothelial cells. Oncogene. 15(18):2169–2177. doi:10.1038/sj.onc.1201380.

Roux KJ, Kim DI, Raida M, Burke B. 2012. A promiscuous biotin ligase fusion protein identifies proximal and interacting proteins in mammalian cells. Journal of Cell Biology. 196(6):801–810. doi:10.1083/jcb.201112098.

Ruan G-X, Kazlauskas A. 2012. VEGF-A engages at least three tyrosine kinases to activate PI3K/Akt. Cell Cycle. 11(11):2047–2048. doi:10.4161/cc.20535.

Salani B, Briatore L, Contini P, Passalacqua M, Melloni E, Paggi A, Cordera R, Maggi D. 2009. IGF-I induced rapid recruitment of integrin beta1 to lipid rafts is Caveolin-1 dependent. Biochem Biophys Res Commun. 380(3):489–492. doi:10.1016/j.bbrc.2009.01.102.

Sala-Valdés M, Ursa A, Charrin S, Rubinstein E, Hemler ME, Sánchez-Madrid F, Yáñez-Mó M. 2006. EWI-2 and EWI-F link the tetraspanin web to the actin cytoskeleton through their direct association with ezrin-radixin-moesin proteins. J Biol Chem. 281(28):19665–19675. doi:10.1074/jbc.M602116200.

Saltz LB, Clarke S, Díaz-Rubio E, Scheithauer W, Figer A, Wong R, Koski S, Lichinitser M, Yang T-S, Rivera F, et al. 2008. Bevacizumab in combination with oxaliplatin-based chemotherapy as first-line therapy in metastatic colorectal cancer: a randomized phase III study. J Clin Oncol. 26(12):2013–2019. doi:10.1200/JCO.2007.14.9930.

Salzer U, Prohaska R. 2001. Stomatin, flotillin-1, and flotillin-2 are major integral proteins of erythrocyte lipid rafts. Blood. 97(4):1141–1143. doi:10.1182/blood.V97.4.1141.

Sampson MJ, Davies IR, Braschi S, Ivory K, Hughes DA. 2003. Increased expression of a scavenger receptor (CD36) in monocytes from subjects with Type 2 diabetes. Atherosclerosis. 167(1):129–134. doi:10.1016/s0021-9150(02)00421-5.

Sanchez AD, Branon TC, Cote LE, Papagiannakis A, Liang X, Pickett MA, Shen K, Jacobs-Wagner C, Ting AY, Feldman JL. 2021. Proximity labeling reveals non-centrosomal microtubule-organizing center components required for microtubule growth and localization. Curr Biol. 31(16):3586-3600.e11. doi:10.1016/j.cub.2021.06.021.

Serru V, Le Naour F, Billard M, Azorsa DO, Lanza F, Boucheix C, Rubinstein E. 1999. Selective tetraspan-integrin complexes (CD81/alpha4beta1, CD151/alpha3beta1, CD151/alpha6beta1) under conditions disrupting tetraspan interactions. Biochem J. 340(Pt 1):103–111.

Sfeir Z, Ibrahimi A, Amri E, Grimaldi P, Abumrad N. 1997. Regulation of FAT/CD36 gene expression: further evidence in support of a role of the protein in fatty acid binding/transport. Prostaglandins Leukot Essent Fatty Acids. 57(1):17–21. doi:10.1016/s0952-3278(97)90487-7.

Shafaq-Zadah M, Gomes-Santos CS, Bardin S, Maiuri P, Maurin M, Iranzo J, Gautreau A, Lamaze C, Caswell P, Goud B, et al. 2016. Persistent cell migration and adhesion rely on retrograde transport of β1 integrin. Nat Cell Biol. 18(1):54–64. doi:10.1038/ncb3287.

Shangary S, Wang S. 2009. Small-Molecule Inhibitors of the MDM2-p53 Protein-Protein Interaction to Reactivate p53 Function: A Novel Approach for Cancer Therapy. Annual Review of Pharmacology and Toxicology. 49(1):223–241. doi:10.1146/annurev.pharmtox.48.113006.094723.

Shelby SA, Castello-Serrano I, Wisser KC, Levental I, Veatch SL. 2023. Membrane phase separation drives responsive assembly of receptor signaling domains. Nat Chem Biol. 19(6):750–758. doi:10.1038/s41589-023-01268-8.

Shenoy-Scaria AM, Dietzen DJ, Kwong J, Link DC, Lublin DM. 1994. Cysteine3 of Src family protein tyrosine kinase determines palmitoylation and localization in caveolae. J Cell Biol. 126(2):353–363. doi:10.1083/jcb.126.2.353.

Shoham T, Rajapaksa R, Kuo C-C, Haimovich J, Levy S. 2006. Building of the Tetraspanin Web: Distinct Structural Domains of CD81 Function in Different Cellular Compartments. Mol Cell Biol. 26(4):1373–1385. doi:10.1128/MCB.26.4.1373-1385.2006.

Shu Q, Li W, Li H, Sun G. 2014. Vasostatin Inhibits VEGF-Induced Endothelial Cell Proliferation, Tube Formation and Induces Cell Apoptosis under Oxygen Deprivation. International Journal of Molecular Sciences. 15(4):6019–6030. doi:10.3390/ijms15046019.

Shukla S, Chen Z-S, Ambudkar SV. 2012. Tyrosine kinase inhibitors as modulators of ABC transporter-mediated drug resistance. Drug Resist Updat. 15(1–2):70–80. doi:10.1016/j.drup.2012.01.005.

Sidak Z. 1967. Rectangular Confidence Regions for the Means of Multivariate Normal Distributions. Journal of the American Statistical Association. 62(318):626–633. doi:10.2307/2283989.

da Silva GB, Pinto JR, Barros EJG, Farias GMN, Daher EDF. 2017. Kidney involvement in malaria: an update. Rev Inst Med Trop Sao Paulo. 59:e53. doi:10.1590/S1678-9946201759053.

Silverstein RL, Febbraio M. 2009. CD36, a Scavenger Receptor Involved in Immunity, Metabolism, Angiogenesis, and Behavior. Sci Signal. 2(72):re3. doi:10.1126/scisignal.272re3.

Simons K, Toomre D. 2000. Lipid rafts and signal transduction. Nat Rev Mol Cell Biol. 1(1):31–39. doi:10.1038/35036052.

Singer SJ, Nicolson GL. 1972. The fluid mosaic model of the structure of cell membranes. Science. 175(4023):720–731. doi:10.1126/science.175.4023.720.

Smith MA, Blankman E, Gardel ML, Luettjohann L, Waterman CM, Beckerle MC. 2010. A Zyxin-Mediated Mechanism for Actin Stress Fiber Maintenance and Repair. Developmental Cell. 19(3):365–376. doi:10.1016/j.devcel.2010.08.008.

Song S, Ewald AJ, Stallcup W, Werb Z, Bergers G. 2005. PDGFRβ+ perivascular progenitor cells in tumours regulate pericyte differentiation and vascular survival. Nat Cell Biol. 7(9):870–879. doi:10.1038/ncb1288.

Stahl A, Hirsch DJ, Gimeno RE, Punreddy S, Ge P, Watson N, Patel S, Kotler M, Raimondi A, Tartaglia LA, et al. 1999. Identification of the Major Intestinal Fatty Acid Transport Protein. Molecular Cell. 4(3):299–308. doi:10.1016/S1097-2765(00)80332-9.

Stipp CS, Kolesnikova TV, Hemler ME. 2003. EWI-2 regulates α3β1 integrin–dependent cell functions on laminin-5. J Cell Biol. 163(5):1167–1177. doi:10.1083/jcb.200309113.

Stirling DR, Swain-Bowden MJ, Lucas AM, Carpenter AE, Cimini BA, Goodman A. 2021. CellProfiler 4: improvements in speed, utility and usability. BMC Bioinformatics. 22(1):433. doi:10.1186/s12859-021-04344-9.

Sulpice E, Bryckaert M, Lacour J, Contreres J-O, Tobelem G. 2002. Platelet factor 4 inhibits FGF2-induced endothelial cell proliferation via the extracellular signal-regulated kinase pathway but not by the phosphatidylinositol 3-kinase pathway. Blood. 100(9):3087–3094. doi:10.1182/blood.V100.9.3087.

Sun S, Dong H, Yan T, Li Junchen, Liu B, Shao P, Li Jie, Liang C. 2020. Role of TSP-1 as prognostic marker in various cancers: a systematic review and meta-analysis. BMC Medical Genetics. 21(1):139. doi:10.1186/s12881-020-01073-3.

Sun X, Fu Y, Gu M, Zhang L, Li D, Li H, Chien S, Shyy JY-J, Zhu Y. 2016. Activation of integrin α5 mediated by flow requires its translocation to membrane lipid rafts in vascular endothelial cells. Proceedings of the National Academy of Sciences. 113(3):769–774. doi:10.1073/pnas.1524523113.

Swerlick RA, Lee KH, Wick TM, Lawley TJ. 1992. Human dermal microvascular endothelial but not human umbilical vein endothelial cells express CD36 in vivo and in vitro. J Immunol. 148(1):78–83.

Taban Q, Mumtaz PT, Masoodi KZ, Haq E, Ahmad SM. 2022. Scavenger receptors in host defense: from functional aspects to mode of action. Cell Communication and Signaling. 20(1):2. doi:10.1186/s12964-021-00812-0.

Tadokoro S, Shattil SJ, Eto K, Tai V, Liddington RC, de Pereda JM, Ginsberg MH, Calderwood DA. 2003. Talin Binding to Integrin ß Tails: A Final Common Step in Integrin Activation. Science. 302(5642):103–106. doi:10.1126/science.1086652.

Tadros A, Hughes DP, Dunmore BJ, Brindle NPJ. 2003. ABIN-2 protects endothelial cells from death and has a role in the antiapoptotic effect of angiopoietin-1. Blood. 102(13):4407–4409. doi:10.1182/blood-2003-05-1602.

Takada Y, Ye X, Simon S. 2007. The integrins. Genome Biol. 8(5):215. doi:10.1186/gb-2007-8-5-215.

Takahashi T, Ueno H, Shibuya M. 1999. VEGF activates protein kinase C-dependent, but Ras-independent Raf-MEK-MAP kinase pathway for DNA synthesis in primary endothelial cells. Oncogene. 18(13):2221–2230. doi:10.1038/sj.onc.1202527.

Talapko J, Škrlec I, Alebić T, Jukić M, Včev A. 2019. Malaria: The Past and the Present. Microorganisms. 7(6):179. doi:10.3390/microorganisms7060179.

Tandon NN, Lipsky RH, Burgess WH, Jamieson GA. 1989. Isolation and characterization of platelet glycoprotein IV (CD36). J Biol Chem. 264(13):7570–7575.

Tao N, Wagner SJ, Lublin DM. 1996. CD36 is palmitoylated on both N- and C-terminal cytoplasmic tails. J Biol Chem. 271(37):22315–22320. doi:10.1074/jbc.271.37.22315.

Taraboletti G, D'Ascenzo S, Borsotti P, Giavazzi R, Pavan A, Dolo V. 2002. Shedding of the matrix metalloproteinases MMP-2, MMP-9, and MT1-MMP as membrane vesicle-associated components by endothelial cells. Am J Pathol. 160(2):673–680. doi:10.1016/S0002-9440(10)64887-0.

Tarrant JM, Robb L, Spriel AB van, Wright MD. 2003. Tetraspanins: molecular organisers of the leukocyte surface. Trends in Immunology. 24(11):610–617. doi:10.1016/j.it.2003.09.011.

Tausig F, Wolf FJ. 1964. Streptavidin- a substance with avidin-like properties produced by microorganisms. Biochemical and Biophysical Research Communications. 14:205–209.

Teese MG, Langosch D. 2015. Role of GxxxG Motifs in Transmembrane Domain Interactions. Biochemistry. 54(33):5125–5135. doi:10.1021/acs.biochem.5b00495.

Termini CM, Lidke KA, Gillette JM. 2016. Tetraspanin CD82 Regulates the Spatiotemporal Dynamics of PKCα in Acute Myeloid Leukemia. Sci Rep. 6(1):29859. doi:10.1038/srep29859.

Terracciano R, Preianò M, Fregola A, Pelaia C, Montalcini T, Savino R. 2021. Mapping the SARS-CoV-2–Host Protein–Protein Interactome by Affinity Purification Mass Spectrometry and Proximity-Dependent Biotin Labeling: A Rational and Straightforward Route to Discover Host-Directed Anti-SARS-CoV-2 Therapeutics. International Journal of Molecular Sciences. 22(2):532. doi:10.3390/ijms22020532.

Thal DR, Griffin WST, Braak H. 2008. Parenchymal and vascular Aβ-deposition and its effects on the degeneration of neurons and cognition in Alzheimer's disease. Journal of Cellular and Molecular Medicine. 12(5b):1848–1862. doi:10.1111/j.1582-4934.2008.00411.x.

Thorne RF, Marshall JF, Shafren DR, Gibson PG, Hart IR, Burns GF. 2000a. The Integrins α3β1 and α6β1 Physically and Functionally Associate with CD36 in Human Melanoma Cells: REQUIREMENT FOR THE EXTRACELLULAR DOMAIN OF CD36*. Journal of Biological Chemistry. 275(45):35264–35275. doi:10.1074/jbc.M003969200.

Thorne RF, Marshall JF, Shafren DR, Gibson PG, Hart IR, Burns GF. 2000b. The Integrins α3β1 and α6β1 Physically and Functionally Associate with CD36 in Human Melanoma Cells: REQUIREMENT FOR THE EXTRACELLULAR DOMAIN OF CD36*. Journal of Biological Chemistry. 275(45):35264–35275. doi:10.1074/jbc.M003969200.

Thorne RF, Ralston KJ, de Bock CE, Mhaidat NM, Zhang XD, Boyd AW, Burns GF. 2010. Palmitoylation of CD36/FAT regulates the rate of its post-transcriptional processing in the endoplasmic reticulum. Biochimica et Biophysica Acta (BBA) - Molecular Cell Research. 1803(11):1298–1307. doi:10.1016/j.bbamcr.2010.07.002.

Togayachi A, Kozono Y, Ikehara Y, Ito H, Suzuki N, Tsunoda Y, Abe S, Sato T, Nakamura K, Suzuki M, et al. 2010. Lack of lacto/neolacto-glycolipids enhances the formation of glycolipid-enriched microdomains, facilitating B cell activation. Proc Natl Acad Sci U S A. 107(26):11900–11905. doi:10.1073/pnas.0914298107.

Trebec-Reynolds DP, Voronov I, Heersche JNM, Manolson MF. 2010. VEGF-A expression in osteoclasts is regulated by NF-κB induction of HIF-1α. Journal of Cellular Biochemistry. 110(2):343–351. doi:10.1002/jcb.22542.

Truong Quang B-A, Lenne P-F. 2014. Membrane microdomains: from seeing to understanding. Frontiers in Plant Science. 5. [accessed 2023 May 1]. https://www.frontiersin.org/articles/10.3389/fpls.2014.00018.

Tuszynski GP, Rothman VL, Murphy A, Siegler K, Knudsen KA. 1988. Thrombospondin promotes platelet aggregation. Blood. 72(1):109–115.

Udenwobele DI, Su R-C, Good SV, Ball TB, Varma Shrivastav S, Shrivastav A. 2017. Myristoylation: An Important Protein Modification in the Immune Response. Front Immunol. 8:751. doi:10.3389/fimmu.2017.00751.

Umlauf E, Mairhofer M, Prohaska R. 2006. Characterization of the Stomatin Domain Involved in Homo-oligomerization and Lipid Raft Association *. Journal of Biological Chemistry. 281(33):23349–23356. doi:10.1074/jbc.M513720200.

Valdramidou D, Humphries MJ, Mould AP. 2008. DISTINCT ROLES OF β1 MIDAS, ADMIDAS AND LIMBS CATION-BINDING SITES IN LIGAND RECOGNITION BY INTEGRIN α2β1. J Biol Chem. 283(47):32704–32714. doi:10.1074/jbc.M802066200.

Vega-Lugo J, da Rocha-Azevedo B, Dasgupta A, Jaqaman K. 2022a. Analysis of conditional colocalization relationships and hierarchies in three-color microscopy images. Journal of Cell Biology. 221(7):e202106129. doi:10.1083/jcb.202106129.

Vega-Lugo J, da Rocha-Azevedo B, Dasgupta A, Jaqaman K. 2022b. Analysis of conditional colocalization relationships and hierarchies in three-color microscopy images. J Cell Biol. 221(7). doi:10.1083/jcb.202106129. [accessed 2023 Apr 3]. https://rupress.org/jcb/article/221/7/e202106129/213216/Analysis-of-conditional-colocalization.

Velling T, Nilsson S, Stefansson A, Johansson S. 2004. β1-Integrins induce phosphorylation of Akt on serine 473 independently of focal adhesion kinase and Src family kinases. EMBO Rep. 5(9):901–905. doi:10.1038/sj.embor.7400234.

Vélot L, Lessard F, Bérubé-Simard F-A, Tav C, Neveu B, Teyssier V, Boudaoud I, Dionne U, Lavoie N, Bilodeau S, et al. 2021. Proximity-dependent Mapping of the Androgen Receptor Identifies

Kruppel-like Factor 4 as a Functional Partner. Molecular & Cellular Proteomics. 20:100064. doi:10.1016/j.mcpro.2021.100064.

Vinogradova O, Velyvis A, Velyviene A, Hu B, Haas T, Plow E, Qin J. 2002. A structural mechanism of integrin alpha(IIb)beta(3) “inside-out” activation as regulated by its cytoplasmic face. Cell. 110(5):587–597. doi:10.1016/s0092-8674(02)00906-6.

Virtanen P, Gommers R, Oliphant TE, Haberland M, Reddy T, Cournapeau D, Burovski E, Peterson P, Weckesser W, Bright J, et al. 2020. SciPy 1.0: fundamental algorithms for scientific computing in Python. Nat Methods. 17(3):261–272. doi:10.1038/s41592-019-0686-2.

Vogel C, Marcotte EM. 2009. Absolute abundance for the masses. Nat Biotechnol. 27(9):825–826. doi:10.1038/nbt0909-825.

Volpert OV, Zaichuk T, Zhou W, Reiher F, Ferguson TA, Stuart PM, Amin M, Bouck NP. 2002. Inducer-stimulated Fas targets activated endothelium for destruction by anti-angiogenic thrombospondin-1 and pigment epithelium-derived factor. Nat Med. 8(4):349–357. doi:10.1038/nm0402-349.

Walia A, Yang JF, Huang Y, Rosenblatt MI, Chang J-H, Azar DT. 2015. Endostatin’s Emerging Roles in Angiogenesis, Lymphangiogenesis, Disease, and Clinical Applications. Biochim Biophys Acta. 1850(12):2422–2438. doi:10.1016/j.bbagen.2015.09.007.

Wang C, Yoo Y, Fan H, Kim E, Guan K-L, Guan J-L. 2010. Regulation of Integrin β1 Recycling to Lipid Rafts by Rab1a to Promote Cell Migration*. Journal of Biological Chemistry. 285(38):29398–29405. doi:10.1074/jbc.M110.141440.

Wang D, Huang HJ, Kazlauskas A, Cavenee WK. 1999. Induction of vascular endothelial growth factor expression in endothelial cells by platelet-derived growth factor through the activation of phosphatidylinositol 3-kinase. Cancer Res. 59(7):1464–1472.

Wang H-X, Kolesnikova TV, Denison C, Gygi SP, Hemler ME. 2011. The C-terminal tail of tetraspanin protein CD9 contributes to its function and molecular organization. J Cell Sci. 124(Pt 16):2702–2710. doi:10.1242/jcs.085449.

Wang J. 2012. Pull and push: Talin activation for integrin signaling. Cell Res. 22(11):1512–1514. doi:10.1038/cr.2012.103.

Wang J, Li Y. 2019. CD36 tango in cancer: signaling pathways and functions. Theranostics. 9(17):4893–4908. doi:10.7150/thno.36037.

Wary KK, Mariotti A, Zurzolo C, Giancotti FG. 1998. A Requirement for Caveolin-1 and Associated Kinase Fyn in Integrin Signaling and Anchorage-Dependent Cell Growth. Cell. 94(5):625–634. doi:10.1016/S0092-8674(00)81604-9.

Wei R, Wu Q, Ai N, Wang L, Zhou M, Shaw C, Chen T, Ye RD, Ge W, Siu SWI, et al. 2021. A novel bioengineered fragment peptide of Vasostatin-1 exerts smooth muscle pharmacological activities and anti-angiogenic effects via blocking VEGFR signalling pathway. Comput Struct Biotechnol J. 19:2664–2675. doi:10.1016/j.csbj.2021.05.003.

Welch BL. 1947. The generalisation of student's problems when several different population variances are involved. Biometrika. 34(1–2):28–35. doi:10.1093/biomet/34.1-2.28.

Welch DR, Hurst DR. 2019. Defining the Hallmarks of Metastasis. Cancer Res. 79(12):3011–3027. doi:10.1158/0008-5472.CAN-19-0458.

Welch S, Spithoff K, Rumble RB, Maroun J. 2010. Bevacizumab combined with chemotherapy for patients with advanced colorectal cancer: a systematic review. Annals of Oncology. 21(6):1152–1162. doi:10.1093/annonc/mdp533.

White NJ. 2022. Severe malaria. Malaria Journal. 21(1):284. doi:10.1186/s12936-022-04301-8.

Wickström SA, Alitalo K, Keski-Oja J. 2002. Endostatin Associates with Integrin α5β1 and Caveolin-1, and Activates Src via a Tyrosyl Phosphatase-dependent Pathway in Human Endothelial Cells1. Cancer Research. 62(19):5580–5589.

Wolven A, Okamura H, Rosenblatt Y, Resh MD. 1997. Palmitoylation of p59fyn is reversible and sufficient for plasma membrane association. Mol Biol Cell. 8(6):1159–1173. doi:10.1091/mbc.8.6.1159.

Wong HS, Jaumouillé V, Freeman SA, Doodnauth SA, Schlam D, Canton J, Mukovozov IM, Saric A, Grinstein S, Robinson LA. 2016. Chemokine Signaling Enhances CD36 Responsiveness toward Oxidized Low-Density Lipoproteins and Accelerates Foam Cell Formation. Cell Reports. 14(12):2859–2871. doi:10.1016/j.celrep.2016.02.071.

Wu S-C, Lo Y-M, Lee J-H, Chen C-Y, Chen T-W, Liu H-W, Lian W-N, Hua K, Liao C-C, Lin W-J, et al. 2022. Stomatin modulates adipogenesis through the ERK pathway and regulates fatty acid uptake and lipid droplet growth. Nat Commun. 13(1):4174. doi:10.1038/s41467-022-31825-z.

Xiong Z, Lo HP, McMahon K-A, Martel N, Jones A, Hill MM, Parton RG, Hall TE. 2021. In vivo proteomic mapping through GFP-directed proximity-dependent biotin labelling in zebrafish. Solnica-Krezel L, White RM, Solnica-Krezel L, Major BM, editors. eLife. 10:e64631. doi:10.7554/eLife.64631.

Xu J, Kurup P, Foscue E, Lombroso PJ. 2015. Striatal-enriched protein tyrosine phosphatase regulates the PTPα/Fyn signaling pathway. J Neurochem. 134(4):629–641. doi:10.1111/jnc.13160.

Xu X, Mao W, Chen Q, Zhuang Q, Wang L, Dai J, Wang H, Huang Z. 2014. Endostar, a Modified Recombinant Human Endostatin, Suppresses Angiogenesis through Inhibition of Wnt/β-Catenin Signaling Pathway. PLOS ONE. 9(9):e107463. doi:10.1371/journal.pone.0107463.

Xue Q, Nagy JA, Manseau EJ, Phung TL, Dvorak HF, Benjamin LE. 2009. Rapamycin Inhibition of the Akt/mTOR Pathway Blocks Select Stages of VEGF-A164–Driven Angiogenesis, in Part by Blocking S6Kinase. Arteriosclerosis, Thrombosis, and Vascular Biology. 29(8):1172–1178. doi:10.1161/ATVBAHA.109.185918.

Yamaoka T, Kusumoto S, Ando K, Ohba M, Ohmori T. 2018. Receptor Tyrosine Kinase-Targeted Cancer Therapy. Int J Mol Sci. 19(11):3491. doi:10.3390/ijms19113491.

Yang L. 2023. Proximity labeling reveals a BIN2 signaling network. The Plant Cell. 35(3):958–959. doi:10.1093/plcell/koad006.

Yang Y, Liu XR, Greenberg ZJ, Zhou F, He P, Fan L, Liu S, Shen G, Egawa T, Gross ML, et al. 2020. Open conformation of tetraspanins shapes interaction partner networks on cell membranes. EMBO J. 39(18):e105246. doi:10.15252/embj.2020105246.

Yao L, Pike SE, Setsuda J, Parekh J, Gupta G, Raffeld M, Jaffe ES, Tosato G. 2000. Effective targeting of tumor vasculature by the angiogenesis inhibitors vasostatin and interleukin-12. Blood. 96(5):1900–1905. doi:10.1182/blood.V96.5.1900.

Yauch RL, Berditchevski F, Harler MB, Reichner J, Hemler ME. 1998. Highly Stoichiometric, Stable, and Specific Association of Integrin α3β1 with CD151 Provides a Major Link to Phosphatidylinositol 4-Kinase, and May Regulate Cell Migration. MBoC. 9(10):2751–2765. doi:10.1091/mbc.9.10.2751.

Yauch RL, Kazarov AR, Desai B, Lee RT, Hemler ME. 2000. Direct Extracellular Contact between Integrin α3β1 and TM4SF Protein CD151 *. Journal of Biological Chemistry. 275(13):9230–9238. doi:10.1074/jbc.275.13.9230.

Yoshizuka N, Chen RM, Xu Z, Liao R, Hong L, Hu W-Y, Yu G, Han J, Chen L, Sun P. 2012. A Novel Function of p38-Regulated/Activated Kinase in Endothelial Cell Migration and Tumor Angiogenesis. Mol Cell Biol. 32(3):606–618. doi:10.1128/MCB.06301-11.

Yu H, Gao M, Ma Y, Wang L, Shen Y, Liu X. 2018. Inhibition of cell migration by focal adhesion kinase: Time-dependent difference in integrin-induced signaling between endothelial and hepatoblastoma cells. Int J Mol Med. 41(5):2573–2588. doi:10.3892/ijmm.2018.3512.

Yu J, Lee C-Y, Changou CA, Cedano-Prieto DM, Takada YK, Takada Y. 2017. The CD9, CD81, and CD151 EC2 domains bind to the classical RGD-binding site of integrin αvβ3. Biochemical Journal. 474(4):589–596. doi:10.1042/BCJ20160998.

Zafra F, Piniella D. 2022. Proximity labeling methods for proteomic analysis of membrane proteins. Journal of Proteomics. 264:104620. doi:10.1016/j.jprot.2022.104620.

Zech T, Ejsing CS, Gaus K, de Wet B, Shevchenko A, Simons K, Harder T. 2009. Accumulation of raft lipids in T-cell plasma membrane domains engaged in TCR signalling. EMBO J. 28(5):466–476. doi:10.1038/emboj.2009.6.

Zeng Y, Tao N, Chung K-N, Heuser JE, Lublin DM. 2003a. Endocytosis of oxidized low density lipoprotein through scavenger receptor CD36 utilizes a lipid raft pathway that does not require caveolin-1. J Biol Chem. 278(46):45931–45936. doi:10.1074/jbc.M307722200.

Zeng Y, Tao N, Chung K-N, Heuser JE, Lublin DM. 2003b. Endocytosis of Oxidized Low Density Lipoprotein through Scavenger Receptor CD36 Utilizes a Lipid Raft Pathway That Does Not Require Caveolin-1 *. Journal of Biological Chemistry. 278(46):45931–45936. doi:10.1074/jbc.M307722200.

Zhang K, Chen J. 2012. The regulation of integrin function by divalent cations. Cell Adh Migr. 6(1):20–29. doi:10.4161/cam.18702.

Zhang K, Li M, Yin L, Fu G, Liu Z. 2020. Role of thrombospondin-1 and thrombospondin-2 in cardiovascular diseases (Review). Int J Mol Med. 45(5):1275–1293. doi:10.3892/ijmm.2020.4507.

Zhang X, Kazerounian S, Duquette M, Perruzzi C, Nagy JA, Dvorak HF, Parangi S, Lawler J. 2009. Thrombospondin-1 modulates vascular endothelial growth factor activity at the receptor level. FASEB J. 23(10):3368–3376. doi:10.1096/fj.09-131649.

Zhang XA, Kazarov AR, Yang X, Bontrager AL, Stipp CS, Hemler ME. 2002. Function of the Tetraspanin CD151–α6β1 Integrin Complex during Cellular Morphogenesis. Mol Biol Cell. 13(1):1–11. doi:10.1091/mbc.01-10-0481.

Zhu J, Luo B-H, Xiao T, Zhang C, Nishida N, Springer TA. 2008. Structure of a complete integrin ectodomain in a physiologic resting state and activation and deactivation by applied forces. Mol Cell. 32(6):849–861. doi:10.1016/j.molcel.2008.11.018.

Zhuo Y, Robleto VL, Marchese A. 2023. Proximity Labeling to Identify β-Arrestin1 Binding Partners Downstream of Ligand-Activated G Protein-Coupled Receptors. International Journal of Molecular Sciences. 24(4):3285. doi:10.3390/ijms24043285.

Zilber M-T, Setterblad N, Vasselon T, Doliger C, Charron D, Mooney N, Gelin C. 2005. MHC class II/CD38/CD9: a lipid-raft–dependent signaling complex in human monocytes. Blood. 106(9):3074–3081. doi:10.1182/blood-2004-10-4094.

Zuidscherwoude M, Dunlock V-ME, van den Bogaart G, van Deventer SJ, van der Schaaf A, van Oostrum J, Goedhart J, In ’t Hout J, Hämmerling GJ, Tanaka S, et al. 2017. Tetraspanin microdomains control localized protein kinase C signaling in B cells. Sci Signal. 10(478):eaag2755. doi:10.1126/scisignal.aag2755.

Chapter 6: Appendices

6.1 Appendix A: Determining Streptavidin Compatible for Biotinylated Protein Capture and Tandem Mass Spectrometry

Cell surface biotinylation is an enzyme-free biotin labelling technique that utilizes Sulfo-NHS-biotin to covalently link biotin to the primary amine of lysine residues. The Sulfo group's negative charge prevents this biotin derivative from entering the cell. Therefore, cell surface biotinylation provides a global map of membrane proteins present in TIME mEmerald-CD36 cells. Initially, the CD36 BAR and cell surface biotinylation proteomes were going to be compared to access proteins enriched and de-enriched within CD36 nanoclusters. However, issues regarding TIME cell viability during cell surface biotinylation prevented it from being used as a control. Nevertheless, the high level of biotinylated proteins produced by cell surface biotinylation allowed the determination of streptavidin beads capturing capacity.

Validation of cell surface biotinylation was performed via immunofluorescence and immunoblot analysis. Cell surface biotinylation of TIME mEmerald-CD36 cells produced homogenous streptavidin AF647 staining, confirming non-discriminate biotinylation of membrane proteins (Figure 6-1, A). A high level of biotinylated proteins was detected in the lysate of mEmerald-CD36 cells treated with cell surface biotinylation via immunoblotting (Figure 6-1, B).

Following validation of cell surface biotinylation, we used lysate from TIME mEmerald-CD36 cells treated with cell surface biotinylation was used to access biotin protein capture for a variety of streptavidin beads. The first beads used for capture were Pierce™ Streptavidin Agarose (ThermoFisher, Waltman, MA, USA). Immunoblot revealed high capture efficiency as few biotinylation proteins are present in the flow-through fraction (Figure 6-2, A). The captured proteins were subsequently submitted to LC-MS/MS. Over 120 proteins were identified, with ~25% being membrane proteins (Table 6-1). However, the end of the chromatogram showed peaks, indicating that our samples contained contaminants (Figure 6-2, A). Therefore, Pierce™ Streptavidin Agarose beads were deemed incompatible with LC-MS/MS in our hands. Magnetic

M280 Dynabeads (ThermoFisher, Waltman, MA, USA) were the 2nd type of streptavidin beads accessed for biotinylated protein capture and compatibility with LC-MS/MS. Magnetic M280 Dynabeads had poor capturing capacity, as many biotinylated proteins were detected in the flow-through (Figure 6-2, B). LC-MS/MS on the captured proteins revealed that the beads were compatible with mass spectrometry, as no large contaminants were detected in the chromatograph (Figure 6-2, B). However, only ~90 proteins were identified, with ~16% being membrane proteins (Table 6-1).

To optimize protein capture, four different magnetic streptavidin beads were tested: M280 Dynabeads, C1 Dynabeads (ThermoFisher, Waltman, MA, USA), MagnaBind (ThermoFisher, Waltman, MA, USA), and Pierce magnetic beads. Flow-through revealed Pierce magnetic and MagnaBind beads to have the highest biotin binding capacity (Figure 6-2, C). Biotinylated protein captured with 300uL of each beads type was submitted to LC-MS/MS. Biotinylated proteins captured using Magnabind beads contained contaminants, whereas Pierce magnetic beads samples were contaminant free (Figure 6-2, C).

Biotinylated proteins captured with the Pierce magnetic beads also had the most proteins identified (380), with ~21% being membrane proteins (Table 6-1). Therefore, Pierce magnetic beads were determined to be optimal for biotinylated capture and compatible with LC-MS/MS. Therefore, Pierce magnetic beads were utilized for biotinylated protein capture of our CD36 BAR samples.

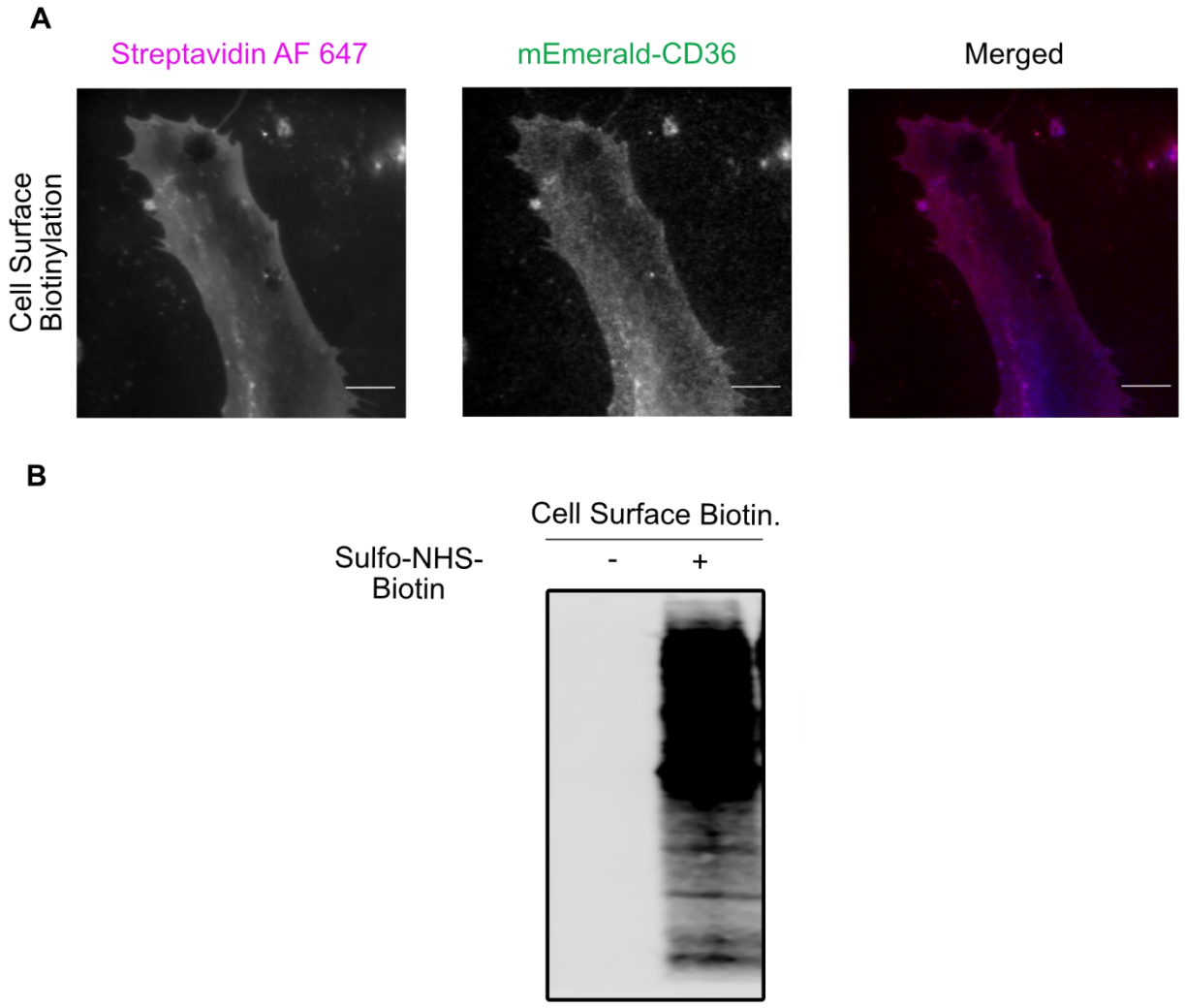

Figure 6-1: Validation of Cell Surface Biotinylation via widefield microscopy (A) and immunoblotting (B).

(A) Widefield fluorescent images of TIME mEmerald-CD36 cells treated with CD36 BAR, CD36 BAR control, and cell surface biotinylation. Bar Scale = 10μm. ***(B)*** *Detection of biotinylated proteins in TIME mEmerald-CD36 lysate treated with CD36 BAR, CD36 BAR control, and cell surface biotinylation with streptavidin IRDye 680RD.*

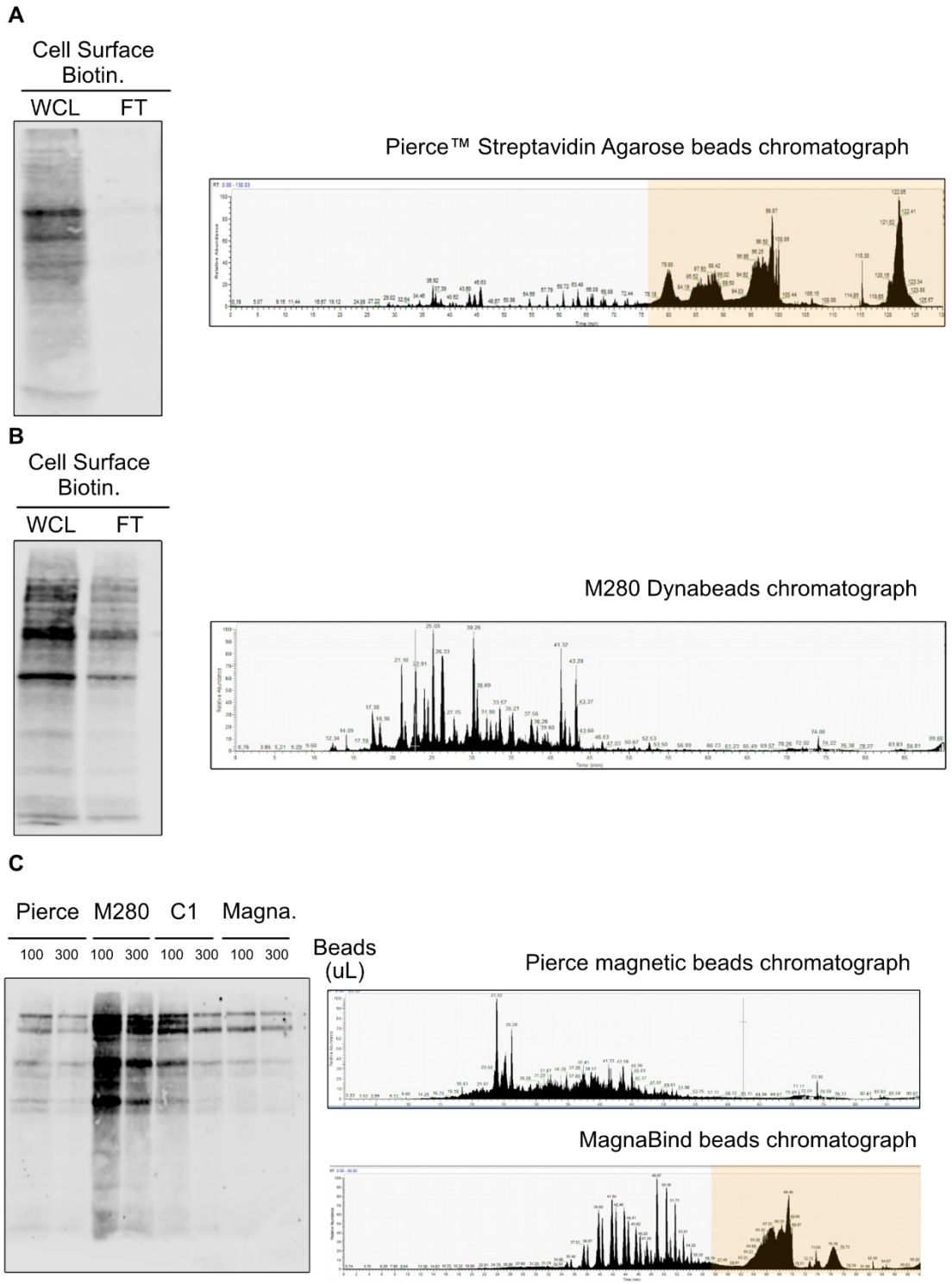

Figure 6-2: Efficiency of biotin protein capture and LC-MS/MS compatibility of agarose and magnetic streptavidin beads.

Analysis of magnetic and agarose streptavidin beads protein capture and compatibility with LC-MS/MS. (A) Biotinylated proteins from cell surface biotinylation lysate were captured using Pierce™ streptavidin agarose beads, and the corresponding chromatograph showed large polymer contaminants in orange. (B) WCL and flow through of biotinylated

protein capture using magnetic Dynabeads M280 streptavidin (M280) and the corresponding chromatograph showing no contaminants. (C) Flow-through of biotinylated proteins captured using Pierce magnetic beads, M280 and C1 Dynabeads, and Magnabeads (Magna). The chromatogram obtained from protein capture using Pierce magnetic beads showed no contaminants, however contaminants are detected (orange) for samples captured using MagnaBind streptavidin beads.

Table 6-1: Summary of identified protein characteristics.

Number of proteins identified, membrane proteins identified and presence of contaminants for cell surface biotinylated protein samples captured with Pierce™ streptavidin agarose, Dynabeads M280, MagnaBind and Pierce magnetic beads.

Beads	Type	Total Proteins Identified	Membrane Proteins Identified (%)	Contaminants Detected in Chromatograph
Pierce™ streptavidin agarose beads	Agarose	129	24.8	Yes
Dynabeads M280	Magnetic	87	16.1	No
MagnaBind beads	Magnetic	151	25.2	Yes
Pierce magnetic beads	Magnetic	380	21.3	No

6.2 Appendix B: Normalization of Protein Intensities for CD36 BAR LC-MS/MS Dataset

LC-MS/MS identified ~800 and ~1000 proteins for CD36 BAR and CD36 BAR control, respectively (Table 6-2). The number of proteins identified is similar for all the replicates within each treatment. However, there was a large variation in average protein intensity between replicates. To nullify the variance and allow for comparisons between CD36 BAR and CD36 BAR control treatments, a novel protein intensity normalization method was developed.

Normalization was performed by finding the common protein identified in all CD36 BAR and CD36 BAR control replicates (Figure 6-3, A). The 367 commonly identified proteins were utilized to determine the normalization factor to be applied to each of the 16 samples (Figure 6-3, A). For each replicate, the average protein intensity of commonly identified proteins were calculated (Figure 6-3, A). The normalization factor was calculated by dividing the average protein intensity for the replicate by the lowest average protein intensity (Figure 6-3, A). CD36 BAR replicate 8 had the lowest average protein intensity (Figure 6-3, A). Therefore, it was used to calculate the normalization factor.

$$Normalization\ Factor = \frac{Average\ protein\ intensity\ for\ the\ commonly\ identified\ 367\ proteins}{BAR\ 8\ average\ protein\ intensity\ for\ the\ commonly\ identified\ 367\ proteins}$$

(Equation 3)

Prior to applying normalization, the CD36 BAR LC-MS/MS data was zero-filled by replacing blank protein intensities values with the minimum protein intensity identified within each sample (Figure 6-3, B). The average protein intensity for each replicate was not affected by zero-filling blank values (Figure 6-4). Normalization was performed by dividing all protein intensities within a sample by their respective normalization factor (Figure 6-3, B). Normalization effectively reduced variation between as the average protein intensity for all replicates is ~ $0.5 * 10^6$ (Figure 6-3, B). Boxplots of the protein intensities for CD36 and Fyn further demonstrate the effectiveness of this method, as the interquartile ranges are greatly reduced after normalization (Figure 6-5).

Normalization of protein intensities reduced variance in the protein intensities among samples allowing us to make statistical comparisons between CD36 BAR and CD36 BAR control data.

$$Ratio = \frac{Average\ protein\ intensity\ of\ protein\ X\ in\ CD36\ BAR}{Average\ protein\ intensity\ of\ protein\ X\ in\ CD36\ BAR\ Control} \quad \textbf{(Equation 4)}$$

Table 6-2: Summary of analyzed samples.

Date submitted, number of proteins identified, and total protein intensity mass spectrometry data for CD36 BAR and CD36 BAR negative control replicates.

Treatment	CD36 BAR Samples							
Sample Number	1	2	3	4	5	6	7	8
Date	2022-04-03	2022-04-03	2022-04-03	2022-04-03	2022-04-03	2022-04-03	2022-04-03	2022-06-15
Number of Proteins Identified	729	823	837	872	853	760	759	799
Total Protein Intensity	1.72e+09	3.40e+09	2.90e+09	1.99e+09	2.28e+09	2.82e+09	2.26e+09	6.65e+08

Treatment	CD36 BAR Negative Control Samples							
Sample Number	1	2	3	4	5	6	7	8
Date	2022-01-10	2022-01-10	2022-01-10	2022-11-10	2022-11-10	2022-11-10	2022-11-10	2022-11-10
Number of Proteins Identified	1112	1083	1075	1090	1024	1025	1020	1045
Total Protein Intensity	3.36e+09	2.84e+09	1.57e+09	2.50e+09	1.07e+09	1.30e+09	2.89e+09	1.65e+09

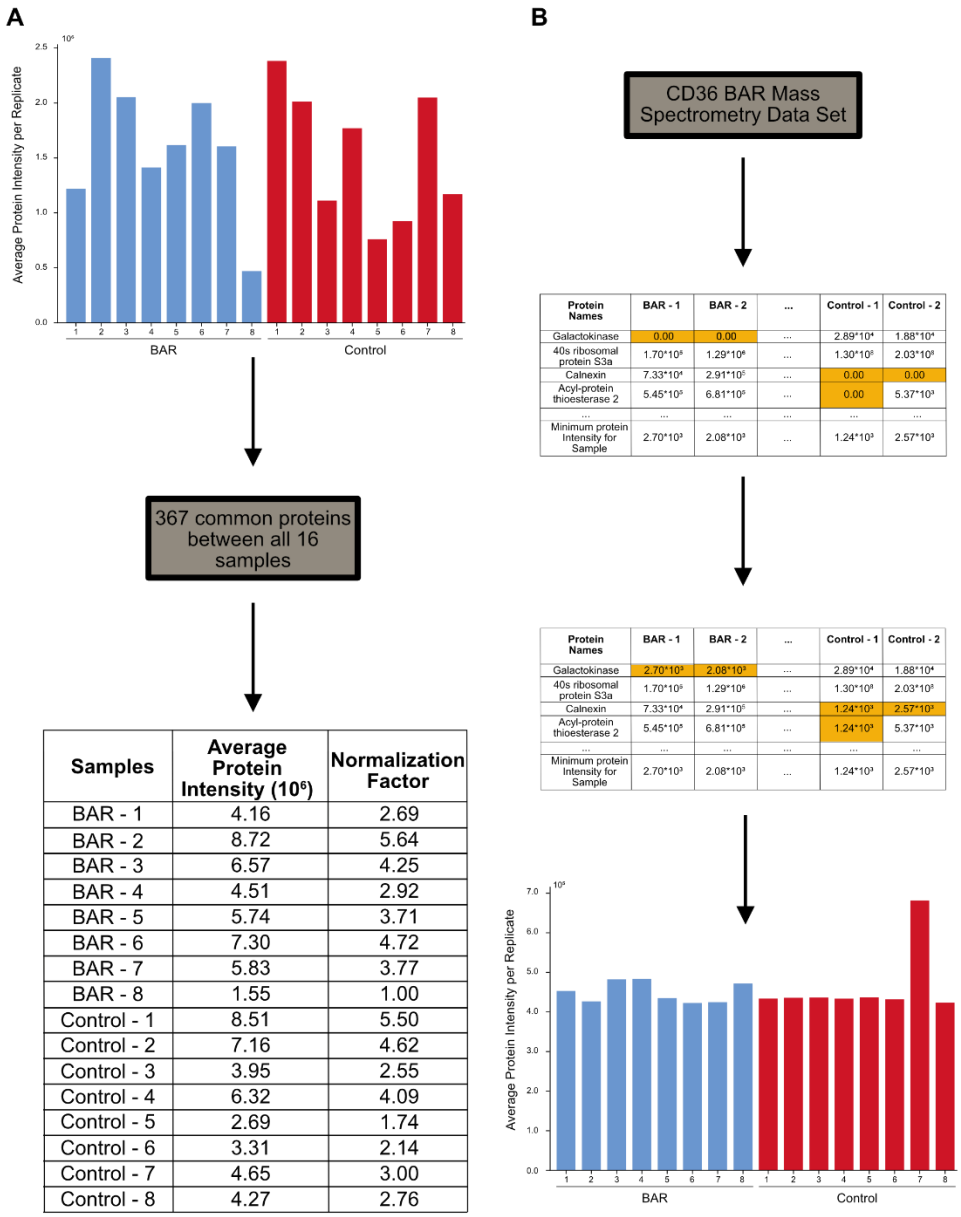

Samples	Average Protein Intensity (10^6)	Normalization Factor
BAR - 1	4.16	2.69
BAR - 2	8.72	5.64
BAR - 3	6.57	4.25
BAR - 4	4.51	2.92
BAR - 5	5.74	3.71
BAR - 6	7.30	4.72
BAR - 7	5.83	3.77
BAR - 8	1.55	1.00
Control - 1	8.51	5.50
Control - 2	7.16	4.62
Control - 3	3.95	2.55
Control - 4	6.32	4.09
Control - 5	2.69	1.74
Control - 6	3.31	2.14
Control - 7	4.65	3.00
Control - 8	4.27	2.76

Figure 6-3: Normalization workflow of CD36 BAR mass spectrometry data protein intensity.

(A) Workflow to determine the normalization factor for each CD36 BAR and CD36 BAR negative-control sample. 367 common proteins were identified between the CD36 BAR and CD36 BAR negative control samples. These common proteins were utilized for the normalization of protein intensities. Normalization factors were calculated by dividing the minimum average protein intensity (indicated in green) by the average protein intensity for the BAR samples. (B) Normalization of CD36 BAR mass spectrometry data. Before normalization, zero-filling was performed by replacing blank values with the minimum protein intensity identified within each sample (local minima). Normalization of protein intensities was obtained by dividing all protein intensities within a sample by their respective normalization factor.

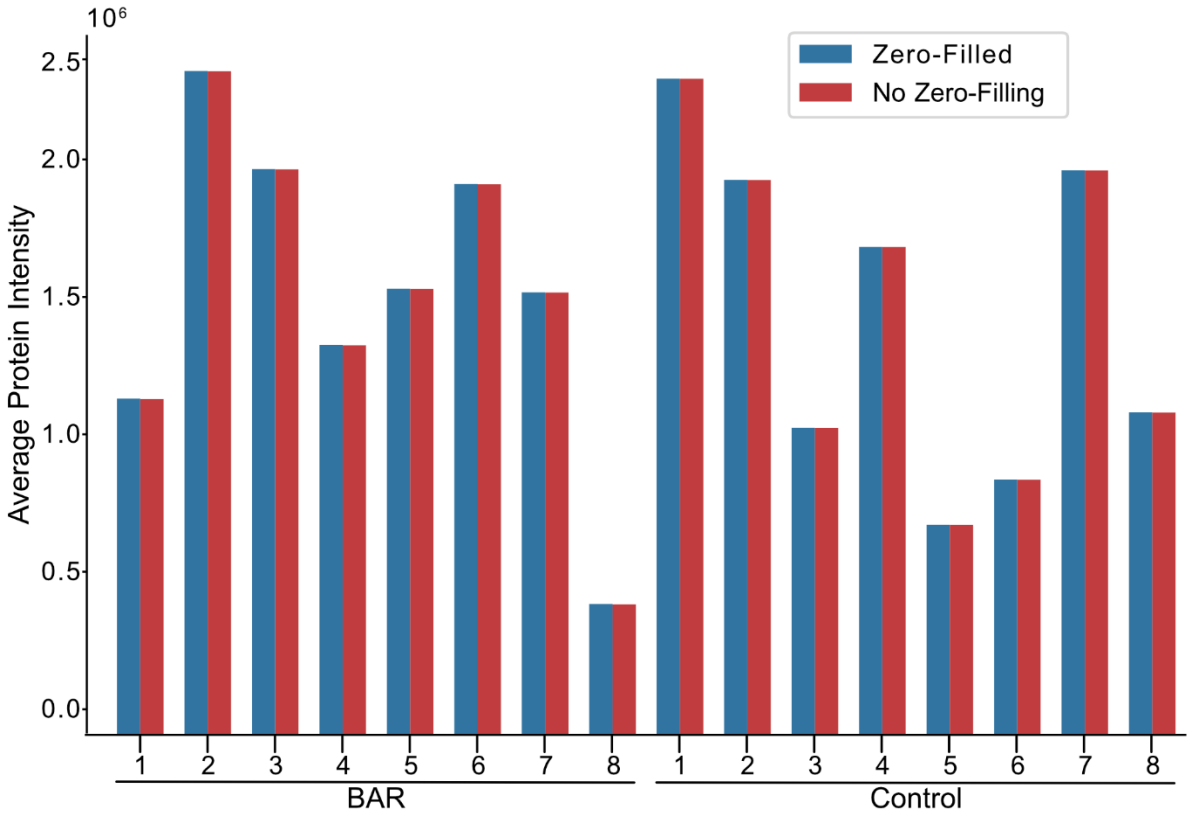

Figure 6-4: Effect of zero-filling on CD36 BAR average protein intensity.

Average protein intensity for CD36 BAR and CD36 control-BAR replicates before (red) and after zero-filling protein intensities (blue). Zero values for each BAR replicate were replaced with their respective protein intensity minima.

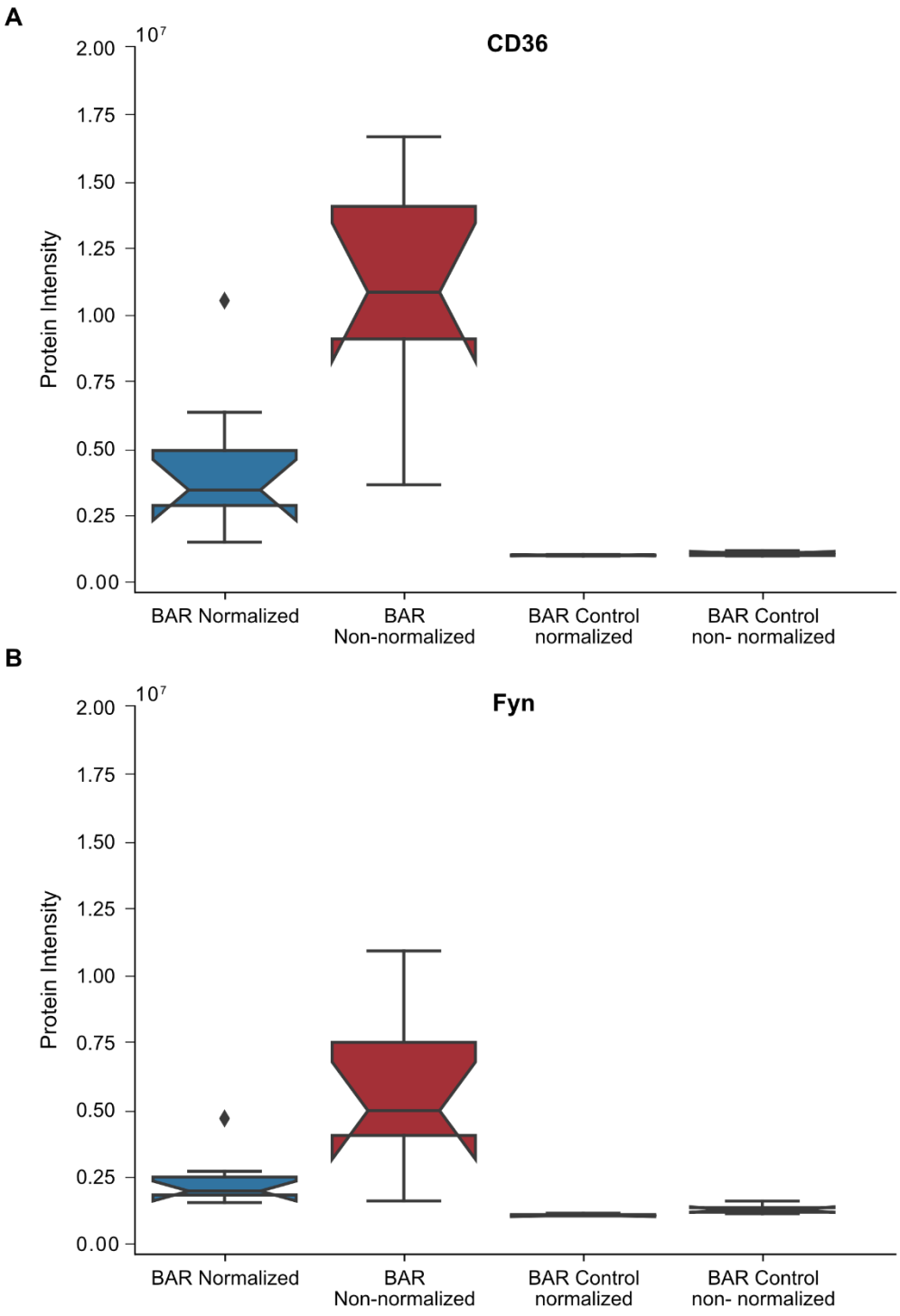

Figure 6-5: Protein levels after normalization.

CD36 (A) and Fyn (B) normalized and non-normalized protein intensity within CD36 BAR and CD36 BAR control datasets. Proteins intensities of CD36 and Fyn were normalized as described in Appendix.

6.3 Appendix C: Complete List of Enriched Proteins within CD36 BAR LC-MS/MS Dataset

Table 6-3: Complete list of proteins enriched in CD36 BAR dataset.

Complete list of proteins identified in CD36 BAR LC-MS/MS with a ratio greater than 2 and p-values less than 0.05. CD36 and Fyn, are highlighted in green, while proteins that are a part of the integrin and tetraspanin family are highlighted in blue and red, respectively.

Protein Name	Ratio	p-value
Neutral alpha-glucosidase AB	179.356	<0.001
40S ribosomal protein S17	149.85	0.007
Disintegrin and metalloproteinase domain-containing protein 10	148.088	0.001
Platelet glycoprotein 4	140.081	0.014
Synaptosomal-associated protein 23	131.331	0.019
Fibulin-1	126.475	0.005
Poliovirus receptor	122.905	0.037
CD81 antigen	121.593	0.010
Junctional adhesion molecule A	112.754	0.028
39S ribosomal protein L38, mitochondrial	105.483	0.033
Cytochrome c oxidase subunit 2	96.256	<0.001
Protein disulfide-isomerase A6	94.529	0.002
Acyl-protein thioesterase 2	92.353	0.002

Endothelial protein C receptor	89.145	0.010
Carbonyl reductase [NADPH] 1	84.315	0.015
Survival motor neuron protein	75.082	0.011
UTP--glucose-1-phosphate uridylyltransferase	74.208	0.016
GTPase KRas	57.731	0.011
Collagen alpha-1(XVIII) chain	53.486	0.001
Heterogeneous nuclear ribonucleoprotein H2	52.501	0.020
C-type lectin domain family 14 member A	51.218	0.026
Cytoplasmic aconitate hydratase	47.163	0.039
Endothelial cell-selective adhesion molecule	42.82	0.004
Elongation factor 1-alpha 1	36.256	0.005
Neuropilin-1	35.567	0.008
Calcium homeostasis endoplasmic reticulum protein	34.354	0.002
Nectin-2	34.069	0.030
Peptidyl-prolyl cis-trans isomerase FKBP8	33.818	0.019
ADAMTS-like protein 1	31.546	0.008
Rab GTPase-activating protein 1	30.341	0.005
Serine/threonine-protein kinase N2	29.76	0.005

cAMP-dependent protein kinase type I-alpha regulatory subunit	29.452	0.018
Collagen alpha-1(VIII) chain	29.311	0.024
Coagulation factor V	28.004	0.007
E3 ubiquitin-protein ligase HUWE1	27.305	0.004
Intercellular adhesion molecule 2	26.437	0.020
Calreticulin	26.087	0.016
Protein Niban 2	22.427	0.012
Integrin alpha-5	22.356	0.001
CD59 glycoprotein	20.217	0.001
Multidrug resistance-associated protein 1	19.265	0.007
EF-hand domain-containing protein D2	18.24	0.003
Peroxiredoxin-2	18.16	0.040
Lon protease homolog, mitochondrial	17.529	0.018
Integrin alpha-3	16.591	<0.001
Integrin beta-1	15.138	0.004
Serum albumin	15.128	0.015
28S ribosomal protein S25, mitochondrial	14.916	0.026
Endoglin	14.862	0.002

Tyrosine-protein kinase Fyn	14.65	0.009
Erythrocyte band 7 integral membrane protein	14.616	0.022
Plexin-D1	14.541	0.002
Integrin alpha-6	14.346	0.015
Splicing factor 3A subunit 3	14.236	0.009
Aminopeptidase N	13.488	0.004
Double-stranded RNA-binding protein Staufen homolog 1	13.216	0.021
Disintegrin and metalloproteinase domain-containing protein 9	13.198	0.034
Y-box-binding protein 1	12.518	0.027
Laminin subunit gamma-1	12.015	0.038
AP-3 complex subunit delta-1	11.786	0.002
Sushi repeat-containing protein SRPX	11.045	0.039
Laminin subunit alpha-4	10.593	0.033
CD9 antigen	10.585	0.014
Transforming growth factor-beta-induced protein ig-h3	10.523	0.012
Thrombospondin type-1 domain-containing protein 4	10.326	0.007
Replication factor C subunit 2	10.225	0.011
Flotillin-2	9.653	0.005

HLA class I histocompatibility antigen, C alpha chain	9.294	<0.001
Annexin A6	8.86	0.027
Protein transport protein Sec24A	8.437	0.004
Hemoglobin subunit alpha	8.32	0.017
NEDD8-conjugating enzyme Ubc12	8.229	0.040
Microtubule-actin cross-linking factor 1, isoforms 1/2/3/5	8.19	0.025
Fibrillin-1	8.087	0.007
Guanine nucleotide-binding protein G(i) subunit alpha-2	8.032	0.005
EGF-containing fibulin-like extracellular matrix protein 1	7.485	0.001
HLA class I histocompatibility antigen, B alpha chain	7.482	0.029
Rab GDP dissociation inhibitor beta	7.43	0.003
Latent-transforming growth factor beta-binding protein 1	7.238	0.034
Mitochondrial-processing peptidase subunit alpha	7.045	0.032
Isoform 2 of CD166 antigen	6.999	0.019
Ran GTPase-activating protein 1	6.981	0.013
TAR DNA-binding protein 43	6.791	0.046
CD109 antigen	6.733	0.005
Thioredoxin-dependent peroxide reductase, mitochondrial	6.666	0.015

26S proteasome non-ATPase regulatory subunit 3	6.655	0.002
Desmoglein-1	6.602	0.001
Platelet endothelial cell adhesion molecule	6.461	<0.001
Ephrin type-A receptor 2	6.411	0.005
Developmentally-regulated GTP-binding protein 1	6.326	0.041
Integrin alpha-2	6.254	0.002
Ras-related protein Rab-7a	6.234	0.046
Catenin alpha-1	6.19	0.016
Breakpoint cluster region protein	6.167	0.012
Guanine nucleotide-binding protein subunit beta-4	6.084	0.016
Activating signal cointegrator 1 complex subunit 2	5.943	0.048
Isoform 4 of Leucine-rich repeat flightless-interacting protein 1	5.911	0.019
Calponin-2	5.878	0.030
DNA-directed RNA polymerase II subunit RPB3	5.873	0.043
Plasminogen activator inhibitor 1	5.725	0.018
CD44 antigen	5.715	0.009
Src substrate cortactin	5.485	0.034
DBIRD complex subunit ZNF326	5.261	0.011

Signal recognition particle subunit SRP68	5.155	0.018
Eukaryotic translation initiation factor 3 subunit A	4.856	0.002
Antithrombin-III	4.815	0.029
Importin subunit alpha-7	4.711	0.041
Tyrosine-protein phosphatase non-receptor type 1	4.695	0.019
Dolichyl-diphosphooligosaccharide--protein glycosyltransferase subunit 1	4.634	0.005
U3 small nucleolar RNA-associated protein 14 homolog A	4.63	0.013
Junction plakoglobin	4.609	0.009
WASH complex subunit 4	4.512	0.011
Isocitrate dehydrogenase [NADP], mitochondrial	4.359	0.008
E3 ubiquitin-protein ligase ARIH1	4.354	0.039
Multimerin-1	4.338	0.038
Peptidyl-prolyl cis-trans isomerase FKBP1A	4.273	0.012
Cadherin-5	4.262	0.005
Basigin	4.192	0.048
Desmoplakin	4.101	0.015
Voltage-dependent anion-selective channel protein 1	3.954	0.036

60S ribosomal protein L23	3.842	0.015
Pyruvate kinase PKM	3.76	0.003
Malate dehydrogenase, mitochondrial	3.701	0.008
Squamous cell carcinoma antigen recognized by T-cells 3	3.573	0.048
Glutamate dehydrogenase 1, mitochondrial	3.495	0.003
Histone-arginine methyltransferase CARM1	3.317	0.004
Nuclear pore complex protein Nup133	3.305	0.043
Multimerin-2	3.304	0.035
Dihydrolipoyl dehydrogenase, mitochondrial	3.286	<0.001
Citrate synthase, mitochondrial	3.26	0.013
Leucine-rich PPR motif-containing protein, mitochondrial	3.256	0.026
A-kinase anchor protein 12	3.194	0.001
60S ribosomal protein L18a	3.11	0.022
Myoferlin	3.055	0.023
AP2-associated protein kinase 1	3.036	0.045
Hexokinase-1	2.928	0.006
Prothrombin	2.921	0.024
Trifunctional enzyme subunit alpha, mitochondrial	2.871	0.006

5'-nucleotidase	2.859	0.044
Peroxidasin homolog	2.761	0.033
60S ribosomal protein L37a	2.704	0.030
Catenin delta-1	2.673	0.001
ATP-binding cassette sub-family F member 1	2.519	0.031
Ras GTPase-activating-like protein IQGAP1	2.461	0.008
Moesin	2.426	0.022
Ankycorbin	2.329	0.018
EH domain-containing protein 2	2.3	0.040
Annexin A2	2.267	<0.001
40S ribosomal protein SA	2.186	0.021
Cell surface glycoprotein MUC18	2.173	0.048
60S ribosomal protein L19	2.084	0.020
Ras-interacting protein 1	2.021	0.013
EH domain-containing protein 4	2.001	0.045

6.4 Appendix D: Conditional Colocalization Figures

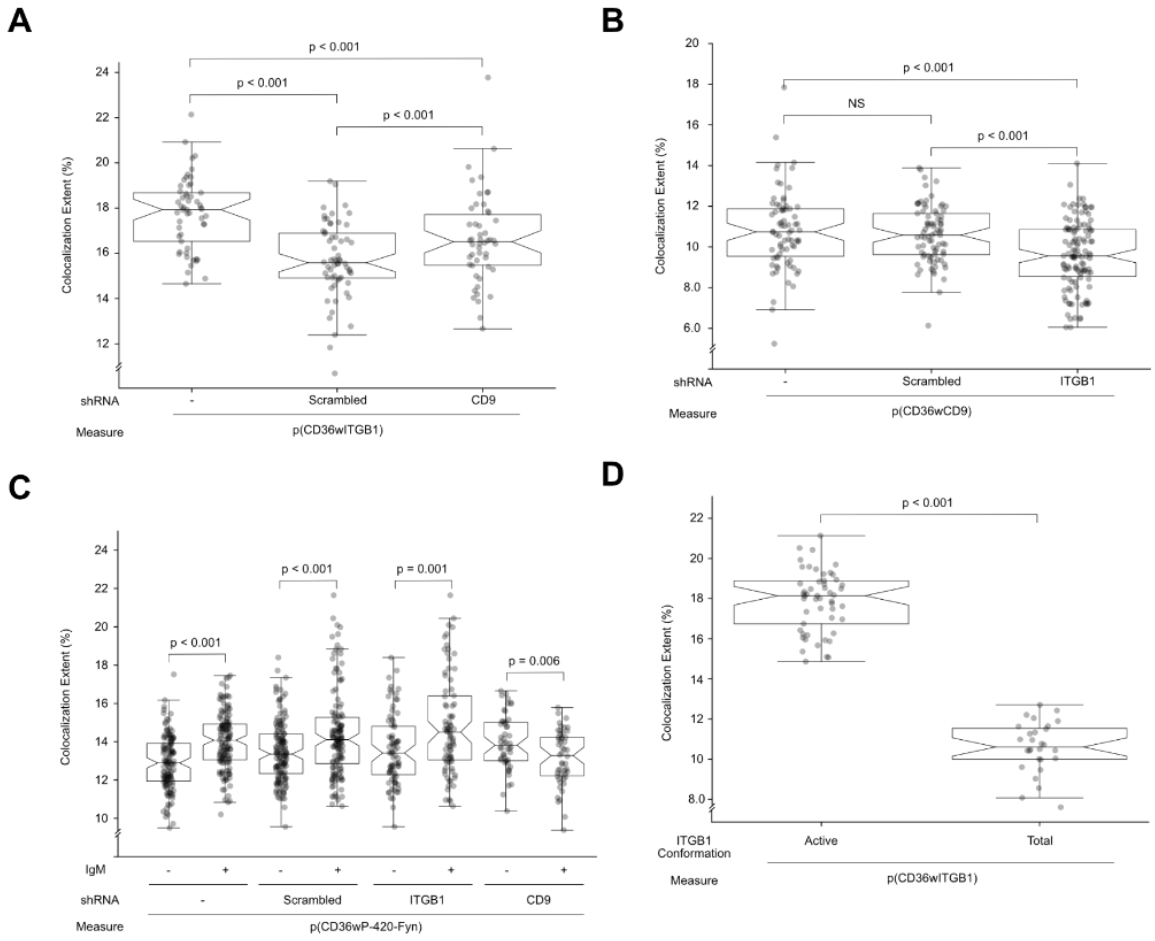

Figure 6-6: Conditional colocalization of CD36 with ITGB1, CD9 and P-Y420-Fyn.

CD36 colocalization with active ITGB1 (A), CD9 (B), P-Y420-Fyn (C) and (D) total ITGB1 in cells with ITGB1 and CD9 inactivation with or without stimulation with mouse anti-IgM CD36. (A) Overall CD36 colocalization with ITGB1 (p(CD36wITGB1)) in response to CD9 KD. 55 cells were imaged across 3 experiments. (B) Overall CD36 colocalization with CD9 (p(CD36wCD9)) in response in ITGB1 KD. 55 cells were imaged across 3 experiments (C) Overall CD36 colocalization with P-Y420-Fyn (p(CD36wP-Y420-Fyn)) in response to ITGB1 KD, CD9 KD, and/or mouse anti-CD36 IgM stimulation. For TIME-HT CD36 WT, 128 and 131 cells were imaged for the unstimulated and stimulated conditions, respectively. For TIME-HT CD36 cells expressing scrambled shRNA, 147 and 135 cells were imaged for the unstimulated and stimulated conditions, respectively. For TIME-HT CD36 cells expressing ITGB1 shRNA, 89 and 78 cells were imaged for the unstimulated and stimulated conditions, respectively. For TIME-HT CD36 cells expressing CD9 shRNA, 50 cells were imaged for the unstimulated and stimulated conditions, respectively. For the ITGB1 and CD9 knockdown cell lines images were collected from 3 different experiments. For TIME HT-CD36 and TIME HT-CD36 cells expressing scrambled shRNA, images were collected over 6 different experiments. (D) Overall colocalization of CD36 with active and total ITGB1 (p(CD36wITGB1)). For CD36's overall colocalization with active ITGB1, 55 cells were imaged across 3 different experiments. For CD36's overall colocalization with total ITGB1, 33 cells were imaged across 2 different experiments.

6.5 *Appendix E: Preliminary F-actin fractionation results*

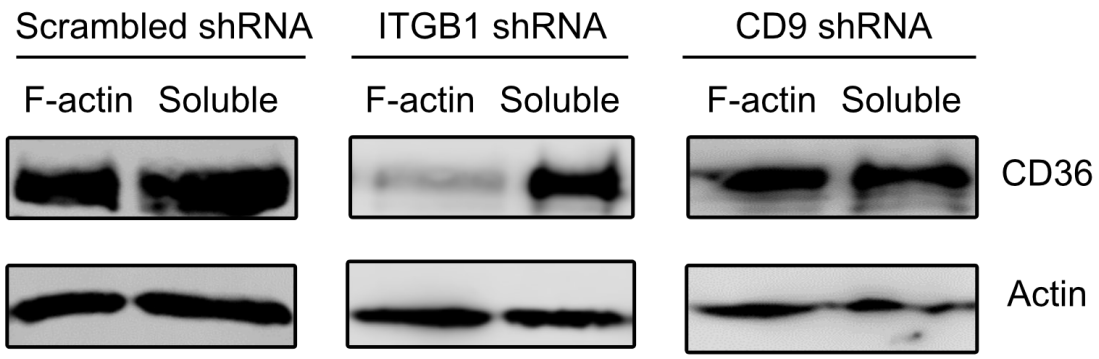

Figure 6-7: Effect of ITGB1 and CD9 shRNA KD on CD36 F-actin Association.

TIME-mEmerald-CD36 cells were grown to ~90% confluency in 6 well plates and induced with 0.5ug of doxycycline for 18 hours prior to performing F-actin separation. After aspirating TIME cell media, cells were lysed using warm 250µL of cytoskeleton stabilizing buffer. Cell lysate was then later centrifuged at 2000 rpm at room temperature for 5 min to pellet unbroken cells. Supernatant was recovered, and then ultracentrifuged at 50,000g at room temperature for 1 hour. Following, Eppendorf tubes were immediately placed on ice. The G-actin fraction (supernatant) was saved in a separate Eppendorf tube, and the remaining F-actin pellet then was depolymerized using F-actin depolymerization buffer.

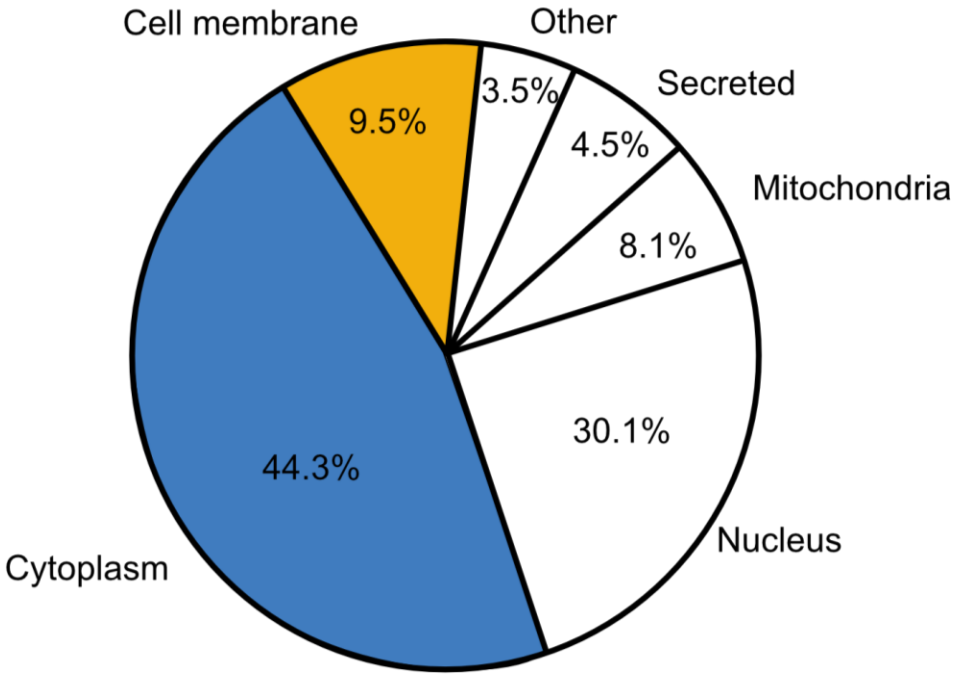

Figure 6-8: Subcellular distribution of TIME mEmerald-CD36 proteome.

TIME mEmerald-CD36 cells grown in a single well of a 6-well plate were incubated with 0.5µg of doxycycline for 18 hours and lysed with 250µL of lysis buffer (150mM NaCl, 50mM Tris-HCl at pH 7.2, 0.2% SDS, 1% Triton X-100, protease inhibitor cocktail) for 30 min on ice. Cell homogenate was harvested using a cell scrapper and centrifuged at 14,000 RPM for 20 minutes at 4℃. 30uL of TIME mEmerald-CD36 of lysate was mixed with 10uL of 4X Laemmli sample buffer (62.5mM Tris pH 6.8, 0.005% bromophenol blue, 10% glycerol, 20% β-mercaptoethanol). Proteins were resolved on 10% SDS-PAGE for 1hr at 150V. Following electrophoresis, the gel was incubated with fixative (50% ethanol and 2% phosphoric acid) for 20min. The gel was washed twice with double-distilled water for 20min, and then stained with blue-silver staining solution (10% phosphoric acid, 20% ethanol, 756 mM ammonium sulphate, 1.4 mM Coomassie Blue G-250) overnight. Following overnight incubation, the gel was washed twice with double-distilled water for 20min. The TIME CD36-mEmerald lane was excised from the gel, further cut into ~0.6mm cubes, and placed into 1.5mL tubes. Gel pieces were destained using 150µL destaining solution (50% 100mM ammonium bicarbonate/ acetonitrile). Gel pieces with destaining solution were heated at 37°C for 10 min. Destaining solution was removed, and destaining was repeated till the gel became transparent. Following destaining, the gel was dehydrated by adding 150µL of 100% acetonitrile to each tube for 5 minutes twice. Acetonitrile was removed, and gel pieces were air dried at 37°C for 15min. Following dehydration, 150µL of reduction solution (3.5 µL of BME in 5ml of 100mM NH_4HCO_3) was added to gel pieces for 30 min at 37°C. Reduction solution was removed, and 150µL of alkylation solution (10 mg/mL IAM in 100 mM NH_4HCO_3) was added to gel pieces for 30 min at 37°C. Excess alkylation solution was removed and gel pieces were washed once with 150µL of 100mM NH_4HCO_3 for 10 min at 37°C. Following washes, gel pieces were dehydrated via two incubations of 150µL of 100% acetonitrile at 37°C for 30min. Acetonitrile was removed, and gel pieces were air dried at 37°C for 15min. Following dehydration, 75 µL of digestion buffer (prepared as 20 µg lyophilized trypsin in 3.3 mL of 50 mM NH_4HCO_3) was added to each tube overnight. Following overnight digestion, digestion buffer was added to a MS V-bottom well plate and 200µL of extraction solution (2% formic acid and 2% ACN in water) was added to gel pieces for 1 hour at 37 °C for extraction of hydrophilic/short peptides. Extraction solution was removed from the 1.5mL tubes and added to the MS V-bottom well plate. A 2nd extraction of hydrophobic/longer peptides was performed by adding 100µL ACN, and 100µL extraction solution to gel pieces for 1 hour at 37°C. The solution for the 2nd extraction was removed from the 1.5mL tubes and added to the same MS V-bottom well plate. Finally, a 3rd extraction was

performed to extract longer and more hydrophobic peptides by adding 100µL ACN, and 100µL of extraction solution to gel pieces for 1 hour at 37°C. Following the incubation, the solution was removed from the 1.5mL tubes and added to the same MS V-bottom well plate. The solution in the MS V-bottom plate was dried via a Genevac®. The dried samples were resolubilized in 20µL of 0.2% formic acid and allowed to set at room temperature for 10min. The 20µL was transferred to a 1.5mL tube and another 20µL was added to the MS V-bottom plate. Following, the 20µL was transferred to the same 1.5mL tube. Following these steps, the 40µL solution was submitted for analysis via LC-MS/MS.